Evaluation of Vertical Ground and Floor Accelerations and Spectra in Elastic RC Frame Buildings Located in Eastern Canada

by

Shahabaldin MAZLOOM

MANUSCRIPT-BASED THESIS PRESENTED TO ÉCOLE DE TECHNOLOGIE SUPÉRIEURE IN PARTIAL FULFILLMENT FOR THE DEGREE OF DOCTOR OF PHILOSOPHY
PH.D.

MONTREAL, MAY 12, 2023

ÉCOLE DE TECHNOLOGIE SUPÉRIEURE
UNIVERSITÉ DU QUÉBEC

BOARD OF EXAMINERS

THIS THESIS HAS BEEN EVALUATED

BY THE FOLLOWING BOARD OF EXAMINERS

Mrs. Rola Assi, Thesis Supervisor
Department of Construction Engineering at École de technologie supérieure

Mr. Tan Pham, President of the Board of Examiners
Department of Mechanical Engineering at École de technologie supérieure

Mrs. Marie-José Nollet, Member of the jury
Department of Construction Engineering at École de technologie supérieure

Mr. Pierre Léger, External Evaluator Independent
Department of Civil, Geological and Mining Engineering at École Polytechnique de Montréal

THIS THESIS WAS PRESENTED AND DEFENDED

IN THE PRESENCE OF A BOARD OF EXAMINERS AND PUBLIC

ON MARCH 17, 2023

AT ÉCOLE DE TECHNOLOGIE SUPÉRIEURE

ACKNOWLEDGMENT

I would like to express my deep and sincere gratitude to my research supervisor, Professor Rola Assi, for her continuous help and support, constant encouragement and skillful guidance throughout this research. I am so glad to have had the opportunity to work with her.

I am also grateful for the financial support provided by my supervisor through the NSERC Discovery Grant RGPIN-2016-05009.

Last but certainly not least, my deepest gratitude goes to my beloved family; my spouse, Sima, who has accompanied me on this path with invaluable and irreplaceable love, and my parents, especially my father, for his constant support and for bearing numerous difficulties during these years to enable me to reach this stage. Finally, I dedicate this thesis to the soul of my mother, whom I never met.

Évaluations des accélérations et spectres verticaux au sol et de plancher dans des bâtiments élastiques en béton armé à ossature résistant aux moments situés dans l'est du Canada

Shahabaldin MAZLOOM

RÉSUMÉ

Alors que les dommages structuraux de bâtiments ont généralement été rares à la suite des récents tremblements de terre modérés et sévères, les dommages associés aux composants non structuraux ont été beaucoup plus répandus et peuvent entraîner des pertes économiques supplémentaires. Dans la plupart des codes et normes, seul l'effet de la composante horizontale a été considéré en relation avec la conception et l'analyse sismique de la structure et des composants non structuraux (CNS), et l'effet de la composante verticale a été moins pris en compte ou complètement négligé. D'autre part, l'effet de l'accélération sismique verticale peut être significatif dans certains cas et affecter gravement les performances structurelles d'un bâtiment et, par conséquent, ses composants non structuraux. Le Code national du bâtiment du Canada (CNB, 2015) se limite principalement à un rapport empirique de 2/3 dans la relation entre l'accélération verticale et horizontale. De plus, l'exigence de prendre en compte la composante sismique verticale est limitée uniquement aux structures de longue portée, aux structures précontraintes et aux structures avec des éléments fortement sollicités sous des charges de gravité.

Dans ce projet, les caractéristiques de la composante verticale des mouvements du sol pour le sol très dense avec une catégorie d'emplacement C dans la région sismique de l'Est du Canada a été étudiée, et une relation a été proposée pour établir l'accélération spectrale verticale de conception en utilisant les rapports d'accélération pseudo-spectrale verticale/horizontale. Pour cela, 248 enregistrements sélectionnés de 67 séismes de cette région avec une magnitude M_w 3.0 et une distance épicentrale (Repi) 150 km ont été étudiés. En raison du manque

d'enregistrements pour le sol ferme selon les critères mentionnés dans cette région, les enregistrements d'autres types de sol que le sol très dense ont été convertis en enregistrements correspondants à la catégorie d'emplacement C en utilisant le logiciel DEEPSOIL. Les rapports V/H PSA calculés ont été calibrés avec ceux obtenus à partir des équations de prédiction des mouvements du sol (GMPEs) compatibles. Les rapports V/H PSA moyens calculés ont dépassé la valeur typique de 2/3 recommandée dans le CNB, en particulier pour les courtes périodes allant jusqu'à 1,3 sec. Un profil des spectres de conception de l'accélération verticale (ADS_{ver}) a été proposé pour la catégorie d'emplacement C à Montréal et comparé à ceux obtenus par les dispositions de l'ASCE/SEI 7-16 (2017) et de l'ASCE 41-17 (2017).

En outre, l'effet de la hauteur du bâtiment et de la flexibilité de la dalle sur la réponse verticale du système de plancher, y compris à différents endroits du plancher et le long de la hauteur du bâtiment en termes d'amplification verticale des accélérations maximales du plancher et des accélérations spectrales du plancher, a été évalué à l'aide de simulations numériques en 3D. Par conséquent, quatre bâtiments en béton armé réguliers de 3, 6, 9 et 12 étages à ossature élastique résistant au moment avec une ductilité limitée pour la catégorie d'emplacement C à Montréal et trois portées identiques de 7,0 mètres dans chaque direction, conçus conformément au Code national du bâtiment du Canada (CNB, 2015), ont été sélectionnés pour cette recherche. De plus, 65 ensembles d'enregistrements historiques relatifs à 31 tremblements de terre sévères du monde entier en tant qu'accélérations temporelles ont été utilisés pour analyser le comportement linéaire de ces structures.

L'amplification maximale de l'accélération verticale maximale au plancher (AMP_V) a été observée au centre de la dalle intérieure des bâtiments, avec des valeurs médianes normalisées maximales allant de 4,0 dans le bâtiment de 3 étages à 1,24 dans le bâtiment de 12 étages. De plus, l'amplification constante de l'accélération spectrale verticale de plancher (ASP_V) a été observée le long de la hauteur des bâtiments. L'impact significatif de la composante verticale du tremblement de terre était plus visible à des périodes plus courtes puisque l'accélération verticale maximale résultait à des périodes inférieures à 0,35 s. Enfin, le ASP_V estimé correspondant à l'accélération verticale du sol d'entrée a été proposé pour les bâtiments types.

Par conséquent, cette étude indique que le mouvement sismique vertical ne doit pas être négligé dans le processus d'analyse et de conception, en particulier dans les bâtiments de faible hauteur.

Mots-clés : Composant non structurel (CNS), mouvement vertical du sol, accélération spectrale de conception verticale (ASC_{ver}), accélération maximale du plancher (AMP), accélération spectrale du plancher (ASP), ossature en béton armé résistant au moment

Evaluation of vertical ground and floor accelerations and spectra in elastic RC frame buildings located in Eastern Canada

Shahabaldin MAZLOOM

ABSTRACT

Whilst significant structural damage to buildings has generally been rare as a result of recent moderate and severe earthquakes, destructive non-structural damage has been much more widespread and can lead to additional economic loss. In most codes and standards, only the effect of the horizontal component has been discussed in relation to seismic design and analysis. The effect of the vertical component has been less considered or completely neglected. However, the effect of vertical seismic acceleration can be more impressive in some cases and severely affect a building's structural performance and, consequently, its non-structural components (NSCs). The National Building code of Canada (NBC, 2015) is mainly limited to an empirical ratio of 2/3 in the relationship between vertical and horizontal acceleration. Also, in this code, the requirement to consider the vertical seismic component is limited only to structures with long spans, pre-stressed structures, and structures with highly stressed elements under gravity loads.

In this project, the characteristic of the vertical component of ground motions for Site Class C in the Eastern Canada seismic region was investigated, and a relation was proposed to establish the vertical design spectral acceleration using the vertical-to-horizontal pseudo-spectral acceleration ratios (V/H PSA) obtained from the selected 248 records of 67 earthquakes of this region with a magnitude $M_w \geq 3.0$ and an epicentral distance (R_{epi}) <150 km. Due to the lack of enough records for very dense soil according to the mentioned criteria in this region, records from other soil types than very dense soil and soft rock were converted to the corresponding records on Site Class C using the software DEEPSOIL. The computed V/H PSA ratios were calibrated with those obtained from compatible Ground Motion Prediction Equations (GMPEs). The computed mean V/H PSA ratios exceeded the typical value of 2/3

recommended in NBC 2015, especially for short periods of up to 1.3 sec. A profile of vertical acceleration design spectra (ADS_{ver}) was proposed for Site Class C in Montreal and compared with those obtained by ASCE/SEI 7-16 (2017) and ASCE 41-17 (2017) provisions.

In addition, the effect of building height and the flexibility of the slab on the vertical response of the floor system, including different locations within the floor and along the building height on the amplification of vertical peak floor accelerations and floor spectral accelerations was assessed. To this end, four 3-D elastic regular RC moment-resisting frame buildings with limited ductility for the location on Site Class C of Montreal. Therefore, 3-, 6-, 9- and 12-storey regular RC buildings with moderately ductile moment-resisting frame systems and three spans of 7.0 meters in each direction, designed in accordance with the National Building Code of Canada (NBC 2015), were selected for this research. Moreover, 65 sets of historical records relating to 31 severe earthquakes from across the world as input time history accelerations were used to analyze the linear behavior of these structures.

The maximum amplification of vertical Peak Floor Acceleration (PFA_V) was observed at the center of the buildings' interior slab, with the maximum median normalized values ranging from 4.0 in the 3-storey building, to 1.24 in the 12-storey building. Moreover, the constant amplification of the vertical Floor Spectral Acceleration (FSA_V) was observed along the building height. The significant impact of the vertical component of the earthquake was more visible at shorter periods since the maximum vertical acceleration resulted at periods of less than 0.35 sec. Finally, the estimated FSA_V corresponding to the input vertical ground acceleration was proposed for the typical buildings. Therefore, this study indicates that the vertical earthquake motion should not be overlooked in the analysis and design process, especially in low-rise buildings.

Keywords: Non-Structural Component (NSC), vertical ground motion, vertical design spectral acceleration (DSA_{ver}), Peak Floor Acceleration (PFA), Floor Spectral Acceleration (FSA), reinforced concrete moment resisting frame

TABLE OF CONTENTS

Page

LIST OF TABLES

Page

LIST OF FIGURES

Page

LIST OF ABREVIATIONS

ASCE	American Society of Civil Engineers
ADS_{hor}	Horizontal Acceleration Design Spectra
ADS_{ver}	Vertical Acceleration Design Spectra
CSA	Canadian Standards Association
EC 8	Eurocode 8
FEMA	Federal Emergency Management Agency
FSA_H	Horizontal Floor Spectral Acceleration
FSA_V	Vertical Floor Spectral Acceleration
GMPE	Ground Motion Prediction Equation
MCE_R	Risk-Targeted Maximum Considered Earthquake
MD	Moderately Ductile
MRF	Moment-Resisting Frame
NBC	National Building code of Canada
NSC	Non-structural Component
OFC	Operational and functional component
PFA_H	Horizontal Peak Floor Acceleration
PFA_V	Vertical Peak Floor Acceleration
PGA_H	Horizontal Peak Ground Acceleration
PGA_V	Vertical Peak Ground Acceleration

PSA_H	Horizontal Pseudo-Spectral Acceleration
PSA_V	Vertical Pseudo-Spectral Acceleration
RC	Reinforced Concrete
UHS	Uniform Hazard Spectra

LIST OF SYMBOLS

a_p	The dynamic amplification factor as per ASCE/SEI 7-16
A_r	The dynamic amplification factor as per NBC 2015
a_{vg}	Design ground acceleration in the vertical direction as per Eurocode 8-1
A_x	Height factor in NBC
C_p	Seismic coefficient for mechanical and electrical equipment
E_C	Young modulus of concrete
E_S	Young modulus of steel
F_a	Acceleration-based site coefficient
f_{cm}	Mean compressive strength of concrete
$F_{p,\ hor}$	Component seismic design force applied horizontally at the center of gravity of the component as per Eurocode 8-1
$F_{p,\ ver}$	Component seismic design force applied horizontally at the center of gravity of the component as per Eurocode 8-1
f_u	Ultimate strength of steel
f_y	Yield strength of steel
h	Average roof height of structure with respect to the base
h_i	Height above the base to level i
h_x	Height above the base to level x
I_E	Importance factor of the building as per NBC 2015
I_p	Component importance factor

M_w	Moment magnitude of an earthquake event
q_a	Behaviour factor of a non-structural element
R_d	Ductility-related force modification factor
R_o	Overstrength-related force modification factor
R_p	Component response modification factor
R_{rup}	Distance from the fault
$S(T)$	Spectral response acceleration value for a period T
$S_a(0.2)$	Spectral response acceleration value at the period of 0.2 sec
S_{aM}	Site-specific MCE_R spectral response acceleration parameter at any period corresponding to the mapped maximum considered earthquake
S_{DS}	Design, earthquake spectral response acceleration parameter at short periods as per ASCE/SEI 7-16
S_{M1}	Spectral acceleration parameter at a period of 1.0 sec corresponding to the mapped maximum considered earthquake adjusted for site class effects
S_{MS}	Spectral response acceleration parameter at short periods adjusted for site class effects
S_p	Horizontal force factor for part or portion of a building and its anchorage
S_S	Spectral acceleration parameter at short periods corresponding to the mapped maximum considered earthquake
$S_{ve}(T)$	Elastic vertical ground acceleration response spectrum
T_a	Fundamental building period defined by NBC 2015
T_L	Long-period transition period as per ASCE/SEI 7-16
T_p	Period of a non-structural component
$V_{p,hor}$	Lateral seismic design force on a part of the structure as per NBC 2015

$V_{p,ver}$	Vertical seismic design force on a part of the structure as per NBC 2015
V_{s30}	Average shear wave velocity in the top 30 m of soil or rock
W_c	Weight per unit volume of concrete
$W_{Ext\ walls}$	Uniform load of exterior walls
$W_{Floors,Finishing}$	Weight of floor finishing
$W_{L,\ Floor}$	Live load of the floor
$W_{L,\ Roof}$	Live load of the roof
$W_{mechanical}$	Mechanical utility floor load
W_p	Weight of non-structural component
$W_{Partitions}$	Weight of partitions
$W_{Roof,\ Finishing}$	Weight of roof finishing
W_{seis}	Seismic weight of building
W_{Snow}	Snow load
z	Height in structure at the point of attachment of component with respect to the base
δ	Measure of dispersion
ε_c	Crushing strain of concrete
ε_{su}	Ultimate strain of steel
γ_a	Importance factor of a non-structural component as per Eurocode 8-1
η	Damping correction factor
ξ	Viscous damping ratio (in percent)

INTRODUCTION

0.1 Context and problem statement

In the past decades, significant progress was made in modelling and predicting the horizontal performance or response of the structural and non-structural components (NSCs) during earthquakes. However, too much damage has been reported as a result of the vertical vibration of the floors or vertical seismic excitations. In most seismic design codes, the effects of the vertical ground acceleration for typical structures are assumed small when compared with the impact of the horizontal one. Recently, many researchers have emphasized the importance of the significant role of a vertical component of ground motion, especially for near-fault areas where buildings may experience a considerable vertical force (Papadopoulou, 1989; Bozorgnia et al., 1995; Papazoglou & Elnashai, 1996; Elgamal & He, 2004). Reports of the 1994 Northridge earthquake indicate damage to structural elements and floor systems, as well as damage to NSCs caused by the vertical component of ground motion, which in some cases was even more than the damage caused by the horizontal component of the earthquake (Papazoglou & Elnashai, 1996). The 1988 Saguenay earthquake is another example in Eastern Canada that caused significant damage to NSCs (Foo & Lau, 2004).

The vertical component of ground motion is characterized by the short period and significant acceleration-to-velocity ratio (a/v), which is mainly related to near-fault earthquake records. In events with dominant P-waves, the peak vertical acceleration varies depending on the earthquake magnitude, soil conditions, and distance from the fault (Bozorgnia et al., 2000). In the near-field region, because the amount of peak vertical acceleration might be higher than the horizontal one, or even the simultaneous occurrence of both components, it is necessary to investigate the vertical component of ground motions in near-field records (Christopoulos et al., 2000; Shrestha, 2009). The vertical component of the earthquake motion is not significantly attenuated in the near-fault region, thus yielding a vertical Peak Ground Acceleration (PGA_V) value closer to the horizontal PGA. The increased distances from the fault causes P-waves to

attenuate and thus reduce the vertical PGA when compared with the horizontal PGA (Christopoulos et al., 2000).

Canada has various active seismic zones, especially in the western and eastern regions. Due to the high frequency of earthquakes in Eastern Canada, the acceleration-to-velocity ratio (a/v) is usually high; therefore, the earthquakes in this region have a high-frequency content in the short period range and can be assimilated to near fault zones. For instance, the Saguenay earthquake in Eastern Canada in 1988 was confirmed with high a/v values for Eastern North America (ENA) records. Therefore, an investigation of vertical acceleration could be necessary and more challenging for this area. On the other hand, in Western Canada, this ratio is usually small or close to unity, indicating low-frequency earthquakes (Christopoulos et al., 2000; Atkinson & Boore, 2006).

In most building codes, the vertical component of the earthquake is introduced as a constant ratio equal to two-thirds of the horizontal acceleration. Yet, the V/H relation is a function of the site class condition, distances to the fault, and earthquake magnitude (Bozorgnia & Campbell, 2004). For instance, for a rock site far from the fault, the V/H ratio is low, but this ratio will be high on a firm soil site. These parameters indicate that in earthquakes with high-frequency contents, the vertical ground motion could be stronger than the horizontal one (Bozorgnia et al., 1996). Therefore, the V/H ratio of 2/3 is overestimated for higher periods and underestimated for short periods, especially in the near-fault region (Bozorgnia et al., 2000; Elgamal & He, 2004). However, to estimate the approximate vertical response spectrum, the horizontal response spectrum at each period range could be calibrated and shifted with more accurate ratios related to the characteristics of the seismic regions. Therefore, this could be an effective method for calibrating the spectra of a large number of selected earthquake records (Bozorgnia et al., 1996; Bozorgnia et al., 2000).

On the other hand, few studies have been conducted regarding the effect of vertical ground acceleration and its corresponding floor acceleration on NSCs. The floor response spectrum or Peak Floor Acceleration (PFA) is generally considered for the seismic analysis and evaluation

of NSCs and their response at different frequencies. The discussed PFA applies to NSCs that are rigid ($T \leq 0.06$ sec) in the direction of investigation. Also, flexible components ($T > 0.06$sec), such as ceiling tiles and panels, mechanical and electrical piping, horizontal HVAC risers, and other similar cases, are more susceptible to experiencing the vibration of floor systems. In the case of vertical components of ground motion, the flexibility of the slabs and beams will amplify the vertical floor acceleration that is transferred to the NSCs.

The amplification of the acceleration through the height of the building was primarily evaluated for the horizontal components of ground motion, whilst the flexibility of the floors was ignored for the vertical floor acceleration assessment. For instance, acceleration-sensitive NSCs, such as ceiling panels, are susceptible to floor vibrations. Therefore, design requirements for such components, which are subjected to strong vertical acceleration, should be provided.

Moreover, there is no explicit method in NBC 2015 to estimate the vertical design spectra; thus, the accuracy of the recommended ratio of 2/3 for the V/H spectra in the NBC should be assessed. Estimating the suitable vertical Uniform Hazard Spectra (UHS) could be an essential step in computing the vertical floor response spectra and improving the seismic design of the NSCs.

0.2 General and specific objectives

The main objective of this research is to improve the seismic design requirements of NSCs attached to reinforced concrete moment-resisting frame buildings subjected to near-field strong vertical ground motion in Eastern Canada. This purpose is detailed into the following specific objectives of the present manuscript-based thesis:

i. Developing an approximate vertical design spectral acceleration for the Site Class C in the Eastern Canada seismic region using the V/H spectral acceleration ratios

of the moderate to severe earthquakes, recorded in very dense soil and soft rock types according to the classification NBC 2015 (Table-A VI-1).

ii. Identification and assessment of building parameters affecting the vertical peak floor acceleration (PFA_V) in the regular, moderately ductile and elastic RC moment-resisting frame buildings and proposing an approximate normalized PFA_V through the building height.

iii. Assessment of the vertical floor response spectra applying the input near-field strong vertical time history acceleration in the moderately ductile low and mid-rise elastic RC moment-resisting frame buildings and proposing the vertical floor spectral acceleration (FSA_V) profiles through the building height.

0.3 Methodology of the research

In the first mentioned research objective, a series of 248 sets of records from 67 historical earthquakes in the Eastern Canada region with a magnitude $M_w \geq 3.0$ and an epicentral distance (R_{epi}) <150 km, were collected to provide an estimate of V/H PSA ratio in the Eastern Canada seismic region for the very dense soils ($360 < V_{s30} < 760$ m/s) known as Site Class C in NBC 15. Then, a profile of vertical acceleration design spectra (ADS_{ver}) corresponding to a 2475-year return period (at 2% per 50 years probability) for Site Class C in Montreal was proposed. The mentioned return period is applied in this objective since it is similar to the one used for standard structures in the current NBC 2015 edition.

Since there are no sufficient records on Site Class C in this region, the selected acceleration time history records from other site classes were converted to the considered Site Class C in NBC 2015 using DEEPSOIL software (Hashash et al., 2019). In this process, the equivalent linear method, using the Pressure-Dependent Modified Kondner Zelasko (MKZ) model of analysis in the frequency domain, was applied in this software. The process of using this

software was explained in detail in ANNEX II. Eventually, the corresponding PSA of the available and converted records, considering a damping ratio equal to 5%, were computed using the PRISM software (Jeong et al., 2011) and then validated by SeismoSignal software (SeismoSoft, 2018). First, the V/H ratios of PGA and PSA and then their mean values were computed. Finally, these ratios were calibrated with those obtained from compatible GMPEs proposed in previous studies by Bozorgnia and Campbell (2004) and Gülerce and Abrahamson (2011), and their proposed equations along with other information, were more comprehensively presented in ANNEX III.

Also, a reliable vertical Acceleration Design Spectra (ADS_{ver}) was derived for Site Class C in Montreal, and the proposed spectra were compared with those derived according to the procedures proposed in the standards ASCE/SEI 7-16 (2017), ASCE 41-17 (2017) and the 2/3 V/H empirical ratio prescribed in NBC 2015.

In the second and third objectives, the effects of building height, the location of the mounted NSCs in the floor plan and along the height of the building on the amplification of vertical acceleration of the earthquakes were assessed. For this purpose, the vertical seismic accelerations in four regular elastic RC moment-resisting frame buildings with limited ductility were evaluated. Therefore, 3, 6, 9, and 12-storey RC office buildings with an overstrength force modification factor, R_o, equal to 1.4 and a ductility-related force modification factor, R_d, equal to 2.5 were designed according to the current provision of the NBC (NBC, 2015a) and the standard CSA-A23.3-14 (CSA-A23.3, 2014) using the ETABS software. It should be mentioned that a regular symmetrical plan with three-by-three 7.0 m spans in each direction, a finished typical floor height of 3.0 m, and a 140 mm RC slab floor system were considered for all the buildings. The selected buildings were supposed to be located on Site Class C in Montreal. Therefore, the Montreal uniform hazard spectrum corresponding to this soil type, with a 2475 return period at a 5% damping ratio, was used to design the buildings.

The buildings were subjected to 65 sets of time history accelerations recorded on Site Class C from 31 strong near-field (R_{rup} < 25 km) earthquakes around the world with the earthquake magnitude, M_W, greater than 5.5, and PGA_{ver} greater than 0.25 g. It is noteworthy that, Strike-Slip (SS), Reverse (RV), Reverse Oblique (RVO), Normal (N), and Normal Oblique (NO) are the types of the selected earthquakes' fault mechanisms. The considered sets of records were used as the input acceleration time history using ETABS software for analysis.

The quantification of the PFA_H and PFA_V through the heights of the mentioned buildings and at the critical nodes at the center of the slabs, at the middle and quarter point of the beam spans, were assessed in the second objective, and the corresponding profile of PFA normalized to the PGA for both horizontal and vertical components were proposed. Moreover, the obtained results of the PFA_h were compared to recommendations provided in NBC 2015, ASCE/SEI 7-16 (2017) and ATC 2018.

In the third objective, the amplification of the vertical floor spectra through the height of the buildings, as well as the fluctuations of the FSA_V at the critical nodes of a floor, were assessed in order to accurately demonstrate the effect of out-of-plane flexibility level of the RC floor systems on FSA_V. Finally, an estimation of the FSA_V corresponding to the input vertical spectral acceleration of ground motion was proposed. The proposed profile curve of FSA_V was compared with those obtained through the AC 156 (2010) equations used to derive vertical floor spectral accelerations.

0.4 Original contributions of the thesis

According to the author's knowledge, the original contributions of this thesis include as follow:

- V/H Pseudo Spectral Acceleration (PSA) ratios were computed for the Eastern Canada seismic region using historical records and applicable GMPMs.

- It was demonstrated that the empirical V/H PSA ratio of 2/3 suggested in most codes is only adequate for periods greater than 1.0 s for eastern Canada site Class C.
- A reliable vertical Acceleration Design Spectra (ADS_{ver}) was derived for Site Class C in Montreal.
- The amplification of the PFA_V and FSA_V along the height and at different locations on a floor of typical RC moment-resisting frame buildings was quantified.
- It was demonstrated that the PFA_V/PFA_H at the rooftop exceeds the empirical ratio of 2/3 and decreases as the building height increases.
- Conclusions and insights into the effect of the out-of-plane flexibility of slabs on PFA_V and FSA_V were highlighted.
- Equations were proposed to derive PFA_V and FSA_V corresponding to the input vertical ground spectral acceleration (GSA_V).
- The approach proposed by AC 156 provisions to derive FSA_V could be generally applied at the rigid nodes of the supporting floor in RC moment-resisting frame buildings.

0.5 Structure of the thesis

This manuscript is presented in four chapters in addition to the introduction and conclusions:

- Chapter 1 covers a literature review of design methods and research carried out to date, on NSCs and the effect of vertical acceleration of earthquakes.

- Chapter 2 presents the importance of the vertical acceleration of moderate to strong earthquakes in the Eastern Canada seismic region. According to the V/H ratios obtained from the spectral acceleration values resulting from the selected earthquakes, a relationship proportional to the horizontal one given in the NBC 2015 was proposed in order to obtain

the vertical design spectrum for this seismic region. The derived paper from this study was published in the Soil Dynamics and Earthquake Engineering journal.

- Chapter 3 focuses on the effect of vertical acceleration on reinforced concrete (RC) moment-resisting frame buildings, analyzed and designed according to the NBC (2015) and CSA-A23.3 (2014). Thus, the amplification of PFA_H and PFA_V in typical buildings was investigated. The corresponding article of this study was published in the Journal of Earthquake Engineering.

- In Chapter 4, the vertical spectral acceleration of the buildings' floors was computed using the earthquakes and buildings archetype of Chapter 3. Subsequently, the vertical Floor Spectral Acceleration (FSA_V), corresponding to the input vertical ground acceleration, was proposed for this building type. Finally, the paper related to the studies of this section was accepted for publishing in the journal of Engineering Structures.

Figure 0.1 illustrates the links between each specific objective, dealt with in the three scientific articles, and the resulting contributions.

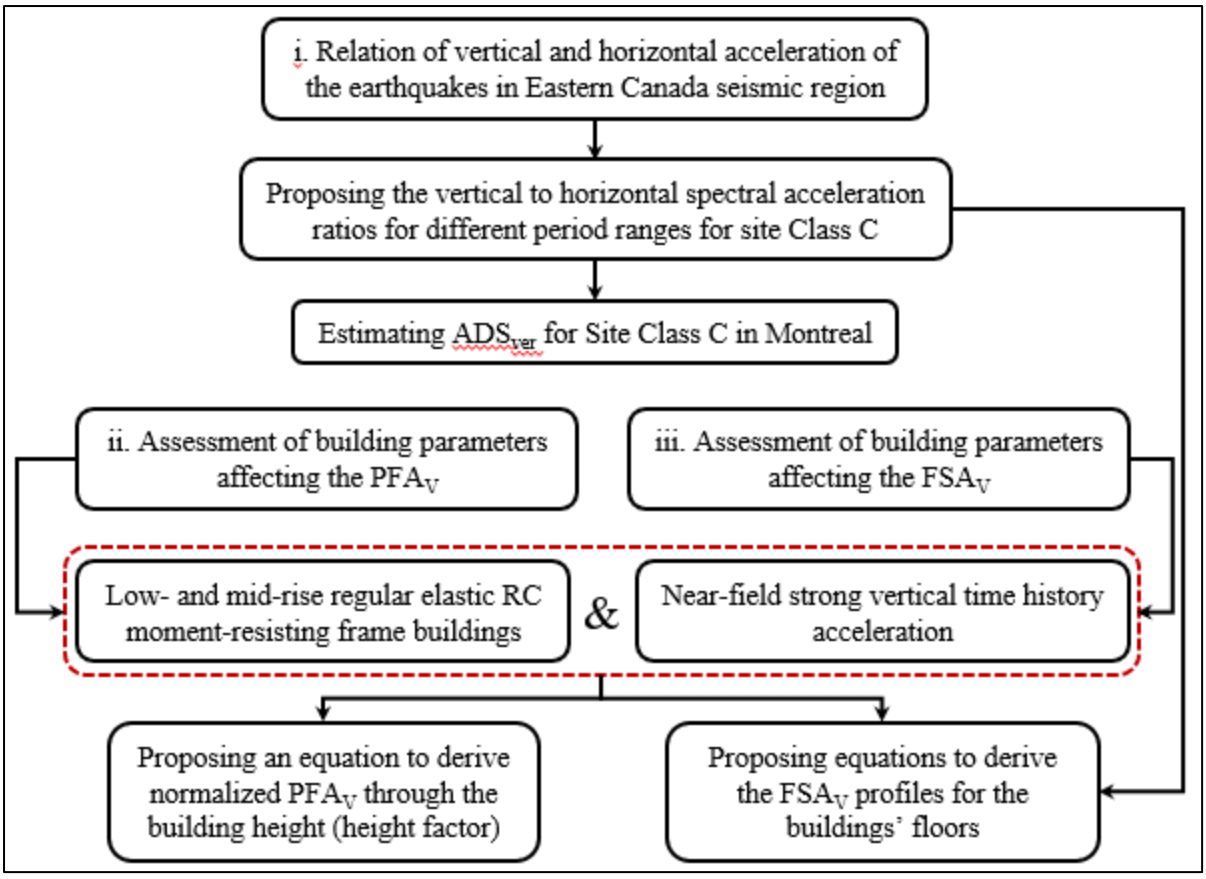

Figure 0.1 Summary of the specific objectives and the links between the contributions within the framework of this thesis

CHAPITRE 1

LITERATURE REVIEW

This Chapter represents a brief description of the seismic importance of NSCs and characteristics of the vertical ground motion and its impact on the seismic response of the structural and NSCs. In addition, the proposed approach of different codes in generating the ground vertical design spectra was presented. Therefore, the suggested equations for vertical design spectra by the codes, including NBC 2015, ASCE7-16 (2017) and Eurocode 8-1 (2004), were given and discussed here. Also, different code recommendations, involved in estimating the horizontal and vertical seismic design force of acceleration-sensitive NSCs, were introduced. Moreover, an overview of the studies conducted on the effect of vertical acceleration on the seismic response of structural elements and NSCs were made.

1.1 Introduction

Very few studies have been dedicated to the vertical seismic response of structures and their NSCs, compared to the horizontal response. Generally, the conducted studies in this field can be divided into two categories. One group investigated the seismic characteristics of the vertical component of the earthquakes either alone or in comparison with the horizontal components; and another assessed the structural behavior of the buildings or at least the NSCs against the vertical components of earthquakes. In each case, the obtained results had a significant effect on the advancement of seismic design relations in most codes and standards, including Eurocode 8-1 (2004), American standards, such as ASCE/SEI 7-16 (2017) and FEMA P-1050-1 (2015), which is a turning point in structural seismic design. In order to better understand what was undertaken in the leading studies, the analysis and results of previous research have been divided according to two categories here.

In the first category, factors that are considered in most studies, related to the characteristics of the vertical component of the earthquakes, with comparison to the horizontal component, the effect of magnitude, the distance from the fault, and the type of soil are considered. The second part, highlights the considerations of past research on the structure's performance against the vertical component of the earthquake, the importance of the building height and the location of the installed NSC in the floor plan. Therefore, greater attention was paid to these cases in this present study. However, the PFA_V and the vertical floor response spectra are the items that have rarely been seen in them. It can even be said that research on the vertical response of the floors has been neglected. Reference to some of the previous studies on this topic are given in the following sections.

1.2 Classification of Non-Structural Components (NSCs)

The elements of a building that are not part of the lateral resisting systems or load-bearing elements, such as piping, partition walls, electrical systems, and equipment, are known as Non-structural Components and Systems (NSCs). These systems have been defined as the Occupational Functional Components (OFCs) in the CSA S832 (CSA-S832, 2014) and Secondary Structures (Gupta, 1984; Chen & Wu, 1999; Taghavi & Miranda, 2008). NSCs provide a necessary operational and functional capability in buildings, which makes them crucial to the seismic performance objectives of the facility (CSA-S832, 2014; NIST GCR 17-917-44 (ATC), 2017).

According to CSA S832 (2014), NSCs are classified into architectural components (external and internal), building services and utilities such as mechanical and electrical facilities and building contents, including standard and specialized components such as elevator systems. A typical building, as illustrated in Figure 1.1, shows different types of NSCs, such as plumbing, electrical equipment, air condition systems, and ceiling panels (Wang, 2008).

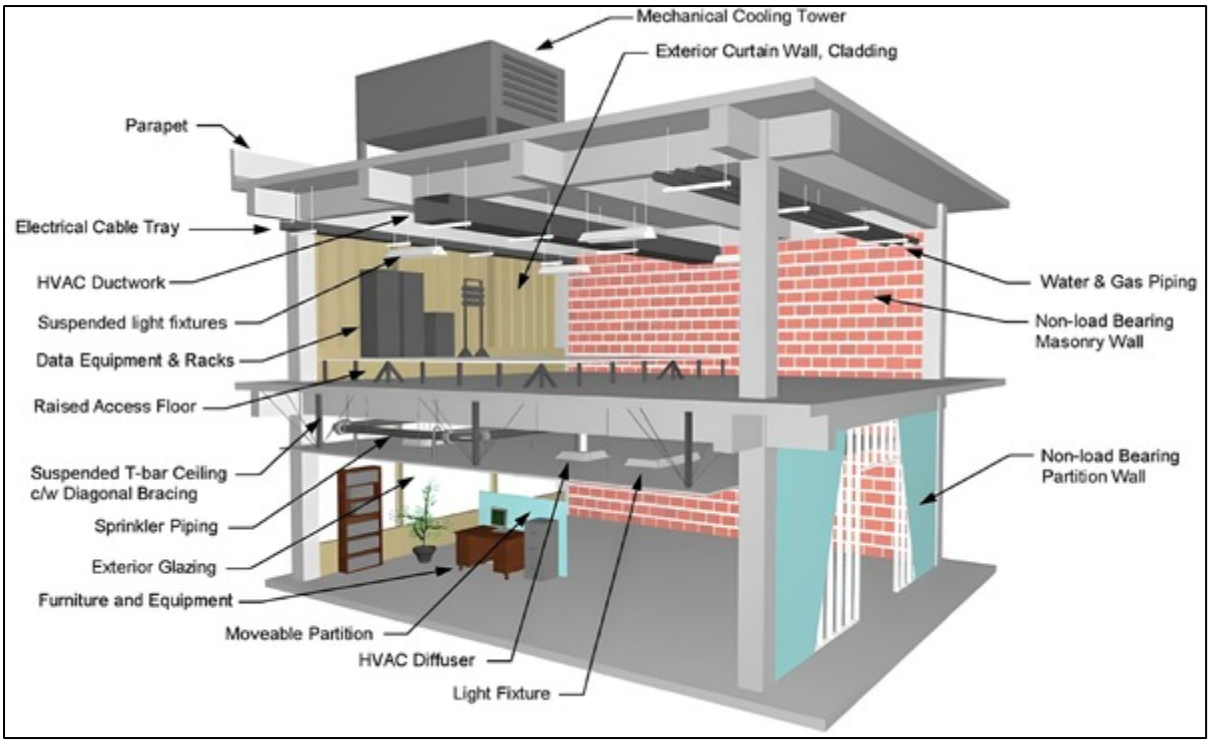

Figure 1.1 Non-structural components of a typical building
Taken from Wang (2008)

In strategic buildings such as fire stations, hospitals and emergency centers, failure of essential services has become an important research topic among engineering communities, after extensive damage to NSCs was observed and reported following recent earthquakes. Examples include the damage of NSCs as a result of the Northridge earthquake in 1994 (Broderick et al., 1994; Bozorgnia et al., 1995; Pekcan et al., 2003) and the Chile earthquake in 2010, resulting in many buildings, including hospitals, fire stations and service centers, being entirely or partially destroyed due to the damage of NSCs (Filiatrault & Sullivan, 2014). Therefore, special attention should be devoted to the seismic design of NSCs in buildings. In general, the experiences obtained from the consequences of recent earthquakes in the world indicate the importance of the seismic design of NSCs, especially in relation to the following areas:

a) Life safety: The failure of NSCs, especially the falling of heavy cladding panels, can cause serious injuries and death. For instance, the failure of cladding panels caused many fatalities in the 2012 earthquake in northern Italy. (Magliulo et al., 2014).

b) Economic loss: NCSs represent the most considerable portion of a building cost, especially in high-importance buildings such as hospitals and museums. Therefore, the failure of NSCs can lead to substantial financial losses. Figure 1.2 shows the economic contribution of structural and non-structural components specified in three different building types (Taghavi & Miranda, 2003).

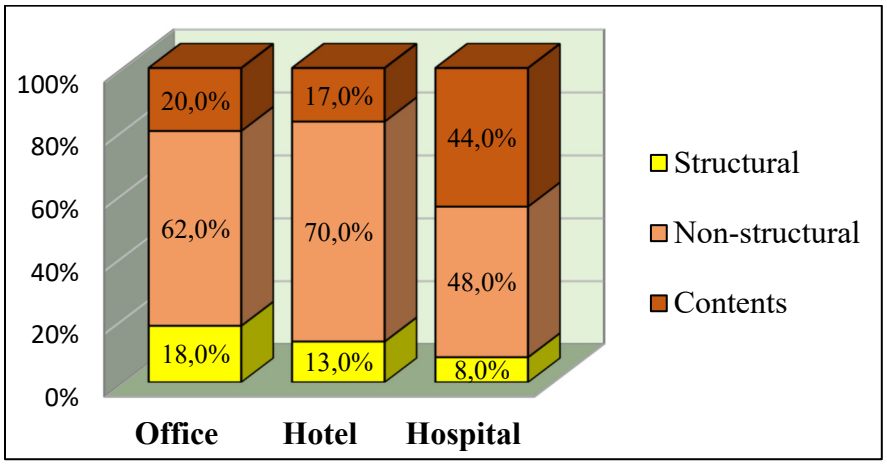

Figure 1.2 Relative value of components for different building types
Taken from Taghavi and Miranda (2003)

During the last decades, many studies have been conducted to investigate the seismic behaviour of structural components and the NSCs attached to them. These studies mainly focused on the horizontal components of ground motion. There is no extensive research related to the vertical component of ground motion since it is generally assumed that buildings are flexible laterally and rigid in the vertical direction (Newmark et al., 1973; Bozorgnia et al., 1996; Christopoulos, 1999; N. N. Ambraseys & J. Douglas, 2003). For NSCs that are attached to rigid vertical elements, such as reinforced concrete columns and shear walls which are axially rigid, the amplification of the vertical acceleration of ground motion could be

negligible. Still, the vertical acceleration amplification cannot be ignored for the NSCs that are attached to the flexible structural elements, such as slabs and beams (Pekcan et al., 2003). It was noticed that the amplification of vertical ground acceleration along the building height varies, based on the location of the investigation; this is related to the out-of-plane flexibilities of the beam and the slab, as well as the frequency contents of the ground motion, which may cause resonance (Wieser et al., 2012).

From a structural viewpoint, NSCs are classified based on engineering demand parameters affecting their response to seismic excitation (FEMA E-74, 2012):

a) Acceleration-sensitive components: The building's seismic inertial forces are the main reason for seismic damage in this case. The suspended ceiling could be a prominent example in this category.
b) Displacement-sensitive components: In this case, the building displacement or inter-storey drift is the main reason for the damage. The cabins of elevators and windows could be an example in this category.
c) Both acceleration and displacement-sensitive elements: A combination of the building's seismic inertial force and displacement causes damage in this category. Heavy walls and sprinklers are examples in this category.

NSCs are also divided into two categories based on their fundamental period. The NSCs with a fundamental period of less than and equal to 0.06 sec are classified as rigid; otherwise, they are classified as flexible (NIST GCR 17-917-44 (ATC), 2017). Furthermore, a NSC is considered light when its mass doesn’t exceed 20% of the floor's total weight or 10% of the total mass of the supporting structure (CSA-S832, 2014).

NSCs are exposed to the acceleration response of the floor or structural elements and are not directly subjected to the acceleration of ground motion. Hence, depending on the location of the NSC within the floor or different levels of the structure, the seismic response can be different (Kumar, 2014).

1.3 Characteristics of the vertical component of ground motion

Some parameters of an earthquake, such as the PGA, the duration, the frequency content, and the energy content are considered, when comparing the characteristics of its horizontal and vertical components. Therefore, P-waves are dominant in earthquakes with a high a/v ratio, mostly in sites close to the fault. That means that the vertical component of the earthquake motion is not attenuated quickly in the near-fault region. As the distance from the fault increases, the P-waves are weakened and thus cause a decrease in the vertical acceleration in comparison with the horizontal acceleration (Christopoulos et al., 2000). Normally, the predominant period range that defines the highest amplitude of vertical acceleration depends on the earthquake's magnitude, the distance from the epicenter, and the soil type conditions. In this regard, the shape of the vertical response spectrum is more different than the horizontal response spectrum (Bozorgnia & Campbell, 2004). Therefore, the main parameters of the earthquake, such as PGA, time duration, energy content and frequency content, should be considered to compare the horizontal and vertical components of an earthquake (Bozorgnia et al., 1996).

It was previously considered that floor systems were completely rigid in all directions, and that vertical acceleration was not affected by changes in the building height or type of floor system. However, floor flexibility can lead to resonance and significant acceleration amplification of the NSCs, especially when the fundamental vertical frequencies of structures are in the range of vertical pulses of ground motions (Lee et al., 2013). Therefore, the studies conducted to investigate the effect of the vertical component of the earthquake on the floor system, including slabs and beams, showed a behavior of the floor systems different from previously assumed rigid one. In addition, in strong earthquakes, it was proved that the vertical displacement of girders increases in the upper levels, which shows that the rigid diaphragm assumption is not accurate in the presence of the vertical component of the ground motion due to the out-of-plane deformations of the floor systems (Bas et al., 2016).

1.4 Relationship of vertical and horizontal components of earthquakes

Most earthquake records consist of two orthogonal horizontal components and one vertical component. The effect of intensity correlations between the three orthogonal components recorded at a specific site on the vertical seismic hazard assessment has not received much research attention (Boore et al., 2006; Campbell & Bozorgnia, 2007). However, since there are common inherent features, such as the magnitude, soil conditions, and distance from the fault, for horizontal and vertical components of an earthquake, then consideration of the dependent and close relationships of the components is inevitable (Campbell & Bozorgnia, 2003; Shirai et al., 2004).

This correlation was introduced much earlier in some studies by Newmark et al. (1973), Campbell (1997), Collier and Elnashai (2001), and Kalkan and Gülkan (2004) through the acceleration ratios of vertical and horizontal components. The vertical-to-horizontal (V/H) ratio estimates the relative vertical component compared to the horizontal one (Gülerce & Abrahamson, 2011). The maximum V/H acceleration ratio of some earthquakes was reported to exceed unity in the near-fault zone (Bozorgnia and Niazi, 1993, Silva 1997, Bozorgnia et al., 1999). For instance, the maximum recorded V/H ratio was equal to 1.79 in the 1994 Northridge earthquake for a site close to the fault. It has been noted that the maximum vertical acceleration depends on the soil conditions, epicentral distance to the site, and earthquake magnitude (Gülerce & Abrahamson, 2011). Investigations into several earthquakes have shown that the V/H ratio for moderate and severe earthquakes with a magnitude between 6.5 and 7.0 is more significant than that of weaker earthquakes with a magnitude between 4.5 and 6.0 (Li et al., 2007).

On the other hand, the time history records show that the maximum horizontal and vertical accelerations do not necessarily occur at the same time. Therefore, the V/H ratio estimates the potential damage and failure to a structure by the combined effect of an earthquake's horizontal

and vertical components, since the modes that are influenced by the vertical motion are at a higher frequency than those affected by the horizontal component (Christopoulos et al., 2000).

1.5 Approaches in codes and standards for seismic design of NSCs subjected to horizontal and vertical excitation

In general, most building codes have similarities in the definition of the lateral design force equation of NSCs. For example, the equation of static horizontal force for acceleration-sensitive NSCs is computed based on the following parameters (CSA-S832, 2014):

- Design PGA;
- Amplification of PFA over the building height relative to the PGA (PFA/PGA) known as the height factor (A_x);
- Amplification of the acceleration at the center of mass of the NSC relative to the PFA known as the A_r factor;
- Ductility of the NSC;

Table 1.1 summarizes the different code equations for the seismic design force of the NSCs subjected to horizontal and vertical excitation in Eurocode 8-1 (2004), NBC 2015) and ASCE/SEI 7-16 (2017). The height factor parameter is based on the linearly increasing acceleration over the building height (ASCE/SEI 41-17, 2017). Moreover, these criteria could apply to the PFAv and its amplification to calculate the vertical seismic design force of the NSCs.

Table 1.1 Seismic design force of NSCs subjected to horizontal and vertical excitation in the codes

Code	Seismic horizontal force	Seismic vertical force
NBC 2015 (2015)	$V_{p,hor} = 0.3F_aS_a(0.2)I_ES_pW_p$	$V_{p,ver} = 2/3V_{p,hor}$

ASCE/SEI 7-16 (2017)	$F_{p,hor} = \frac{0.4 a_p S_{DS} I_p W_p}{R_p}(1 + 2\frac{z}{h})$	$F_{p,ver} = 0.2 S_{DS} W_p$
Eurocode8-1 (2004)	$F_{p,hor} = \frac{S_{a,hor} \cdot \gamma_a}{q_a} . W_p$	$F_{p,ver} = \frac{S_{a,ver} \cdot \gamma_a}{q_a} . W_p$

No specific equation is provided for vertical seismic design forces in Canadian provisions, and it is only limited to the empirical 2/3 of the horizontal one. In Canada, the design provisions of NSCs were first published in 1953 in the NBC edition and have been gradually updated so that with each edition, the design requirements for the horizontal seismic design force of the NSCs are improved (Assi & McClure, 2015; Asgarian, 2017).

In the equations presented by NBC 2015, F_a is the acceleration-based site class coefficient which is a function of the site class condition, and $S_a(0.2)$ is the response acceleration spectrum at the period of 0.2 sec (based on a 2% probability of exceedance in 50 years). I_E is the importance factor of the building (1.0, 1.3 or 1.5); S_p is computed from Equation 1.1.

$$S_p = C_p A_r A_x / R_p \tag{1.1}$$

The maximum and minimum values of S_p could be 4.0 and 0.7, respectively. C_p is the component factor and represents the risk to the life safety associated with the failure of the component and varies from 0.7 to 1.5 for the low risk to high risk, respectively. A_r is the component force amplification factor which is a function of the NSC and structure's natural frequencies; A_x is the height factor which is a linear amplification of acceleration through the height of the building computed from the following equation:

$$a_p = A_x = 1 + 2\, h_x / h_n \tag{1.2}$$

The component response modification factor, R_p, represents the component's energy-absorption capacity, which varies from 1.25 to 5.0. The vertical seismic force of the NSCs in

NBC 2015 is based on the codified V/H acceleration ratio, which can lead to an unrealistic response in the case of near-fault site conditions (Asgarian, 2017; Assi et al., 2017).

On the other hand, an almost similar formulation for the horizontal seismic design force of NSC was suggested in ASCE/SEI 7-16 (2017). A height factor similar to that given in the NBC 2015 can be seen in this equation, in which z or h_x is the location of the attached component in the height of the structure with respect to the base, and h or h_n is the height of the structure. In the presented equation, S_{DS} is the spectral acceleration at the short period, which is computed as $F_a S_a(0.2)$. However, the vertical seismic design force of NSCs is just a function of S_{DS} and the component weight.

The method described in Eurocode 8-1 (2004) deals separately with horizontal and vertical seismic action. Therefore, in the equations presented in the Table 1.1, the components are qualified with similar importance and behavior factor in horizontal and vertical directions and are generated based on the design accelerations, S_a, defined in equation 1.3 (Eurocode 8-1, 2004).

$$S_{av} = \frac{a_{vg}}{g} \times C_{av} \tag{1.3}$$

Where C_{av} is the coefficient amplification of the floor spectrum, in particular depending on the damping of the sub-system composed by the NSCs and its fixations, and a_{vg} is the vertical acceleration (Ministère du Logement & Ministère de l'Écologie, 2014).

The coefficient $C_{av}=2.0$ represents the maximum value of the amplification due to the floor response spectra when the ratio between the natural period of the NSC and that of its supporting structure is less than 0.5. The suspended ceilings on the underside of floors exemplify this case (Eurocode 8-1, 2004).

1.6 Codes approaches on deriving vertical design spectra

Suggested methods to derive vertical design response spectra are provided in the following codes:

1.6.1 NBC 2015

There is no specified method to derive the vertical design spectra. The relationships between the vertical and horizontal response spectra acceleration are indicated to obtain the vertical design spectra, which should be more based on the site and soil conditions. Also, using the empirical factor of 2/3 is designated for the V/H ratio and applied to the horizontal target spectra to generate the vertical one was recommended in this code.

1.6.2 Eurocode 8-1

Due to the vertical component of ground motion, the elastic vertical response spectrum $S_{ve}(T)$, is represented by equations 1.4 to 1.7 in Eurocode 8-1 (2004).

$$0 \le T \le T_B \qquad S_{ve}(T) = a_{vg}\left[1 + \frac{T}{T_B}(3.0\eta - 1)\right] \qquad (1.4)$$

$$T_B \le T \le T_C \qquad S_{ve}(T) = a_{vg} \times 3.0\eta \qquad (1.5)$$

$$T_C \le T \le T_D \qquad S_{ve}(T) = a_{vg} \times 3.0\eta\left[\frac{T_C}{T}\right] \qquad (1.6)$$

$$T_D \le T \le 4.0\ sec \qquad S_{ve}(T) = a_{vg} \times 3.0\eta\left[\frac{T_C.T_D}{T^2}\right] \qquad (1.7)$$

Where a_{vg} is designed ground acceleration in the vertical direction on the ground type A in the determined category in Eurocode 8-1 (2004), in cases where the value of a_{vg} is greater than

0.25g (2.5 m/s²), consideration of the vertical component of the seismic ground motion will be essential. η is the damping correction factor with a reference value of $\eta=1$ for the 5% damping ratio, ξ, of the structure that can be determined from equation 1.8:

$$\eta = \sqrt{10/(5+\xi)} \tag{1.8}$$

T_B and T_C are the lower and upper limits of the period of the constant spectral acceleration branch, respectively, and T_D is the value defining the beginning of the constant displacement response range of the spectra. The National Annex gives the values of T_B, T_C, T_D, and a_{vg} for each type of vertical spectrum to be used in each region. The use of two types of vertical response spectra is recommended for five ground types A, B, C, D and E, as shown in Table 1.2, to account for the influence of local ground conditions on seismic action. It should be noted that the site classification provided in the Eurocode 8-1 (2004) is presented in Table-A VI-3.

Table 1.2 Recommended values of parameters describing the vertical elastic response spectra

Taken from Eurocode 8-1 (2004)

Spectrum	**a_{vg}/a_g**	**T_B**	**T_C**	**T_D**
TYPE 1	0.9	0.05	0.15	1.0
TYPE 2	0.45	0.05	0.15	1.0

If the earthquakes have a surface-wave magnitude M_s, of less than 5.5, choosing the Type 2 spectrum is recommended. In other words, for the seismic surface magnitude equal to and greater than 5.5, the Type 1 spectrum is recommended. The recommended elastic vertical response spectra for the classified types of Table 1.2 is illustrated in Figure 1.3 (continuous lines).

When the ductile behavior of the components is considered, the elastic analysis based on the reduced response spectra is used. Therefore, a design spectrum, $S_{vd}(T)$, is defined for each

direction of seismic ground motion according to equations 1.9 to 1.12 and shown for the classified types in Figure 1.3 (dashed lines):

$$0 \le T \le T_B \qquad S_{vd}(T) = a_{vg}\left[\frac{2}{3} + \frac{T}{T_B}\left(\frac{2.5}{q} - \frac{2}{3}\right)\right] \qquad (1.9)$$

$$T_B \le T \le T_C \qquad S_{vd}(T) = a_{vg} \times \frac{2.5}{q} \qquad (1.10)$$

$$T_C \le T \le T_D \qquad S_{vd}(T) = a_{vg} \times \frac{2.5}{q} \times \left[\frac{T_C}{T}\right] \ge \beta . a_{vg} \qquad (1.11)$$

$$T_D \le T \qquad S_{vd}(T) = a_{vg} \times \frac{2.5}{q} \times \left[\frac{T_C . T_D}{T^2}\right] \ge \beta . a_{vg} \qquad (1.12)$$

The behavior factor, q, is an approximate ratio of the seismic forces the structure would experience in accordance with elastic response and 5% damping. A value of 1.5 is considered for concrete buildings and 1.5 to 2.0 for steel or composite steel-concrete structures.

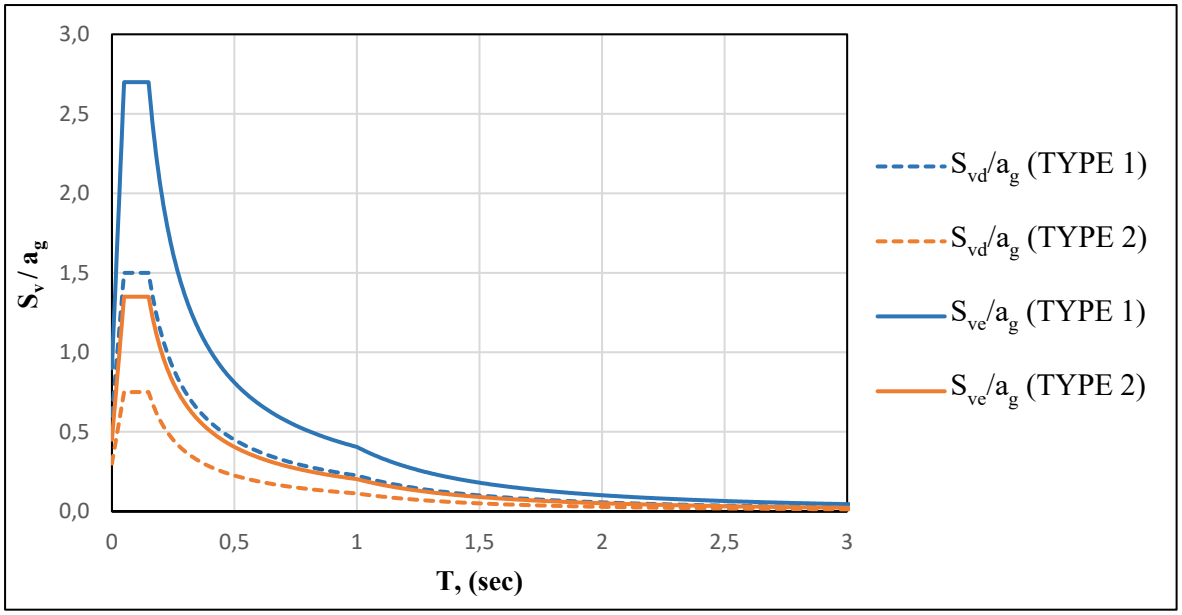

Figure 1.3 Recommended vertical elastic response spectra (S_{ve}) and vertical design spectra for elastic analysis (S_{vd}) in the Eurocode8-1 (2004) for 5% damping ratio

A behavior factor equal to or less than 1.5 could be generally adequate for structural and nonstructural components when considering the vertical component of ground motion; therefore, values greater than 1.5 should be justified for the analysis. The lower bound factor, β, is generally used for the horizontal design spectrum, and the value of 0.2 is recommended for both vertical and horizontal design spectra.

1.6.3 ASCE/SEI 7-16 and NEHRP 2015

The design response spectral acceleration for vertical ground motion, S_{av}, is computed as two-thirds of the maximum considered for risk-targeted vertical response spectral acceleration, S_{aMv}.

It should be mentioned that the prescribed seismic design requirements for the vertical ground motions only apply to the structures located in site categories C, D, E, and F (ASCE/SEI 7-16, 2017). Therefore, where the site-specific methods are not used, the maximum considered risk-targeted vertical response spectral acceleration, S_{aMv}, is developed according to different vertical period of vibration (FEMA P-1050-1, 2015; ASCE/SEI 7-16, 2017) as provided in equations 1.13 to 1.16.

$$T_v \leq 0.025sec \qquad S_{aMv} = 0.3C_vS_{MS} \tag{1.13}$$

$$0.025 \leq T_v \leq 0.05\ sec \qquad S_{aMv} = 20C_vS_{MS}(T_v - 0.025) + 0.3C_vS_{MS} \tag{1.14}$$

$$0.05 \leq T_v \leq 0.15\ sec \qquad S_{aMv} = 0.8C_vS_{MS} \tag{1.15}$$

$$0.15 \leq T_v \leq 2.0\ sec \qquad S_{aMv} = 0.8C_vS_{MS}\left(\frac{0.15}{T_v}\right)^{0.75} \tag{1.16}$$

Where S_{MS} is the risk-targeted maximum considered earthquake response spectral acceleration parameter at short periods, T_v is the fundamental vertical period. C_v is the vertical coefficient defined according to the spectral response parameters at short periods and site classes in accordance with Table 1.3 (ASCE/SEI 7-16, 2017). The linear interpolation is conducted for the interstitial values. The information on the soil types category in these codes, presented in Table-A VI-2, is similar to NBC 2015.

Table 1.3 Vertical coefficient C_v

Taken from FEMA P-1050-1 (2015) and ASCE/SEI 7-16 (2017)

***MCE*$_R$ Response Spectral Parameter at Short Periods**	**Site Class**		
	A & B	**C**	**D & E & F**
$S_S \geq 2.0$	0.9	1.3	1.5
$S_S = 1.0$	0.9	1.1	1.3
$S_S = 0.6$	0.9	1.0	1.1
$S_S = 0.3$	0.8	0.8	0.9
$S_S \leq 0.2$	0.7	0.7	0.7

For instance, the vertical design response spectra for Site Class C, according to the described equations for different tabulated C_v and S_{Ms}, are shown in Figure 1.4.

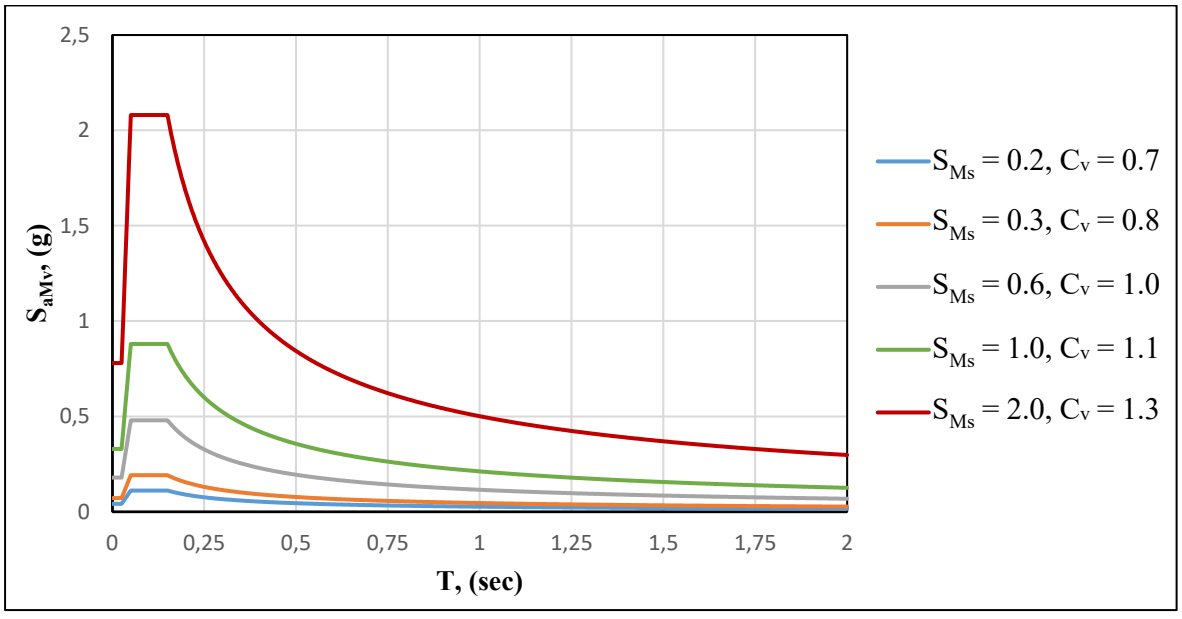

Figure 1.4 Design vertical response spectra for the Site Class C
Adapted from ASCE/SEI 7-16 (2017)

Equation 1.7 calculates the MCE_R response spectral acceleration parameters at short periods, S_{Ms}.

$$S_{Ms} = F_a S_s \tag{1.17}$$

Where S_s is the mapped MCE_R of the response spectral response parameter for the short periods and F_a and F_v are the short-period and long-period site coefficients, respectively determined as tabulated in part 11.4.4 of the ASCE/SEI 7-16.

Instead of using the above method, a site-specific study may be carried out for the period less than 2.0 sec periods, but the obtained value should not be less than 80% of the values from the presented equations. However, for the vertical period greater than 2.0 sec, the vertical response spectrum must be extracted from the site-specific procedure (FEMA P-1050-1, 2015). In addition, the value of the vertical design response spectrum should be greater than one-half (1/2) of the corresponding components for the horizontal response spectrum, S_{ah}, determined in accordance with the general or site-specific procedures (FEMA P-1050-1, 2015).

All relations and definitions in NEHRP for design vertical response spectrum are almost similar to those of the ASCE/SEI 7-16 standard with the difference in the applied symbols in this provision (FEMA P-1050-1, 2015; ASCE/SEI 7-16, 2017).

1.7 Importance of the vertical ground acceleration

Bozorgnia et al. (2000) investigated comprehensive datasets of the near-field strong ground motions with magnitudes ranging from 4.7 to 7.7 and distances less than 60 km from the fault. Data consisting of more than 2800 PGA taken from 48 earthquakes and 1300 response spectra

from 33 earthquakes were studied to develop an equation to estimate the relationship between the vertical and horizontal PGA and PSA. Values of V/H spectral acceleration ratios greater than 1.5 were obtained at periods less than 0.1 sec (short period range) in soft soil type. It was then concluded that this ratio strongly depends on the fault distance, local site conditions and periods, and a minor function of faulting mechanisms and magnitude. Therefore, the attenuation models for both horizontal and vertical PGA and acceleration response spectra as a function of the earthquake magnitude, distance from the epicenter, ground profile type and fault mechanism were developed.

Campbell and Bozorgnia (2003) studied the relationship between the horizontal and vertical components using more than 85 records sets of earthquakes with magnitudes of 4.7 to 7.7 and consisting of up to 443 corrected and 960 uncorrected accelerograms. Based on the characteristics of the earthquakes consisting of distance from the fault, earthquake magnitude, faulting mechanism and site class condition, the PGA and 5% damped PSA for the horizontal and vertical components and their relations in the form of equations were generated. Moreover, it was observed that the events with reverse and thrust-faulting mechanisms have a large amplitude at short periods. Subsequently, it was concluded that a vertical ground motion has higher amplitudes at short periods and near the epicenter. Also, the vertical acceleration of the earthquakes on the firm soil sites is relatively higher due to the less inelastic attenuation and lack of non-linearity effects.

Bozorgnia and Campbell (2004) conducted comprehensive studies on the effect of earthquake magnitude, distance from the fault, local site conditions and faulting mechanism for the V/H acceleration ratio of the PGA and PSA from more than 400 earthquake databases. The results show that earthquake magnitude and distance effect is much more prominent at short periods for firm soil, and there is no significant effect for firm rock. However, the higher periods are not sensitive to earthquake magnitude and fault distance. The V/H ratios were higher at a short period range (less than 0.25 sec) for all mentioned parameters. Therefore, the effect of the earthquake magnitude and distance from the fault and site conditions, especially for firm soil sites, are significant, while the effect of the faulting mechanism is not important. On the other

hand, the analysis of the Site Class condition demonstrated that the V/H ratio could exceed unity at the firm soil sites. The ratio is amplified in short periods for earthquakes with large magnitudes and near-field sites.

Different earthquake databases from the 1999 Chi-Chi, Taiwan and the 1999 Kocaeli and Duzce, Turkey, were used by Elnashai et al. (2004) to study the characteristics of the vertical ground motions. The strong vertical records from these three earthquakes were selected to propose an equation which estimates the vertical response spectra at various damping ratios. The maximum acceleration range in this equation was determined between 0.05 sec to 0.15 sec (corner periods) for near-field sites, and 0.05 sec to 0.20 sec for the far-field sites.

Ambraseys and Douglas (2005) used 595 data records of strong vertical ground motions from European and Middle Eastern earthquakes to propose an equation to estimate the PGA_V and PSA_V for 5% damping for periods between 0.05 and 2.5 sec. All records were chosen from the shallow crustal earthquakes in the 5.0 to 7.6 magnitude range and distance from the fault less than 100 km for different Site Classes. Then, the effect of the faulting mechanism and the local site conditions and their role in deriving the ground motion equation were investigated. It was concluded that the effect of the local site conditions is more prominently than other parameters. In the study by Gülerce & Abrahamson (2011) on the characteristics of the vertical ground motion, two main approaches for developing the vertical hazard spectra were assessed. In the first approach, the vertical ground motion prediction equation (GMPE) and in the second approach, the GMPE of V/H spectral acceleration ratio were developed. The first method is to develop an independent equation for the vertical and horizontal components based on the earthquake magnitude and distance from the faults. The second method generates an equation to derive the V/H ratio directly, which can be applied to scale the horizontal acceleration spectrum. Therefore, more than 2684 sets of recordings for vertical and horizontal components from 127 earthquakes were used to investigate the parameters mentioned to derive the V/H equation.

1.8 Effect of the vertical ground acceleration on the response of structures and NSCs

According to the research by Newmark and Hall (1982), columns and wall elements are particularly vulnerable to the vertical component of ground motion in compression. Moreover, the floor systems, including slabs, beams, or other horizontal and cantilevered elements, where the amplification factors for vertical response may be relatively large and cause to amplify the acceleration, which leads to an increase in the shear or moment force of the elements.

Mohit and Shimazu (1987) proved that the rotational stiffness of the beam ends would be reduced, and deflection at the middle of the span would be increased due to the vertical acceleration. This increase will continue approximately until the first yielding of the RC section at the critical point of the beam, which is not addressed in code design provisions.

Broderick et al. (1994) concluded that the effect of vertical components of ground motions is typically less pronounced in the perimeter and corner columns than in the interior columns. Perimeter and corner columns receive more seismic forces from horizontal motions than those in the interior area, as the perimeter and corner columns provide resistance to overturning created by the horizontal acceleration of ground motion. In addition, the contribution of gravity forces is larger for interior columns, since the effect of overturning is negligible at interior columns. For the first vertical mode of vibration of moment frame buildings, the effects of the vertical components of ground motion are less in the columns at the lower stories than in the upper stories. That is because the relative change in the pre-existing static axial load is more significant in the upper stories. In other words, the sensitivity of the columns to the vertical component of ground motions is greater in the upper stories than in the lower levels.

Papazoglou and Elnashai (1996) investigated two modes of shear and compression failures caused by the vertical component of ground motion for RC structures. They found that failure in the RC structures subjected to the vertical component of strong earthquakes depends on the amount of tension or compression force in the columns.

Yamanouchi and Hasegawa (1996) conducted an analytical study on buildings ranging from one to 8-stories. The most significant effect of the vertical acceleration was observed on the interior columns, which are most heavily loaded, and the exterior columns were affected mainly by the horizontal acceleration.

Christopoulos (1999) studied the non-linear behavior of a 6-storey steel moment-resisting frame system subjected to near-fault vertical acceleration and found a significant effect of vertical shaking on the rotational ductility, strain rate, and axial load. He concluded that the strain rate increases, especially at the panel zone area of the beam-to-column connections.

Pekcan et al. (2003) conducted linear elastic time history analysis on two buildings with flexible floor systems. The horizontal and vertical responses of the selected buildings were assessed and compared with the experimental test guidelines, and the seismic response of NSCs was evaluated. The obtained results showed that the imposed seismic acceleration affects the floor systems due to the out-of-plane behavior of the slab. Also, the results indicated that the peak vertical floor acceleration could be greater than the horizontal ones for the buildings subjected to the near-field ground motions.

Kim & Elnashai (2008) conducted experimental and analytical tests with the simulated vertical acceleration of ground motions to calculate the axial tension in vertical structural elements. However, the interaction of the tension and shear strength in these elements could be more disruptive. A numerical simulation of the same RC buildings showed that the axial tension in vertical elements such as shear walls and columns is insignificant and only leads to decreased shear resistance.

Wieser et al. (2012) investigated the influence of relative height within the building, ductility levels, and out-of-plane flexibility of the floor system using the vertical acceleration of ground motions. The mentioned study considered a 3-storey hospital building and three office

buildings consisting of 3, 9 and 20 stories with steel moment-resisting systems. Both linear and non-linear analyses were used to develop the finite element models. Elastic behavior was assumed for the floor decks and steel frames, and the fiber section modelling was used to investigate the non-linearity of beam-column connection elements. Despite the constant and unchanged acceleration in the column joints, the significant vertical acceleration amplification was observed away from the column supports due to the out-of-plane flexibility of the floor system. In addition, a significant amplification of vertical acceleration was observed in the middle of the floor bays as a result of the out-of-plane flexibility of the floor systems.

The results obtained from the experiments of Furukawa et al. (2013) at Tohoku University show a strong influence of input vertical acceleration on the response of acceleration-sensitive NCSs; this effect is particularly significant for elements located at open bays rather than those located close to the columns. Therefore, vertical floor accelerations are greatly influenced by the location of the component on a floor, along with the height of the building and the characteristics and properties of the floor system.

Moschen et al. (2014) studied PFA_V demands on NSCs and assumed them to be rigid in the vertical direction. Steel moment-resisting frame buildings ranging from 1 to 21 stories were analyzed by applying the recorded vertical acceleration of ground motions. It should be noted that only the rigid NSCs mounted close to the columns and at the mid-span length of the regular steel moment-resisting frames were evaluated. However, the effect of the vertical acceleration of ground motion on the slabs was not evaluated. The obtained results demonstrated that vertical acceleration is amplified through the height of buildings away from the columns.

Ryan et al. (2016) did an experimental test to study how the PGA_V is amplified from the column to the middle of the slab. They found that this amplification ranges from 3.0 near the column to 6.0 at approximately the middle of the slab. Also, by increasing the vibration period of the slab, the amplification factor increased. On the other hand, the results obtained from the experimental tests and numerical simulation of the slab by Guzman Pujols & Ryan (2018)

indicate that the single vertical mode at higher floors mainly dominates the slab response due to the vertical vibration. Furthermore, it was demonstrated that the response of the NCSs is highly dependent on the vibration and acceleration of the floor system and the deflection of the slabs.

Marshall et al. (2017) studied the behavior of a 6-storey steel special moment resisting frame of an office building by selecting a set of near and far field earthquakes, and the analysis was done by applying the earthquake first in the horizontal direction only, then in both vertical and horizontal directions. It was found that consideration of the vertical acceleration has little impact on the lateral storey drift of the structure, while there is a significant impact on the column axial forces. Furthermore, since the load tributary area for interior columns is larger than the exterior columns, it is clear that the impact of the vertical acceleration on the interior is more than the outer columns.

1.9 Summary and conclusion

This chapter explains the importance of NSCs from the seismic point of view and their responses to severe earthquakes. Also, the recommendation of code provisions such as Eurocode 8-1 (2004), NBC 2015, and ASCE/SEI 7-16 (2017) for the horizontal, vertical seismic design force of NSCs was presented. Although in these codes, most attention was paid to the horizontal seismic design, the vertical component of the earthquake is less discussed. For instance, the estimation of the vertical seismic design force of NSCs in the Canadian standard is confined to 2/3 of the horizontal one. In some cases, such as at the middle of the open bays, this amount could be underestimated. Furthermore, even the relationship presented in ASCE/SEI 7-16 (201), which incorporates a dead load scale factor of $0.2S_{DS}$, indicates that the effect of vertical acceleration is not taken into account to obtain the vertical seismic force of NSCs.

The previous studies indicated the importance of the location variation on the floor and along the building height. Therefore, it is necessary to investigate the amplification of vertical acceleration in both PFA_V and FSA_V, which are related to the rigid and flexible NSCs. In this regard, this research is a path to address the shortcomings of the codes, especially NBC 2015, in order to improve them. Accordingly, since limited studies have focused on vertical floor response spectra, especially in a 3D building model, part of this study focused on developing a method to define the vertical floor spectra for RC moment-resistant frame buildings. On the other hand, to improve design requirements and NSCs subjected to vertical seismic loading, proper design vertical spectra should be provided.

Moreover, in this chapter, it was highlighted that a few studies had been conducted on the importance of the vertical component of earthquakes. Although a few codes, such as ASCE/SEI 7-16 (2017) and Eurocode 8-1 (2004), developed some formulations to generate the vertical design spectra for their seismic region, NBC has still not provided any relationship or equation for obtaining the vertical design spectra in different seismic regions of Canada, and it is just limited to the empirical value of 2/3 for V/H spectral ratio. As discussed in this literature review, the previous research demonstrated that this ratio is underestimated for the near-field and strong ground motions and might be overestimated for far-field areas. Also, due to the importance of the vertical component of the earthquakes in the Eastern Canada seismic region, this study proposed a solution to derive vertical design spectra for this region. Hence, the importance of the vertical seismic ground motion in Eastern Canada was highlighted in the first objective, and eventually, the vertical design spectra were proposed.

CHAPITRE 2

ESTIMATE OF V/H SPECTRAL ACCELERATION RATIOS FOR FIRM SOIL SITES IN EASTERN CANADA

Shahabaldin Mazloom[a] and Rola Assi[b]

[a, b] Department of Construction Engineering, École de Technologie Supérieure, 1100 Notre-Dame West, Montreal, Quebec, Canada H3C 1K3

Paper published in *Soil Dynamics and Earthquake Engineering*[1], May 2022

Abstract

This study aims to provide an estimate of vertical-to-horizontal (V/H) pseudo-spectral acceleration (PSA) ratios in the Eastern Canada seismic region for firm soils ($360 < V_{s30} < 760$ m/s) referred to as Site Class C in the National Building Code of Canada (NBC). According to previous studies, the 2/3 V/H empirical ratio prescribed in NBC is deemed overestimated for far-field areas and underestimated for near-field areas. In this study, the V/H PSA ratios were computed for 248 records from 67 historic earthquakes in the Eastern Canada region with a magnitude $M_w \geq 3.0$ and an epicentral distance (R_{epi}) <150 km. Given the lack of available records for Site Class C in this region, sets of records from other site classes, mostly Site Class A (Hard rock), were selected and converted to the corresponding records on Site Class C. To this end, the equivalent linear method, using the Pressure-Dependent Modified Kondner Zelasko (MKZ) model of analysis in the frequency domain was selected using the software DEEPSOIL. Computed V/H PSA ratios were then calibrated with those obtained from available Ground Motion Prediction Equations (GMPEs) compatible with Site Class C of the

[1] Mazloom, S., & Assi, R. (2022). Estimate of V/H Spectral Acceleration Ratios for Firm Soil Sites in Eastern Canada. Soil dynamics and earthquake engineering, 159, 107350. DOI: https://doi.org/10.1016/j.soildyn.2022.107350

studied region. The computed mean V/H PSA ratios were found to exceed the common value of 2/3 recommended in most codes, especially for short periods up to 1.3 sec, and new V/H ratios were proposed as a function of the fundamental period of the building. Finally, a profile of vertical acceleration design spectra (ADS_{ver}) was proposed for Site Class C in Montreal and compared with those obtained by ASCE/SEI 7-16 and ASCE 41-17 provisions.

Keywords: Acceleration Design Spectra (ADS), Site Class, Ground Motion Prediction Equation (GMPE), Pseudo Spectral Acceleration (PSA), Eastern Canada seismic region

2.1 Introduction

The effects of vertical ground motions have generally been neglected in the seismic design of typical structures and assumed to be minor compared with the effects of horizontal ground motions, since buildings are typically considered stiff enough in the vertical direction (Bozorgnia et al., 1998). Yet, structural damage to buildings and bridges due to the detrimental effect of the vertical component of the ground motion was reported following major earthquakes (Goltz, 1994; Papazoglou & Elnashai, 1996; Kim et al., 2011). For instance, the Northridge Fashion Center building experienced shear cracking and total collapse of floors due to vertical floor oscillations (Hilmy & Masek, 1994). Subsequently, it was concluded that the induced shear and flexural failure resulted from the severe vertical motion of the quake, which caused a significant reduction in the ductility and moment capacity of the reinforced concrete columns (Papazoglou & Elnashai, 1996). In another example, the high acceleration of the vertical ground motion generated during the 2012 M_w 5.8 Mirandola earthquake was determined to lie at the root of the total or partially observed failures of structures (Breccolotti & Materazzi, 2016).

Furthermore, several recent studies have highlighted the importance of considering the vertical component of ground motions in the seismic design of non-structural components (N. N. Ambraseys & John Douglas, 2003; Bozorgnia & Campbell, 2004; Shrestha, 2009; Gülerce &

Abrahamson, 2011; Moschen et al., 2016; Assi et al., 2017), especially in the near-fault areas, where the vertical component of the ground motion is characterized by a high-frequency content and large acceleration-to-velocity (a/v) ratio (Tso et al., 1992; Christopoulos, 1999). For instance, a high a/v ratio that reached 5.51 was recorded at Chicoutimi-Nord station during the 1998 M_w 5.9 Saguenay earthquake (Tso et al., 1992).

It is thus clear that the vertical component of an earthquake affects the structural behaviour of floor systems and, consequently, their non-structural components; therefore, its quantification and characterization should be given thorough consideration in the analysis and design of buildings (Pekcan et al., 2003; Wieser et al., 2012; Moschen et al., 2015). Most past studies in Eastern North America (Haghshenas et al., 2008), including Eastern Canada, focused solely on the horizontal components of ground motions. Consequently, developing vertical acceleration design spectra based on the seismological characteristics of the region under consideration becomes essential.

Two main approaches are proposed in the literature to derive the vertical design spectra for a given site. The first approach consists of computing the vertical spectra independently from the horizontal spectra using vertical Ground Motion Prediction Equations (GMPEs). This approach is known as the independent vertical ground motion model approach and was discussed and comprehensively applied in studies undertaken by Bozorgnia & Campbell (2004, 2016b) and Gülerce & Abrahamson (2011). The vertical Uniform Hazard Spectra (UHS) are constructed by estimating the spectral amplitudes at specific periods for a given return period, using the Probabilistic Seismic Hazard Analysis (PSHA), and considering earthquake events which are most likely to produce the target spectral amplitude for a given period (McGuire, 1995; Baker, 2011). The main drawbacks of this approach are the lack of available data necessary to develop vertical GMPEs as high-frequency records are needed, while most processed data have a high-frequency cut-off of 40 Hz (Graizer, 2012). In addition, since this approach does not consider the correlation of the three components for each earthquake (Gülerce & Abrahamson, 2011), this could generate a possible mismatch between

the horizontal and vertical controlling earthquakes. On the other hand, the second approach consists of deriving the vertical design spectra by applying a scaling factor to available horizontal design spectra often developed using the conventional 5% damping ratio (N. N. Ambraseys & John Douglas, 2003; Bozorgnia & Campbell, 2004; Gülerce & Abrahamson, 2011; Bozorgnia & Campbell, 2016a). This approach is adopted in most codes due to its simplicity and deemed appropriate to a great extent since it considers the dependent relationships of the horizontal and vertical components of an earthquake, especially their standard inherent features such as the magnitude, soil conditions, and distance from the fault, (Campbell & Bozorgnia, 2003; Shirai et al., 2004). Therefore, this approach is used in this study to derive the vertical acceleration design spectrum (ADS_{ver}) for Montreal.

Currently, the National Building code of Canada (NBC, 2015a) proposes to obtain the vertical ADS by multiplying the available horizontal ones by a constant empirical ratio equal to 2/3. Most studies focusing on deriving the V/H PSA ratios have concluded that this ratio is not a constant value and could be higher at short periods and in the near-fault areas, especially on the rock sites known as Site Class A (Bozorgnia et al., 1996; N. N. Ambraseys & John Douglas, 2003; Bozorgnia & Campbell, 2004; Gülerce & Abrahamson, 2011) Therefore, the empirical ratio of 2/3 used for vertical design purposes in the nuclear industry was not recommended (McGuire et al., 2001). For instance, an analysis by Bozorgnia and Campbell (2004) for the V/H ratio in near-field sites demonstrated that this ratio can exceed unity at firm soil (Site Class C) and could be amplified for earthquakes with large magnitudes, especially at the short period range. In another example, a vertical Peak Ground Acceleration (PGA_{ver}) of 1.3g was recorded in the 1976 M_w 7.0 Gazli earthquake, while the horizontal Peak Ground Acceleration (PGA_{hor}) was equal to 0.7g (Shteinberg et al., 1980). This high V/H ratio could be attributed to reduced inelastic attenuation and a lack of nonlinear site effects (Campbell & Bozorgnia, 2003; Ambraseys et al., 2005). The study by McGuire et al. (2001) for the Western United States (WUS) and Central and Eastern United States (CEUS) seismic regions concluded that the V/H ratio is independent of the fault distance for data recorded at rock sites located at distances ranging from 20 km to 1000 km, while it is dependent on the earthquake magnitude for sites

in the CEUS seismic region. On the other hand, the investigation of databases in the WUS and CEUS region indicated large V/H ratios at higher frequencies and at very close distances (R_{rup} < 50km) and strong earthquake magnitude (M_w > 5.5) for the hard rock site conditions (McGuire et al., 2001). Meanwhile, no correlation was observed between the earthquake magnitude and the increasing distance from the fault for both firm soil and rock sites.

In seismic events with dominant P-waves, the amount of peak vertical acceleration varies depending on the earthquake magnitude, soil conditions, and distance from the fault (Bozorgnia et al., 2000). The vertical component of the earthquake motion is not significantly attenuated in the near-fault region, which yields vertical PGA values close to horizontal PGA. On the other hand, an increase in the distance from the fault causes P-waves to attenuate, thus reducing the vertical PGA compared to the horizontal PGA (Christopoulos et al., 2000). Therefore, this study focuses on near-fault ground motions where the adverse effect of vertical ground motions needs special attention.

In particular, this paper focuses on assessing the accuracy of the 2/3 V/H ratio proposed in NBC for Eastern Canada and then proposing a profile of vertical acceleration design spectra (ADS_{ver}) corresponding to a 2475-year return period (at 2% per 50 years probability) for Site Class C in Montreal. It should be noted this return period is adopted for this study since it is similar to the one used for standard structures in the current NBC 2015 edition.

First, the records collected from different site classes were converted to very dense soil known as Site Class C in NBC 2015 using the software DEEPSOIL (Hashash et al., 2019); then, the V/H PGA and PSA ratios were computed for each record, and the mean values were used to scale the horizontal design spectra (ADS_{hor}). Finally, these ratios were compared with those calculated using compatible GMPEs proposed in previous studies by Bozorgnia and Campbell (2004) and Gülerce and Abrahamson (2011). These selected reference models are deemed largely compatible with the region of our investigation since they were developed based on ground motions gathered from different sources around the globe. Eventually, the proposed

ADS_{ver} was compared with those derived according to the procedures proposed in the standards ASCE/SEI 7-16 (ASCE/SEI 7-16, 2017) and ASCE 41-17 (ASCE/SEI 41-17, 2017).

2.2 Collection of ground motions in Eastern Canada region

In this study, a database composed of 248 records culled from 67 earthquakes (1982-2015), having a magnitude M_w greater than 3.0 and an epicentral distance (R_{epi}) less than 150 km, was selected. The earthquake records of events that occurred between 1992 and 2008 were extracted from the Ground Motion Databases channel of the Engineering Seismology Toolbox, while earthquake records for events that occurred from 2010 to 2015 were extracted from the Interactive Ground Motion Maps for Southern Ontario presented by the Engineering Seismology Toolbox in the Earthquake Data Auto-Processor (EDAP) Project (Seismotoolbox, 2019). The records for the Miramichi and Saguenay earthquakes that occurred in 1982 and 1988, respectively, were taken from the website of Natural Resources Canada (NRCAN, 2001). Also, some records were taken from the Pacific Earthquake Engineering Research Center (PEER-NGA, 2018) for the Central and Eastern North American region and Strong-Motion Cosmos Virtual Data Center (VDC, 2018), respectively. The selected records are filtered and digitalized with high sampling rates of 40 Hz (67 sets), 100 Hz (164 sets), and 200 Hz (17 sets).

For each of the selected ground motions, the name, date, station name, magnitude, site class, epicentral distance, focal depth, and average shear wave velocity at each station are presented in Table-A I-1. Then, the attributed earthquake moment magnitudes were completed from the USGS website (2018) and the Bent (2009) databases. The conversion expression used to determine the moment magnitude scaling of earthquakes is based on the expressions given in Macias Carrasco et al. (2010) and Sonley and Atkinson (2005). Some other supplementary information for some earthquakes, such as event names and site classes, was extracted from other references, including the Incorporated Research Institutions for Seismology (IRIS,

2018), the U.S. Geological Survey (USGS, 2018) and Natural Resources Canada (NRCAN, 2015).

The selected earthquakes were recorded on 4 different site classes based on V_{s30} criterion according to the NBC 2015 (NBC, 2015a): class A (hard rock, $V_{s30} > 1500$ m/s), class B (rock, $760 < V_{s30} \leq 1500$ m/s), class C (very dense soil and soft rock, $360 < V_{s30} < 760$ m/s), and class D (stiff soil, $180 < V_{s30} < 360$ m/s). Figure 2.1 shows the number of records per site class. It is noteworthy that most selected data were recorded on bedrock (203 out of 248); therefore, the lack of sufficient databases for Site Class C according to the given criteria is quite obvious. For this reason, the DEEPSOIL software (Hashash et al., 2019) was used to convert all records to their equivalent on Site Class C using the Pressure-Dependent Modified Kondner Zelasko (MKZ) model (Kondner & Zelasko, 1963) implemented in this software. An average shear wave velocity, V_{s30}, of 450m/s was used in the conversion process since prescribed by NBC 2015 for Site Class C, and it is an average value typical of firm soil in Eastern Canada.

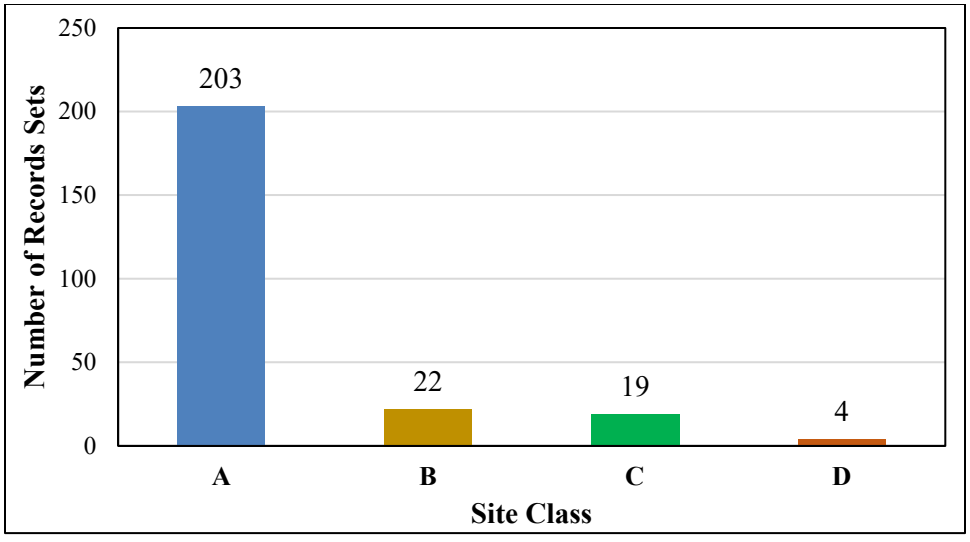

Figure 2.1 Cumulative number of records taken from different site classes

Since very little soil nonlinearity is expected in Site Cass C, the equivalent linear method of analysis based on Frequency Domain solution type (Hashash et al., 2019) was used. This

simplified conversion approach is considered accurate enough for the sake of this study. Also, the automatic profile generation proposed in this software was used in the conversion process based on the reference shear wave velocity V_{s30} taken equal to 450 m/s due to the lack of precise details about the characteristics of the soil layers of the sites where data were recorded. This assumption is considered acceptable for design purposes since in line with the current NBC provisions that consider the column of soil made of a 1D single layer. Eventually, the acceleration response spectra were computed for each record converted to Site Class C, called converted records, considering a damping ratio equal to 5%. In this regard, the PRISM software (Jeong et al., 2011) was used to compute the pseudo-spectral acceleration (PSA) for each record, and results were validated by SeismoSignal software (SeismoSoft, 2018).

2.3 Computation of the PGA and PSA ratios of the records

2.3.1 Geometric means of the horizontal components

Most sets of records consist of three orthogonal components, two being in the horizontal direction and one in the vertical direction. In this study, the geometric mean of the horizontal components was used in the evaluation of V/H PGA and PSA ratios, as shown in Equations 2.1 and 2.2, respectively. In these equations, H1 and H2 correspond to the two orthogonal directions of the horizontal components for PGA and PSA.

$$PGA_{hor} = \sqrt{PGA_{H1} \times PGA_{H2}} \tag{2.1}$$

$$PSA_{hor} = \sqrt{PSA_{H1} \times PSA_{H2}} \tag{2.2}$$

This method was recommended in Acerra et al. (2004), Picozzi et al. (2005), Boore et al. (2006), Campbell & Bozorgnia (2007), Haghshenas et al. (2008), Pileggi et al. (2011), Stewart et al. (2011), NBC (2015b), and ASCE/SEI 7-16 (2017). In fact, the theoretical results by Boore et al. (2006) and Albarello & Lunedei (2013) demonstrate that the correlated horizontal

ground motion records have one rotation angle, which will be equal or close to zero when the geometric mean is used. On the other hand, the minimum horizontal spectral value could occur over a limited range of the rotation angles and will be a strong function of the correlation form. Accordingly, the maximum value will not be a strong function of the component correlation form, and thus, any fractal measurement represented by the geometric mean value will be closer to the maximum than to the minimum value (Boore et al., 2006). In addition, this method reflects the correlation between the acceleration components recorded at each station (Huang et al., 2016).

Moreover, since the V/H PSA ratio represents the frequency-dependent characterization of the components, and it inherently accounts for site class, fault distance, and earthquake magnitude impacts, using two horizontal components separately was deemed non-practical (Bartosh & Bouaanani, 2014).

2.3.2 V/H PGA ratios (PGA_{ver}/PGA_{hor})

The peak ground acceleration (PGA) plays an essential role in stabilizing the zero period ordinate of the response spectra (N. N. Ambraseys & John Douglas, 2003). The vertical-to-horizontal PGAs of the considered records were computed using Equation 2.3.

$$\left(\frac{V}{H}\right)_{PGA} = \frac{1}{n}\sum \frac{PGA_{ver}}{\sqrt{PGA_{H1} \times PGA_{H2}}} \tag{2.3}$$

PGA_{H1} and PGA_{H2} were described previously, PGA_{ver} is the vertical peak ground acceleration, and n is the number of selected records (248). The characteristics of the components for different seismic zones were explored using this approach in past studies carried out by Newmark et al. (1973), Abrahamson and Litehiser (1989), Campbell (1997), Collier and Elnashai (2001), and Kalkan and Gülkan (2004). A mean PGA ratio of 0.78 was found for the 248 sets of records, which is 16.9% larger than the 2/3 empirical ratio recommended in NBC

and other codes and standards. We can also note that the minimum V/H PGA ratio of 0.17 corresponds to the 1998 M_w 3.2 Lac-Ministuk earthquake at R_{epi} 89.70 km. In comparison, the maximum V/H PGA ratio of 2.53 corresponds to the 2000 M_w 3.7 Baie-Saint-Paul earthquake at R_{epi} 73.96 km. Therefore, the obtained ratios are unrelated to the magnitude and the epicentral distance.

On the other hand, generating the vertical design spectra by scaling the horizontal UHS with a constant PGA ratio assumes a constant relation throughout the shorter and higher frequency levels (Bozorgnia & Campbell, 2004). Since the modes that are influenced by the vertical ground motion are at a higher frequency level than those affected by the horizontal component, this constant ratio does not properly reflect the potential damage and failure to a structure caused by the combined effect of the horizontal and vertical components of an earthquake. Therefore, this approach is inappropriate and will not be used in this study.

2.3.3 V/H PSA ratios (PSA_{ver}/PSA_{hor})

Generally, the V/H PSA ratios are represented as a function of fault distance, earthquake magnitude, and soil conditions (Siddiqqi & Atkinson, 2002; N. N. Ambraseys & John Douglas, 2003; Bozorgnia & Campbell, 2004, 2016a). The peaks of horizontal and vertical spectra for an earthquake recorded at a given station do not necessarily occur at the same time (US NRC, 2014). Therefore, the computed V/H PSA ratio at a station provides an approximate estimation of the vertical component relative to the horizontal one (Christopoulos et al., 2000; N. N. Ambraseys & John Douglas, 2003). However, in the absence of the target vertical spectra, the V/H PSA ratios from the ground motion records for a given site class can be applied to define vertical spectra as a fraction of horizontal design spectra (NBC, 2015b).

In the following, the mean V/H PSA relations will be deduced from the V/H ratios at specified periods in the horizontal and vertical acceleration response spectra. Similar to the previous method, this ratio is first computed for each record by using the geometric mean of the pair of

horizontal spectral accelerations at specified periods of vibration, as shown in Table 2.1, and subsequently, all of them are averaged out, as presented in Equation 2.4.

$$\left(\frac{V}{H}\right)_{PSA,i} = \frac{1}{n}\left(\sum \frac{PSA_{ver}}{\sqrt{PSA_{H1} \times PSA_{H2}}}\right)_i \tag{2.4}$$

Where $(V/H)_{PSA,i}$ represents the mean V/H PSA ratio at the i^{th} period of vibration. PSA_{H1} and PSA_{H2} were described previously; PSA_{ver} and n are the vertical pseudo-spectral acceleration and the number of selected records, respectively. The computed mean V/H PSA ratios with the 95% confidence levels are presented in Table 2.1 and Figure 2.2.

Table 2.1 Computed V/H PSA ratios for converted records to Site Class C collected in Eastern Canada

T (sec)	Upper Bound 95% Confidence Level	Mean V/H ratio	Lower Bound 95% Confidence Level	T (sec)	Upper Bound 95% Confidence Level	Mean V/H ratio	Lower Bound 95% Confidence Level
0.01	0.88	0.82	0.77	**0.8**	0.91	0.86	0.81
0.02	0.94	0.86	0.80	**0.9**	0.89	0.84	0.79
0.04	0.83	0.77	0.72	**1.0**	0.89	0.84	0.79
0.05	0.79	0.74	0.69	**1.1**	0.88	0.83	0.78
0.06	0.78	0.74	0.69	**1.2**	0.87	0.83	0.78
0.075	0.78	0.73	0.69	**1.3**	0.87	0.82	0.77
0.08	0.79	0.74	0.69	**1.4**	0.86	0.81	0.77
0.09	0.80	0.75	0.70	**1.5**	0.85	0.80	0.76
0.1	0.81	0.76	0.70	**1.6**	0.85	0.80	0.76
0.15	0.89	0.83	0.77	**1.7**	0.85	0.80	0.76
0.2	0.88	0.82	0.77	**1.8**	0.85	0.80	0.76
0.26	0.89	0.84	0.78	**1.9**	0.85	0.80	0.76

0.3	0.90	0.85	0.79	**2.0**	0.85	0.80	0.76
0.4	0.88	0.83	0.78	**2.5**	0.85	0.79	0.74
0.5	0.91	0.85	0.80	**3.0**	0.85	0.80	0.75
0.6	0.91	0.85	0.80	**3.5**	0.88	0.82	0.77
0.7	0.92	0.86	0.81	**4.0**	0.87	0.82	0.77

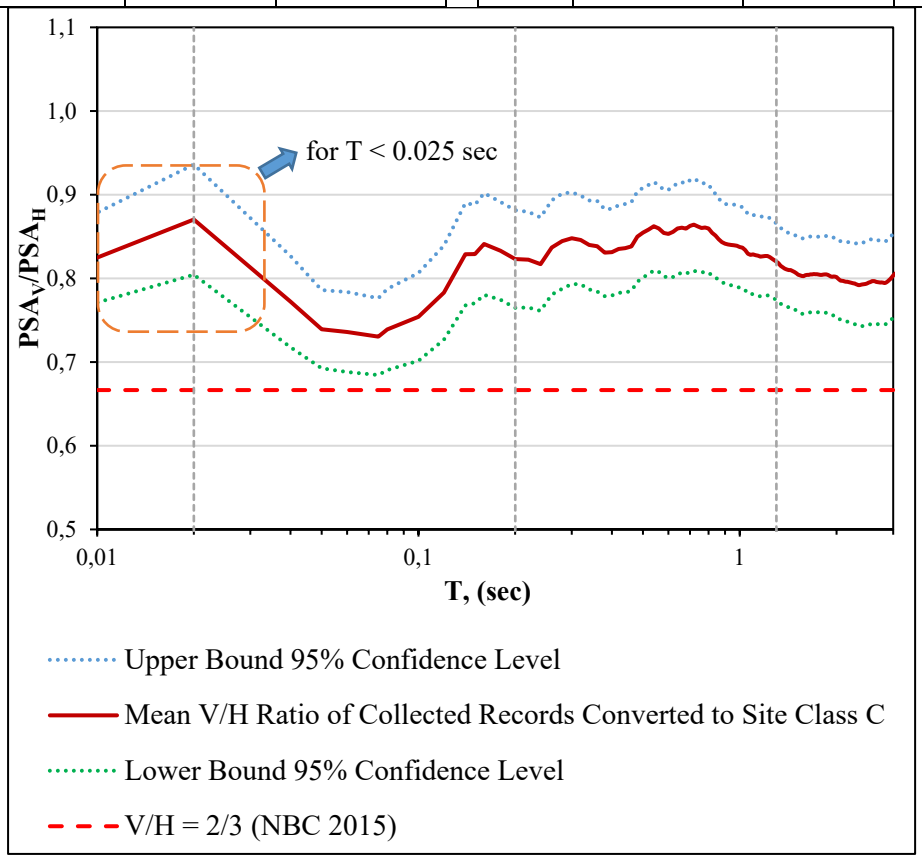

Figure 2.2 The mean and confidence levels of V/H PSA ratios for converted records on Site Class C Eastern Canada

As shown in Figure 2.2, the computed mean V/H PSA ratios for the studied events are greater than 2/3 at all periods. For better interpretation and exploitation of the obtained results, the obtained V/H PSA ratios were divided into four period intervals. A maximum mean value of 0.87 was obtained up to a period of 0.02 sec (T = 0.02 sec). This ratio decreased over the interval period interval of 0.02 to 0.2 sec. It should be noted that since most recorded data used

in the present study were digitized with 100 samples/sec, the results for the lower periods ($T < 0.025$ sec or even < 0.04 sec) may not be reliable, especially for the vertical components as was reported by Graizer (2012). Therefore, the actual V/H ratios for this period range (the orange box shown in Figure 2.2) could be higher than the obtained ratios.

Furthermore, the ratio is almost uniform (with a value of about 0.8) in the $1.30 \leq T \leq 3.0$ sec period range. Nevertheless, the V/H PSA ratio pattern is non-uniform at very short periods, with increasing values observed for periods ranging from 0.2 to 1.3 sec, which highlights the importance of the vertical ground motion component in the short period range for the Eastern Canada earthquakes.

It can be concluded that a constant ratio of 0.86, which is equivalent to the mean value (0.83) plus the standard deviation (0.03), is a reasonable estimate for the period ranges less than 1.0 sec ($T \leq 1.0$ sec) for Site Class C. Beyond that range, this ratio reaches an average value of 0.73, which is close to the empirical value of 2/3 recommended in NBC 2015; therefore, it is suggested to keep this ratio unchanged for periods larger than 1.0 sec.

In order to validate the results obtained from the converted records, the V/H ratios from available records on Site Class C (19 in total) were computed and shown in Figure 2.3. It can be noted that the calculated mean ratios of these records are a little greater than the empirical value of 2/3 at almost all periods. In this case, the ratio of 0.86, equivalent to the average ratio (0.78) + the standard deviation (0.08), was concluded for $T \leq 1.0$ sec, which corroborates the ratios obtained from the converted records (248 in total) on Site Class C. A decrease in the acceleration ratio was also observed in the period range of 0.02 to 0.2 sec (Figure 2.3), thus confirming the decreasing ratio pattern in this interval as previously explained and shown in Figure 2.2. It can then be concluded from Figures 2.2 and 2.3 that the obtained results for original and converted records are in good agreement.

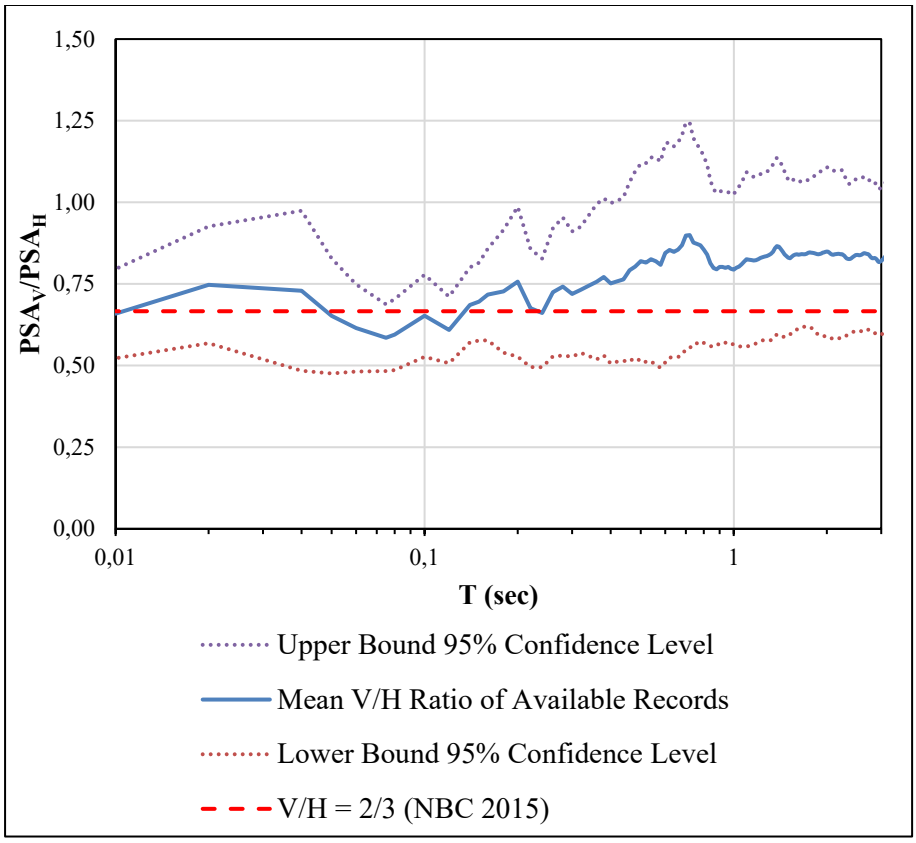

Figure 2.3 V/H PSA ratios for available records on Site Class C in Eastern Canada

2.4 Comparison of the computed V/H PSA ratios with applicable GMPEs

Ground Motion Prediction Equations (GMPEs) relate ground motion intensity measures to variables describing the earthquake source, path, and site effects. While horizontal GMPEs were proposed in the studies by Atkinson (2004) and Atkinson and Boore (2006) for the Eastern Canada seismic region, as yet, such equations are not available for the vertical direction.

In order to validate the V/H PSA ratios computed previously from converted records (Section 2.3.3), results were compared to ratios resulting from two selected Ground Motion Prediction Equations (GMPEs) proposed by Bozorgnia and Campbell (2004) and Gülerce and Abrahamson (2011) that are deemed compatible with the Eastern Canada region. In fact, the

GMPE of V/H ratios proposed by Bozorgnia & Campbell (2004) could be valid for shallow crustal earthquakes in worldwide active tectonic regions with earthquake magnitudes greater than 5.0 ($M_w \geq 5.0$), distances of less than 100 km from the fault, and Strik-Slip, Reverse, Reverse Oblique, Thrust, and Normal fault mechanisms. In addition, this model is the basis for the proposed Risk-Targeted Maximum Considered Earthquake, MCE_R, of the vertical response spectral acceleration, S_{aMv}, in American standards such as ASCE/SEI 7-16 and ASCE 41-17, as will be explained in more detail in Section 2.5.1. On the other hand, the proposed GMPE for the V/H ratios proposed by Gülerce & Abrahamson (2011) was developed based on earthquakes selected throughout the world and could be applied to distances from the source of up to 200 km for the Western United States (WUS) and up to 100 km for other regions. This model is also adequate for events with moment magnitude ranging from 5.0 to 8.5 for Strike-Slip[1] and 5.0 to 8.0 for Normal[2] and Dip-Slip[2] faults. More details of the abovementioned characteristics of the selected GMPEs are shown in Table 2.2.

Table 2.2 Characteristics of the GMPEs used in this study

GMPEs	Magnitude Range	Epicentral Distance Range (km)	Period Range (sec)	Response Variables	Damping ratios
Bozorgnia & Campbell (2004)	$M_w \geq 5.0$	0 – 100	0 – 4.0	PSA	5 %
Gülerce & Abrahamson (2011)	[1]M_w 5.0 to M_w 8.5 [2]M_w 5.0 to M_w 8.0	0 – 100	0 – 10.0	PSA	5 %

The selected M-R scenarios (Moment magnitude-fault distance) used for the chosen GMPEs are based on those proposed by Atkinson (2004) and Atkinson and Boore (2006) for the Eastern Canada seismic region. These include the moment magnitude of M_w 6.0 at the fault distances from 10 to 15 km and 20 to 30 km, and the moment magnitude of M_w 7.0 at the fault distances from 15 km to 25 km and 50 km to 100 km, as detailed in Table 2.3. It is considered that earthquake magnitudes of 6.0 and 7.0 provide a high margin of confidence level to evaluate results obtained from converted records of this study. Eleven sets of records per suite, as recommended in NBC 2015, for Site Class C (V_{S30} = 450 m/s) were considered. Therefore, a

total of 44 V/H PSA ratios were computed for each selected GMPE, as shown in Table 2.3. Eventually, for illustrative purposes, the proposed PSA ratios based on the GMPEs are presented in Table 2.4 and Figure 2.4, along with those obtained from the 248 sets of converted records.

Table 2.3 Considered M-R scenarios used for the selected GMPEs

M_w	R_{epi} (km)										
6.0	10	10.5	11	11.5	12	12.5	13	13.5	14	14.5	15
	20	21	22	23	24	25	26	27	28	29	30
7.0	15	16	17	18	19	20	21	22	23	24	25
	50	55	60	65	70	75	80	85	90	95	100

Table 2.4 Computed mean V/H PSA ratios at different periods from converted records and selected GMPEs

T (sec)	This study	Bozorgnia & Campbell (2004)	Gülerce & Abrahamson (2011)
0.01	0.82	0.77	0.72
0.02	0.86	0.82	0.72
0.03	0.85	0.87	0.84
0.04	0.770	0.93	0.96
0.05	0.74	0.98	1.04
0.075	0.73	0.99	1.02
0.10	0.76	0.88	0.89
0.15	0.83	0.70	0.74
0.20	0.82	0.58	0.65
0.26	0.84	0.52	0.56
0.30	0.85	0.48	0.53
0.40	0.83	0.46	0.49
0.50	0.85	0.43	0.47
0.75	0.86	0.42	0.50
1.0	0.84	0.44	0.54
1.5	0.80	0.45	0.57
2.0	0.80	0.51	0.60

3.0	0.80	0.53	0.62
4.0	0.82	0.50	0.65

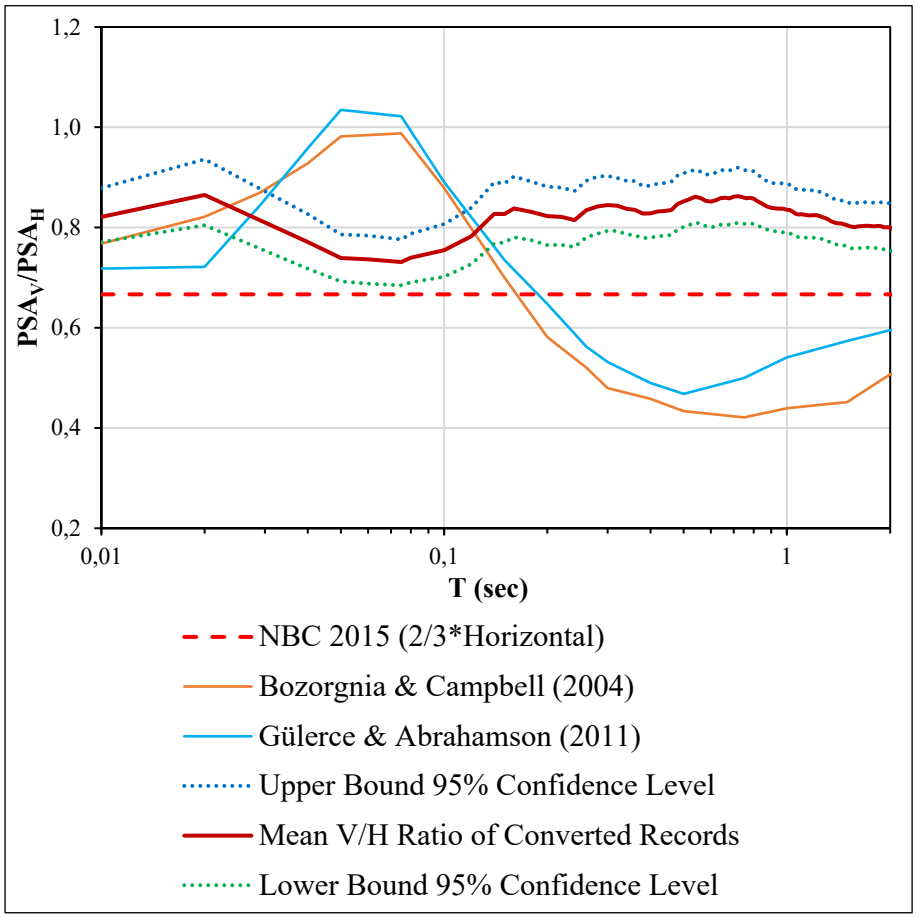

Figure 2.4 V/H PSA ratios from converted records and selected GMPEs for Site Class C

As shown in Table 2.4 and Figure 2.4, the values of V/H PSA ratios obtained from the GMPEs proposed by Bozorgnia and Campbell (2004) and Gülerce and Abrahamson (2011) are close, particularly in the short period range up to 0.5 sec. Both models yield an average ratio of 0.84, which is higher than 2/3, for short periods of less than 0.2 sec. Also, the conservative ratio of 0.90, including the sum of the average value and the standard deviation for the periods ranging up to 1.0 sec ($T \leq 1.0$ sec), is concluded, which is very close to the proposed one (0.86) in Section 2.3.3. On the other hand, lower ratios were obtained for periods greater than 1.0 sec.

Therefore, to determine the vertical design spectra, for T > 1.0 sec, it is recommended that the horizontal design spectra be scaled by the suggested ratio of 2/3 in the NBC.
Comparing the presented models' results with those obtained from the converted records shows the difference in the acceleration ratio in the period interval of 0.02 to 0.2 sec. Despite the reduction in the acceleration ratio of converted earthquakes, the increase was observed in the proposed equations (GMPEs), which could be due to the faults type or lack of sufficient strong near-field earthquakes in the region of this study.

2.5 Proposed Vertical Acceleration Design Spectra (ADS_{ver}) for Site Class C in Montreal

2.5.1 Using the converted records

In this section, the vertical acceleration design spectra (ADS_{ver}) corresponding to a 2475-year return period for Site Class C in Montreal are obtained according to the computed V/H PSA of concerted records. In this case, the vertical design spectral response acceleration for a period of T can be calculated by multiplying the horizontal acceleration design spectra ($S_{hor}(T)$) proposed in the National Building Code of Canada (NBC, 2015a; NRCAN, 2015) by the mean V/H PSA ratios computed in Section 2.3 at defined spectral periods, as given in Equation 2.5.

$$S_{ver}(\mathrm{T}) = \left(\frac{V}{H}\right) \times S_{hor}(T) \tag{2.5}$$

It should be noted that the design spectral response acceleration (S(T)) at a specified period is deduced from 5% damped spectral response acceleration for a period of T ($S_a(T)$), according to the procedure described in NBC 2015 as presented through Equation 2.6.

$$S(T) = F(T) \times \mathrm{S}_a(T) \tag{2.6}$$

Where F(T) is the site coefficient for spectral acceleration at each period determined in NBC 2015 for different site classes, that is equal to 1.0 at all periods for the reference Site Class C.

However, for a period less than 0.2 sec, S(T) = F(0.2) S_a(0.2) or F(0.5) S_a(0.5), whichever is larger.

It should be mentioned that the 5% damped horizontal spectral response acceleration for a period of T, $S_{a,hor}$(T) were given in NBC 2015 for different regions in Canada. First, the horizontal design response spectral acceleration, S_{hor}(T), for Site Class C in Montreal is computed using Equation 2.6, then the corresponding vertical design response spectral acceleration, S_{ver}(T), is obtained using Equation 2.5.

Since the computed mean V/H PSA ratios of the converted records exceeded the empirical ratio of 2/3 recommended in the NBC 2015 and most codes, it is concluded that the vertical component of ground motions at short periods is important for the Eastern Canada seismic region, especially at periods less than 1.0 sec. In total, from an engineering standpoint, it appears that for obtaining S_{ver}(T), there is no significant difference between NBC 2015 (2/3 × S_{hor}(T)) and the proposed spectra ((average of V/H + standard deviation) × S_{hor}(T)) for periods T ≥ 1.0 sec. Therefore, it is appropriate to suggest using S_{ver}(T) = 0.86 × S_{hor}(T) for T ≤ 1.0 sec and 0.67 otherwise for each location in the Eastern Canada seismic region.

The computed vertical acceleration design spectra, S_{ver}(T), using the proposed coefficient obtained from the V/H ratios converted records of this study and NBC 2015 (2/3 × S_{hor}(T)), were presented in Figure 2.5.

2.5.2 Using the equations proposed in ASCE/SEI 41-17 and ASCE/SEI 7-16

In order to develop the vertical and horizontal design spectra corresponding to the Risk-Targeted Maximum Considered Earthquake, MCE_R, the American Standards (ASCE/SEI 7-16, 2017; ASCE/SEI 41-17, 2017) propose a series of equations for different period ranges. In the absence of site-specific procedures, the Risk-Targeted Maximum Considered Earthquake of the vertical response spectral acceleration, S_{aMv}, is developed according to the vertical period as provided in the form of equations. The corresponding MCE_R vertical and horizontal

response spectra for these standards are presented in Tables 2.5 and 2.6, respectively. S_{MS} and S_{M1} are the maximum risk-targeted considered earthquake response spectral accelerations for the 5% damping ratio at short periods and at a period of 1.0 sec, respectively, and can be adjusted to account for different site classes. T_v is the vertical period, and C_v is the vertical coefficient defined in terms of S_S (Table 2.7) according to the spectral response parameters at short periods for different site classes. The values of the equivalent seismic parameters for Site Class C in Montreal are available in SEAOC and OSHPD Seismic Design Maps (SEAOC/OSHPD, 2019), as presented in Table 2.8. It should be noted that the DSA_{ver} considered for the nonlinear design range of the building in these standards is determined as 2/3 of the MCE_R of the elastic one (FEMA P-1050-1, 2015; ASCE/SEI 7-16, 2017).

The MCE_R for the vertical response spectral acceleration, S_{aMv}, in the first three equations is known for a short period and can be defined by the amplitude of the 5% damped vertical spectral acceleration at 0.1 sec and by the V/H spectral ratio. The first and third equations are controlled by the vertical peak ground acceleration (PGA_{ver}) and the short-period V/H spectral ratio at 0.1 sec, respectively. The second equation is the interface of the first and second period-dependent equations (Campbell & Bozorgnia, 2009; ASCE/SEI 7-16, 2017). The period domains of the V/H ratio are a function of the site condition and distance from the source of the earthquakes. The last part of the vertical elastic spectra, as defined in the fourth equation, is considered as the mid-period range and shows the decay of the spectrum inversely to the vertical period (Campbell & Bozorgnia, 2009; FEMA P-1050-1, 2015; ASCE/SEI 7-16, 2017).

Table 2.5 Vertical MCE_R elastic design spectra
Taken from FEMA P-1050-1 (2015) and ASCE/SEI 7-16 (2017)

Period Range	**Vertical (S_{aMv})**
$T_v \leq 0.025\ sec$	$0.3C_vS_{MS}$
$0.025 \leq T_v \leq 0.05\ sec$	$20C_vS_{MS}(T_v - 0.025) + 0.3C_vS_{MS}$
$0.05 \leq T_v \leq 0.15\ sec$	$0.8C_vS_{MS}$

$0.15 \leq T_v \leq 2.0\ sec$	$0.8C_vS_{MS}(0.15/T_v)^{0.75}$

Table 2.6 Horizontal MCE_R elastic design spectra
Taken from FEMA P-1050-1 (2015) and ASCE/SEI 7-16 (2017)

Period Range	Horizontal (S_{aMh})
$0 \leq T \leq T_0$	$[0.4 + 0.6 \times T/T_0] \times S_{MS}$
$T_0 \leq T \leq T_S$	S_{MS}
$T_S \leq T \leq T_L$	S_{M1}/T
$T \geq T_L$	$(S_{M1} \cdot T_L)/T^2$

Table 2.7 Values of vertical coefficient C_v
Taken from FEMA P-1050-1 (2015) and ASCE/SEI 7-16 (2017)

MCE_R Response Spectral Parameter at Short Periods	***Site Class***		
	A & B	***C***	***D & E & F***
$S_S \geq 2.0$	0.9	1.3	1.5
$S_S = 1.0$	0.9	1.1	1.3
$S_S = 0.6$	0.9	1.0	1.1
$S_S = 0.3$	0.8	0.8	0.9
$S_S \leq 0.2$	0.7	0.7	0.7

Table 2.8 Equivalent seismic parameters corresponding to Site Class C in Montreal
Taken from SEAOC/OSHPD (2019)

Codes	***S_S***	***S_1***	***F_a***	***F_v***	***S_{MS}***	***S_{M1}***	***T_0***	***T_S***	***T_L***	***C_v***
ASCE 7-16 & NEHRP 2015	0.418	0.099	1.3	1.5	0.543	0.149	0.055	0.273	6.0	0.879
ASCE 41-17	0.453	0.107	1.3	1.5	0.589	0.161	0.055	0.273	6.0	0.902

The horizontal and vertical design spectra with a 2% probability of exceedance in 50 years were computed for Site Class C in Montreal based on the equations given in ASCE 7-16 and ASCE 41-17 using equivalent parameters, as illustrated in Figure 2.5.

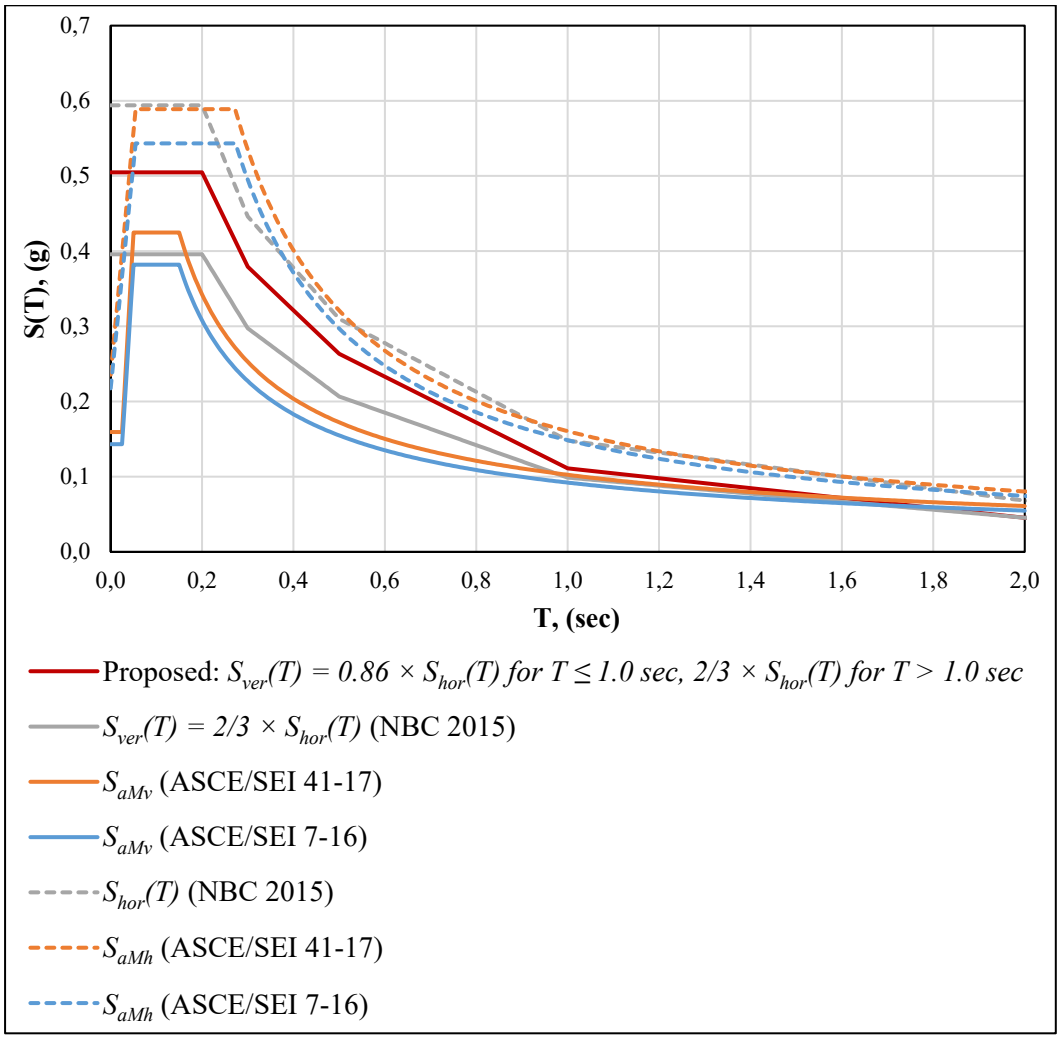

Figure 2.5 Proposed $S_{ver}(T)$ and calculated Vertical Acceleration Design Spectra based on ASCE/SEI 41-17, ASCE/SEI 7-16 (S_{aM}), and NBC 2015 for Site Class C in Montreal

As shown in Figure 2.5, the proposed vertical design spectra obtained from the converted records of this study yielded higher values than those obtained from the American Standards and even from NBC 2015 (2/3 $S_{hor}(T)$).

Comparing the NBC 2015 ADS_{hor} to those obtained using ASCE/SEI 41-17 standard (Figure 2.5), a close resemblance could be observed mainly at longer periods, greater than 1.0 sec (Figure 2.5). Nevertheless, spectral acceleration values higher than 2/3 of the horizontal values are observed at period ranges of 0.05 to 0.2 sec in ASCE/SEI 41-17. On the other hand, values yielded by ASCE/SEI 41-17 are higher than NBC values for periods less than 0.15 sec.

2.6 Summary and conclusion

This paper constitutes an effort to develop an accurate estimate of the vertical acceleration design spectra (ADS_{ver}) as a ratio of the horizontal acceleration design spectra, using a database of 248 records of earthquakes in Eastern Canada (for years from 1982 to 2015). These records were selected for moderate earthquakes with magnitude M_w ranging between 3.0 and 5.9 and an epicentral distance of less than 150 km. Due to the lack of earthquakes recorded on reference Site Class C of NBC, the selected records, mostly recorded on Site Class A, were converted to Site Class C using the equivalent linear method of analysis based on Frequency Domain Solution (Hashash et al., 2019) proposed in the DEEPSOIL software. In the conversion process, the automatic profile generation based on the target shear wave velocity of 450 m/s was used due to the unavailable specific soil characteristics of the sites.

The calculated V/H PSA ratios exceeded the empirical ratio of 2/3, suggested in most codes, at all period ranges, which spotlights the importance of considering the vertical component of ground motions in the seismic analysis of non-structural components located in the Eastern Canada region. The accuracy of V/H PSA ratios for records converted to Site Class C was validated by ratios obtained from the small number of earthquakes records available for Site Class C (19 sets of records). The same ratio of 0.86 (average of V/H + Standard Deviation) was obtained in both cases for the periods up to 1.0 sec ($T \leq 1.0$ sec). These findings were corroborated with ratios (0.84) obtained using the GMPEs proposed by Bozorgnia and Campbell (2004) and Gülerce & Abrahamson (2011). For the periods greater than 1.0 sec (T

> 1.0 sec), this value reaches the average ratio of 0.73, considered very close to the empirical value of 2/3. On the other hand, the average equivalent ratio for this period range (T > 1.0 sec) using the selected GMPEs yields a value less than 2/3 (0.53 and 0.64 for the models by Bozorgnia and Campbell (2004) and Gülerce & Abrahamson (2011), respectively), that is why a ratio of 2/3 is suggested. Therefore, it was concluded that obtaining ADS_{ver}, by scaling the $S_{hor}(T)$ using the ratio of 2/3 ($2/3 \times S_{hor}(T)$) is appropriate for periods T > 1.0 sec. On the other hand, it is proposed to use a ratio of 0.86 to determine the vertical design spectra ($S_{ver}(T) = 0.86 \times S_{hor}(T)$) for $T \leq 1.0$.

Furthermore, the proposed vertical acceleration design spectra (ADS_{ver} or $S_{ver}(T)$) for Site Class C in Montreal at a 2475-year return period were compared with spectra derived using the equations proposed by the ASCE 7-16 and ASCE 41-17 standards. While ADS_{hor} ($S_{hor}(T)$) values of NBC 2015 are very close to (S_{aMh}) values obtained from ASCE/SEI 41-17 (Figure 2.5) at all period ranges, derived ADS_{ver} ($S_{ver}(T)$) from the ratios proposed in this study yield higher values than the aforementioned standards, especially for the shorter periods (Figure 2.5). Therefore, the outcomes of this study through the analysis done for the earthquakes in the Eastern Canada seismic region allowed a reliable derivation of vertical acceleration design spectra and highlighted the importance of considering the vertical component in the seismic design process.

CHAPITRE 3

ESTIMATION OF VERTICAL PEAK FLOOR ACCELERATION DEMANDS IN ELASTIC RC MOMENT-RESISTING FRAME BUILDINGS

Shahabaldin Mazloom[a] and Rola Assi[b]

[a, b] Department of Construction Engineering, École de Technologie Supérieure,
1100 Notre-Dame West, Montreal, Quebec, Canada H3C 1K3

Paper published in *Journal of Earthquake Engineering*[2], November 2022

Abstract

This paper assesses the vertical seismic accelerations in four 3-D elastic RC moment-resisting frame buildings with limited ductility, designed according to the National Building Code of Canada (NBC 2015). 65 near-fault strong motions recorded on dense soil were considered. The greatest amount of amplification of vertical acceleration was observed at the center of the buildings' interior slab, with maximum median normalized values ranging from 4.0, in the 3-storey building, to 1.24, in the 12-storey building. This study indicates that the vertical earthquake motion should not be overlooked in the analysis and design process, especially in low-rise buildings.

Keywords: Non-Structural Component (NSC), vertical Peak Floor Acceleration (PFA_V), vertical Peak Ground Acceleration (PGA_V), amplification of acceleration, reinforced concrete (RC) moment-resisting frame system

---

[2] Mazloom, S., & Assi, R. (2022). Estimation of the Vertical Peak Floor Acceleration Demands in Linear Elastic RC Moment-Resisting Frame Buildings. Journal of Earthquake Engineering. DOI: https://doi.org/10.1080/13632469.2022.2148018

3.1 Introduction

Reports from recent earthquakes, such as the 1994 M_w 6.7 Northridge earthquake, indicate that structural elements and floor systems failures and damage to non-structural components (NSCs) are triggered by the vertical component of ground motion. In contrast, there was minor damage reported in association with the lateral resisting system of buildings exposed to the horizontal components of the same ground motions (Papazoglou & Elnashai, 1996). The 1988 M_w 5.9 Saguenay earthquake is an example of an event in Eastern Canada that caused considerable damage to NSCs (Foo & Lau, 2004).

While most codes and standards, such as ASCE/SEI 7-16 (ASCE/SEI 7-16, 2017), ATC 2018 (ATC, 2018), and Eurocode 8-1 (Eurocode 8-1, 2004), propose certain relationships to compute vertical seismic design accelerations, others such as NBC 2015 (NBC, 2015a) in Canada only propose a constant empirical value of 2/3 to relate vertical-to-horizontal (V/H) accelerations. Therefore, the vertical seismic force of NSCs in NBC 2015 is based on the codified constant V/H acceleration ratio, leading to an inaccurate evaluation of their response in the case of near-fault site conditions (Asgarian, 2017; Assi et al., 2017).

Generally, the horizontal seismic forces for NSCs are estimated by considering three key parameters: ground motions applied to the base of the building, dynamic amplification due to the resonance between the supporting structure and NSCs, and the height factor related to the filtering and amplification of input ground motion through the building height. The latter parameter is based on the linearly increasing acceleration over the height of the structure (NBC, 2015a).

The vertical component of ground motions usually has high-frequency content, which leads to the induction of very high fundamental vertical frequencies in the vertical direction (Papadopoulou, 1989). Meanwhile, reinforced concrete structures are characterized by a high stiffness in the vertical direction as their vertical period typically ranges from 0.05 sec to 0.25

sec (Dana et al., 2014). Therefore, considering the out-of-plane floor flexibility could lead to the resonance and to a significant amplification of structural and non-structural components when the fundamental vertical frequencies of the structures are in the range of the vertical pulses of ground motions (Papazoglou & Elnashai, 1996; Lee et al., 2013). In fact, the flexibility of the slab and, consequently, its out-of-plane floor vibrations are generally the main factors contributing to the vertical amplification of floor accelerations. Moreover, floor accelerations are present at locations varying from areas close to columns to those at the center of the slab (Furukawa et al., 2013), a fact which is currently overlooked in design codes. A study by Bozorgnia et al. (1998) conducted on instrumented RC buildings during the 1994 Northridge earthquake showed an amplification of vertical accelerations ranging from 2.4 to 4.7 for the nodes close to the shear wall edges and for nodes at the center of the slabs, respectively.

Several researchers have recently focused on investigating the amplification of vertical ground motion through the building floor system, including slabs and girders (Papadopoulou, 1989; Pekcan et al., 2003; Wieser et al., 2012; Guzman Pujols & Ryan, 2018). Floor systems, including slabs, beams, or other horizontal and cantilever elements, can be affected by amplified vertical accelerations, which lead to an increase in the shear force or moment of the elements (Newmark & Hall, 1982).

A study by Pekcan et al. (2003) indicated that the elastic vertical floor response spectra in two RC buildings with flexible floor systems are affected by the out-of-plane flexibility of the slab as the maximum response was obtained at around 7.0 to 10 Hz (0.1 to 0.14 sec). Furthermore, results demonstrated that the peak vertical floor accelerations could be amplified by as much as five times the vertical peak ground acceleration and often greater than the horizontal peak floor acceleration in buildings subjected to near-field ground motions.

Moreover, an analytical study by Moschen et al. (2015) conducted on regular steel moment-resisting frames ranging from 1 to 21-storeys, subjected to recorded near-fault and strong

ground motions, concluded that vertical acceleration is amplified through the height of buildings away from the columns. An assessment of the amplification of vertical peak floor accelerations for mounted rigid NSCs indicated that elements located at open bays, i.e., at locations away from columns and relatively close to girders or at the center of slabs, are subjected to vertical acceleration that could reach four times the acceleration of elements located close to the columns. In addition, the out-of-plane flexibility of the floor systems caused a significant amplification of the floor response spectra demands for NSCs located at the center of the slab. Therefore, vertical floor accelerations are highly influenced by the component's location on a specific floor, the element's location along the height of the building, and the characteristics of the floor system (Moschen, 2016).

Similarly, Wieser et al. (2012) investigated the influence of the relative height within the building and the out-of-plane flexibility of the floor system on the vertical acceleration demands on NSCs. A 3-storey hospital building and three office buildings consisting of 3, 9, and 20 storeys with steel moment-resisting frame systems were used in the study. An elastic behavior was assumed for the floor decks and steel frames, while fiber sections were used to model the nonlinearity in the beam-column connection. Notwithstanding the constant and unchanged acceleration in the columns' joints, a significant vertical acceleration amplification was observed away from the column supports due to the out-of-plane flexibility of the floor system, in which the amplification of the vertical acceleration for the selected 3-storey building exceeded the value of 2.0 at the center of the slab bays.

In this context, an experimental test was conducted by Ryan et al. (2016) to assess the amplification of peak vertical accelerations in a 5-storey steel moment frame building. It was shown that the amplification ranged from approximately 3.0, near the column, to 6.0, at the center of the slab bay, highlighting the significant amplification at the center of the slab away from the column. Also, the amplification factor rose by increasing the period of vibration of the slab. The current design procedure for NSCs presented in the seismic design codes is thus inappropriate to accurately assess the amplification of vertical floor accelerations.

Additionally, Bas et al. (2016) noted a significant vertical displacement of the beams mainly at the top storeys of structures subjected to strong earthquakes, such as the 1979 M_w 6.5 Imperial Valley, 1995 M_w 6.9 Kobe, and 1999 M_w 7.6 Kocaeli earthquakes, which indicates that the out-of-plane deformation of the slab is must not be neglected in the presence of the vertical component of a ground motion.

The present study aims to investigate the effects of building height and location of the mounted NSCs, in floor plan along the height of the building, on the amplification of a vertical earthquake component. Therefore, four low- to medium-rise RC frame buildings with 3, 6, 9, and 12 storeys were designed according to the National Building Code of Canada (NBC, 2015a) and CSA-A23.3-14 (CSA-A23.3, 2014) provisions. The buildings were supposed to be located in Montreal, which is a moderate seismic zone; therefore, they were designed for seismic forces corresponding to a limited ductility. The buildings were subjected to 65 sets of time history accelerations recorded on Site Class C from 31 strong near-field earthquakes worldwide. To this end, different nodes on the floors were considered, and the corresponding normalized vertical Peak Floor Acceleration (PFA_V) profile and the vertical-to-horizontal (PFA_V/PFA_H) ratio were drawn for each node. The Peak Floor Acceleration (PFA) demand to Peak Ground Acceleration (PGA) ratio is referred to as the normalized Peak Floor Acceleration.

3.2 General assumptions of the study

3.2.1 Description of selected archetype buildings

In this study, 3, 6, 9, and 12-storey archetype reinforced concrete office buildings with moderately ductile moment-resisting frame systems were designed according to current provision of the NBC (NBC, 2015a) and CSA-A23.3-14 (CSA-A23.3, 2014) standard, with an overstrength force modification factor, R_o, equal to 1.4 and a ductility-related force modification factor, R_d, equal to 2.5. A regular symmetrical plan with three-by-three 7.0 m

spans in each direction, a finished typical floor height of 3.0 m, and a 140 mm RC slab floor system were considered for all the buildings, as shown in the elevation and plan views in Figure 3.1. The selected buildings were supposed to be located in Montreal on very dense soil known as Site Class C according to the soil classification and criteria specified in NBC 2015, with an average shear wave velocity between 360 and 760 m/sec. The Montreal uniform hazard spectrum corresponding to Site Class C, with a 2475 return period at a 5% damping ratio, was used to design the buildings.

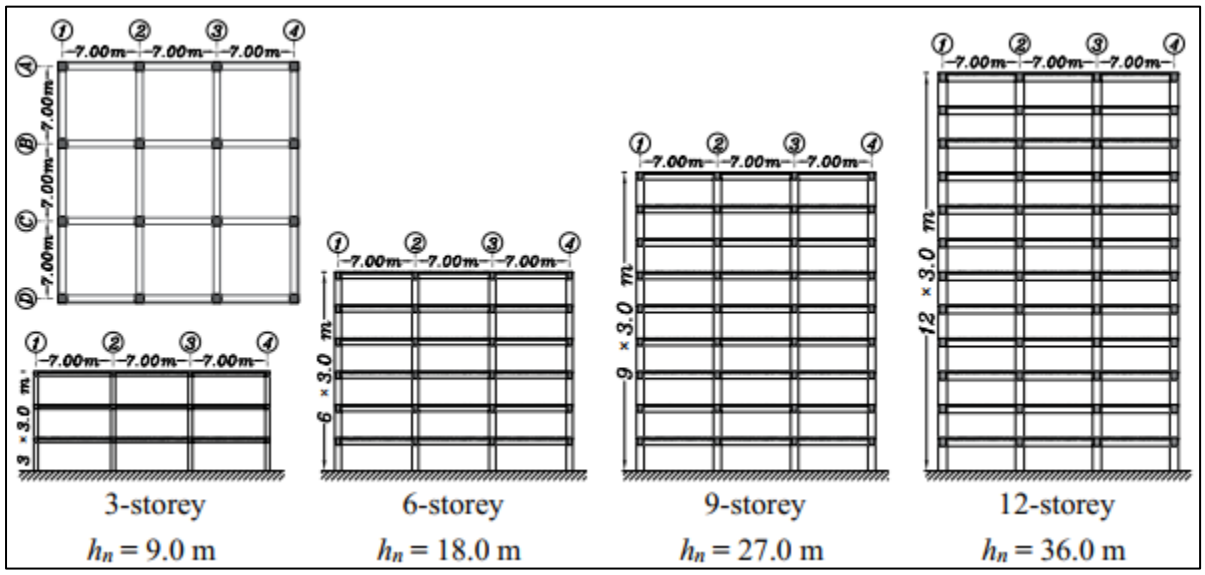

Figure 3.1 Plan and elevation views of the archetype RC moment-resisting frame buildings used in this study

The input information, including material properties and the gravity load types of the different floors, are presented in Tables 3.1 and 3.2, respectively. 3D finite element models of the buildings were generated using the ETABS software (CSI, 2017). The diaphragm on all floors was modelled using 500 × 500 mm meshes with finite element shells to account for their in-plane stiffness in the horizontal direction and out-of-plane flexibility in the vertical direction. For all the models, classical Rayleigh damping with a ratio of 5%, which is applicable for RC buildings, was considered. This value is generally assigned to the fundamental mode and to

the higher modes where the total effective mass participation is over 95%. For the vertical direction, a damping ratio of 5% was also considered.

Table 3.1 Material properties of the selected buildings

Material	Material Parameter	Values Used	Units
Concrete	Mean compressive strength, f_{cm}	35	N/mm^2
	Weight per unit volume, W_c	24	kN/m^3
	Modulus of elasticity, E_c	30.5	kN/mm^2
	Crushing strain, ε_c	0.003	----
Steel	Yield strength, f_y	400	N/mm^2
	Ultimate strength, f_u	440	N/mm^2
	Young's modulus, E_s	200	kN/mm^2
	Ultimate strain, ε_{su}	0.002	----

Table 3.2 Load types and values used for the buildings design

Load Type	$W_{Roof\ Finishing}$	$W_{Floors\ Finishing}$	$W_{mechanical}$	$W_{Partitions}$	$W_{L,\ Roof}$	$W_{L,\ Floors}$	W_{Snow}	$W_{Ext.walls}$
Amount (kPa)	0.7	0.5	0.5	1.0	1.0	2.4	2.48	1.2 kN/m

All elements were modelled with the effective stiffness, EI_{eff}, as a fraction of the gross stiffness, EI_g, as suggested in CSA-A23.3-14, with modifiers equal to 0.40, 0.70, and 0.20 for the beams, columns, and slabs, respectively. The obtained optimum cross-sectional dimensions (in mm) of the structural elements are presented in Tables 3.3 and A II-1 to A II-16 in Appendix II.

Table 3.3 Cross-sectional dimensions of the buildings' elements

Structure Reference	Columns		Beams (b×h)	
	Internal	External	X-direction	Y-direction
3-storey	400×400	400×400	350×400	350×400
6-storey	600×600	600×600	400×600	400×600
9-storey	700×700	700×700	500×650	500×650

12-storey	800×800	800×800	600×750	600×750

As shown in Table 3.4, the buildings' fundamental lateral periods, resulting from modal analysis, increase with the number of floors or height of the building. Their values are greater than those obtained using the NBC equations for low-rise buildings (3- and 6-storey), while they exceed the NBC values for medium-rise buildings (9- and 12-storey). In contrast, the variation in the vertical period is very negligible. Therefore, it can be concluded that the vertical period for RC moment frame buildings is a function of the floor system type, i.e., slabs and beams, rather than the number of storeys, which complies with observations resulting from the studies conducted by Papazoglou & Elnashai (1996) and Lee et al. (2013).

Table 3.4 Fundamental horizontal and vertical periods of the buildings

Building	**NBCC 2015:** $T_a = 1.5 \times 0.075(h_n)^{3/4}$	T_h	T_V
	(sec)	**(sec)**	**(sec)**
3-Storey	0.59	0.87	0.31
6-Storey	0.98	0.97	0.30
9-Storey	1.33	1.23	0.30
12-Storey	1.65	1.32	0.29

The lateral and vertical mode shapes for the exterior frame of the buildings are shown in Figures 3.2.(a) and 4.2.(b), respectively. Obtained results indicate that the slab response due to vertical vibration is mainly dominated by a single vertical mode on rooftops, which is similar to the results obtained by Pujols & Ryan's (2018) experimental tests performed on a 5-storey steel moment-resisting frame structure.

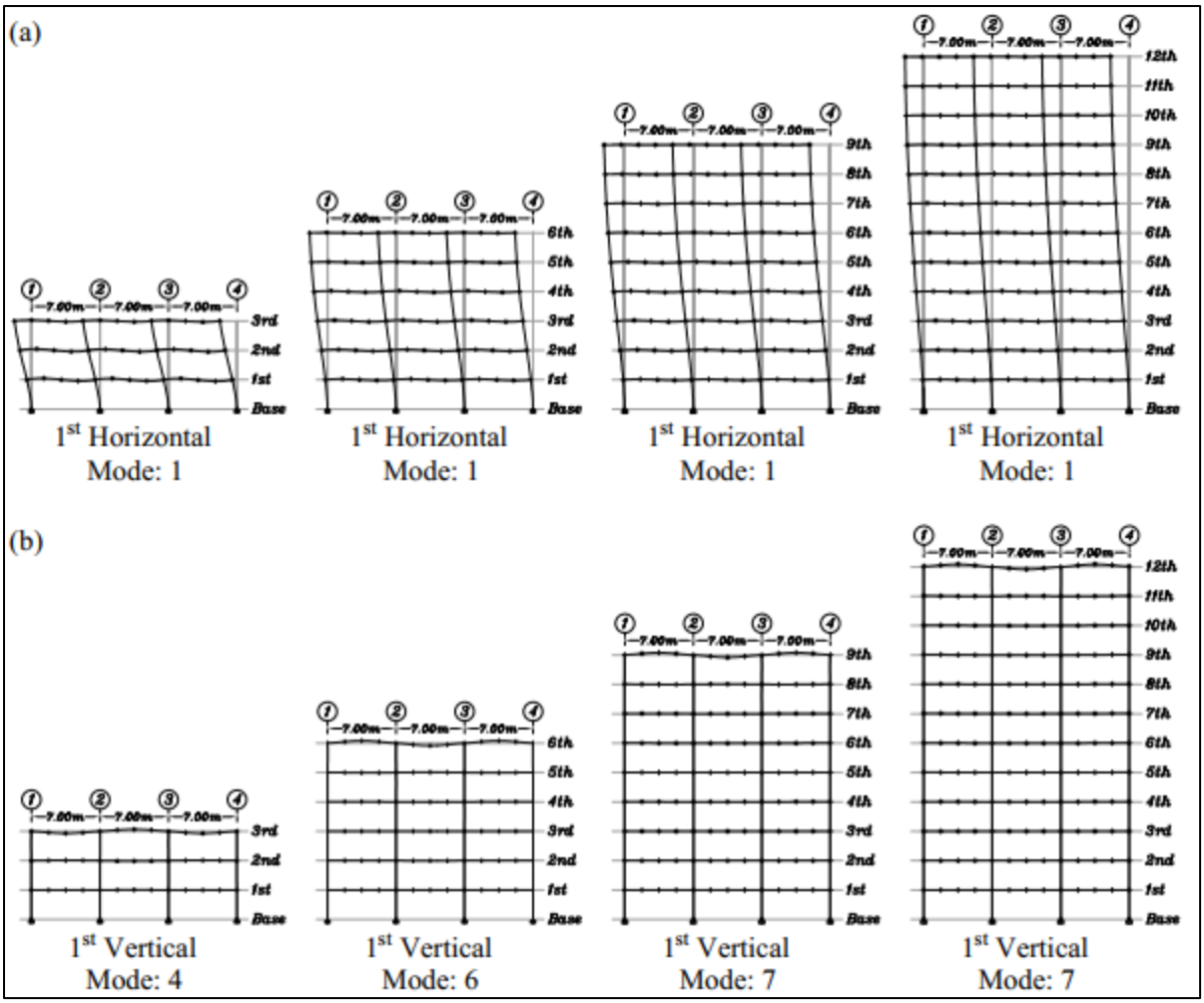

Figure 3.2 Fundamental lateral and first vertical mode shapes of the exterior frames

3.2.2 Selection of input ground motions

A suite of 65 sets of ground motions resulting from 31 strong near-field earthquakes that occurred worldwide was selected according to the following criteria:

- Earthquake magnitude, M_W, greater than 5.5 ($5.5 < M_W < 8.0$);
- Recorded at Site Class C ($360 \text{ m/s} \leq V_{S30} \leq 760 \text{ m/s}$);
- Distance to the fault is less than 25 km ($0.0 < R_{rup} < 25$ km) (near-field);
- Peak ground vertical acceleration (PGA_{ver}) is greater than 0.25 g ($PGA_{ver} > 0.25$ g);

- Fault mechanism (FM): Strike-Slip (SS), Reverse (RV), Reverse Oblique (RVO), Normal (N), Normal Oblique (NO).

The horizontal and vertical time history records retrieved from the Pacific Earthquake Engineering Research Center website (PEER-NGA, 2018) are presented in Table-A V-1 (Appendix III).

Each set of records consists of three orthogonal components, two in the horizontal direction and one in the vertical direction. Since two horizontal acceleration records are available for each set, the horizontal components' geometric mean is used to get a single horizontal Peak Ground Acceleration (PGA_{hor}), as shown in Equation 3.1. In this equation, H_1 and H_2 correspond to the two orthogonal directions of the horizontal PGA components:

$$PGA_{hor} = \sqrt{PGA_{H1} \times PGA_{H2}} \tag{3.1}$$

This method was recommended in ASCE/SEI 7-16 (2017) and by several researchers (Acerra et al., 2004; Picozzi et al., 2005; Campbell & Bozorgnia, 2007; Haghshenas et al., 2008; Stewart et al., 2011; Albarello & Lunedei, 2013; NBC, 2015b). Since the correlated horizontal ground motion records have one rotation angle equal to or close to zero, the maximum value may not be a strong function of the component correlation form. On the other hand, the minimum horizontal spectral values could occur over a limited range of the rotation angles and will be a strong function of the correlation form. Thus, any fractal measurement represented by the geometric mean value could be closer to the maximum than to the minimum value (Boore et al., 2006).

The corresponding acceleration response spectra for both horizontal and vertical components of the selected seismic records are shown in Figure 3.3, where the gray curves represent the Pseudo-Spectral Acceleration (PSA) for each single record, and the red curves shown are the

median spectra. Also, the 16th and 84th percentiles of the spectra are represented in dashed line curves, individually.

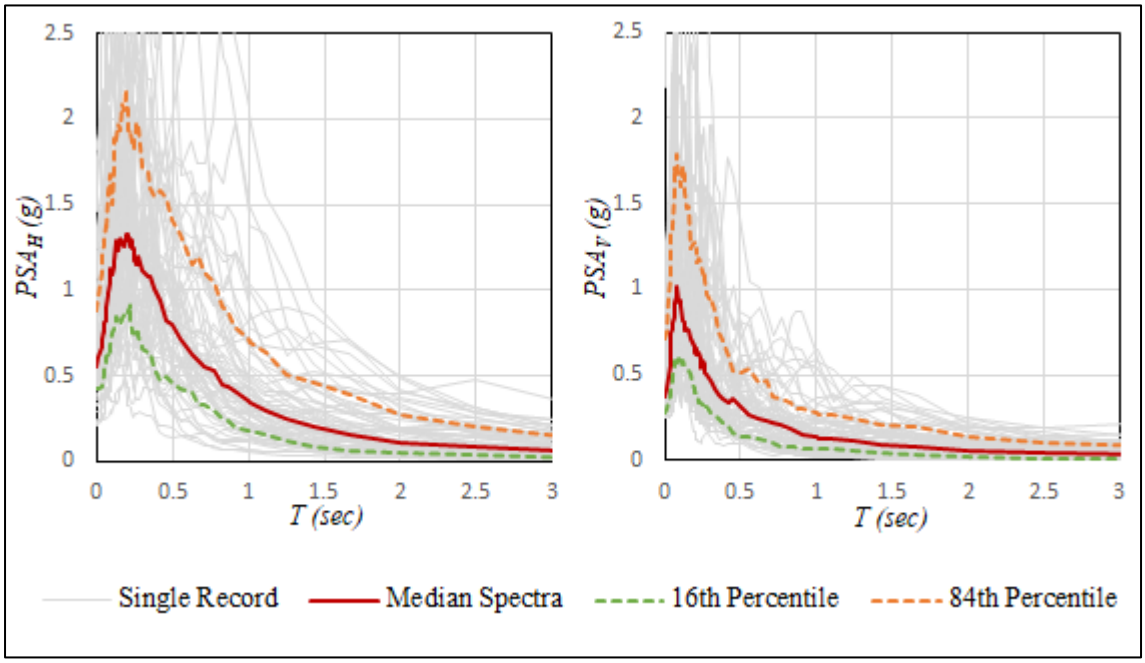

Figure 3.3 Pseudo-Spectral Acceleration of the horizontal and vertical seismic motion records with 5% damping ratio

3.3 Parametric study and discussion of the obtained results

To investigate the effects of building filtering on the amplification of the vertical earthquake component, as compared to the horizontal component and compute the PFA_V/PFA_H ratio, the archetype buildings were subjected to the time history acceleration records described in the previous sections. A series of critical nodes were considered on the beams and slabs of the RC floor system at all floor elevations, as illustrated in Figure 3.4. Specifically, the nodes were selected at the center of the slabs (S_1, S_2, and S_3) and the at the middle and quarter point of the beam spans (B_L, B_M, and B_R).

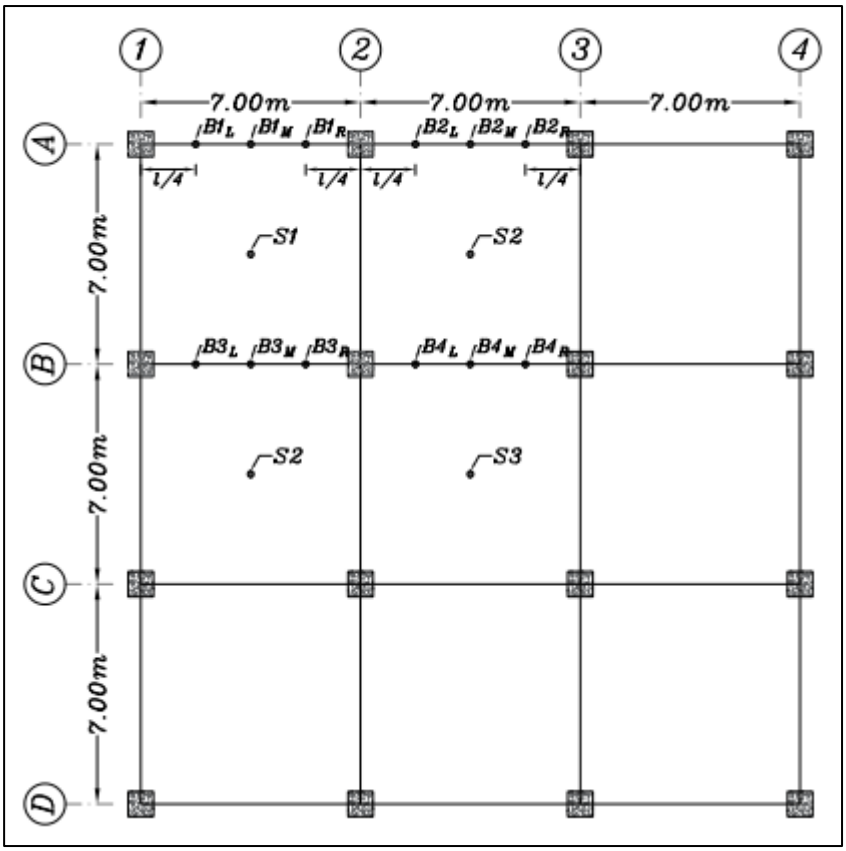

Figure 3.4 Selected critical nodes on the beams and slabs

3.3.1 Effect of location and height variation on amplification of PFA

In this section, the amplification or attenuation of the horizontal and vertical PFA through the height of each building was investigated separately. Individual, median, 16th, and 84th percentile results are shown in Figures 3.5 to 3.12. Since diaphragms above ground level are rigid in the horizontal direction, a single horizontal peak floor acceleration value can be concluded for all nodes of a typical floor.

3.3.1.1 Normalized Horizontal Peak Floor Acceleration profiles

The normalized horizontal Peak Floor Acceleration profiles, PFA_H, along each building height are presented in Figure 3.5. The gray lines represent the results of the 65 pairs of horizontal components computed as the geometric mean values. The bold and dashed lines constitute the computed median, 16th, and 84th percentile values. In addition, the obtained median normalized PFA_H values and their corresponding 84th percentile values (median + standard deviation) are presented in Table 3.5 for the selected buildings.

As presented in Figure 3.5.(a), a linearly increasing median PFA_H was obtained for the 3-storey building, with an amplification of 40% at the rooftop. The median normalized PFA_H profile for the 6-, 9-, and 12-storey buildings presented in Figures 3.5.(b), 3.5.(c), and 3.5.(d) display an oscillating wave with no amplification along the height, except at the rooftop, where a 44%, 40%, and 34% amplification was respectively obtained.

The obtained results were compared to recommendations provided in NBC 2015 and ASCE/SEI 7-16 (2017), as given in Equation 3.2. This equation shows a linear relationship proportional to the location of the component, h_x, relative to the height of the structure, h_n, with a maximum value of 3.0 at the rooftop.

$$A_x = 1 + 2h_x/h_n \tag{3.2}$$

On the other hand, the results were also compared to the Applied Technology Council (ATC, 2018) provision based on observations from instrumented buildings, as given in Equation 3.3.

$$\frac{PFA_H}{PGA_H} = 1 + \min\left\{1/T_a, 2.5\right\}.\left(h_x/h_n\right) + max\left\{\left[1 - \left(0.4/T_a\right)^2\right], 0\right\}.\left(h_x/h_n\right)^{10} \tag{3.3}$$

where T_a is the fundamental period of the building, which is computed from Equation 3.4 specified in the ASCE/SEI 7-16 (2017).

$$T_a = C_t h_n^x \tag{3.4}$$

Values of 0.0466 and 0.9 are assumed for the coefficients C_t and x, respectively, in the RC moment-resisting frame buildings.

In general, NBC 2015, ASCE/SEI 7-16, and ATC 2018 yield overly conservative results, especially for low-rise buildings. However, the results of the NBC 2015 and ASCE/SEI 7-16 show a linear and constant amplification for all buildings. Compared to the results of this study, it can be concluded that the amplification profiles of NBC 2015 and ASCE/SEI 7-16, shown in Figure 3.5, are exaggerated, especially for the mid-rise buildings. On the other hand, it can be seen that the ATC 2018 gives more reasonable results than the other mentioned codes, especially for mid-rise buildings. However, it still gave a very conservative result for the 3-storey building, even as compared to NBC 2015 and ASCE/SEI 7-16 (2017). The ATC 2018 profile almost coincides with the results obtained for mid-rise buildings, and is relatively conservative on the upper floors, while ASCE/SEI 7-16 and NBC 2015 show excessive results for all floor levels.

In view of the above results, an amplification profile which linearly increases from 1.0 at the ground level to 1.5 at the floor before the rooftop was proposed, and then a constant factor of 2.0 at the buildings' rooftops was deemed adequate, covering the 84th percentile values. To this end, the relationship presented in Equation 3.5 can be provided:

$$A_x = \begin{cases} 1 + 0.5\dfrac{h_x}{h_{n-1}}, & 0 \le x \le n-1 \\ 2, & Rooftop \end{cases} \tag{3.5}$$

where n is the number of the building floors, h_x is the height from above the base to level x, and h_n is the total height of the building.

Table 3.5 Computed median and 84th percentile values of normalized PFA_H of the building nodes

Normalized Height	3-storey Median Value	3-storey 84th Percentile
1.00	1.37	2.17
0.67	1.17	1.59
0.33	1.01	1.36
0.00	1	1

Normalized Height	6-storey Median Value	6-storey 84th Percentile
1.00	1.44	1.97
0.83	0.80	1.45
0.67	0.84	1.23
0.50	1.09	1.43
0.33	0.97	1.24
0.17	0.78	0.90
0.00	1	1

Normalized Height	9-storey Median Value	9-storey 84th Percentile
1.00	1.40	2.03
0.89	0.83	1.46
0.78	0.80	1.21
0.67	0.94	1.33
0.56	0.89	1.36
0.44	0.94	1.35
0.33	1.03	1.36
0.22	0.94	1.14
0.11	0.82	0.91
0.00	1	1

Normalized Height	12-storey Median Value	12-storey 84th Percentile
1.00	1.34	1.81
0.92	0.96	1.50
0.83	0.65	1.14
0.75	0.76	1.10
0.67	0.87	1.19
0.58	0.88	1.20
0.50	0.78	1.16
0.42	0.85	1.15
0.33	0.98	1.22
0.25	0.98	1.13
0.17	0.80	0.97
0.08	0.84	0.92
0.00	1	1

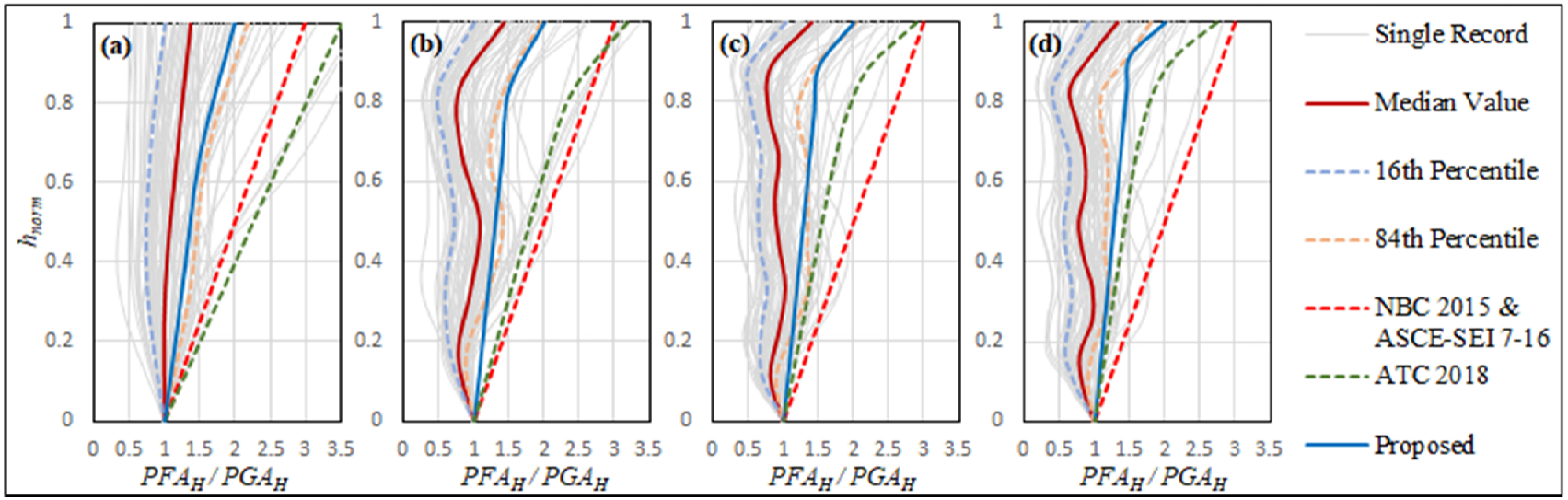

Figure 3.5 Proposed profiles of the normalized PFA_H at all nodes of the floor in (a) 3-storey, (b) 6-storey, (c) 9-storey, and (d) 12-storey buildings

3.3.1.2 Normalized Vertical Peak Floor Acceleration profiles

The following sections will discuss the median and 84th percentile values of the normalized PFA_V profiles for each building at selected nodes.

3.3.1.2.1 The 3-storey building

A significant acceleration amplification through the height was observed at the slab nodes (Table 3.6 and Figure 3.6), especially at the center of the interior slab, S3, where a rooftop amplification of 5.8 (84th percentile) was reached, almost twice the value obtained at node S1 (2.81). The acceleration amplification increases linearly until the first floor, and then remains almost constant up to the rooftop.

Table 3.5 Normalized median and 84th percentile PFA_V values at slab nodes of the 3-storey building

Normalized Height	S1		S2		S3	
	Median Value	84th Percentile	Median Value	84th Percentile	Median Value	84th Percentile
1.00	2.18	2.81	2.73	3.70	3.96	5.82
0.67	2.34	2.97	2.80	3.79	4.45	5.79
0.33	2.23	2.91	2.78	3.72	4.22	5.66
0.00	1	1	1	1	1	1

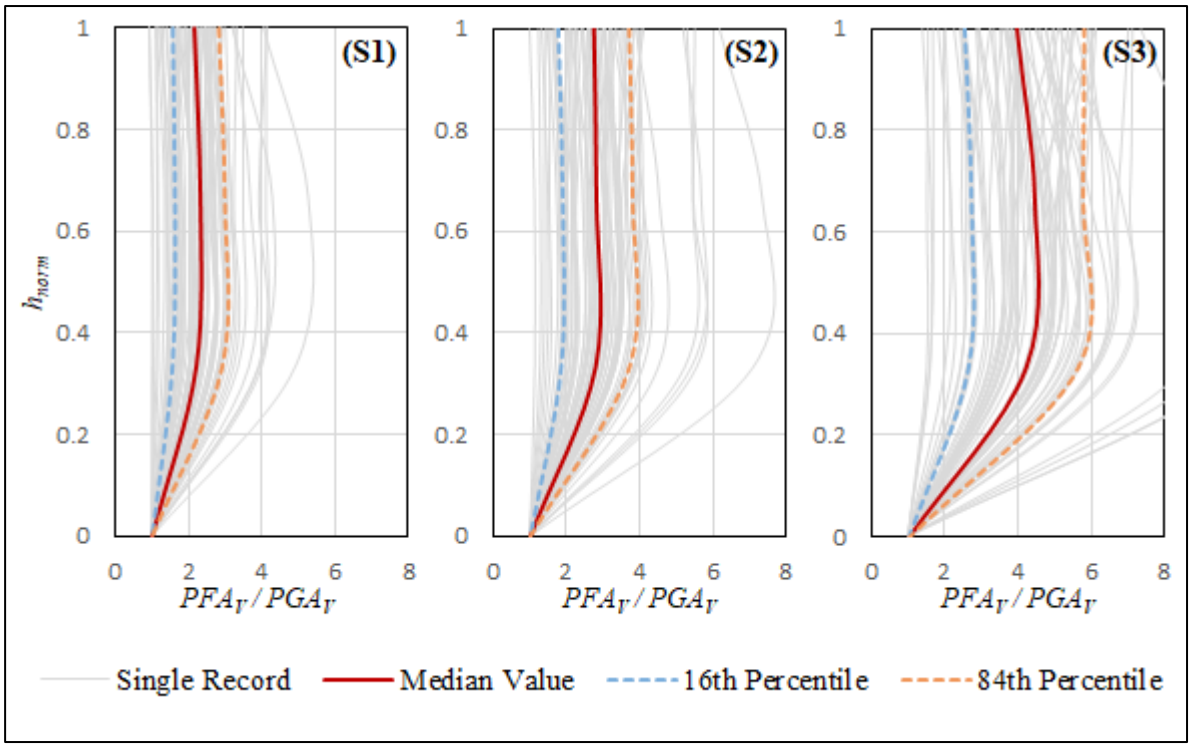

Figure 3.6 Profiles of the normalized PFAV at the center of the slabs of the 3-storey building

As for the considered nodes for the beams, shown in Figure 3.7, a slight amplification based on the computed 84th percentile PFAV was observed at nodes of beam B4 (B4$_L$, B4$_M$, and M4$_R$) and at the middle of beam B3 (B3$_M$), while the other beam nodes were not subjected to acceleration amplification (Table 3.7).

Table 3.6 Normalized median and 84th percentile PFA$_V$ values at beam nodes of the 3-storey building

Normalized Height	$B3_L$		$B3_M$		$B3_R$	
	Median Value	84th Percentile	Median Value	84th Percentile	Median Value	84th Percentile
1.00	0.81	1.02	0.87	1.20	0.81	0.94
0.67	0.84	1.00	0.94	1.19	0.84	1.02
0.33	0.83	1.00	0.89	1.15	0.84	1.00
0.00	1	1	1	1	1	1

Normalized Height	$B4_L$		$B4_M$		$B4_R$	
	Median Value	84th Percentile	Median Value	84th Percentile	Median Value	84th Percentile
1.00	0.94	1.23	1.23	1.69	0.94	1.23
0.67	0.89	1.13	1.24	1.56	0.89	1.13
0.33	0.92	1.12	1.17	1.54	0.92	1.12
0.00	1	1	1	1	1	1

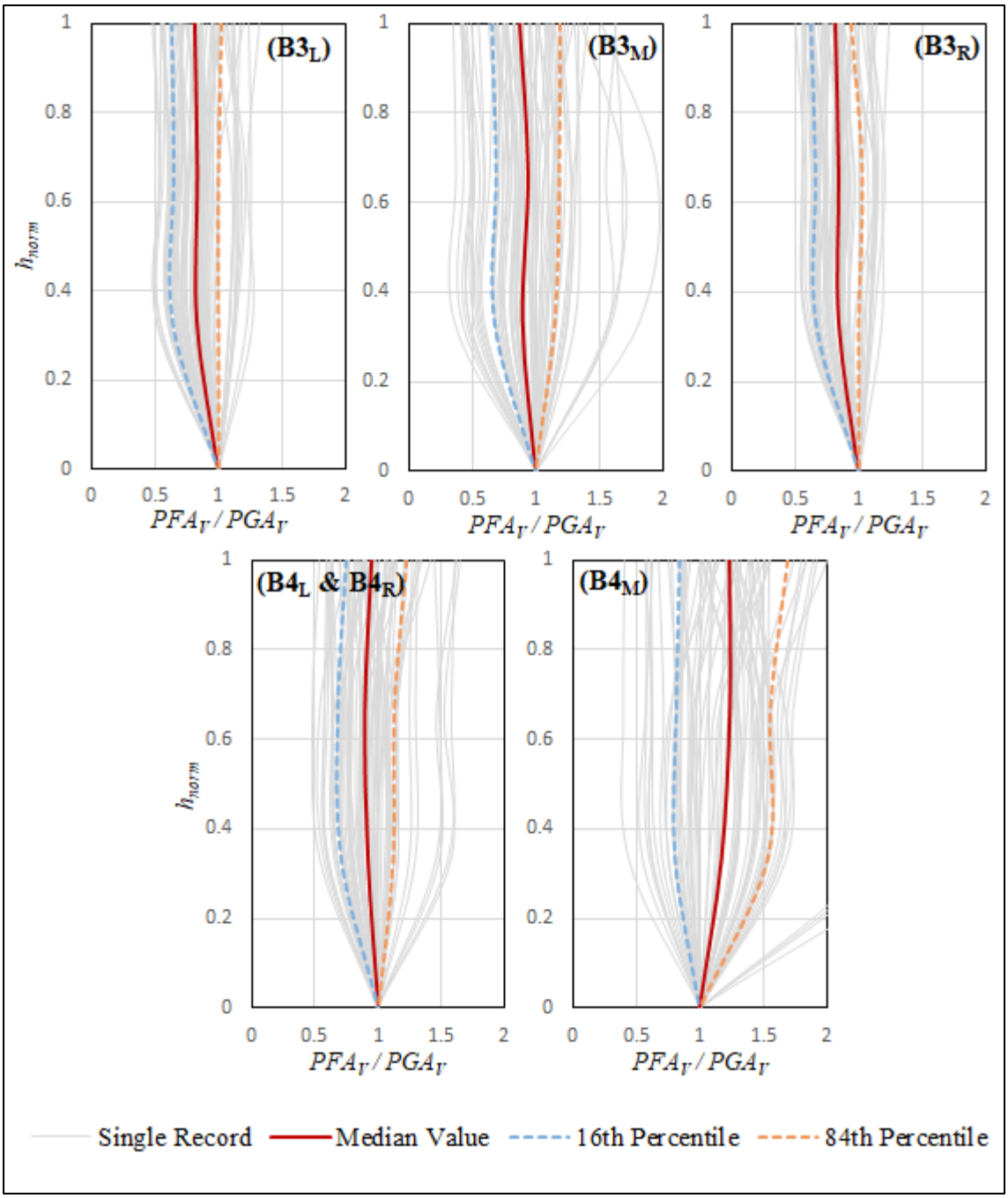

Figure 3.7 Profiles of the normalized PFAv for the considered beam nodes of the 3-storey building

3.3.1.2.2 The 6-storey building

As presented in Table 3.8 and Figure 3.8, the amplification of vertical acceleration for the node at the center of the corner slab, S1, was reduced as compared to the 3-storey building, and a constant normalized median PFAv equal to the unit value through the building height was obtained. However, the 84th percentile values from 1.20 to 1.34 show that an amplification can still be considered for this node. As mentioned earlier, a greater amplification is noted among the nodes at the center of the interior slab, S3, than on other floor nodes, 3.30 times the values at node S1.

Table 3.7 Normalized median and 84th percentile PFAv values at slab nodes of the 6-storey building

Normalized Height	S1		S2		S3	
	Median Value	84th Percentile	Median Value	84th Percentile	Median Value	84th Percentile
1.00	1.00	1.31	1.45	1.92	3.30	4.21
0.83	1.02	1.34	1.51	2.11	3.55	4.66
0.67	1.00	1.29	1.46	2.02	3.47	4.47
0.50	0.99	1.27	1.43	1.97	3.43	4.44
0.33	0.99	1.24	1.39	1.92	3.38	4.33
0.17	1.00	1.20	1.34	1.84	3.30	4.22
0.00	1	1	1	1	1	1

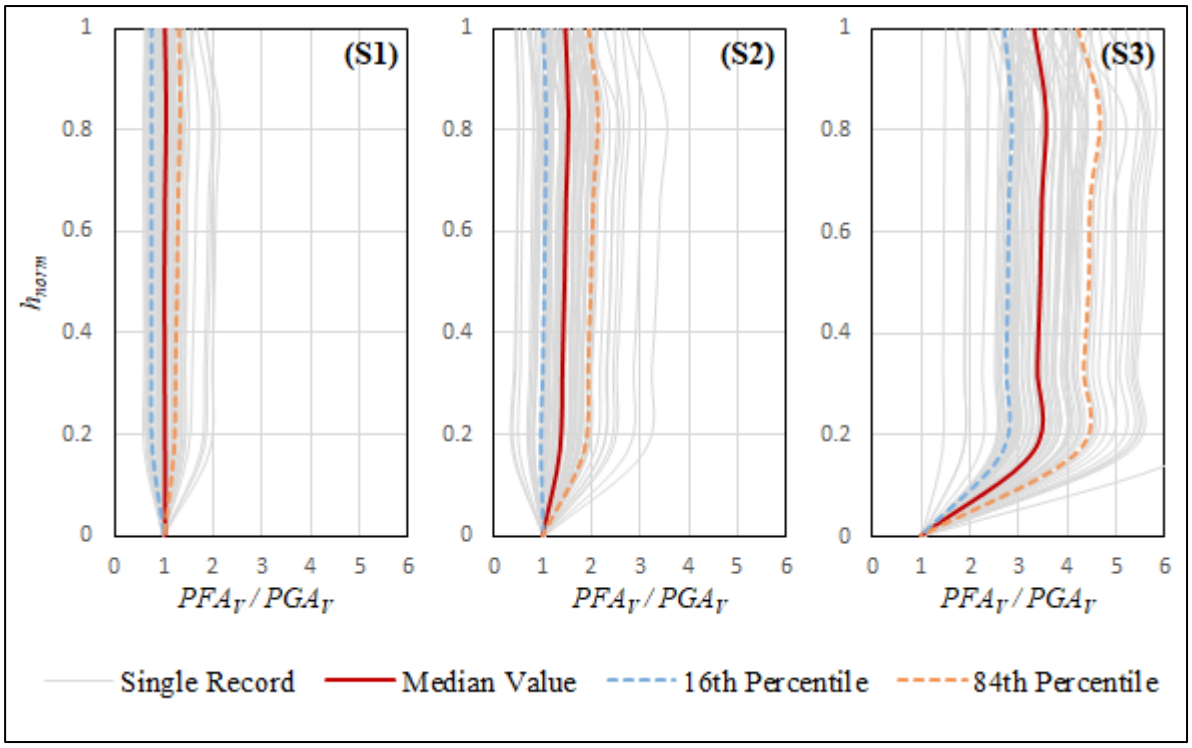

Figure 3.8 Profiles of the normalized PFA_V at the center of the slabs of the 6-storey building

No significant changes in acceleration were found on the beams for the considered nodes. However, a very slight amplification of vertical acceleration was noted on the mid-beam nodes of the interior frame, B4, which for the node at the middle of the beam, $B4_M$, was a little greater than for the side nodes, $B4_L$ and $B4_R$, as presented in Table 3.9 and illustrated Figure 3.9.

Table 3.8 Normalized median and 84th percentile PFAV values at beam nodes of the 6-storey building

Normalized Height	$B4_L$		$B4_M$		$B4_R$	
	Median Value	84th Percentile	Median Value	84th Percentile	Median Value	84th Percentile
1.00	1.04	1.08	1.08	1.14	1.04	1.08
0.83	1.03	1.06	1.07	1.11	1.03	1.06
0.67	1.04	1.06	1.07	1.12	1.04	1.06
0.50	1.03	1.06	1.07	1.11	1.03	1.06
0.33	1.03	1.06	1.07	1.11	1.03	1.06
0.17	1.04	1.06	1.07	1.11	1.04	1.06
0.00	1	1	1	1	1	1

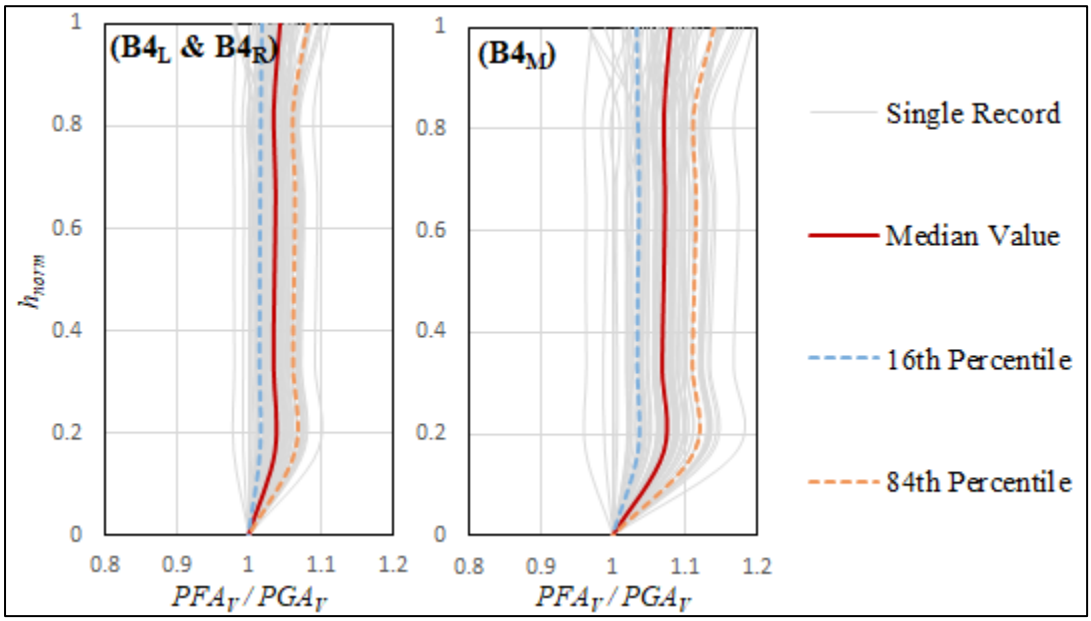

Figure 3.9 Profiles of the normalized PFAV for the considered beam nodes of the 6-storey building

3.3.1.2.3 The 9-storey building

In this building, the computed median normalized PFAV at the slab nodes, shown in Table 3.10 and Figure 3.10, represents no amplification at node S1 and a slight amplification at node S2, while a significant amplification is still observed at node S3. The amplification of 3.2, 1.5, and

1.10 through the computed 84th percentile could be considered for nodes S3, S2, and S1, respectively.

Table 3.9 Normalized median and 84th percentile PFA$_V$ values at slab nodes of the 9-storey building

Normalized Height	S1		S2		S3	
	Median Value	84th Percentile	Median Value	84th Percentile	Median Value	84th Percentile
1.00	0.92	1.11	1.10	1.44	2.56	3.11
0.89	0.92	1.11	1.17	1.47	2.67	3.24
0.78	0.93	1.11	1.19	1.51	2.71	3.28
0.67	0.93	1.10	1.17	1.49	2.68	3.22
0.56	0.92	1.09	1.16	1.48	2.67	3.20
0.44	0.92	1.09	1.14	1.47	2.64	3.17
0.33	0.92	1.08	1.12	1.45	2.62	3.13
0.22	0.92	1.07	1.10	1.42	2.59	3.08
0.11	0.92	1.04	1.04	1.26	2.13	2.46
0.00	1	1	1	1	1	1

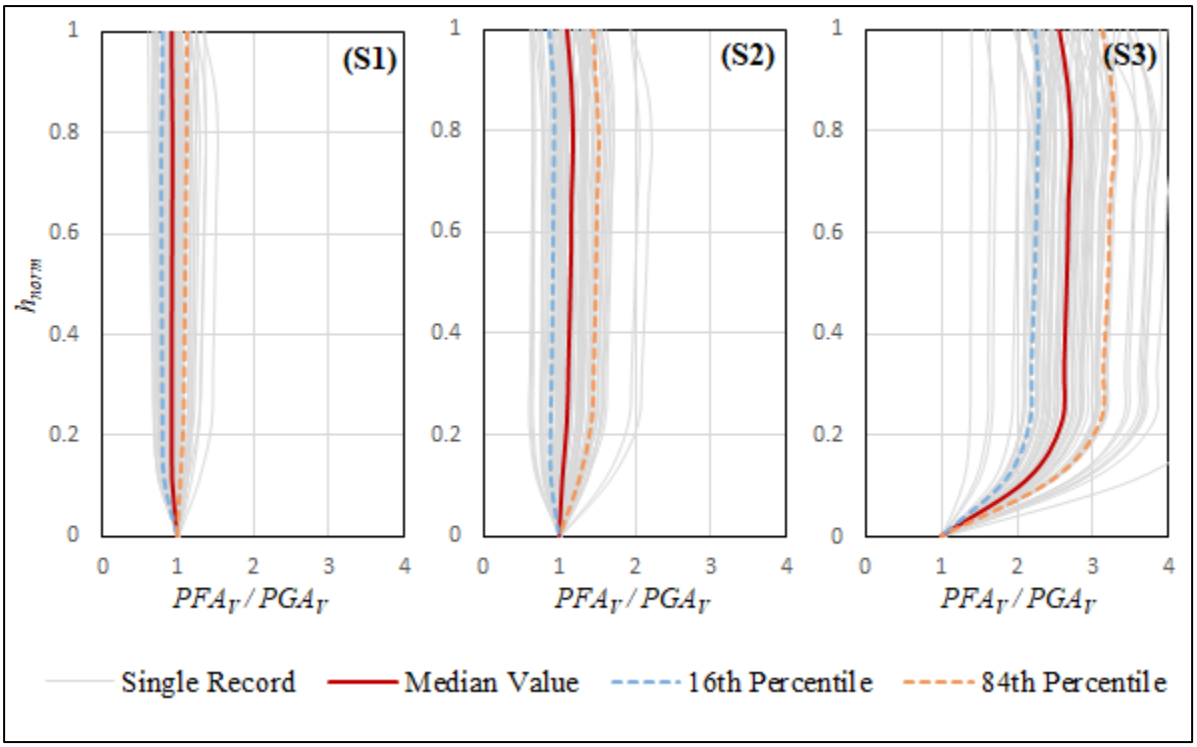

Figure 3.10 Profiles of the normalized PFA_V at the center of the slabs of the 9-storey building

Accordingly, there was no amplification of vertical floor acceleration at the beam nodes of this building, except at the mid-span beam of the interior frame, as shown in Table 3.11 and Figure 3.11, where a very low amplification was seen for the side ($B4_L$, $B4_R$) and mid-span ($B4_M$) nodes.

Table 3.10 Normalized median and 84th percentile PFA_V values at beam nodes of the 9-storey building

Normalized Height	$B4_L$		$B4_M$		$B4_R$	
	Median Value	84th Percentile	Median Value	84th Percentile	Median Value	84th Percentile
1.00	1.02	1.04	1.04	1.07	1.02	1.04
0.89	1.02	1.03	1.04	1.06	1.02	1.03
0.78	1.02	1.03	1.03	1.06	1.02	1.03
0.67	1.02	1.03	1.04	1.06	1.02	1.03
0.56	1.02	1.03	1.04	1.06	1.02	1.03
0.44	1.02	1.03	1.03	1.06	1.02	1.03
0.33	1.02	1.03	1.03	1.06	1.02	1.03
0.22	1.02	1.03	1.03	1.06	1.02	1.03
0.11	1.01	1.02	1.02	1.04	1.01	1.02
0.00	1	1	1	1	1	1

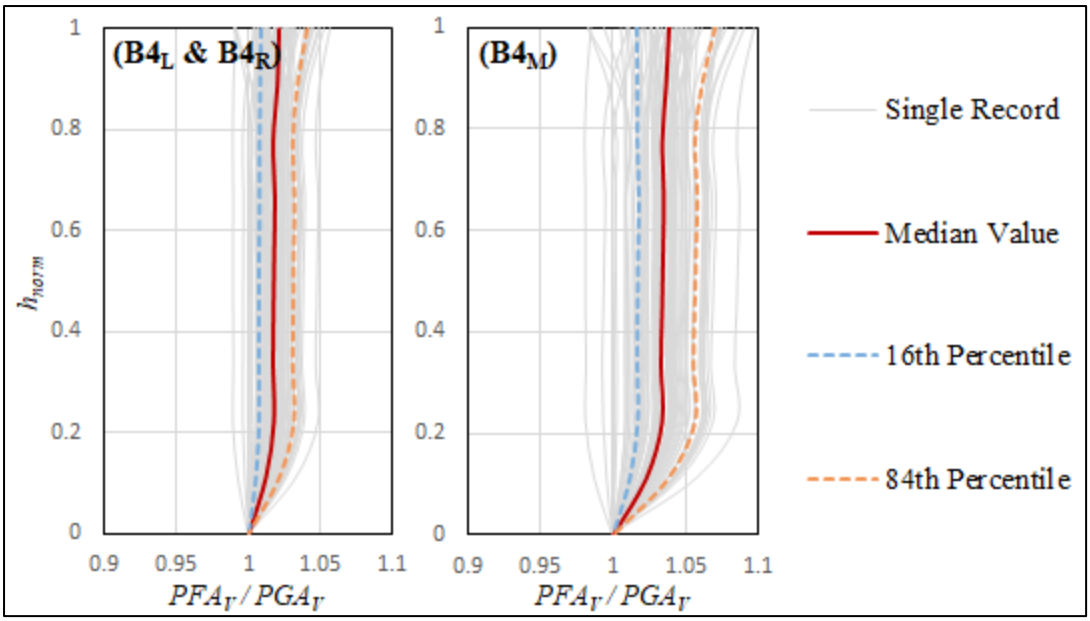

Figure 3.11 Profiles of the normalized PFAv for the considered beam nodes of the 9-storey building

3.3.1.2.4 The 12-storey building

For this building, the amplification of vertical acceleration was only observed at the center of the interior slab, S3, as illustrated in Figure 3.12. According to the computed 84th percentile, presented in Table 3.12, an amplification of 35% could be observed along the building's floors. On the other hand, no amplification of vertical acceleration was found for the other nodes.

Table 3.11 Normalized median and 84th percentile PFAv values at slab nodes of the 12-storey building

Normalized Height	S1		S2		S3	
	Median Value	84th Percentile	Median Value	84th Percentile	Median Value	84th Percentile
1.00	0.84	0.96	0.84	0.95	1.24	1.35
0.92	0.82	0.98	0.83	0.98	1.24	1.36
0.83	0.82	0.98	0.83	0.98	1.24	1.36
0.75	0.83	0.98	0.83	0.98	1.24	1.36
0.67	0.83	0.98	0.83	0.98	1.24	1.35
0.58	0.83	0.98	0.83	0.98	1.24	1.35

0.50	0.83	0.98	0.83	0.98	1.23	1.34
0.42	0.83	0.98	0.84	0.98	1.23	1.34
0.33	0.84	0.98	0.84	0.98	1.22	1.33
0.25	0.84	0.98	0.84	0.98	1.22	1.32
0.17	0.85	0.98	0.85	0.98	1.21	1.31
0.08	0.85	0.98	0.85	0.98	1.21	1.30
0.00	1	1	1	1	1	1

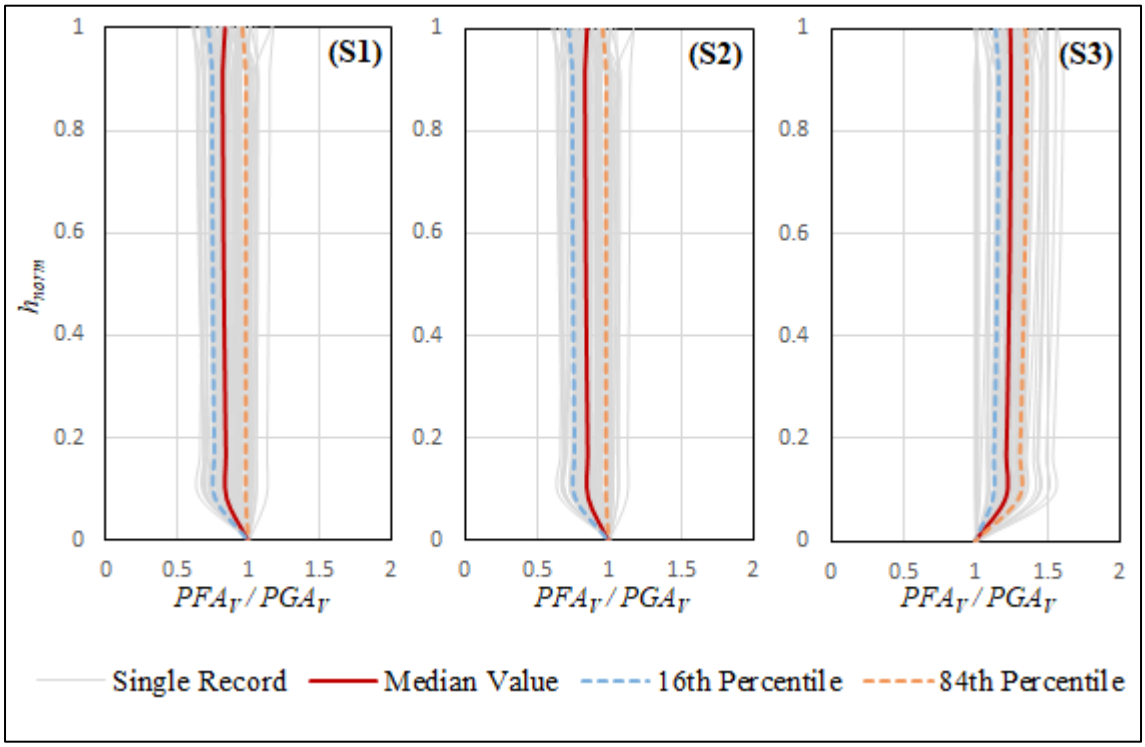

Figure 3.12 Profiles of the normalized PFA_V at the center of the slabs of the 12-storey building

3.3.2 Proposed PFA_V demands in the selected buildings

The predicted normalized PFA_V for the slabs (continuous lines) illustrated in Figure 3.13 shows that the amplification linearly decreases as the building height increases. The profiles presented indicate how important it is to consider the vertical component of near-fault strong-motion earthquakes, especially in the case of low-rise buildings. Since an almost constant acceleration

amplification was experienced along the floors of each building, the following relations (Equation 3.6) as a function of the number of the building floors (n) could be used to estimate the amplification of the vertical floor acceleration of the slabs denoted as A_{ver} in the low- and medium-rise buildings (dotted lines in Figure 3.13):

$$A_{ver} = \begin{cases} 3.5 - 0.2n, & \text{for the corner slab node (S1)} \\ 4.5 - 0.3n, & \text{for the side slab node (S2)} \\ 7.5 - 0.5n, & \text{for the interior slab node (S3)} \end{cases} \quad (3.6)$$

As shown in Figure 3.13, the effect of the location variation on the floor is also quite evident. The vertical acceleration gradually increases from the center of the corner slab, S1, to the side slab node, S2, and then rises strongly to the center of the interior slab, S3.

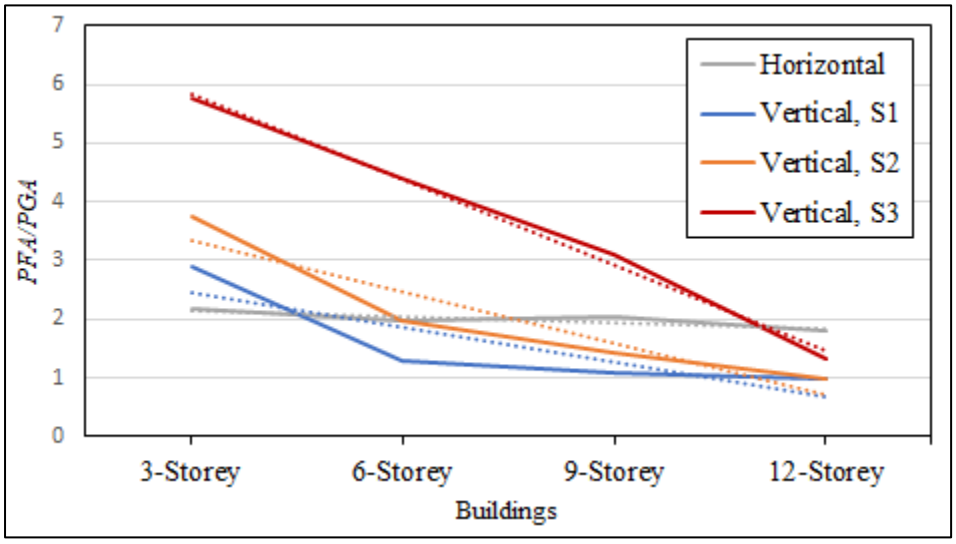

Figure 3.13 Computed and suggested normalized PFA_V profiles of the slabs' node demands and the normalized PFA_H at the buildings' rooftop versus the number of floors per building

Compared with input horizontal ground acceleration on the floors, the results once again illustrate the importance of considering the vertical component of earthquakes in shorter buildings. Regarding the height effect investigation, the vulnerability of the low-rise buildings is still quite evident, as shown in Figure 3.14 for the PFA_V/PFA_H ratio at the buildings' rooftops. The sensitivity of the selected 3- to 9-storey buildings to the vertical ground motion

for the node at the center of the interior slab, S3, is quite apparent and outclasses the horizontal component of earthquakes as the ratio exceeds 2/3 in all cases.

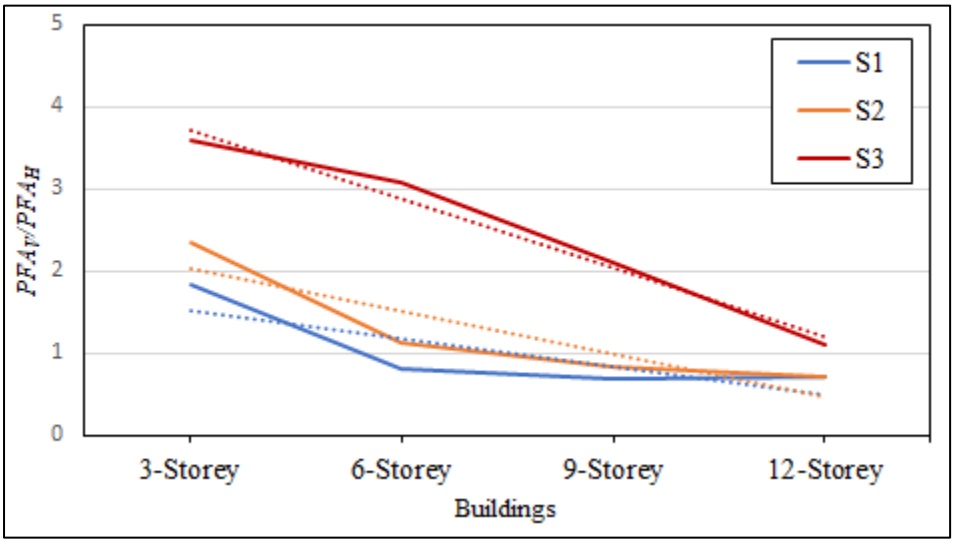

Figure 3.14 Profiles of the building height effect on PFA_V/PFA_H of the slab nodes at the buildings' rooftops

3.3.3 Dispersion of the normalized Peak Floor Acceleration

Since the seismic peak ground acceleration response can be approximated by a lognormal distribution (Kupper, 1971), the record-to-record variability of the normalized horizontal and vertical peak floor accelerations could be quantified through the unbiased estimator of dispersion (Shome & Cornell, 1999). In order to validate the normalized horizontal, vertical, and V/H peak floor accelerations, the dispersion measure, δ, was computed according to the provided standard deviation of the natural logarithms of the data presented in Equation 3.7 (Shome & Cornell, 1999).

$$\delta = \left[\frac{\sum_{i=1}^{n}(\ln x_i - \ln \hat{x})^2}{n-1}\right]^{\frac{1}{2}} \tag{3.7}$$

According to the basic parameters of this study, n is the number of ground motion records equal to 65, x_i is the normalized peak floor acceleration (PFA) demand due to the ith record calculated from PFA/PGA for each node, and $\hat{x}$ is the median or central value computed from Equation 3.8 given in Shome and Cornell (1999).

$$\hat{x} = exp\left[\frac{\sum_{i=1}^{n} ln\, x_i}{n}\right] \tag{3.8}$$

In this regard, the dispersion was estimated at slab nodes of the 3- and 6-storey buildings subjected to the 65 sets of time history acceleration recorded on Site Class C, as illustrated in Figures 3.15 and 3.16, respectively.

As can be seen, the dispersion of normalized horizontal PFA is almost identical in all nodes for each building. The maximum horizontal dispersion, d_H, of 0.44 was obtained on the top floor of the 3-storey building. The corresponding maximum amount of 0.54 was observed on the fifth floor of the 6-storey building.

The estimated dispersion ranges are $0.29 \leq d_H \leq 0.44$ and $0.14 \leq d_H \leq 0.54$ from the first level to the rooftop of the 3- and 6-storey buildings, respectively, which corresponds to the oscillation margin due to variability records observed in earthquake response analysis.

On the other hand, the maximum vertical dispersion, d_V, of 0.42 for the interior slab node, S3, of the 3-storey building, and 0.41 for the node at the center of the side slab, S2, of the 6-storey structure, was observed for all floors. In the 6-storey building, there is generally a considerable vertical dispersion for the nodes at the center of the slabs. Only a negligible dispersion of around 0.03 was obtained for the beam nodes, as shown in Figure 3.16.(a). However, the vertical dispersion in the 3-storey building is much more variable, ranging from 0.06 to 0.42, which is more significant for the slab nodes and the interior frame than for other nodes, as shown in Figure 3.15.(a).

A value of 0.38 was obtained for the PGA_V/PGA_H ratio dispersion, $d_{V/H}$, and the maximum dispersion for the nodes at the 3-storey building rooftop ranged from 0.48 to 0.58, as shown in Figure 3.15.(c). A maximum dispersion value of 0.7 was observed for the interior slab node for the fifth floor of the 6-storey building, as shown in Figure 3.16.c. The dispersions are almost identical for the other nodes through the building height.

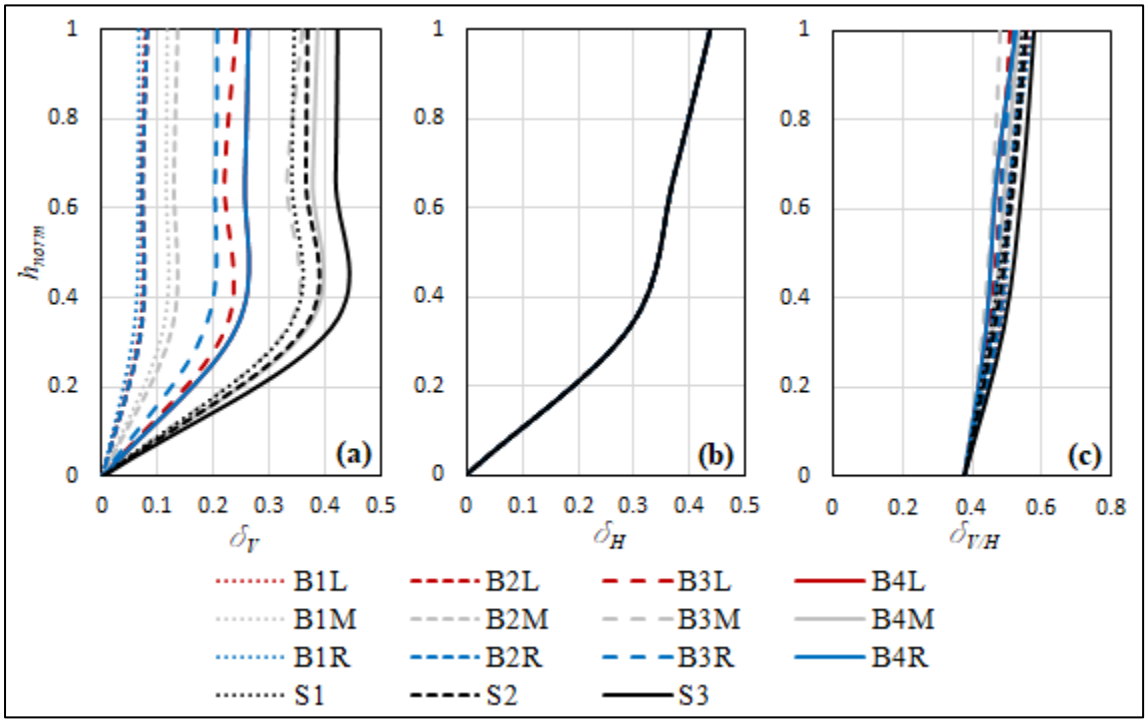

Figure 3.15 Dispersion of the normalized a) vertical, b) horizontal, and c) PFA_V/PFA_H of the 3-storey building

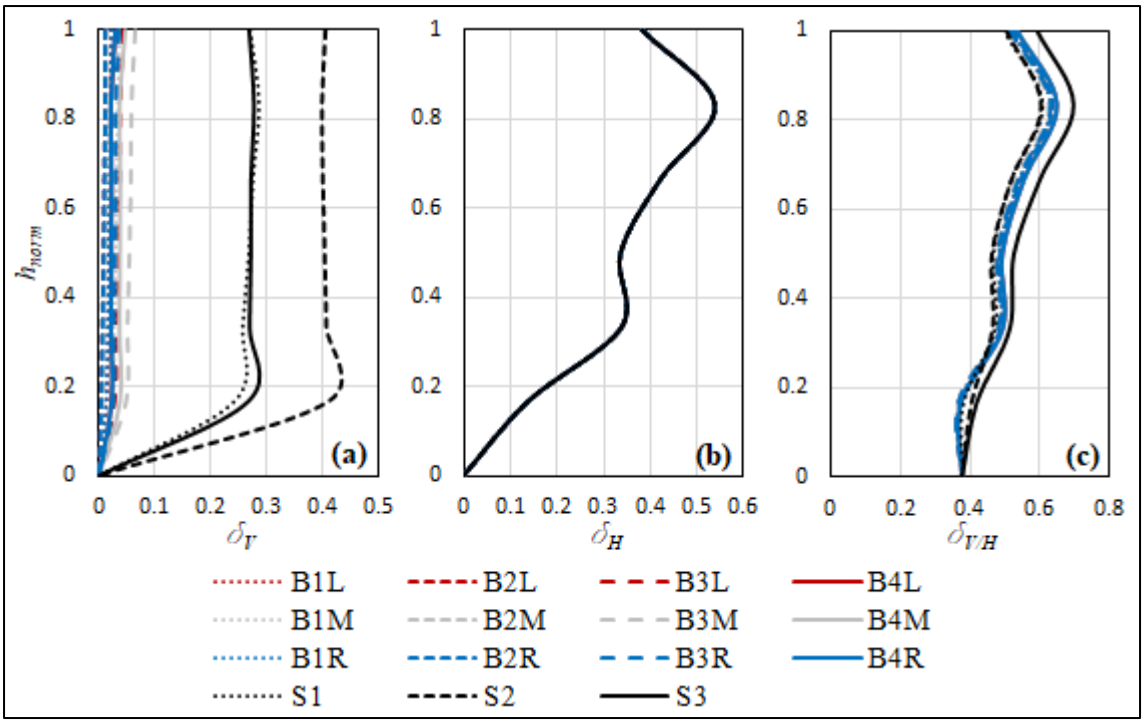

Figure 3.16 Dispersion of the normalized a) vertical, b) horizontal, and c) PFA_V/PFA_H of the 6-storey building

3.4 Summary and conclusion

In this study, the horizontal and vertical Peak Floor Acceleration, PFA_H and PFA_V, normalized with respect to the corresponding Peak Ground Acceleration, PGA, were quantified in four typical elastic low- and medium-rise multi-storey RC moment-resisting buildings. The archetype structures were supposed to be located in Montreal on a Site Class C and designed based on NBC 2015 and CSA-A-23.3-14 provisions. The buildings were subjected to 65 sets of time history accelerations recorded on Site Class C that were selected from 31 strong earthquakes based on specific criteria. The absolute peak floor accelerations were statistically assessed along the building heights for the nodes at the center of the slabs and at the beams' spans.

Significant amplifications of PFA_V through the building height were observed, with a downward trend at the center of the interior (S3), side (S2), and corner (S1) slabs. Also, an

almost constant amplification was generally observed through the height of the buildings. In contrast, practically no amplification was seen on the beam nodes for the exterior frame of the buildings, except in the case of the 3-storey building top floor, where an amplification of 23% was reached at the mid-span of the interior frame beam.

Results show that the normalized PFA_V decreases as the structure's height increases along the beam span or at the slab bay. In this regard, the median normalized PFA_V at the rooftop interior slab ranged from 4.45, for the 3-storey building, to 1.24, for the 12-storey building.

On the other hand, the normalized PFA_H was assessed to emphasize how it differed from the normalized PFA_V demand as a function of the building height. A median amplification of PGA_H, equal to 1.37, 1.44, 1.40, and 1.34, was found for the rooftop of the 3-, 6-, 9-, and 12-storey buildings, respectively. This indicates that the linearly increasing NBC 2015 profile resulting in an amplification of 3.0 at the rooftop is too conservative.

The computed PFA_V/PFA_H at the rooftop exceeds the empirical ratio of 2/3 proposed in NBC 2015 and decreases as the building height increases. From the modal analysis perspective, very little change was observed in the first computed vertical periods of the buildings. In contrast, the first horizontal periods increase as the number of floors or height of the building increases. Moreover, the obtained results highlight the importance of modelling assumptions associated with the distribution of active seismic masses at floor levels since the amplification of vertical accelerations is closely linked to the location within the floor.

The equations proposed in this study for both horizontal and vertical normalized PFA profiles were calibrated according to the results obtained with relatively simple and regular building models. Therefore, the equations herein must be further assessed before being applied in the design.

CHAPITRE 4

VERTICAL FLOOR SPECTRA IN LOW AND MID-RISE ELASTIC RC MOMENT-RESISTING FRAME BUILDINGS

Shahabaldin Mazloom[a] and Rola Assi[b]

[a, b] Department of Construction Engineering, École de Technologie Supérieure,
1100 Notre-Dame West, Montreal, Quebec, Canada H3C 1K3

Paper submitted for publication in *Engineering Structures*[3], December 2022

Abstract

To examine how floor spectral accelerations affect the design force of flexible Non-Structural Components (NSCs), the present study discusses the estimation of floor response spectra resulting from strong vertical seismic motion. 3-, 6-, 9- and 12-storey reinforced concrete buildings with moderately ductile moment-resisting frame systems, designed in accordance with the National Building Code of Canada (NBC 2015) were selected for this research. 65 sets of historical records relating to 31 severe earthquakes from across the world were used to analyze the linear behavior of these structures. A constant amplification of the Vertical Floor Spectral Acceleration (FSA_V) was observed along the building height. This amplification was noticeably elevated for slab nodes, especially at the center of the interior slab and in shorter buildings. Furthermore, the vertical component of the earthquake had a greater impact at shorter periods, since the maximum vertical acceleration occurred at periods lasting less than 0.35 sec. Finally, equations to estimate FSA_V corresponding to the input vertical ground acceleration were proposed for typical code-conforming RC frame buildings.

[3] Manuscript Number: ENGSTRUCT-D-22-06744

Keywords: Non-structural component (NSC), vertical floor spectral acceleration (FSA_V), vertical acceleration of ground motion, RC moment-resisting frame, height effect

4.1 Introduction

Non-structural components (NSCs) constitute the highest cost element in a typical building. Statistical reviews show that in the United States, they account for 82, 87, and 92 percent of the total construction costs for offices, hotels and hospital buildings, respectively (Miranda & Taghavi, 2003). Reports indicate that during earthquakes, while many structures are spared from damage, NSCs generally lose their function either partially or entirely due to seismic events (Filiatrault & Sullivan, 2014). During many strong earthquakes, including the 1988 M_w 5.9 Saguenay Earthquake (Mitchell et al., 1989), the 1994 M_w 6.7 Northridge earthquake (McGavin & Patrucco, 1994) and the 2011 M_w 6.2 Christchurch Earthquake (Baird et al., 2014), losses related to NSC damage were much higher than those associated with structural damage.

The seismic performance of NSCs in a building is crucial for its post-earthquake operation and function. Obtaining an accurate estimation of the NSC seismic design force is one of the most important design factors allowing to ensure optimal NSC performance (Kehoe & Hachem, 2003). The design force of NSCs is primarily a function of their ductility and seismic demand. The seismic demand for its part depends on ground motion features. These amplify the ground motion at the location where the component is mounted and subsequently amplify the motion of the NSCs due to resonance with the building at a certain period (Freeman, 1998). The floor response spectrum, also known as the floor spectral acceleration (FSA), provides a reasonable and accurate estimate of the non-structural design force (Kehoe & Hachem, 2003). For this purpose, considerable effort is required to collect the appropriate acceleration time history records for the time history analysis process (Freeman, 1998). Floor response spectra have been used for the seismic design of NSCs as one of the critical facilities in nuclear power plants (Gupta, 1984; Kehoe & Hachem, 2003).

Recent studies have considered the horizontal seismic response estimation of NSCs, including Taghavi and Miranda (2012), Medina (2013), Petrone et al. (2016), Asgarian (2017), Anajafi and Medina (2018), Kazantzi et al. (2020), Berto et al. (2020), and Filiatrault et al. (2021). On the other hand, few studies have focused on the importance of the vertical acceleration component along the building height and the vertical seismic response of floors; thus, the vertical seismic design force of NSCs has been largely overlooked. Previously, it was assumed that buildings were rigid enough in the vertical direction, and therefore, analysis of the vertical acceleration response was ignored, even though there was concern that the out-of-plane floor flexibility of floors could lead to resonance and significant amplification of spectral acceleration (Pekcan et al., 2003; Lee et al., 2013). In fact, strong near-field earthquakes have larger peak spectral acceleration values in the period range of 0.3 to 0.7 sec (Mase et al., 2018). It turns out that the fundamental period of low- and mid-rise buildings is often included in this period range, and severe damages to the low- and mid-rise buildings were reported during the Tarlay earthquake in Northern Thailand (Mase, 2020; Mase et al., 2021). However, observations during the Northridge earthquake showed a considerable effect of vertical accelerations on sprinkler systems, which were damaged or destroyed due to a lack of vertical seismic design force prediction (McGavin & Patrucco, 1994).

Codes and standards have not fully addressed the vertical seismic force, and building analysis against the vertical component of an earthquake, and their main focus remains on the impact of horizontal seismic components. Likewise, Canadian codes and standards, such as NBC (2015) and CSA-S832 (2014), contain limited provisions related to the vertical seismic design of NSCs; it is merely confined to the practical value of 2/3 for the vertical to the horizontal spectral acceleration of ground motion, with the recommendation that all NSCs and their connections must be designed to resist a vertical seismic force. Therefore, in the absence of detailed data on vertical accelerations for the considered site, a vertical seismic force equal to 2/3 of the horizontal one could be regarded as (CSA-S832, 2014).

In the Canadian code (NBC 2015) and American standard (ASCE/SEI 7-16), almost the same path is proposed to calculate the lateral seismic design force of NSCs. The only difference is that there is no relationship or ratio for the vertical acceleration of the floor in ASCE/SEI 7-16. On the other hand, applying a V/H ratio of 2/3 to obtain the vertical acceleration of the floor can still be considered in NBC 2015. The seismic design procedure for the lateral force of NSCs prescribed in NBC 2015 pointed to the spectral response acceleration value at 0.20 sec, which shows the importance of the acceleration at this period.

In ASCE/SEI 7-16 (2017), a constant vertical seismic design force equal to $0.2S_{DS}Wp$, is suggested for components located above ground level. Here, S_{DS} is the short-period site-specific design response spectral acceleration, and W_p is the component weight. The floor response spectrum can be used as a basis for determining the horizontal seismic design force for NSCs by multiplying the acceleration by the component weight, W_p, and the Importance Factor, I_p, and then dividing the product by the response factor, R_p, (ASCE/SEI 7-16, 2017).

In a study by Pekcan et al. (2003), the generated horizontal and vertical floor acceleration spectra for two existing elastic reinforced concrete (RC) buildings (5 and 8 storeys) subjected to near-fault strong ground motions led to a significant amplification of the vertical acceleration, which exceeded the horizontal acceleration due to the out-of-plane flexibility of the floor systems, especially at the short period range of 0.1 to 0.15 sec. Furthermore, the obtained vertical pseudo-spectral acceleration of the floors for the two buildings showed a significant acceleration at shorter periods that reaches a value of approximately 12.0g at a 0.15 sec period.

In the study by Wieser et al. (2012), the floor slab systems in four steel moment-resisting frame buildings (a 3-storey office, a 3-storey hospital, a 9-storey office, and a 20-storey office building), with fundamental vertical periods of 0.33 sec to 0.07 sec. The incremental dynamic analysis method was used to evaluate the floor response of these buildings subjected to sets of records from 21 ground motions. The normalized vertical floor acceleration spectra were

compared at each of the buildings' floor columns and open-bay locations. It was shown that the columns only contributed to the transmission of vertical acceleration from the ground to the upper floors of the building, and a minor effect on the vertical floor acceleration was observed in the beam-column connections. However, a noticeable amplification in vertical acceleration was also observed at the open-bay location of the floors. This influence indicates what is up to a four-fold increase in the vertical acceleration at the open-bay locations versus that at the column joints. It is worth noting that greater amplification was obtained at the open-bay nodes for the shorter buildings compared to the taller buildings. Moreover, it was concluded that the vertical acceleration of the NSCs depends on their fundamental periods as well as on their locations on the building floor plan. Furthermore, it is independent of the relative height of the building, structural period, and level of ductility.

In an E-Defense test by Ryan et al. (2016), the seismic response of a full-scale 5-storey fixed base, steel moment-resisting frame building, including a suspended ceiling-partition wall-sprinkler piping system, was critically assessed. As a result, a single vibration mode with periods ranging from 0.07 to 0.13 sec was acquired for the floor slabs. Also, the vertical spectral acceleration was amplified by an average value ranging from 3.0g to 6.0g from the shake table to the center of the floor slab, which significantly damaged the mentioned NSCs.

The present study investigated the vertical response of NSCs' demands on reinforced concrete moderately ductile moment-resisting frame buildings. The research was thus conducted by evaluating the vertical floor spectral acceleration (FSA_V) in 3-, 6-, 9-, and 12-storey RC archetype buildings located at Site Class C (Montreal), designed according to NBC 2015 and CSA-A23.3 (2014). An elastic analysis was conducted using a total of 65 vertical acceleration time history records from 31 strong, near-field earthquakes around the world, recorded on Site Class C. Next, the amplification of the vertical floor spectra through the height of the buildings, as well as the fluctuations of the FSA_V at the critical nodes of a floor, were assessed in order to accurately demonstrate the effect of out-of-plane flexibility level of the RC floor systems on FSA_V. Finally, an estimation of the FSA_V corresponding to the input vertical spectral

acceleration of ground motion was proposed, and the results of this study were compared with those used in the Codes and Standards.

4.2 Selection of ground motions

Sixty-five sets of ground motion records resulting from 31 strong near-field earthquakes worldwide selected from the PEER-NGA Database (PEER-NGA, 2018) were used for this study. Details of these records and the criteria for their selection are presented in a previous study by Mazloom and Assi (2022). However, only the vertical time history records were taken into account for the investigation of the vertical response time history analysis of the floors.

A statistical analysis of the records selected, accounting for the record-to-record variability of ground motion sets in the forms of median spectra, of 16^{th} and 84^{th} percentiles, for a damping ratio of 5%, were shown in Figure 4.1. A comparison of the horizontal and vertical response spectra obtained allows to prove the importance of vertical spectral acceleration in the short-period range. The computed median values of the ground response spectra indicate a maximum vertical acceleration of 1.012g at the 0.0833 sec (12 Hz) period. On the other hand, a maximum horizontal acceleration (1.33g) was obtained at the 0.20 sec (5 Hz) period in the horizontal acceleration spectra.

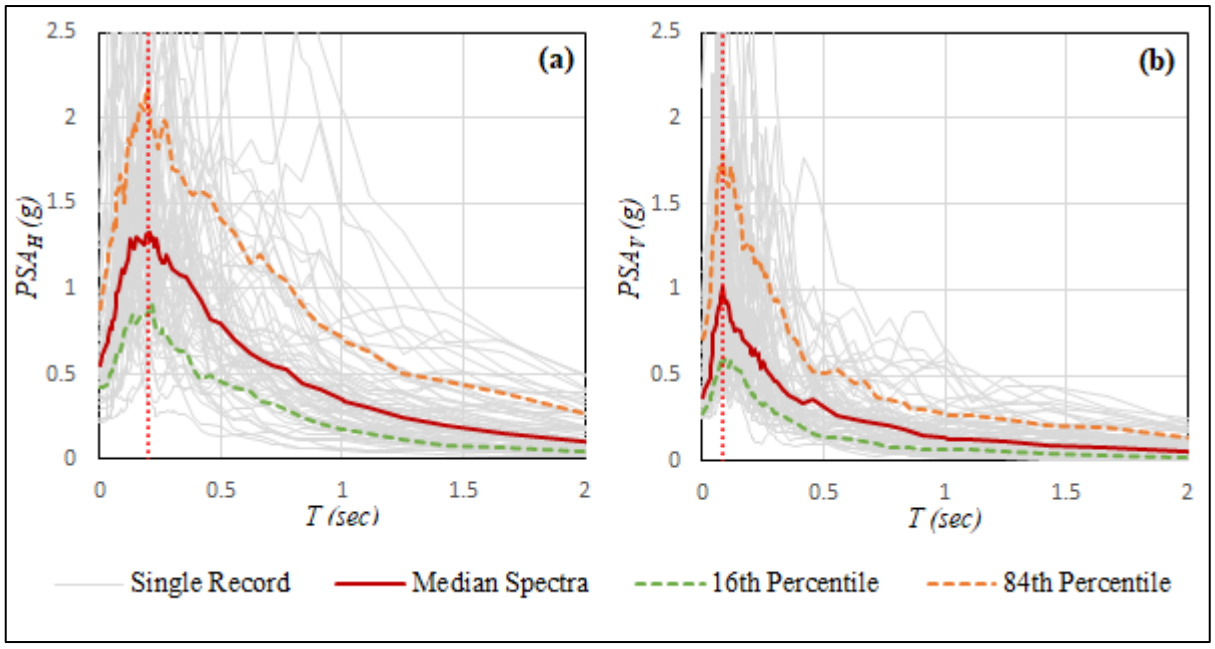

Figure 4.1 (a) Horizontal and (b) Vertical response spectra of the selected ground motion records for the 5% damping ratio

Equation 4.1 presents a proposed relationship according to the median vertical response spectra, $S_{ver}(T)$, as obtained from the input earthquakes of this study, and the corresponding spectral curve is illustrated in Figure 4.2:

$$GSA_V = S_{ver}(T) = \begin{cases} (1 + 22.5T)PGA_V & T \leq 0.067 \text{ sec } (f \geq 15\ Hz) \\ 2.5PGA_V & 0.067 \leq T \leq 0.125\ (8 \leq f \leq 15\ Hz) \\ 0.43\ PGA_V/T^{0.85} & 0.125 \leq T \leq 0.67\ (4 \leq f \leq 8\ Hz) \\ 0.4\ PGA_V/T & T \geq 0.67 \text{ sec } (f \leq 4\ Hz) \end{cases} \quad (4.1)$$

where T and PGAv denote the period and vertical peak ground acceleration in seconds and g, respectively. In the equation, the proposed ground spectral acceleration (GSAv) was established based on the PGAv. It is worth noting that the maximum acceleration in the 0.067 to 0.125 sec period range is prescribed as 2.5 times that of the PGAv. Also, the effect of the maximum acceleration at the shorter period range was shown, considering a period limit of less than 0.67 sec (f ≥ 4 Hz).

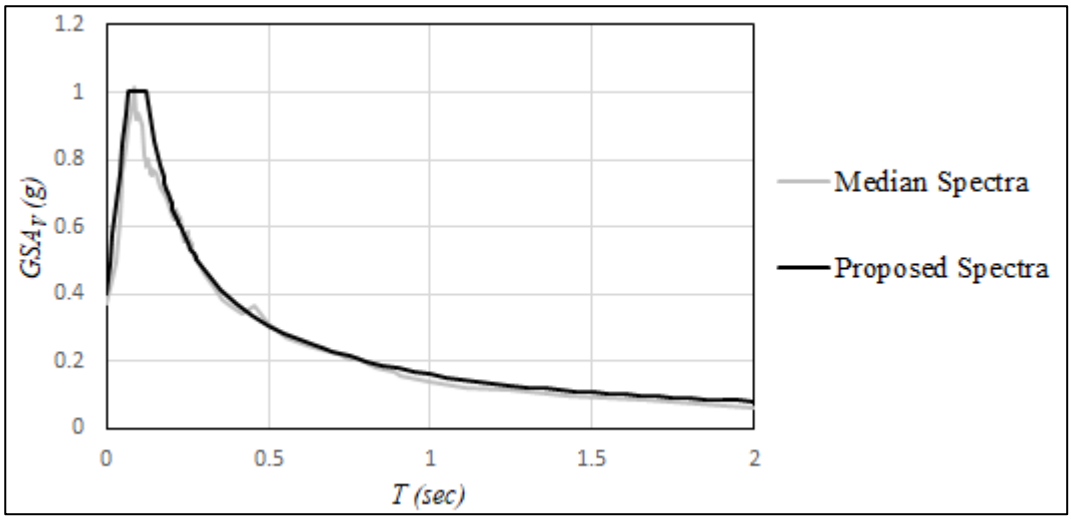

Figure 4.2 Proposed vertical response spectra of the selected ground motion corresponding to 5% damping

4.3 Building selected for the analysis

The current study focuses on low- to mid-rise concrete buildings, which constitute the majority of structures in Canada. Four moderately ductile RC moment-resisting frame models of 3-, 6-, 9- and 12-storey structures located on very dense soil (Site Class C in NBC 2015) in Montreal, designed according to the NBC 2015 and CSA-A23.3-14, were considered. All the buildings have the same symmetrical floor plan, with a 3-span frame and 7.0 m span length to minimize torsion effects.

All buildings have a finished floor height of 3.0 m, and a 140 mm RC slab floor system, as illustrated in the elevation and plan views in Figure 3. Shell elements were used to model the slab in order to account for out-of-plane flexibility in the vertical direction. The buildings were modelled according to the effective stiffness suggested in the standard CSA-A23.3-14, with the modifiers equal to 0.4, 0.70, and 0.20 for the beams, columns, and slabs, respectively. It is worth noting that all beams were modelled and designed as T-sections. The optimal cross-sectional dimensions (in mm) of the buildings' frames are presented in Table 4.1. More detailed

information about the design and analysis of these prototype frames can be found in the study by Mazloom and Assi (2022).

Table 4.1 Cross-sectional dimensions of the buildings' elements
Taken from Mazloom & Assi (2022)

Structure Reference	Columns		Beams (b×h)	
	Internal	External	X-direction	Y-direction
3-storey	400×400	400×400	350×400	350×400
6-storey	600×600	600×600	400×600	400×600
9-storey	700×700	700×700	500×650	500×650
12-storey	800×800	800×800	600×750	600×750

As shown in Figure 4.3, the computed first vertical modal period of the building indicates almost the same values for all selected buildings, with a slight increase seen as the height or the number of floors decreases. This is consistent with the studies by Papazoglou & Elnashai (1996) and Lee et al. (2013). Therefore, the floor system reveals a more essential role in affecting the vertical mode of the structure than does the number of floors in the building.

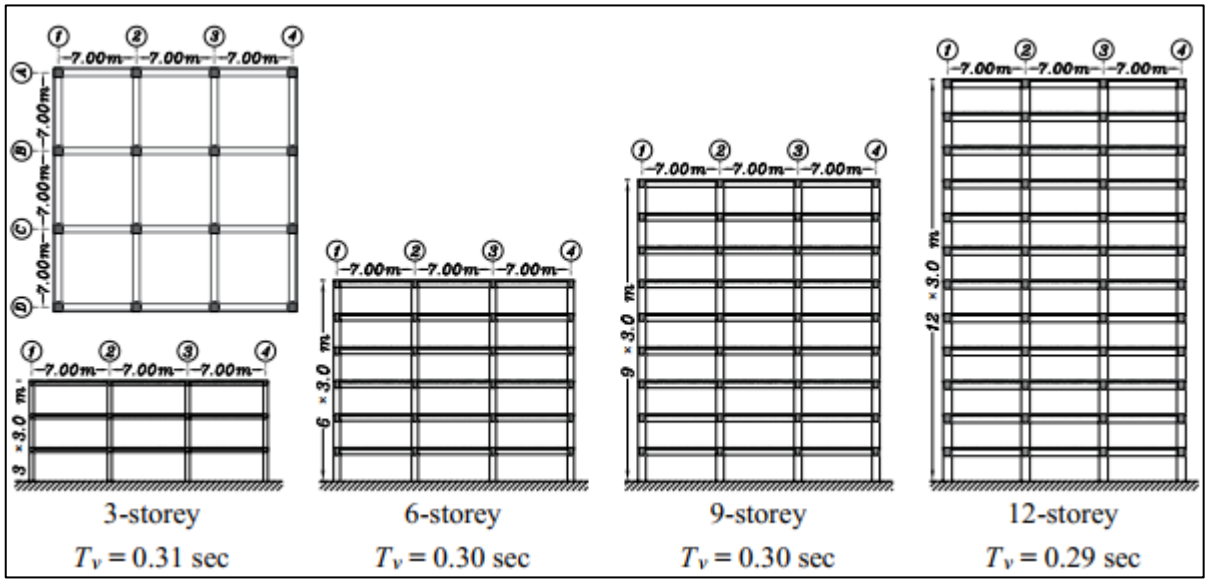

Figure 4.3 Plan and elevation views of the archetype RC moment-resisting frame buildings used in this study, along with the vertical period of the structures' first mode

Comparing the vertical periods for the first 12 modes of the selected buildings, presented in Table 4.2, shows close period values to the first 12 vertical periods of the floors in the first modes. The results indicate that the building response due to vertical vibration is mainly dominated by a single vertical mode of the floor, which is consistent with the results of the experimental tests by Guzman Pujols and Ryan (2018) carried out on a 5-storey steel moment-resisting frame structure.

Table 4.2 First 12 vertical periods of the selected buildings and floors

Mode	3-Storey	6-Storey	9-Storey	12-Storey	Floors
1	0.31	0.30	0.30	0.29	0.29
2	0.30	0.29	0.29	0.28	0.26
3	0.30	0.29	0.29	0.28	0.26
4	0.28	0.29	0.29	0.28	0.24
5	0.27	0.29	0.29	0.28	0.22
6	0.27	0.29	0.29	0.28	0.22
7	0.27	0.26	0.29	0.28	0.21
8	0.26	0.24	0.29	0.28	0.21
9	0.25	0.24	0.29	0.28	0.18
10	0.23	0.23	0.25	0.28	0.12
11	0.22	0.23	0.25	0.28	0.12
12	0.22	0.23	0.25	0.28	0.11

4.4 Results of elastic Vertical Floor Spectral Accelerations

In this section, the responses of the floors subjected to vertical acceleration time histories were computed for each building. Hence, the corresponding FSA_V with a 5% damping ratio at each floor was computed with respect to the ground motions selected as the input GSA_V. The obtained FSA_V of the buildings' floors are illustrated in Figures 4.4 to 4.7. The grey lines represent the FSA_V corresponding to the input of 65 records of past earthquakes, and the computed median spectra, the 16^{th} and the 84^{th} percentiles (median ± standard deviation), are plotted in bold, continuous and dashed lines, respectively. It is worth noting that the response spectra of the floors were measured at the center of the interior slab. The reason for this node choice is based on the results obtained in the study by Mazloom and Assi (2022) and the explanation in section 4.6.

4.4.1 The 3-storey building

The FSAv obtained for each floor of the 3-storey building is presented in Figure 4.4. Maximum accelerations of 10.97g and 11.74g were found on the FSAv curve for the first and second floors, respectively, at the 0.21 sec period. In addition, the maximum value of 10.42g on the FSAv curve was obtained for the rooftop at the 0.23 sec period. A nominal decrease in acceleration is observed from the second floor to the rooftop, which can generally be ignored. The obtained results indicate that the maximum accelerations correlate to the higher modes of the floors. On the other hand, the first eight modes of the floors are almost close to each other from the period 0.29 to 0.21 sec. Therefore, only one maximum acceleration value is observed in the obtained curve. This is consistent with the results of the experimental study by Ryan et al. (2016), which found that the slab vibrations were dominated by the single-mode response.

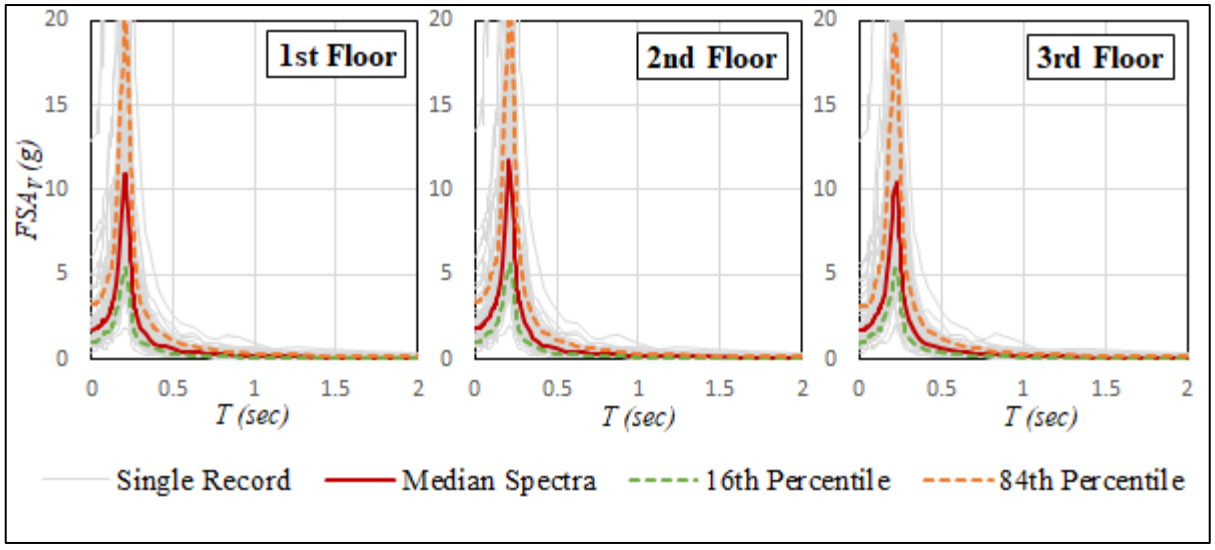

Figure 4.4 Computed FSAv at the center of the interior slab of the 3-storey building

4.4.2 The 6-storey building

The obtained FSAv for the 6-storey building floors shown in Figure 4.5 indicate the maximum acceleration of 5.75g to 6.22g at the 0.20 sec period for the 1st to the 5th floors of the building. A negligible decrease in this maximum acceleration to a value of 6.15g at the 0.20 sec period

can be observed on the building rooftop. As in the case of the 3-storey building, since the modes are close to each other, only one maximum value (single peak) can be seen in the spectral curves of the floors.

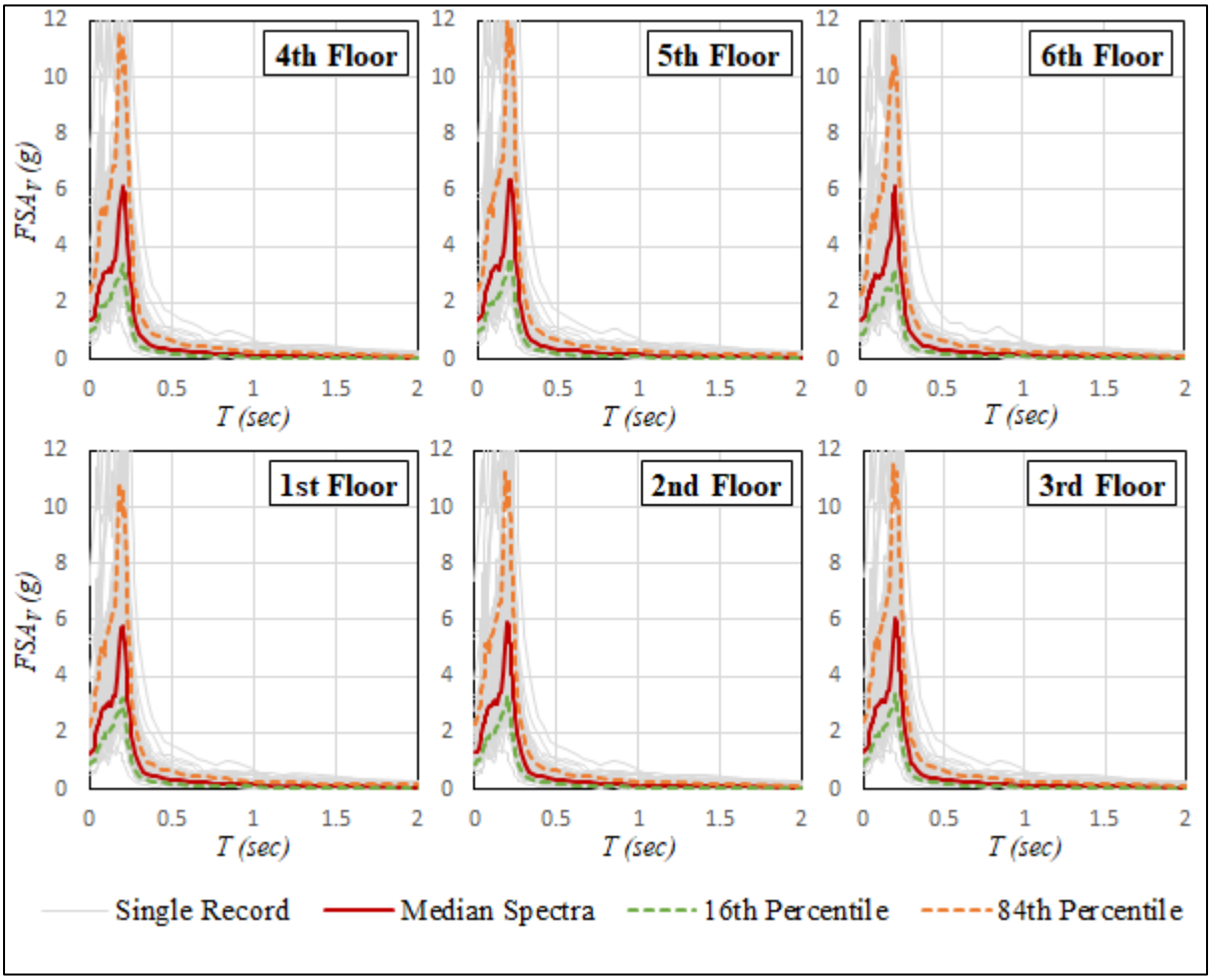

Figure 4.5 Computed FSAV at the center of the interior slab of the 6-storey building

4.4.3 The 9-storey building

The FSAV presented in Figure 4.6 for the 9-storey building floors shows a constant amplification at all floors relative to the ground level. The maximum vertical acceleration on the FSAV curves from the 1st to the 8th floors was slightly amplified in the ranged values from

3.74g to 4.21g at 0.20 sec. However, this amplification decreases around this period (0.21 sec) to a value of 3.56g. It should be noted that the maximum vertical acceleration value occurred at the same period as the 3- and 6-storey buildings, which corresponds to the higher modes (modes 6 and 7) of the floor.

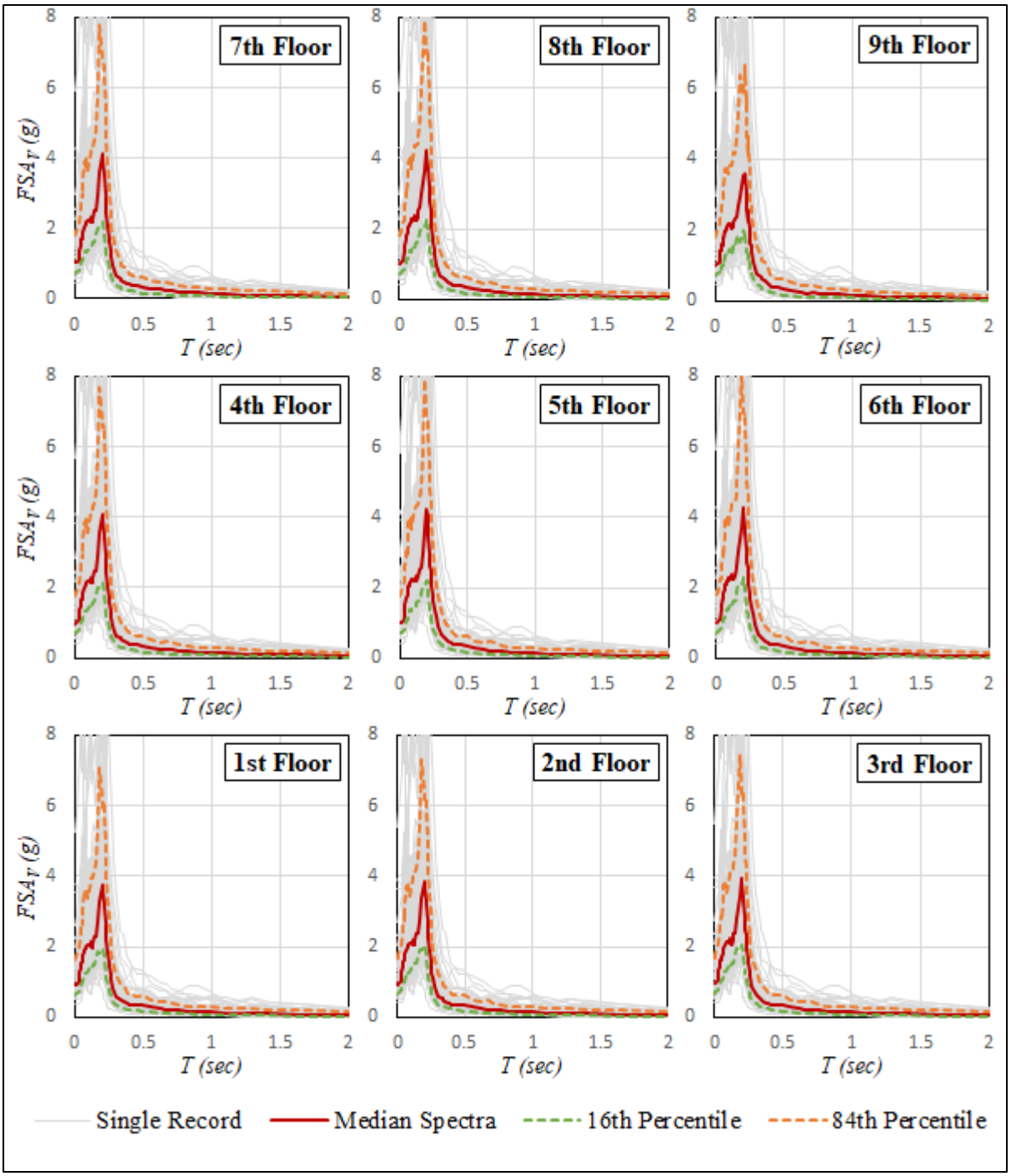

Figure 4.6 Computed FSAv at the center of the interior slab of the 9-storey building

4.4.4 The 12-storey building

The obtained results, illustrated in Figure 4.7, demonstrate that there is almost no amplification of vertical acceleration for the 12-storey building relative to the input vertical spectral acceleration at the base of the structure. Yet, the FSA_V and the maximum values on these spectral curves indicate that the acceleration is slightly higher than the ground acceleration, but only in the 0.23 to 1.0 sec period interval. Two maximum peaks were observed along the spectral curve of the floors. The first maximum vertical acceleration was seen at the 0.083 sec (12 Hz) period, with a value of 0.76g to 0.80g. It should be noted that the maximum vertical acceleration of the median input ground spectra was obtained at this period, with a value of 1.012g; therefore, a partial attenuation at this period can be concluded. Moreover, the second maximum vertical acceleration of the floors was observed at about 0.26 sec (second mode of the floor) with the same range values obtained for the first peak (0.76g to 0.80g). Therefore, it can be concluded that the first and second peaks (maximum vertical acceleration on the FSA_V curves) correspond to the maximum acceleration of the ground and second vertical mode of the floor.

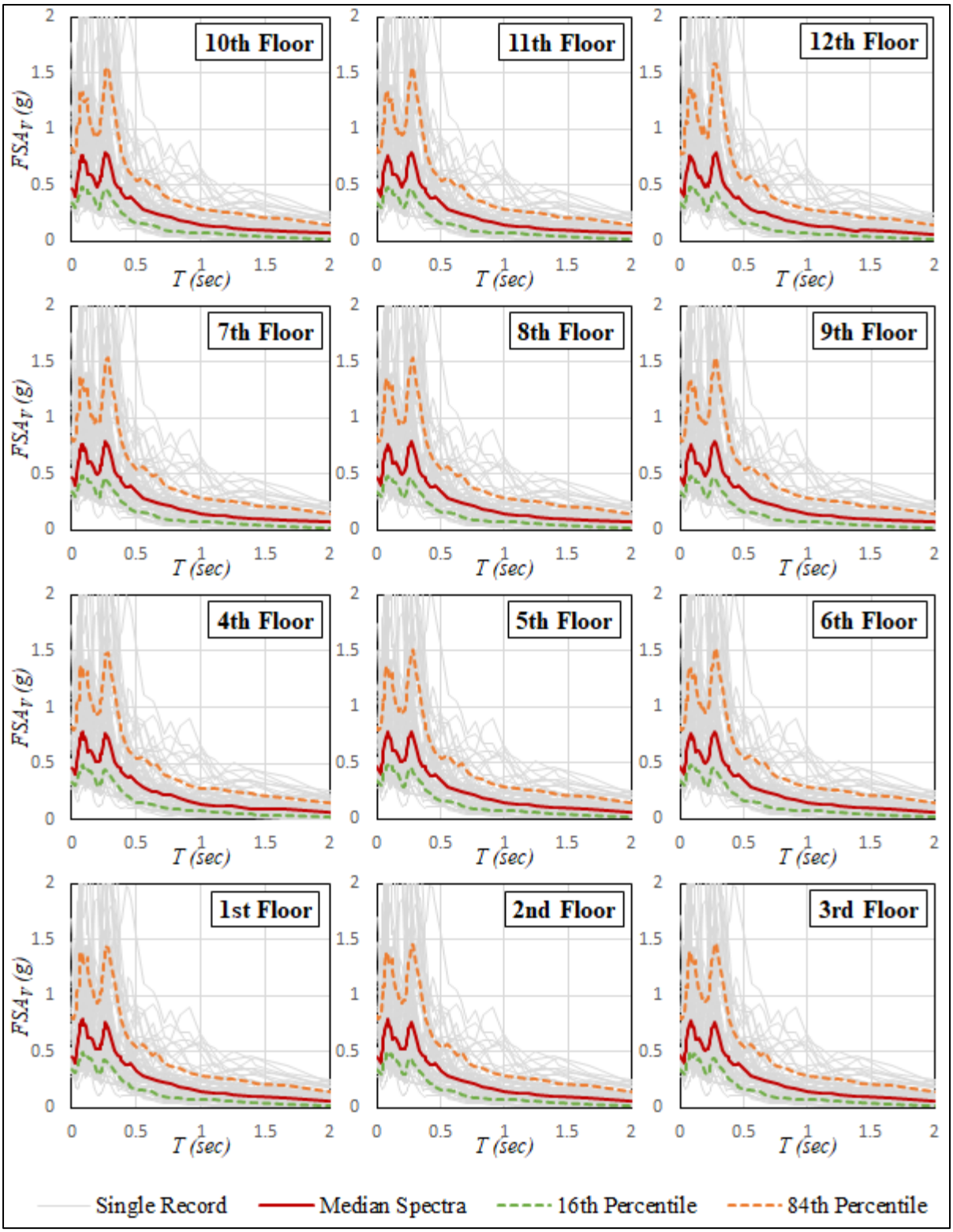

Figure 4.7 Computed FSA_V at the center of the interior slab of the 12-storey building

4.5 Conclusions on the amplification of median FSA_V through the building height

The median floor spectra for each building obtained through the building heights and rooftops are presented in Figures 4.8 and 4.9, respectively. It can be noted that there is a significant amplification of vertical acceleration from the ground to the first level, with a constant amplification continuing throughout the height of the 3-, 6-, and 9-storey buildings. Conversely, the amplification of FSA_V increases with a decrease in the structures' height such that no amplification is observed in the 12-storey building, so that upper floor levels experience FSA_v values, which are almost equal to the GSA_v. This difference in acceleration can clearly be seen in Figure 4.9, which can affirm the importance of considering the vertical component of an earthquake in low-rise buildings, especially in connection with resulting non-structural damage from more severe earthquakes.

A comparison among the floor acceleration spectra for each building shows that the more out-of-plane flexible nodes of the shorter buildings impose larger vertical acceleration to NSCs than taller buildings, which low- to medium rise buildings have a frequency synchronized with the fundamental vertical frequency of the floor. In fact, a higher number of floors provides more potential for out-of-phase interaction of floor vibrations, which acts as a tuned mass damper (Wieser et al., 2012). Furthermore, it was evident that the vertical acceleration of the ground motion is transferred to each floor of the building through the columns and walls that are axially rigid. Hence, due to the high rigidity of the columns, the vertical acceleration of each floor at the column joints on the floor is equal to the vertical ground acceleration. The findings obtained in this study are consistent with the research work conducted by Reinhorn et al. (2010) and Wieser et al. (2012).

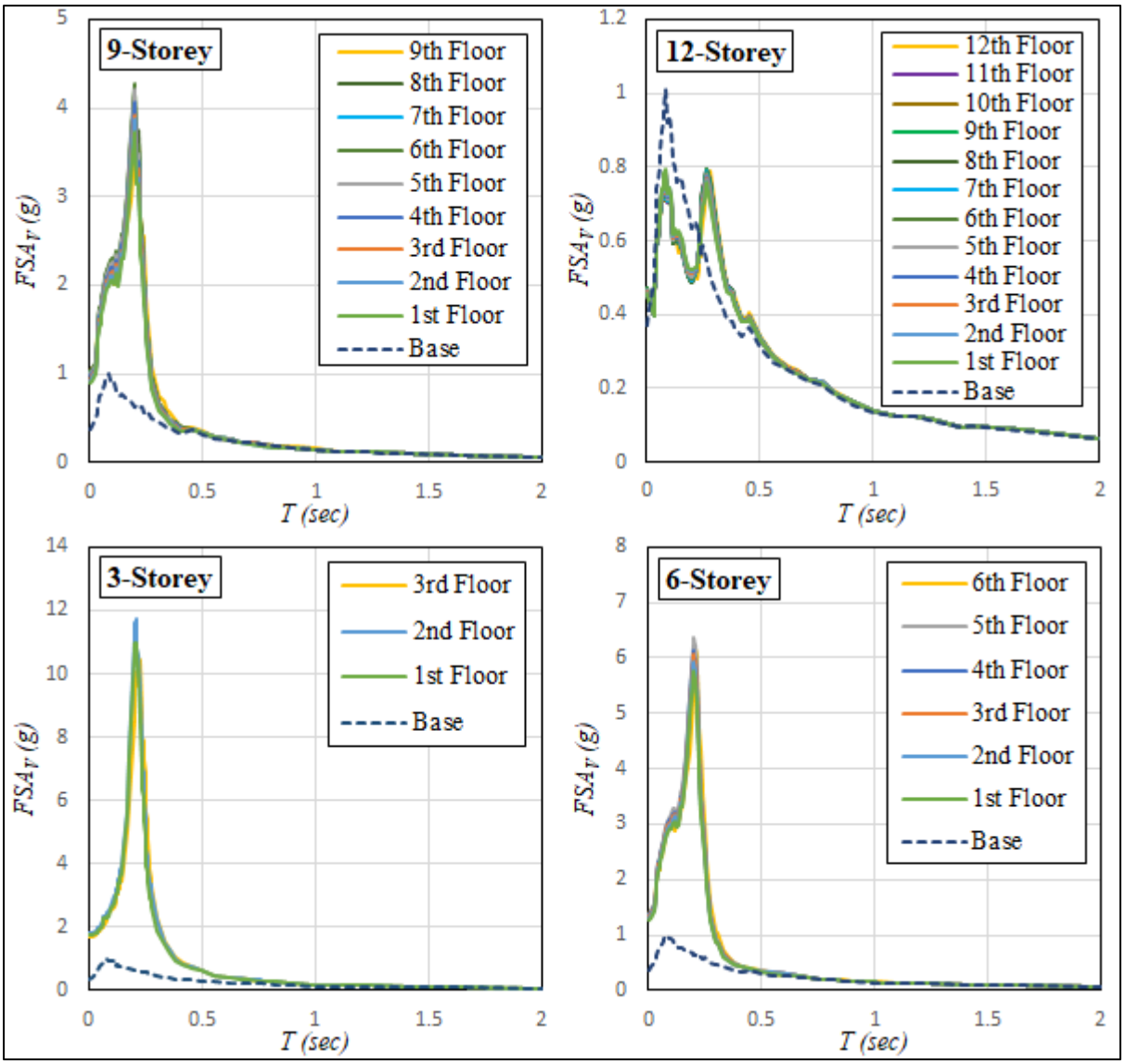

Figure 4.8 Median FSAv through the building height at the center of the interior slab

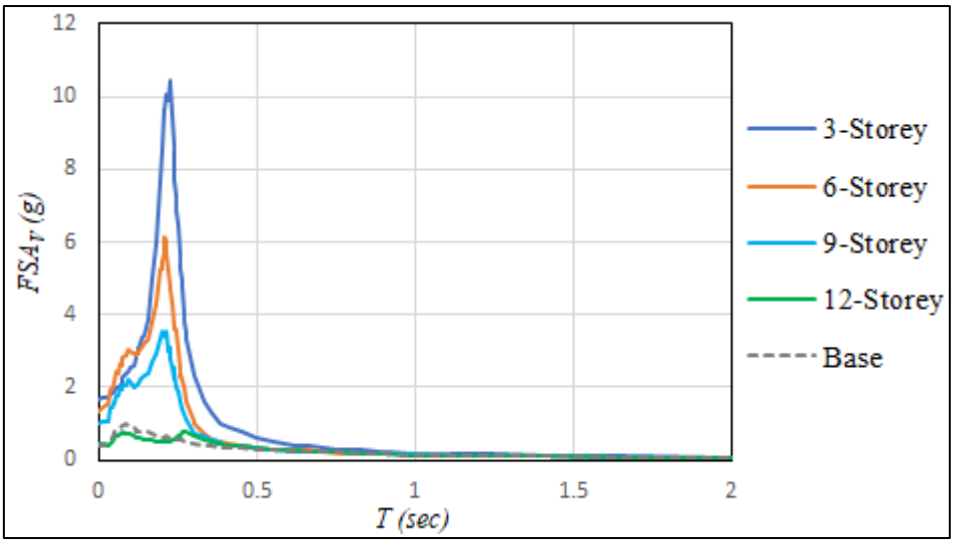

Figure 4.9 Comparison of the median FSA_V of buildings' rooftops at the center of the interior slab

4.6 The effect of the mounting location on the floor plan

In this research, the amplification of the FSA_V for the considered nodes on the floor, as shown in Figure 4.10, was investigated for the 6-storey building rooftop. The results presented in Figure 4.11 demonstrate a significant amplification of vertical spectral acceleration at the center of the slabs. Nevertheless, the greatest amplification was observed at the center of the interior slab, S3, and no amplification was observed for the nodes that were considered on the beams and columns. Unlike the horizontal floor spectral acceleration, FSA_H, which shows almost the same spectral curve for all of the points on the floor due to the in-plane rigidity of the floor systems, the spectral curve of the vertical acceleration spectra varies at each node of the floors. Moreover, the spectra were amplified from rigid out-of-plane locations, close to the columns, to more flexible out-of-plane locations, at the center of the slab bays and even at the middle of the beam spans. Therefore, the importance of the out-of-plane flexibility effect for the floors, especially in the slabs, is further highlighted here for the vertical acceleration of ground motions.

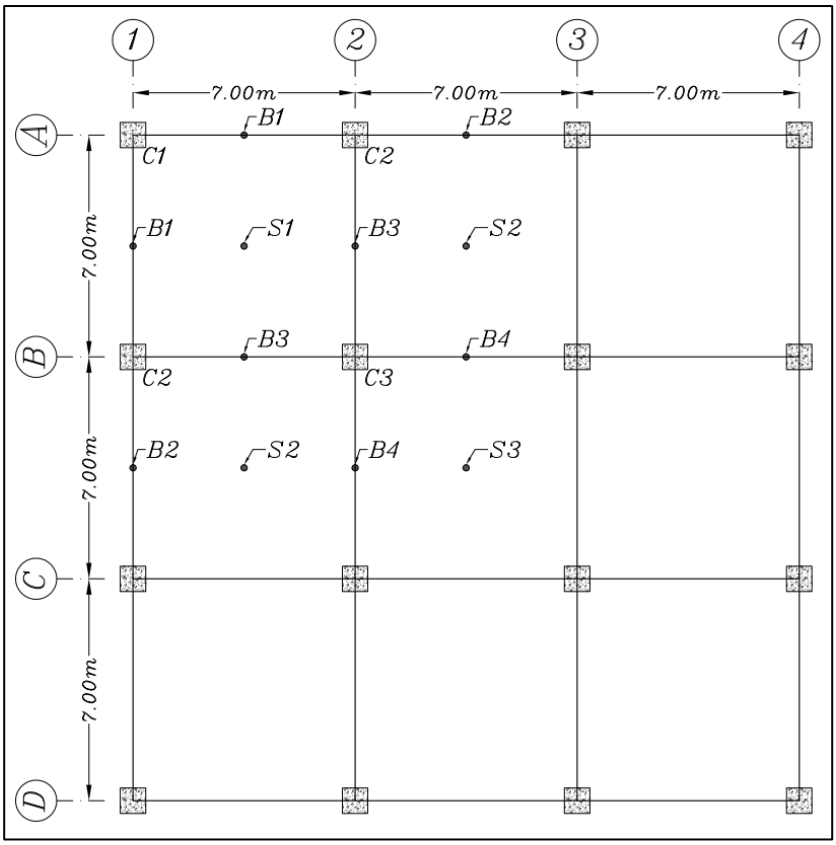

Figure 4.10 Considered critical nodes on the building floors

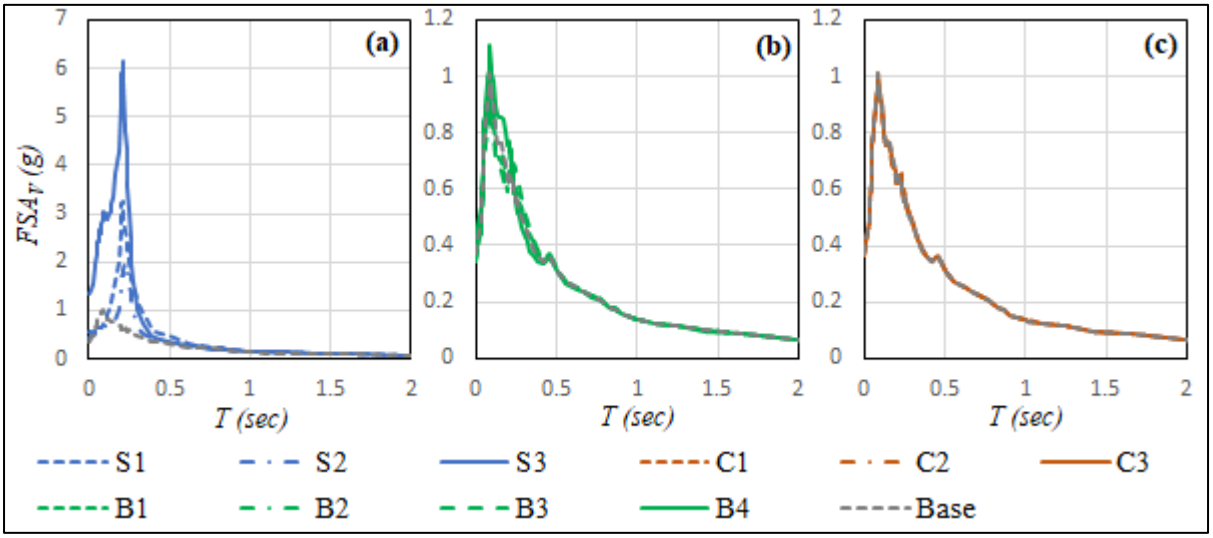

Figure 4.11 Median FSAv of the 6-storey rooftop at different considered nodes: (a) slab nodes, (b) beam nodes and (c) column nodes

4.7 Proposed FSA_V based on obtained results from the selected buildings

In this section, relationships were proposed to estimate the FSA_V of the buildings according to the number of floors and the input vertical ground acceleration. As explained in Sections 4.5 and 4.6, although for a specific node, similar vertical floor spectra can be defined along the height of the building for all floors, a single spectrum cannot be specified for all points of a floor. On the other hand, the buildings demonstrate different behaviors according to their overall height. Therefore, they were divided into two categories to generate the vertical spectra of the floors. Firstly, the relationship for the critical nodes of the buildings shorter than 12 storeys generally includes the nodes located at the center of the interior bays. The second category is related to the other floor nodes of all buildings, typically related to the nodes located far from the center of the slabs, and also for all the floor nodes of the buildings exceeding 12 storeys in height. The relationships corresponding to the first and second categories are presented in Equations 4.2 and 4.3, respectively. By categorizing the period ranges, a sub-equation was generated for each period range according to the available acceleration amplitude. Each sub-equation was derived based on the best-fitting curve such that by entering the period, the acceleration obtained for each building could be close to the unsmoothed curve. Both the graphical and numerical fit results were examined to determine the best fit, and the suitable trend on a scatter plot that matched the initial curve was selected. Linear, exponential and polynomial trendlines were used to this end.

For the node at the center of the inner slabs, in buildings shorter than 12 storeys ($n < 12$) with a 5% damping ratio:

$$FSA_V = \begin{cases} (a \cdot T + b) \times PGA_V & T \leq 0.167\,\text{sec}\ \ (f \geq 6.0\,Hz) \\ (0.11a + 1.34) \times S_{ver}(0.2) & 0.167 \leq T \leq 0.25 \\ \dfrac{c}{T^4} PGA_V + S_{ver}(T) & T \geq 0.25\,\text{sec}\ \ (f \leq 4.0\,Hz) \end{cases} \quad (4.2)$$

For other nodes of the floor (except the center of the slabs) in buildings shorter than 12 storeys ($n < 12$), and for all floor nodes of buildings taller than 12 storeys ($n \geq 12$) with a 5% damping ratio:

$$FSA_V = \begin{cases} S_{ver}(T) & T \leq 0.067\,\text{sec}\ \ (f \geq 15\ Hz) \\ 2.5PGA_V & 0.067 \leq T \leq 0.25 \\ 17.4 \times 10^{-3} PGA_V/T^3 + S_{ver}(T) & T \geq 0.25\,\text{sec}\ \ (f \leq 4.0\ Hz) \end{cases} \quad (4.3)$$

In these equations, *a*, *b*, and *c* are the fixed values obtained according to the number of floors, n, for each building, through the proposed Equations 4.4 to 4.6.

$$a = 225 - 85 \ln n \quad (4.4)$$

$$b = 5.0 - 0.25n \quad (4.5)$$

$$c = \frac{1}{6.04} - \frac{\ln n}{16.33} \quad (4.6)$$

The vertical floor spectral curves for all buildings derived from the proposed relationships were presented separately for each building in Figure 4.12. Additionally, the proposed FSA_V relative to the proposed input GSA_V are illustrated in Figure 4.13, which shows the spectral amplification and effect of the building height. The obtained smooth FSA_V curves show almost the same spectral values in all buildings for periods longer than 0.67 sec. Finally, it should be mentioned that the proposed FSA_V equations were used according to the median spectral curves calibrated to the results obtained in the considered typical regular buildings. Hence, further analytical investigations in this field may be required for other building types in order to confirm these relationships.

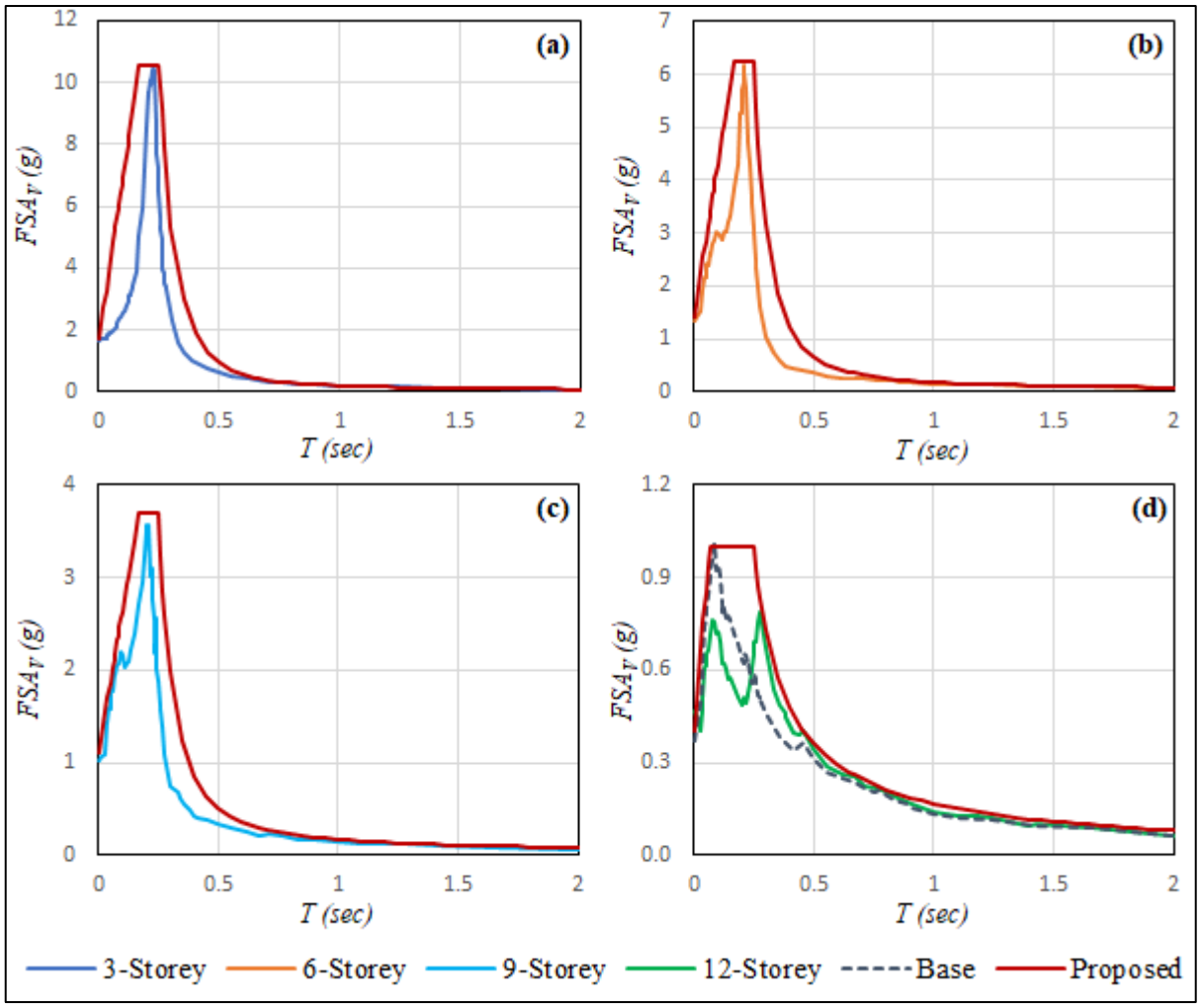

Figure 4.12 Proposed FSAv for the calibrated results obtained for the considered building types: (a) 3-storey, (b) 6-storey, (c) 9-storey, and (d) 12-storey buildings

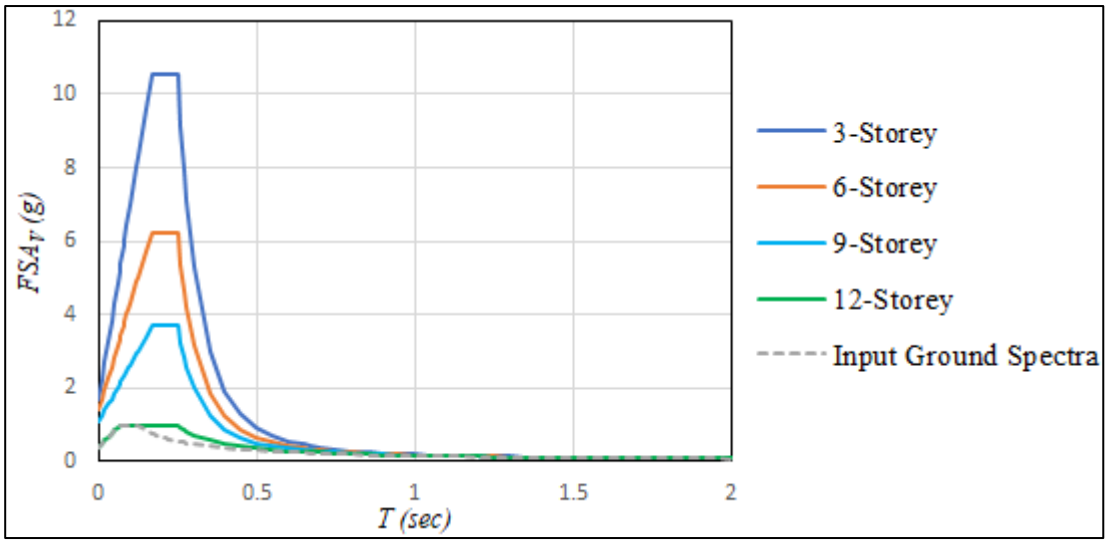

Figure 4.13 Proposed FSAv of this study for the selected buildings' floors with respect to the proposed GSAv

4.8 Parametric Validation of the Proposed Equations for FSAv

In order to validate the proposed FSAv equation for the flexible nodes, the FSAv of the 6-storey RC moment resisting frame buildings with different spans length of 5.0, 7.0 and 9.0 m were computed considering the four near-field strong earthquakes shown in Table 4.4. Secondly, the effect of floor height was also investigated by comparing the FSAV of the reference 6-storey building using floor heights of 3.0 m and 4.5 m shown in Figure 4.15.

The buildings were designed according to the procedure outlined in Section 4.3. The buildings' plans with elevation views and their corresponding details of sections were shown in Figure 4.14 and Table 4.3, respectively.

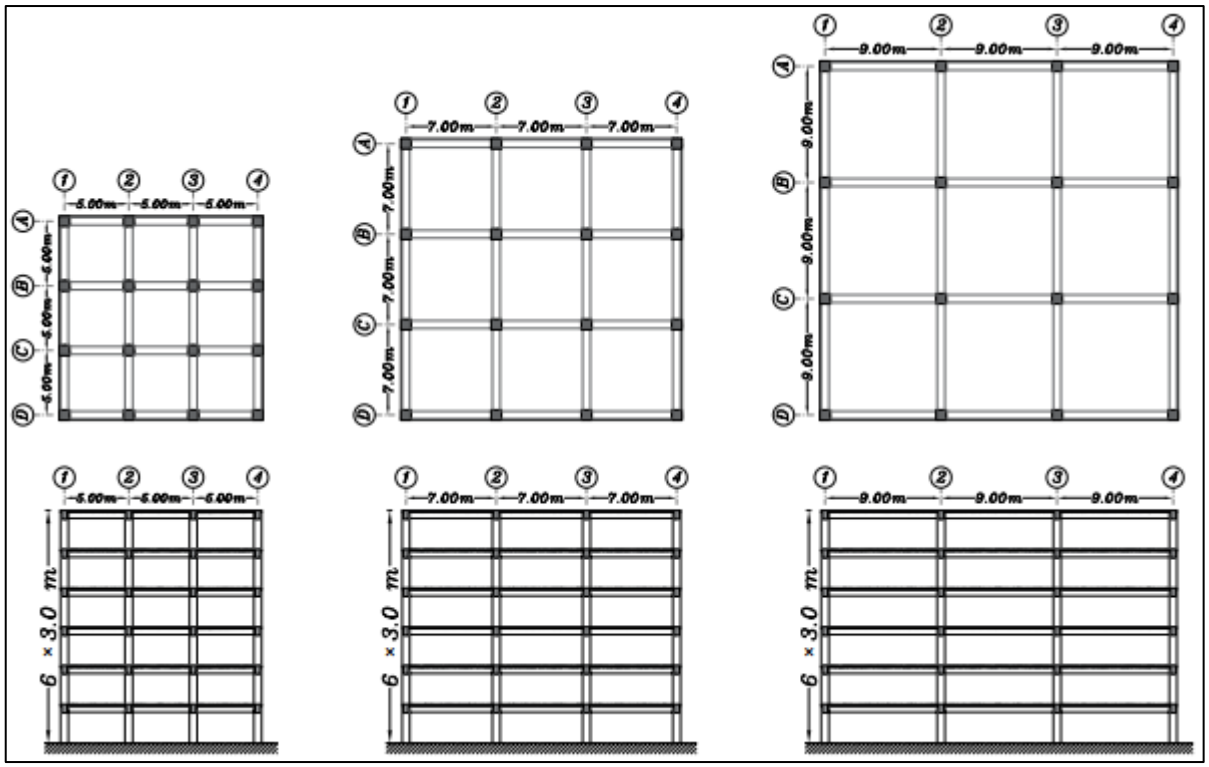

Figure 4.14 Selected 6-storey buildings with different span lengths to apply the proposed FSAv equation

Table 4.3 Cross-sectional dimensions of the 6-storey buildings' elements with (a) 5.0 m, (b) 7.0 m, and (c) 9.0 m span lengths

Structure Reference	Columns		Beams (b×h)	
	Internal	External	X-direction	Y-direction
a	450×450	450×450	350×450	350×450
b	600×600	600×600	400×600	400×600
c	700×700	700×700	500×700	500×700

Table 4.4 Selected earthquake records for validating the proposed FSAv for the flexible nodes

Earthquake	Date	M_W	Station	R_{jb} (km)	R_{rup} (km)	Site Class	PGA_V (g)
Friuli, Italy-01	1976/05/06	6.5	Tolmezzo	14.97	15.82	C	0.28
Nahanni, Canada	1985/12/23	6.76	Site 1	2.48	9.6	C	2.28
Tottori, Japan	2000/10/06	6.61	SMNH01	5.83	5.86	C	0.64

Niigata, Japan	2004/10/23	6.63	NIG028	0.46	9.79	C	0.44

The results presented in Figure 4.15 show that peak spectral values decrease with an increase in span length. Multiple vibration modes contributed to the floor response in building with larger spans length, as demonstrated by the multiple peaks in the FSAv profile, were concluded. In this case, the period interval of successive modes increases, so the maximum acceleration values also decrease. Moreover, the obtained FSAv profiles from the proposed equation, for the flexible nodes, in all considered cases show an almost perfect match with the selected earthquakes.

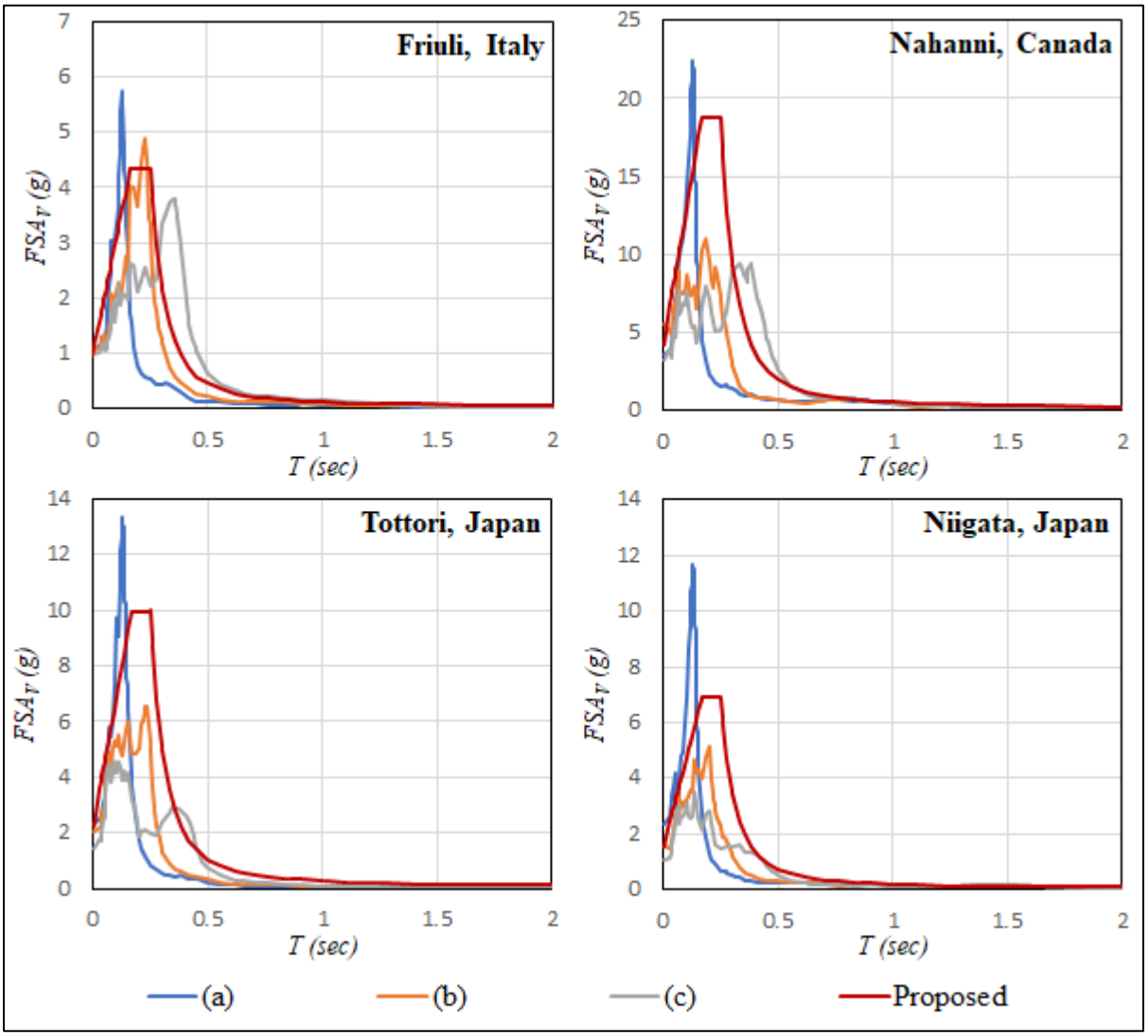

Figure 4.15 Obtained FSAv from the proposed and considered input time-history acceleration for 6-story buildings with (a) 5.0 m, (b) 7.0 m, and (c) 9.0 m span lengths

Moreover, to assess the effect of the floor height, the 6-storey building with the span length of 7.0 m was redesigned for the same building plan but with a finished height of the floors equal to 4.5 m. The elevation views and section details of considered buildings are given in Figure 4.16 and Table 4.5, respectively. For this purpose, the same four earthquake records presented in Table 4.4 were selected as the input vertical acceleration time histories.

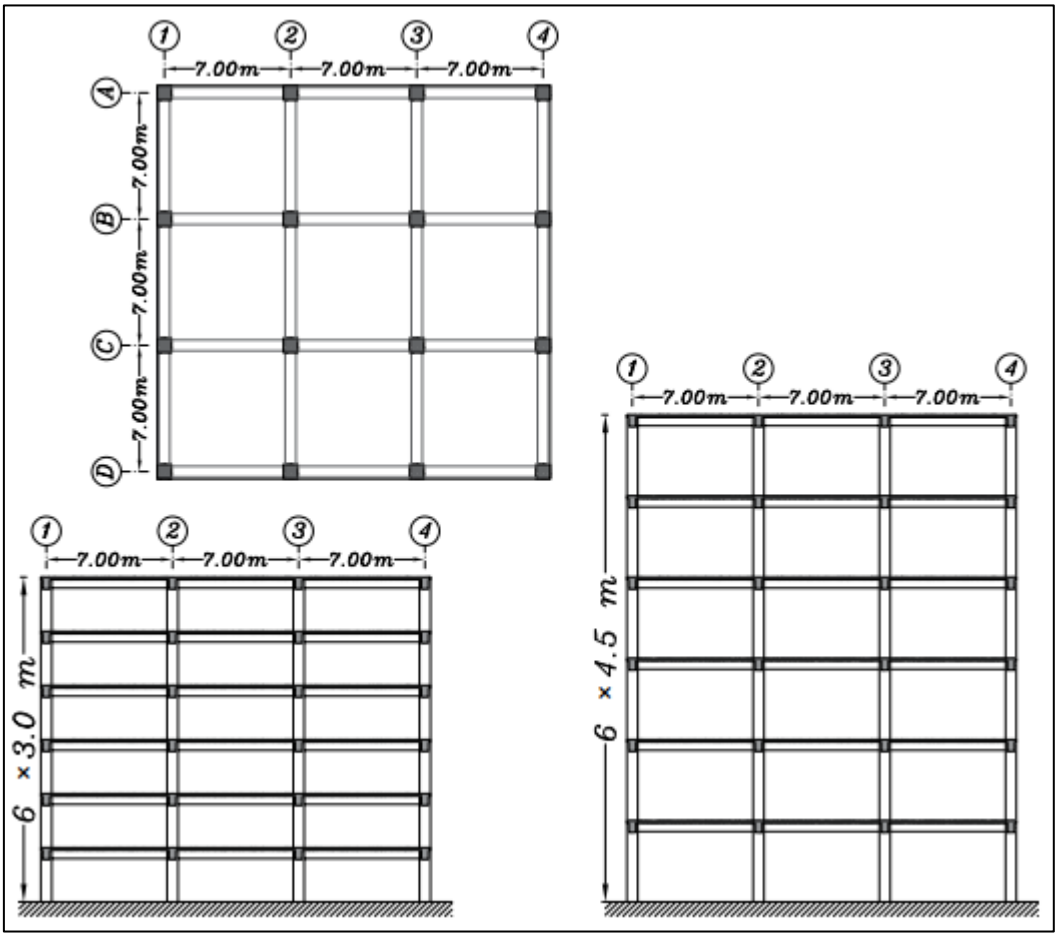

Figure 4.16 Selected 6-storey buildings with different floors height

Table 4.5 Cross-sectional dimensions of the 6-storey buildings' elements with (a) 3.0 m and (b) 4.5 m floors height

	Columns	Beams (b×h)

Structure Reference	Internal	External	X-direction	Y-direction
a	600×600	600×600	400×600	400×600
b	700×700	700×700	500×700	500×700

The results indicate that changing the height of the floors does not affect the vertical spectral accelerations of the floors, as illustrated in Figure 4.17.

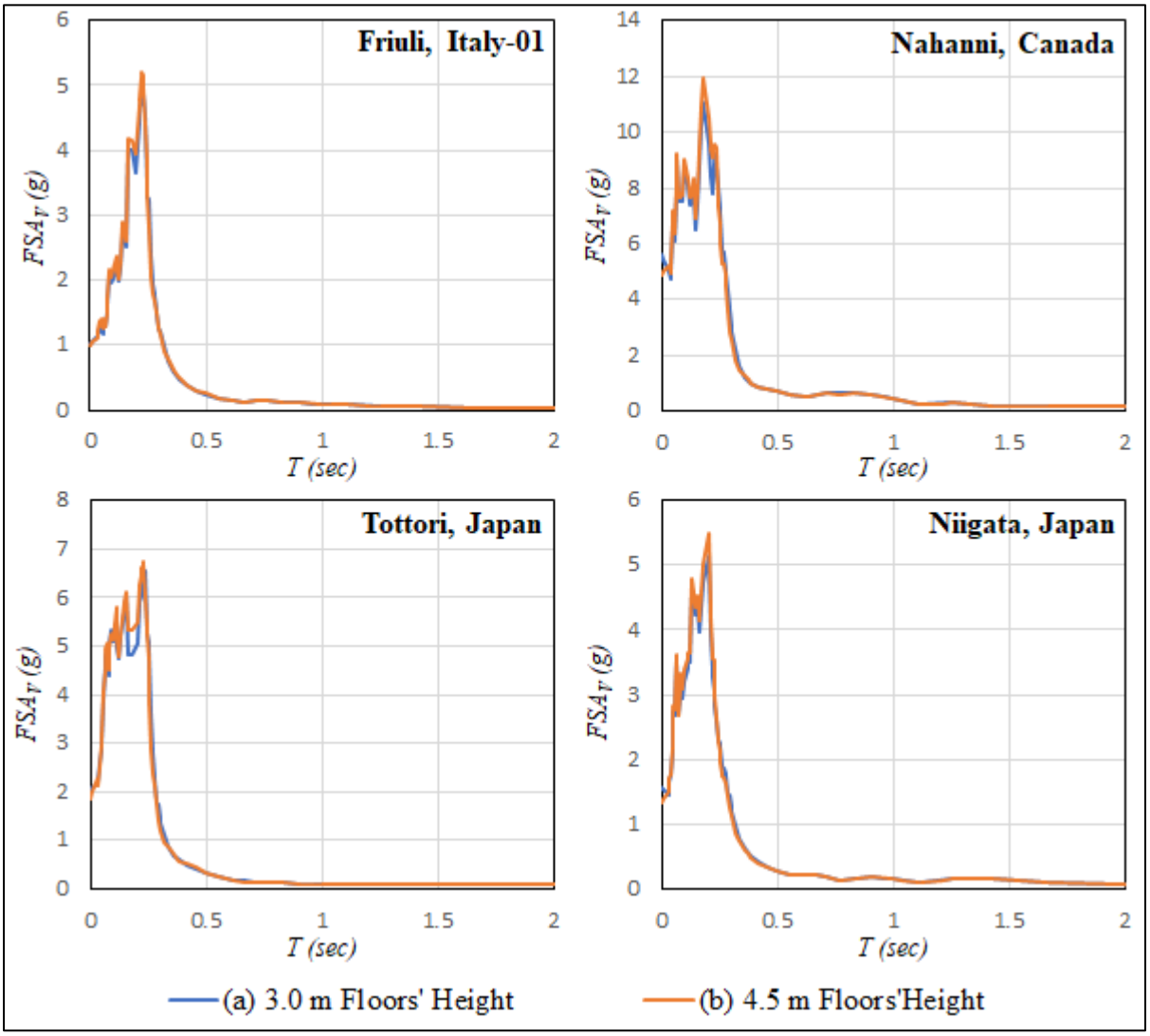

Figure 4.17 Comparison of the obtained FSA_V for two 6-storey buildings with different heights of the floors (a) 3.0 m, and (b) 4.5 m

4.9 Comparison of proposed FSA_V with AC 156 provisions

The results obtained from this study were compared with those obtained through the AC 156 (2010) equations used to derive horizontal and vertical floor spectral accelerations. Generally, the solutions referenced in the provisions to obtain the vertical spectral acceleration of the floors and seismic design force are based on the assumption of rigid floors at all mounting locations (Wieser et al., 2012). While this assumption is only valid for the nodes near columns and shear walls, which is not suitable for the nodes that can vibrate freely in the vertical direction, such as the nodes located at the center of a slab.

The method suggested in AC 156 provisions, known as the Required Response Spectrum (RRS), generates the seismic design force of NSCs according to the minimum requirements for the seismic qualification shake table test. The method presented in this standard is applicable for NSCs with a fundamental period of less than 0.75 sec, and is presented in Equation 4.7, for the horizontal and vertical RRS, as illustrated in Figure 4.18:

$$FSA_H = \begin{cases} \left(\frac{4}{3} - \frac{0.04}{T}\right) A_{FLX} - \left(\frac{1}{3} - \frac{0.04}{T}\right) A_{RIG} & T \leq 0.12 \\ A_{FLX} & 0.12 \leq T \leq 0.75 \\ \left(0.1 + \frac{0.675}{T}\right) A_{FLX} & T \geq 0.75 \end{cases} \quad (4.7)$$

where T is the period, A_{FLX} and A_{RIG} are the horizontal spectral acceleration for the flexible and rigid components, respectively, and are defined by Equations 4.8 and 4.9 in the horizontal direction. It should be noted that the value of A_{FLX} is limited to a maximum of 1.6 times the S_{DS}.

$$A_{FLX,H} = S_{DS}\left(1 + 2\frac{z}{H}\right) \quad (4.8)$$

$$A_{RIG,H} = 0.4S_{DS}\left(1 + 2\frac{z}{H}\right) = 0.4A_{FLX,H} \quad (4.9)$$

Also, these equations could be applied to the corresponding A_{FLX} and A_{RIG} in the vertical direction. The difference is that in the vertical seismic design force of NSCs proposed in ASCE/SEI 7-16 (2017), no amplification of acceleration is considered for the vertical response. Therefore, z may be taken as zero, and as a result, Equations 4.10 and 4.11 could be presented for the vertical spectral acceleration of the flexible and rigid components:

$$A_{FLX,V} = \frac{2}{3} A_{FLX,H} \tag{4.10}$$

$$A_{RIG,V} = \frac{2}{3} A_{RIG,H} = \frac{2}{3} \times 0.4 A_{FLX,H} \tag{4.11}$$

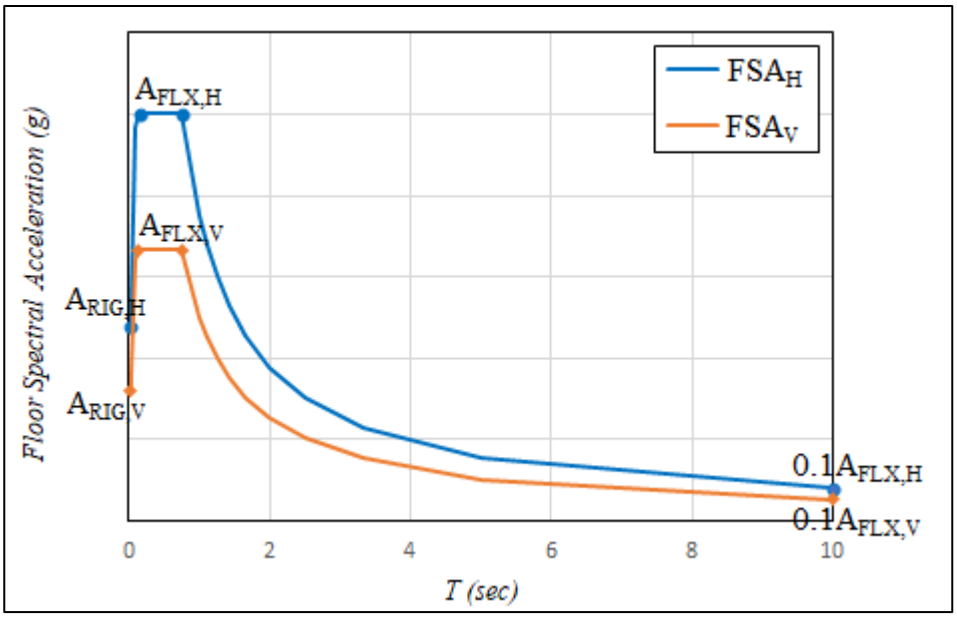

Figure 4.18 Horizontal and Vertical Required Response Spectrum (RRS) for the components at a 5% damping ratio

Taken from AC 156 (2010)

Figure 4.19 presents a comparison of the results for the rigid nodes of the buildings' rooftops, such as column nodes on the floor plan, obtained from the proposed equation of this study with considered code. As can be seen, maximum vertical accelerations equal to 0.724 was obtained at the period range of 0.12 to 0.75 sec. In contrast, the maximum acceleration of the proposed

spectra in this study is equal to 1.0 at the 0.067 to 0.25 sec period range. Also, it can be seen that using spectra proposed in the AC 156 yields underestimated values for shorter periods (T < 0.3 sec) and overestimated values for larger period ranges.

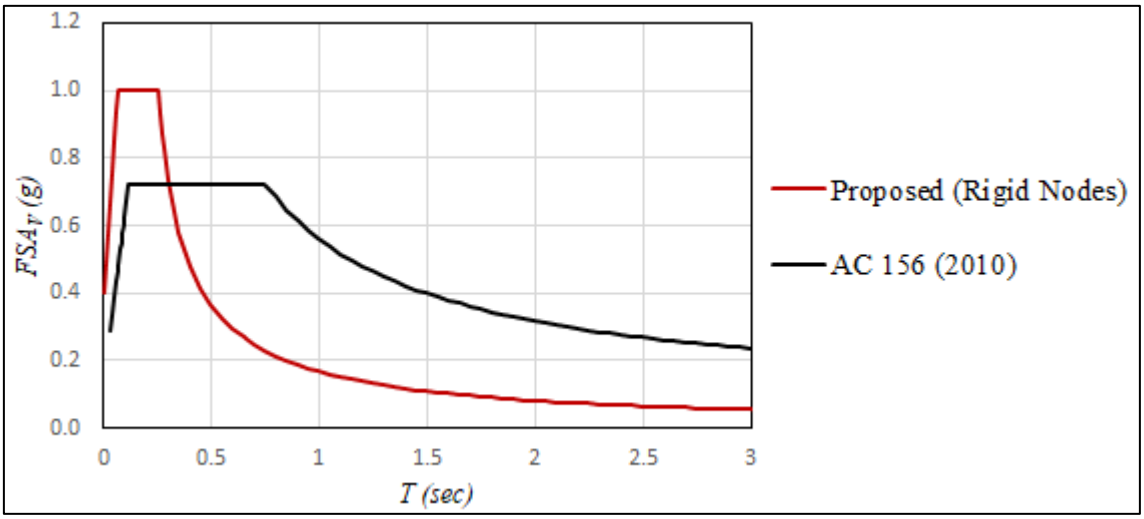

Figure 4.19 Comparison of FSAv proposed in this study for rigid nodes of rooftops with the one proposed in AC 156

4.10 Summary and conclusion

In this paper, the FSAv of four RC moment-resisting frame building archetypes designed according to NBC 2015 for the moderate ductility level, and exposed to 65 vertical acceleration time histories from 31 strong ground motions, were measured. The amplification of the FSAv along the height of each building and at different locations on a floor was assessed. The results show a high amplification at the center of the slabs, which was most critical for the interior slab bay. The spectra were amplified from a place close to the columns to the center of the slabs. Furthermore, a very intense spectral resonance was observed from the base to the first floors, especially for shorter buildings up to 9 stories. Then, the amplification was near-constant along the buildings' upper floors at all periods for the slab nodes. Also, the amplification of the FSAv from mid-rise to low-rise buildings increased drastically at the center of the interior slab.

Equations were proposed to derive the smoothed FSA_V for conventional RC moment-resisting frame buildings based on the median FSA_V obtained from the studied buildings with respect to the aforementioned input GSA_V. In this context, the equations were divided into two categories: one equation for the nodes at the center of the interior slab of the buildings lower than 12 storeys, and another one for the rigid nodes of all buildings close to the columns, as well as for all floor nodes of 12-storey and higher structures. The FSA_V obtained from the proposed equations for the studied buildings and corresponding to the selected GSA_V were presented as smoothed curves, in which the effect of the structure's height was also fully considered.

In addition, parametric analysis was performed to validate the adequacy of the proposed equations to derive FSA_V by varying the span length and the height of the floor. The results indicated that the proposed FSA_V for the flexible nodes was almost consistent with those obtained when the buildings with three different span lengths were subjected to strong earthquakes. Furthermore, it was also proved that the height of floors does not cause a change in the values of FSA_V.

It was also found that FSA_V demands on NSCs specified by AC 156 (2010) are unrealistic and conservative for tall structures and underestimated for short (shorter than mid-rise) structures. The vertical required response spectrum, defined by the AC 156 provisions, conservatively estimates the vertical acceleration demands on the NSCs attached to the columns of the building. Still, it fails to account for the acceleration amplification due to the out-of-plane flexibility of floors located away from the columns. Therefore, it can be confirmed that the approach proposed in the codes could be generally applied to the rigid nodes of the floor. However, for the rigid nodes, using the empirical ratio of 2/3 for the vertical to the horizontal spectral acceleration of the floors, proposed in this standard, provides overestimates spectral values for periods greater than 0.3 sec and underestimates for less than this period.

It is worth mentioning that the results from this study show the importance of accounting for the vertical acceleration in the shorter period within the range of less than 0.67 sec ($f \geq 1.5$Hz).

CONCLUSION

The conducted research in this thesis highlighted the importance of considering the vertical component of earthquakes in the Eastern Canadian seismological region, most notably in the analysis and design of NSCs attached to buildings. The key findings resulting from fulfilling the three specific objectives can be summarized in the following:

The first objective of this research consisted of proposing an accurate estimate of the vertical acceleration design spectra (ADS_{ver}) as a ratio of the horizontal acceleration design spectra (ADS_{hor}) for Site Class C in Eastern Canada. To this end, 248 earthquake horizontal and vertical time history records from moderate earthquakes of this region with a magnitude, M_w, greater than 3.0, recorded on sites with an epicentral distance of less than 150 km, were considered. Due to a lack of data on site Class C, the equivalent linear analysis, based on the Frequency Domain Solution recommended by Hashash et al. (2019) implemented in the DEEPSOIL software, was used to convert the accelerations recorded on a site with a specific shear wave velocity to the target average shear wave velocity of 450 m/s suggested in NBC 2015 as a reference for Site Class C. The accuracy of the conversion technique was checked by comparing the obtained V/H PSA ratios of the converted records with those from a small number of earthquakes records (19 in total) available for Site Class C. A similar ratio of 0.86 (average of V/H + Standard Deviation) was obtained for both available and converted records at a period range of less than 1.0 sec. According to the analysis done in this section, the following keys outcomes were obtained:

- The calculated V/H PSA ratios exceeded the empirical ratio of 2/3, suggested in most codes, at all period ranges, which highlights the importance of considering the vertical component of ground motions in the seismic analysis of NSCs located in the Eastern Canada region.
- The V/H acceleration ratio for periods less than 1.0 sec is almost consistent with the obtained ratios using the GMPEs proposed by Bozorgnia and Campbell (2004) and Gülerce & Abrahamson (2011).

- The ratio for the periods greater than 1.0 sec reached an average value of 0.73, which could be considered very close to the empirical value of 2/3. On the other hand, the average of the obtained ratios by GMPEs of the models by Bozorgnia and Campbell (2004) and Gülerce & Abrahamson (2011) yields a value of less than 2/3.
- For Eastern Canada seismic region, the ADS_{ver} ($S_{ver}(T)$) for Site Class C was proposed by scaling the $S_{hor}(T)$ using the ratio of 0.86 for the period less than 1.0 and 2/3 for periods greater than 1.0 sec.
- The obtained ADS_{ver} for Site Class C in Montreal, at a 2475-year return period, yielded higher values than the spectra derived by the proposed equations in ASCE 7-16 and ASCE 41-17 standards, especially for the shorter periods.

Second, the effect of the vertical ground motion on floor acceleration demands in typical RC moment-resisting frame buildings floor was evaluated. To this end, four regular elastic, low- to mid-rise multi-storey RC moment-resisting frame buildings, located in Montreal on Site Class C and designed according to NBC 2015 and CSA-A-23.3-14 provisions were subjected to 65 sets of time history accelerations recorded on Site Class C that were selected from 31 near field and strong worldwide earthquakes with magnitude greater than 5.5 ($M_W > 5.5$), a distance of less than 25 km from the epicenter ($R_{epi} < 25$ km), and PGA_{ver} greater than 0.25 g ($PGA_{ver} > 0.25$ g). It is worth noting that the fault mechanisms are Strike-Slip (SS), Reverse (RV), Reverse Oblique (RVO), Normal (N), and Normal Oblique (NO).

Both the PFA_H and PFA_V normalized with the corresponding PGA were statistically computed through the building heights, at the nodes at the center of the slabs and at the beams' spans, and the following main findings were concluded:

- An almost constant amplification of PFA_V through the building height was observed with an upward trend from the nodes near the columns to the center of the slabs. The most considerable amplification was obtained at the center of the mid-slab.
- No amplification of PFA_V was seen on the beams of the exterior frames, except in the 3-storey building rooftop, where the normalized amplification reached the value of 1.23 at the mid-span of the interior frame beam.

- By increasing the building's height, the amplification of PFA_V at the beam span or at the slab bay decreased. The median normalized PFA_V at the interior slab node of the building rooftops decreased from 4.45 for the 3-storey building to 1.24 for the 12-storey building.
- The median amplification of PGA_H, equal to 1.37, 1.44, 1.40, and 1.34, was found for the 3-, 6-, 9-, and 12-storey building rooftops, respectively that confirms the NBC 2015 amplification profile, which has a linear trend and showed that the normalized amplification of 3.0 at the rooftop is conservative.
- At the rooftop of the buildings, the obtained PFA_V/PFA_H exceeds the proposed empirical ratio of 2/3 in NBC 2015; however, as the height of the building increases, this ratio decreases.
- While the fundamental horizontal periods increased with the increase in the number of floors, the modal analysis of the buildings showed very little difference in the first vertical periods of the buildings.

Finally, the FSA_V of the selected buildings exposed to the same 65 vertical acceleration time histories from 31 strong ground motions were computed, and their amplification through the height of buildings was assessed. The following conclusions were derived from the obtained results:

- High amplification of FSA_V at the center of the slabs, especially in the interior slab, was observed. Therefore, the spectra were amplified from a place close to the columns to the centre of the slabs.
- A severe resonance of the FSA_V was observed from the base to the floors, especially for the shorter buildings. The FSA_V profile was constantly amplified along the buildings' floors at all periods.
- As the height of the building decreases, the PFA_V amplification tends to increase drastically.
- Two equations were proposed to derive the smoothed FSA_V curves for elastic regular RC moment-resisting frame structures from the input GSA_V. First, for the interior slab

nodes of the shorter buildings up to 9 stories, and secondly, for the nodes close to the columns for all buildings, and also the slab nodes of 12-storey structures and higher.

- The FSAv obtained using the equations proposed in this study is higher than the FSAv obtained using the empirical ratio of 2/3, as suggested by NBC 2015 and ATC 156 (2010).
- The importance of considering the vertical acceleration was highlighted at the shorter period within the range of less than 0.67 sec ($f \geq 1.5$Hz).

RECOMMENDATIONS FOR FUTURE STUDIES

Extensive efforts were made in the current thesis to emphasize the importance of considering the vertical component of an earthquake. However, more analytical studies are still necessary for future investigations to confirm and expand the observations obtained. Therefore, to complete this study and better investigate the subject, the author recommends the following future studies:

- Expand the derivation of the vertical spectral acceleration and the V/H PSA ratio for different Site Classes in the Eastern Canada seismic region.

- Derive the vertical spectral acceleration and the V/H PSA ratio in the Western Canada seismic region and compare results with those in Eastern Canada.

- In the seismic design of structures and NSCs, the vertical acceleration response assessment of the floors, including PFA_V and FSA_V, in different types of RC and steel Seismic Force Resisting Systems (SFRS) can provide a better pattern for developing the proposed PFA_V and FSA_V equations.

- Perform a parametric study to investigate the effect of the span length, the type of slab and building irregularity on the amplification of PFA_V and FSA_V.

- Investigate the effect of floor height on the vertical acceleration response of the floor can be a very interesting study, especially for low-rise buildings, i.e. to see whether increasing the floor height increases the amplification of vertical acceleration. As the floor height increases, the possibility of column buckling increases; therefore, an induced vertical acceleration can probably be effective in buckling failure.

- Perform a non-linear time-history analysis of the slabs to evaluate of effect of nonlinearity on the amplification of vertical floor accelerations and spectra.

ANNEX I

SELECTED EARTQUAKES FOR THE EASTERN CANADA SEISMIC REGION USED IN THE FIRST PAPER

Table-A I-1 Selected ground motions

No.	Earthquake	Date	EQ_{lat}	EQ_{lon}	M_w	Depth (km)	Station	STN_{lat}	STN_{lon}	V_{S30} (m/s)	Site Class	R_{epi} (km)
1	Miramichi	1982/03/31	47.00	-66.57	4.9	5.0	Indian Brook, NB	46.9788	-66.5803	2000	A	0.80
							Mitchell Lake Road, NB	47.0342	-66.6103	2000	A	3.90
							Loggie Lodge, NB	46.9692	-66.5290	2000	A	4.10
							Holmes Lake, NB	46.9455	-66.5945	2000	A	6.00
2	Miramichi	1982/05/06	47.00	-66.60	3.5	5.0	Loggie Lodge, NB	46.9692	-66.5290	2000	A	4.10
3	Saguenay	1988/11/25	48.117	-71.183	5.9	29.0	Chicoutimi-Nord, QC	48.4898	-71.0123	2000	A	43.39
							St-André-Du-Lac-St-Jean, QC	48.3249	-71.9886	2000	A	64.38
							Les Éboulements, QC	47.5485	-70.3258	2000	A	89.91
							Baie-St-Paul, QC	47.4275	-70.5156	2000	A	90.52
							La Malbaie, QC	47.6553	-70.1527	2000	A	92.59
							St-Lucie-de-Beauregard, QC	46.7418	-70.0160	2000	A	96.61
							Tadoussac, QC	48.1432	-69.7189	2000	A	109.02
							Saint-Ferréol, QC	47.1244	-70.8266	2000	A	113.41
							Rivière-Ouelle, QC	47.4680	-70.0096	2000	A	113.70
							St-Pascal, QC	47.5262	-69.8049	2000	A	122.40
							Quebec City, QC	46.7792	-71.2756	2000	A	149.01
4	Crique Rouge	1992/11/17	45.77	-74.93	4.0	16.0	Glen Almond, QC	45.7033	-75.4783	2000	A	43.24
5	Lac-du-Cerf	1993/05/06	46.3	-75.53	3.0	16.3	Glen Almond, QC	45.7033	-75.4783	2000	A	66.55
6	Salaberry-de-Valleyfield	1993/07/30	45.26	-74.12	3.3	8.1	Glen Almond, QC	45.7033	-75.4783	2000	A	116.94
7	Lac-Nominingue	1993/08/30	46.46	-75.06	3.2	14.5	Glen Almond, QC	45.7033	-75.4783	2000	A	90.22
8	La Malbaie	1993/12/01	47.47	-70.16	3.0	18.0	La-Malbaie, QC	47.5483	-70.3267	2000	A	15.27
9	Mont-Laurier	1993/12/25	46.49	-75.62	3.6	18.0	Glen Almond, QC	45.7033	-75.4783	2000	A	88.26
10	Saint-Joseph-de-la-Rive	1993/12/30	47.45	-70.36	3.3	6.2	La-Malbaie, QC	47.5483	-70.3267	2000	A	11.23
11	Port-au-Saumon	1994/09/25	47.77	-69.96	3.8	17.0	La-Malbaie, QC	47.5483	-70.3267	2000	A	36.95
12	Cheneville	1995/02/15	45.9	-75.04	3.0	18.0	Glen Almond, QC	45.7033	-75.4783	2000	A	40.45
13	Saint-Philippe	1995/09/12	45.6	-74.44	3.2	18.0	Glen Almond, QC	45.7033	-75.4783	2000	A	81.61

Continued Table-A I-1

No.	Earthquake	Date	EQ_{lat}	EQ_{lon}	M_W	Depth (km)	Station	STN_{lat}	STN_{lon}	V_{S30} (m/s)	Site Class	R_{epi} (km)
14	Lac-Aubin	1996/03/14	45.92	-74.4	4.0	18.0	Glen Almond, QC	45.7033	-75.4783	2000	A	87.08
15	Lac-Quinn	1996/12/31	46.49	-75.71	3.0	18.0	Glen Almond, QC	45.7033	-75.4783	2000	A	89.38
16	Lac-Aubin	1997/05/24	45.91	-74.24	3.7	18.0	Glen Almond, QC	45.7033	-75.4783	2000	A	98.81
17	Baie-Saint-Paul	1997/08/20	47.54	-70.29	3.2	7.5	St-Roch-des-Aulnaies, QC	47.2425	-70.1978	2000	A	33.84
							Rivière-Ouelle, QC	47.4706	-70.0064	2000	A	22.68
							St-André, QC	47.7036	-69.6897	2000	A	48.59
							Misère, QC	47.4567	-70.4125	2000	A	13.07
							Ste-Mathilde, QC	47.693	-70.09	2000	A	22.70
18	La Malbaie	1997/10/28	47.67	-69.91	4.3	11.3	St-Roch-des-Aulnaies, QC	47.2425	-70.1978	2000	A	52.29
							Rivière-Ouelle, QC	47.4706	-70.0064	2000	A	23.35
							St-André, QC	47.7036	-69.6897	2000	A	16.93
							Misère, QC	47.4567	-70.4125	2000	A	44.59
							Ste-Mathilde, QC	47.693	-70.09	2000	A	13.73
							St-Siméon, QC	47.8264	-69.8922	2000	A	17.46
19	Les Grands-Deserts	1997/11/06	46.8	-71.42	4.9	22.5	St-Roch-des-Aulnaies, QC	47.2425	-70.1978	2000	A	105.02
							Rivière-Ouelle, QC	47.4706	-70.0064	2000	A	130.51
							Misère, QC	47.4567	-70.4125	2000	A	105.67
							Ste-Mathilde, QC	47.693	-70.09	2000	A	141.36
20	Lac-Ministuk	1998/01/10	48.19	-70.91	3.2	18.0	St-Roch-des-Aulnaies, QC	47.2425	-70.1978	2000	A	118.20
							Rivière-Ouelle, QC	47.4706	-70.0064	2000	A	104.75
							St-André, QC	47.7036	-69.6897	2000	A	105.88
							Misère, QC	47.4567	-70.4125	2000	A	89.70
							Ste-Mathilde, QC	47.693	-70.09	2000	A	82.46
							St-Siméon, QC	47.8264	-69.8922	2000	A	85.93
							La-Malbaie, QC	47.5483	-70.3267	2000	A	83.67
21	Fort-Coulonge	1998/02/26	46.08	-76.36	3.2	18.0	Glen Almond, QC	45.7033	-75.4783	2000	A	80.16
22	Papineauville	1998/04/18	45.58	-74.97	3.6	18.0	Glen Almond, QC	45.7033	-75.4783	2000	A	41.87

Continued Table-A I-1

No.	Earthquake	Date	EQ_{lat}	EQ_{lon}	M_w	Depth (km)	Station	STN_{lat}	STN_{lon}	V_{S30} (m/s)	Site Class	R_{epi} (km)
23	La Conception	1998/07/30	46.19	-74.8	4.0	10.0	Glen Almond, QC	45.7033	-75.4783	2000	A	75.45
24	Lac-Saguay	1999/06/18	46.47	-75.1	3.0	18.0	Glen Almond, QC	45.7033	-75.4783	2000	A	90.21
25	Morin-Heights	1999/10/31	45.86	-74.3	3.7	18.0	Glen Almond, QC	45.7033	-75.4783	2000	A	93.12
26	Ajax, Ontario	1999/11/26	43.7	-78.98	3.3	5.0	Sadowa, ON	44.7694	-79.1417	2000	A	119.74
27	Saint-Pascal	2000/06/15	47.67	-69.8	3.2	11.4	St-Roch-des-Aulnaies, QC	47.2425	-70.1978	2000	A	56.23
							Rivière-Ouelle, QC	47.4706	-70.0064	2000	A	27.07
							St-André, QC	47.7036	-69.6897	2000	A	9.07
							Misère, QC	47.4567	-70.4125	2000	A	51.77
							Ste-Mathilde, QC	47.693	-70.09	2000	A	21.88
							St-Siméon, QC	47.8264	-69.8922	2000	A	18.73
							La-Malbaie, QC	47.5483	-70.3267	2000	A	41.79
28	Baie-Saint-Paul	2000/07/12	47.56	-71.06	3.7	18.0	St-Roch-des-Aulnaies, QC	47.2425	-70.1978	2000	A	73.96
							Rivière-Ouelle, QC	47.4706	-70.0064	2000	A	79.84
							St-André, QC	47.7036	-69.6897	2000	A	104.03
							Misère, QC	47.4567	-70.4125	2000	A	50.03
							Ste-Mathilde, QC	47.693	-70.09	2000	A	74.27
							St-Siméon, QC	47.8264	-69.8922	2000	A	92.39
							La-Malbaie, QC	47.5483	-70.3267	2000	A	55.11
29	Baie-Saint-Paul	2000/07/12	47.55	-71.08	3.0	18.0	St-Roch-des-Aulnaies, QC	47.2425	-70.1978	2000	A	74.77
							Rivière-Ouelle, QC	47.4706	-70.0064	2000	A	81.21
							St-André, QC	47.7036	-69.6897	2000	A	105.70
							Misère, QC	47.4567	-70.4125	2000	A	51.26
							Ste-Mathilde, QC	47.693	-70.09	2000	A	75.97
							St-Siméon, QC	47.8264	-69.8922	2000	A	94.18
							La-Malbaie, QC	47.5483	-70.3267	2000	A	56.60

Continued Table-A I-1

No.	Earthquake	Date	EQ_{lat}	EQ_{lon}	M_w	Depth (km)	Station	STN_{lat}	STN_{lon}	V_{S30} (m/s)	Site Class	R_{epi} (km)
30	Charlevoix	2001/05/22	47.65	-69.92	3.1	11.4	St-Roch-des-Aulnaies, QC	47.2425	-70.1978	2000	A	49.95
							Rivière-Ouelle, QC	47.4706	-70.0064	2000	A	21.00
							St-André, QC	47.7036	-69.6897	2000	A	18.26
							Misère, QC	47.4567	-70.4125	2000	A	42.80
							Ste-Mathilde, QC	47.693	-70.09	2000	A	13.61
							St-Siméon, QC	47.8264	-69.8922	2000	A	19.75
							La-Malbaie, QC	47.5483	-70.3267	2000	A	32.56
31	Cap-Chat	2002/01/20	49.49	-66.95	3.6	30.0	Islets-Caribou, QC	49.5217	-67.2719	2000	A	23.54
32	Notre-Dame-des-Prairies	2002/02/11	46.06	-73.46	3.3	10.0	Montreal, QC	45.5025	-73.6231	2000	A	63.34
33	Au-Sable-Forks	2002/04/20	44.53	-73.73	5.1	18.0	Montreal, QC	45.5025	-73.6231	2000	A	108.59
							Adirondack Community, NY	43.38	-73.66	1250.7	B	124.69
							Hanover (Dartmouth College)	43.70	-72.28	375.6	C	142.95
							Lisbon, NH	44.24	-71.92	1043	B	143.08
							Newcomb, NY	43.97	-74.22	1503	A	73.01
34	Au-Sable-Forks	2002/04/20	44.58	-73.73	3.6	18.0	Montreal, QC	45.5025	-73.6231	2000	A	103.04
35	Port-Cartier	2002/07/23	49.59	-66.95	3.5	18.0	Islets-Caribou, QC	49.5217	-67.2719	2000	A	24.46
36	Baie-Saint-Paul	2002/08/17	47.33	-70.51	3.3	13.3	St-Roch-des-Aulnaies, QC	47.2425	-70.1978	2000	A	25.51
							Rivière-Ouelle, QC	47.4706	-70.0064	2000	A	41.05
							St-André, QC	47.7036	-69.6897	2000	A	74.39
							Misère, QC	47.4567	-70.4125	2000	A	15.90
							Ste-Mathilde, QC	47.693	-70.09	2000	A	51.29
							St-Siméon, QC	47.8264	-69.8922	2000	A	72.15
							La-Malbaie, QC	47.5483	-70.3267	2000	A	27.95
37	Saint Regis Falls	2003/04/08	44.62	-74.37	3.2	11.9	Glen Almond, QC	45.7033	-75.4783	2000	A	148.69
							Keeseville, NY	44.5524	-73.6861	2000	A	54.74
							Montreal, QC	45.5025	-73.6231	2000	A	114.46
							Ottawa, ON	45.3942	-75.7167	1914	A	136.61

Continued Table-A I-1

No.	Earthquake	Date	EQ_{lat}	EQ_{lon}	M_W	Depth (km)	Station	STN_{lat}	STN_{lon}	V_{S30} (m/s)	Site Class	R_{epi} (km)
38	La Malbaie	2003/06/13	47.7	-70.09	3.6	11.1	St-Roch-des-Aulnaies, QC	47.2425	-70.1978	2000	A	51.57
							Rivière-Ouelle, QC	47.4706	-70.0064	2000	A	26.30
							St-André, QC	47.7036	-69.6897	2000	A	29.99
							Misère, QC	47.4567	-70.4125	2000	A	36.33
							Ste-Mathilde, QC	47.693	-70.09	2000	A	0.78
							St-Siméon, QC	47.8264	-69.8922	2000	A	20.42
							La-Malbaie, QC	47.5483	-70.3267	2000	A	24.51
39	Les-des-Plages	2003/08/20	46.01	-74.95	3.0	18.0	Glen Almond, QC	45.7033	-75.4783	2000	A	53.32
							Montreal, QC	45.5025	-73.6231	2000	A	117.53
							Ottawa, ON	45.3942	-75.7167	1914	A	90.84
40	La Baie	2004/05/04	47.94	-70.67	3.0	22.0	St-Roch-des-Aulnaies, QC	47.2425	-70.1978	2000	A	85.36
							Rivière-Ouelle, QC	47.4706	-70.0064	2000	A	72.12
							St-André, QC	47.7036	-69.6897	2000	A	77.85
							Misère, QC	47.4567	-70.4125	2000	A	57.16
							Ste-Mathilde, QC	47.693	-70.09	2000	A	51.34
							St-Siméon, QC	47.8264	-69.8922	2000	A	59.43
							La-Malbaie, QC	47.5483	-70.3267	2000	A	50.61
41	Port Hope	2004/08/04	43.68	-78.24	3.2	4.0	Acton, ON	43.6087	-80.0624	966	B	147.01
							Deloro Mine, ON	44.5177	-77.6186	2000	A	105.66
							Prince Edward County, ON	43.934	-76.9939	1000	B	104.03
							Pickering, ON	43.9643	-79.0714	403	C	73.90
							St. Catherines, ON	43.2096	-79.1705	415	C	91.64
							Tyneside, ON	43.095	-79.8702	404	C	147.08
							Wesleyville, ON	43.9236	-78.397	1137	B	29.90
							Port Colborne, ON	42.8844	-79.3115	1000	B	123.56
							Toronto-Leslie Street Spit, ON	43.6136	-79.3433	303	D	89.50

Continued Table-A I-1

No.	Earthquake	Date	EQ_{lat}	EQ_{lon}	M_w	Depth (km)	Station	STN_{lat}	STN_{lon}	V_{S30} (m/s)	Site Class	R_{epi} (km)
42	Val-David	2005/03/03	45.06	-74.2	3.0	18.0	Alfred, ON	45.6283	-74.8842	1000	B	82.87
							Glen Almond, QC	45.7033	-75.4783	2000	A	122.95
							Montreal, QC	45.5025	-73.6231	2000	A	66.85
							Morin-Heights	45.887	-74.2127	2000	A	92.07
43	Rivière-du-Loup	2005/03/06	47.75	-69.73	4.70	13.3	St-Roch-des-Aulnaies, QC	47.2425	-70.1978	2000	A	66.56
							Rivière-Ouelle, QC	47.4706	-70.0064	2000	A	37.39
							St-André, QC	47.7036	-69.6897	2000	A	5.98
							Misère, QC	47.4567	-70.4125	2000	A	60.75
							Ste-Mathilde, QC	47.693	-70.09	2000	A	27.70
							St-Siméon, QC	47.8264	-69.8922	2000	A	14.82
							Les Éboulements, QC	47.5485	-70.3258	2000	A	50.00
							HQ. CHAR, QC	47.69	-70.25	1026	B	39.44
44	Notre-Dame-de-Pontmain	2005/05/25	46.27	-75.62	3.2	18.0	Alfred, ON	45.6283	-74.8842	1000	B	91.36
							Glen Almond, QC	45.7033	-75.4783	2000	A	64.03
							Morin-Heights, QC	45.887	-74.2127	2000	A	116.73
							Ottawa, ON	45.3942	-75.7167	1914	A	97.78
45	Fort-Coulonge	2005/07/04	46.25	-76.9	3.1	14.5	Algonquin Park, ON	45.9544	-78.0509	354	D	94.73
							Glen Almond, QC	45.7033	-75.4783	2000	A	125.70
							Ottawa, ON	45.3942	-75.7167	1914	A	132.30
							Pembroke, ON	45.6773	-77.2466	591	C	69.16
							Plevna, ON	45.0396	-77.0754	2000	A	135.43
46	La Minerve	2005/09/06	46.27	-75.29	3.0	19.5	Alfred, ON	45.6283	-74.8842	1000	B	78.04
							Glen Almond, QC	45.7033	-75.4783	2000	A	64.75
							Morin-Heights, QC	45.887	-74.2127	2000	A	93.48
							Ottawa, ON	45.3942	-75.7167	1914	A	102.96

Continued Table-A I-1

No.	Earthquake	Date	EQ_{lat}	EQ_{lon}	M_w	Depth (km)	Station	STN_{lat}	STN_{lon}	V_{S30} (m/s)	Site Class	R_{epi} (km)
47	Georgian Bay	2005/10/20	44.68	-80.48	3.8	11.0	Acton, ON	43.6087	-80.0624	966	B	123.84
							Bruce Peninsula, ON	44.2437	-81.4423	282	D	90.57
							Buck Lake, ON	45.4423	-79.3989	1000	B	120.11
							Collingwood, ON	44.4491	-80.3013	500	C	29.36
							Elora Gorge, ON	43.6755	-80.4374	1078	B	111.88
							Killbear Provincial Park, ON	45.3566	-80.2132	2000	A	78.19
							Lindsay, ON	44.3541	-78.7802	945	B	139.72
							Pickering, ON	43.9643	-79.0714	403	C	137.59
							Sadowa, ON	44.7694	-79.1417	2000	A	106.32
							Tobermory, ON	45.2257	-81.5234	1000	B	102.21
							Toronto-Leslie Spit, ON	43.6136	-79.3433	303	D	149.45
48	Franklin	2006/01/09	45.03	-73.9	3.7	15.0	Glen Almond, QC	45.7033	-75.4783	2000	A	144.41
							Montreal, QC	45.5025	-73.6231	2000	A	56.90
							Morin-Heights, QC	45.887	-74.2127	2000	A	98.48
							Ottawa, ON	45.3942	-75.7167	1914	A	148.12
49	Thurso	2006/02/25	45.65	-75.23	4.1	20.0	Alfred, ON	45.6283	-74.8842	1000	B	27.02
							Glen Almond, QC	45.7033	-75.4783	2000	A	20.20
							Montreal, QC	45.5025	-73.6231	2000	A	126.28
							Murphy's Point, ON	44.77	-76.2648	2000	A	127.21
							Ottawa, ON	45.3942	-75.7167	1914	A	47.45
							Lake Ozonia, NY	44.6197	-74.5829	1425	B	125.16
50	Acadia	2006/10/03	44.367	68.147	3.87	10	Saint-George, NB	45.1184	-66.8420	2000	A	134.85
							Waterville, ME	44.5640	-69.6626	694.5	C	122.07
51	Baie-Saint-Paul	2006/04/07	47.38	-70.46	3.8	24.5	St-Roch-des-Aulnaies, QC	47.2425	-70.1978	2000	A	25.02
							Rivière-Ouelle, QC	47.4706	-70.0064	2000	A	35.62
							St-André, QC	47.7036	-69.6897	2000	A	68.18
							Misère, QC	47.4567	-70.4125	2000	A	9.26
							Ste-Mathilde, QC	47.693	-70.09	2000	A	44.58
							Saint-Siméon, QC	47.8264	-69.8922	2000	A	65.47
							La-Malbaie, QC	47.5483	-70.3267	2000	A	21.25
52	Sainte-Anne-des-Monts	2006/05/28	49.56	-66.28	3.1	18.0	Islets-Caribou, QC	49.5217	-67.2719	2000	A	71.78

Continued Table-A I-1

No.	Earthquake	Date	EQ_{lat}	EQ_{lon}	M_w	Depth (km)	Station	STN_{lat}	STN_{lon}	V_{S30} (m/s)	Site Class	R_{epi} (km)
53	Eagle Lake	2006/07/14	46.85	-68.65	3.5	5.0	St-Roch-des-Aulnaies, QC	47.2425	-70.1978	2000	A	125.27
							Rivière-Ouelle, QC	47.4706	-70.0064	2000	A	123.75
							St-André, QC	47.7036	-69.6897	2000	A	123.27
							Ste-Mathilde, QC	47.693	-70.09	2000	A	143.65
							Saint-Siméon, QC	47.8264	-69.8922	2000	A	143.51
							La-Malbaie, QC	47.5485	-70.3258	2000	A	148.70
54	Smooth Rock Falls	2006/12/07	49.51	-81.53	3.7	16.0	Kapuskasing, ON	49.4504	-82.5079	2000	A	71.04
							McAlpine Lake, ON	50.0244	-79.7635	2000	A	139.32
							Otter Rapids, ON	50.1818	-81.6286	500	C	75.12
							Timmins, ON	48.4659	-81.3032	2000	A	117.41
55	Lac Saint-Crepin	2007/10/01	47.06	-76.88	3.6	17.0	Belleterre, QC	47.398	-78.6874	2000	A	141.71
							Val-d'Or, QC	48.1901	-77.7573	2000	A	141.98
56	Rivière-du-Loup	2008/11/15	47.74	-69.74	3.7	13.3	Rivière-Ouelle, QC	47.4706	-70.0064	2000	A	36.04
							St-André, QC	47.7036	-69.6897	2000	A	5.53
							Misère, QC	47.4567	-70.4125	2000	A	59.52
							Saint-Siméon, QC	47.8264	-69.8922	2000	A	14.90
							La-Malbaie, QC	47.5483	-70.3267	2000	A	48.90
57	Brownsburg-Chatham	2010/02/28	45.715	-74.464	3.2	17.5	Alfred, ON	45.6283	-74.8842	2000	A	34.08
							Potsdam, NY	44.57	-74.9819	653.6	C	133.79
58	Val-des-Bois	2010/06/23	45.91	-75.49	5.1	16.4	Alfred, ON	45.6283	-74.8842	2000	A	57.99
							Orleans; Innes Road, ON	45.4515	-75.511	1700	A	52.94
							Pembroke, ON	45.6773	-77.2466	591	C	138.13
							SUNY Potsdam, NY	44.6634	-74.9732	555	C	114.07
59	Hawkesbury	2011/03/16	45.581	-74.553	3.6	12.8	Alfred, ON	45.6283	-74.8842	2000	A	26.33
							Flat Rock, Altona, NY	44.835	-73.5883	1200.6	B	112.34
							SUNY Potsdam, NY	44.6634	-74.9732	555	C	107.35
60	Thurso	2011/09/18	45.578	-75.213	3.5	12.5	Alfred, ON	45.6283	-74.8842	2000	A	26.21
							SUNY Potsdam, NY	44.6634	-74.9732	555	C	103.54
61	Verchères	2012/10/10	45.711	-73.257	3.7	14	Alfred, ON	45.6283	-74.8842	2000	A	126.91
							Flat Rock, Altona, NY	44.835	-73.5883	1200.6	B	100.91

Continued Table-A I-1

No.	Earthquake	Date	EQ_{lat}	EQ_{lon}	M_w	Depth (km)	Station	STN_{lat}	STN_{lon}	V_{S30} (m/s)	Site Class	R_{epi} (km)
62	Hawkesbury	2012/11/06	45.601	-74.591	3.5	6.5	Flat Rock, Altona, NY	44.835	-73.5883	1200.6	B	115.99
							Glen Almond, QC	45.7033	-75.4783	2000	A	69.92
							Ottawa, ON	45.3942	-75.7167	1914	A	90.80
							SUNY Potsdam, NY	44.6634	-74.9732	555	C	108.60
63	Shawville	2013/05/17	45.74	-76.345	4.5	13	Alfred, ON	45.6283	-74.8842	2000	A	114.28
							Bancroft, ON	45.0198	-77.928	2000	A	147.47
							Glen Almond, QC	45.7033	-75.4783	2000	A	67.54
							Ottawa, ON	45.3942	-75.7167	1914	A	62.28
							Pembroke, ON	45.6773	-77.2466	591	C	70.43
							Plevna, ON	45.0396	-77.0754	2000	A	96.64
64	Shawville	2013/05/17	45.746	-76.345	3.3	14	Alfred, ON	45.6283	-74.8842	2000	A	114.35
							Bancroft, ON	45.0198	-77.928	2000	A	147.83
							Glen Almond, QC	45.7033	-75.4783	2000	A	67.58
							Ottawa, ON	45.3942	-75.7167	1914	A	62.70
							Pembroke, ON	45.6773	-77.2466	591	C	70.50
							Plevna, ON	45.0396	-77.0754	2000	A	97.18
65	Saddlebrook	2013/05/21	45.438	-74.197	3.0	18	Alfred, ON	45.6283	-74.8842	2000	A	57.62
							Flat Rock, Altona, NY	44.835	-73.5883	1200.6	B	82.40
							Glen Almond, QC	45.7033	-75.4783	2000	A	104.07
							Ottawa, ON	45.3942	-75.7167	1914	A	118.85
							SUNY Potsdam, NY	44.6634	-74.9732	555	C	105.65
66	Hawkesbury	2015/07/15	45.47	-74.54	3.5	14.5	Alfred, ON	45.6283	-74.8842	2000	A	32.10
							Flat Rock, Altona, NY	44.835	-73.5883	1200.6	B	102.85
							Glen Almond, QC	45.7033	-75.4783	2000	A	77.52
							Ottawa, ON	45.3942	-75.7167	1914	A	92.31
67	NE of Shawville	2015/09/09	45.764	-76.344	3.2	14.5	Alfred, ON	45.6283	-74.8842	2000	A	114.50
							Bancroft, ON	45.0198	-77.928	2000	A	148.98
							Glen Almond, QC	45.7033	-75.4783	2000	A	67.66
							Ottawa, ON	45.3942	-75.7167	1914	A	63.90
							Pembroke, ON	45.6773	-77.2466	591	C	70.81
							Plevna, ON	45.0396	-77.0754	2000	A	98.85

ANNEX II

CONVERSION TECHNIQUE USING DEEPSOIL SOFTWARE

Detailed explanations about the instruction and operation of this software are given in the tutorial note prepared by Hashash et al. (2019). In addition, a brief explanation of the method of using this software related to this study was provided in this section as the following steps:

- **Step 1:**

In the following, all analytical items considered at this step were presented as well as Figure-A II-1:

- **Analysis Method:**

The linear method does not give precise and correct results, and since there were not enough soil databases, the Equivalent Linear Method of Analysis is applied.

- **Solution Type:**

Time and frequency domains as the Solution Types were considered in this software, and Frequency Domain Solution is just applicable to the Equivalent Linear Method.

- **Default Soil Model:**

Whether in equivalent linear or nonlinear methods, the shear stiffness and damping of the soil are related to the developed shear strains in the soil sample with the aid of a constitutive soil model. The model used in DEESOIL is the pressure-dependent hyperbolic model, which defines the interrelationship between the stresses and strains developed in soil subjected to a cyclic loading-unloading phenomenon. Generally, the development of cyclic shear stress due to the cyclic strains or vice versa is governed by Massing and Extended Massing rules (Park, 2003). The hyperbolic model is defined as a strain-dependent model and as a modification on the original strain-independent hyperbolic Kondner and Zelasko model, popularly known as

the Pressure-Dependent Modified Konder Zelasko (MKZ) (Kondner & Zelasko, 1963) backbone curve, which defines the stress-strain relationship for loading-unloading and this soil model was considered in this software (Kumar et al., 2014).

- **Profile Generation Type:**

Because the details of the soil layers for the site were not completely available, it was reasonable to consider the Automatic Profile Generation to get precise results for the conversion purpose. On the other hand, since the Equivalent Linear method was adopted as the solution type, which mainly involves the nonlinearity of the soils, the Automatic Profile Generation could be the best option according to the thickness of the layer.

- **Frequency Type:**

In the part Maximum Layer Thickness, the required Maximum Frequency is specified. In this study, the maximum frequency of 50, 100, and 200 Hz were selected. A frequency of 100 Hz was considered for the precise and logical progression of this operation, as shown in Figure-A II-2. Also, the software could automatically find the frequency of the input earthquake.

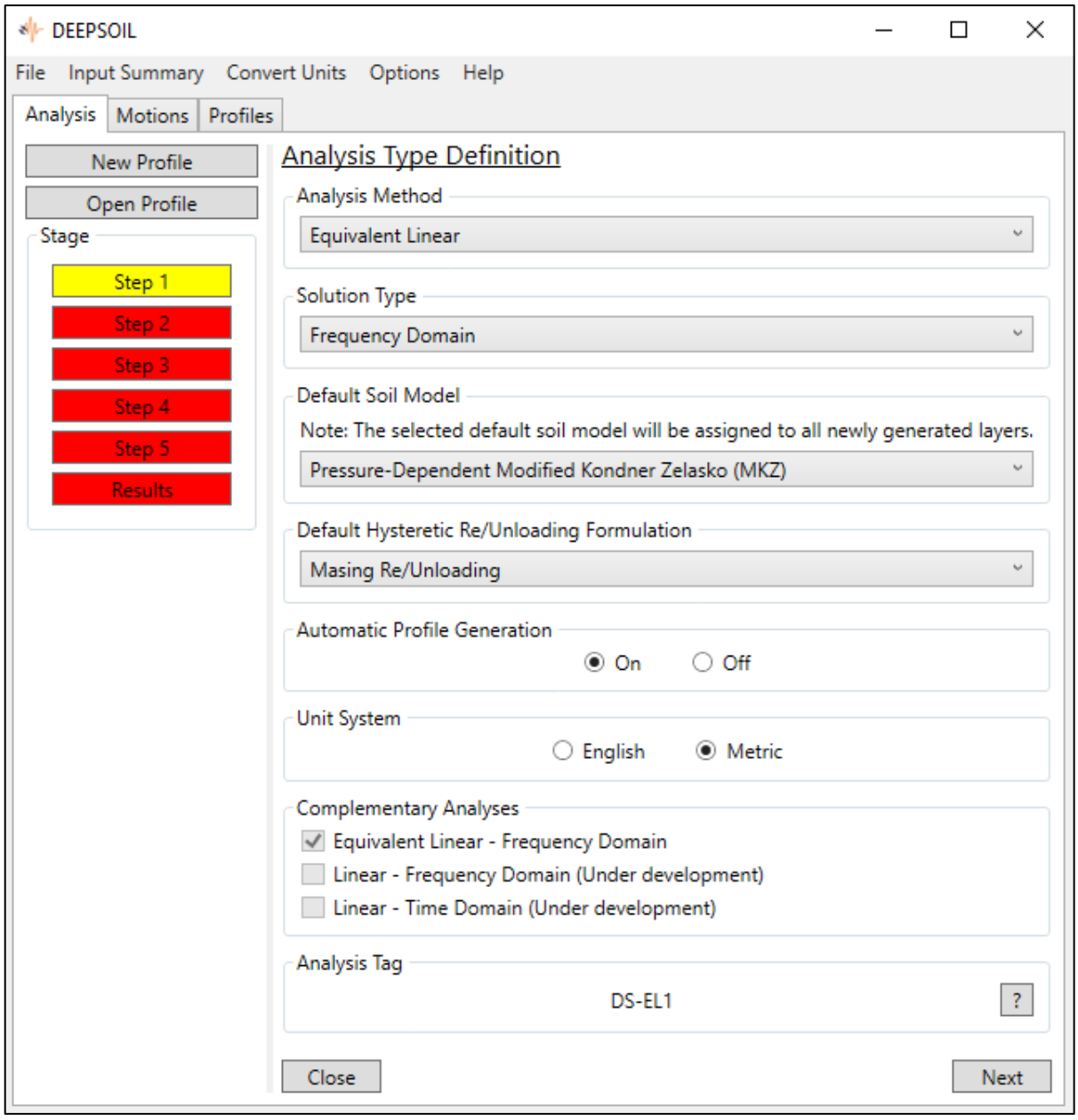

Figure-A II-1 Considered analysis type definition in the conversion of time history acceleration

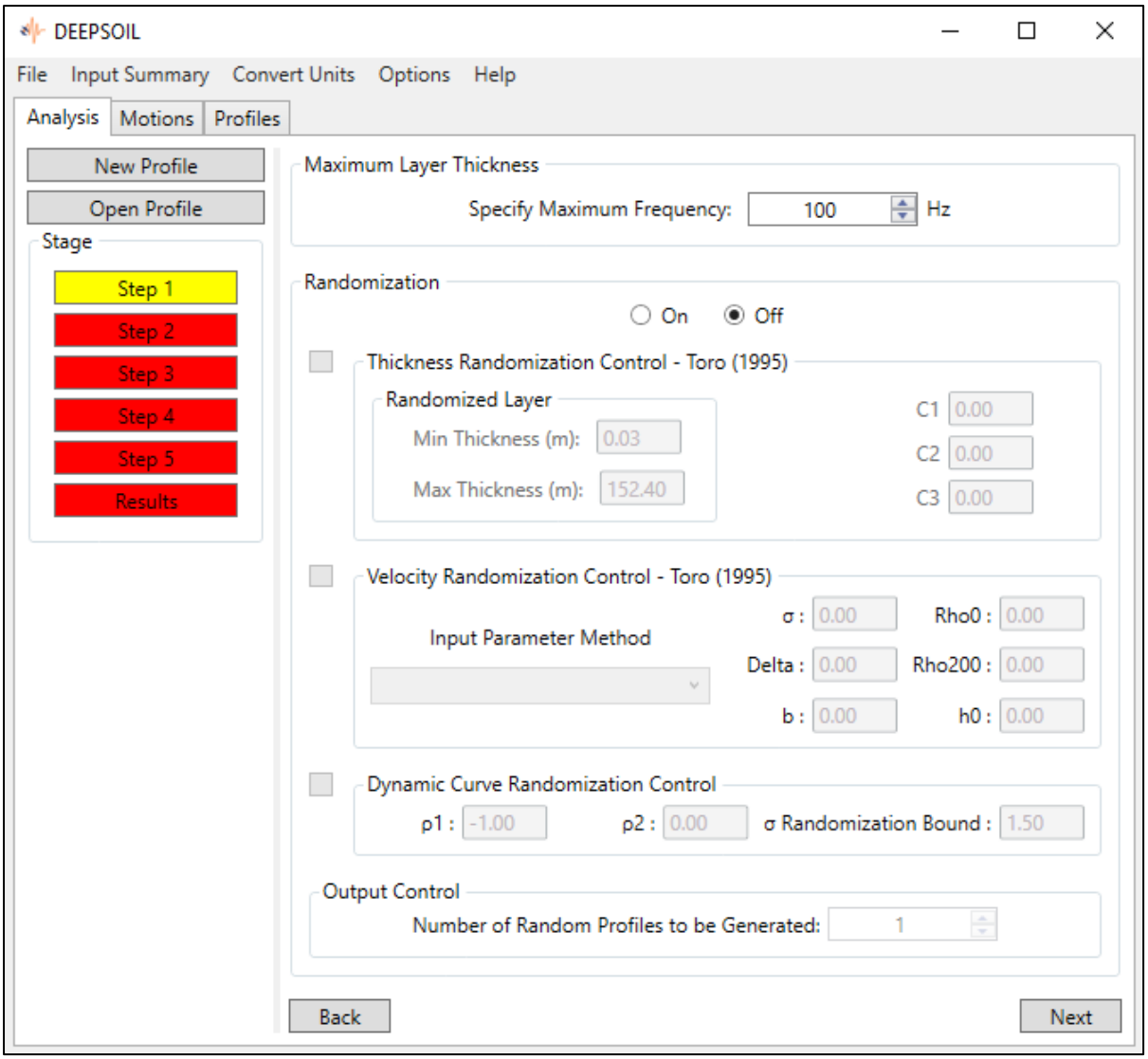

Figure-A II-2 Maximum considered frequency in the conversion process

➢ **Step 2:**

- **Soil Profile Definition**

In the next step, the layer properties of the soil profile, including thickness, unit weight, and Effective Vertical Stress, are entered to the software. In this process, the thickness of the layer was given as a focal depth of the earthquake, and the soil unit weight of the layer could be approximately estimated knowing its shear wave velocity (Look, 2007). The corresponding

shear wave velocity and shear modulus, the soil's density, could be calculated according to the online reference by Dhari (2019). It should be mentioned that the Effective Vertical Stress could be automatically computed by entering the thickness and unit weight of the layer.

In addition, the target shear wave velocity (450 m/s), indicating the soil type in the surface layer, is also entered into the software.

The sand and clay are two options for the Mean Layer Reference Curve that should be defined in the following process. The Seed and Idriss (Mean) (Seed & Idriss, 1970), and Vucetic and Dobry (Vucetic & Dobry, 1991; Vucetic, 1992) reference curves were selected as the Mean Layer Reference for the sand and clay, respectively. The Mean layer properties of the soil with layer reference curve of the sand and clay were illustrated in Figure-A II-3 and Figure-A II-4, respectively.

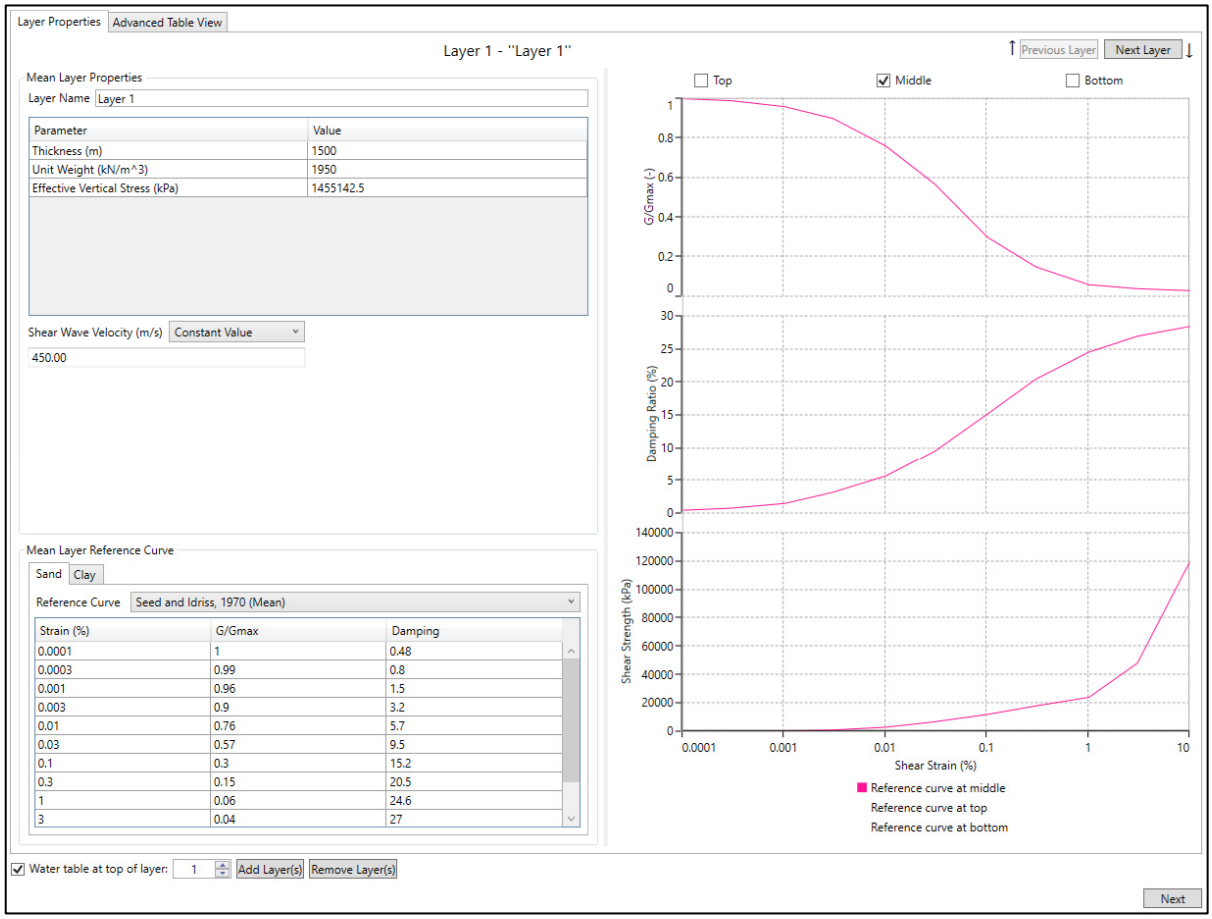

Figure-A II-3 Mean layer properties of the soil and the mean layer reference curve of the sand

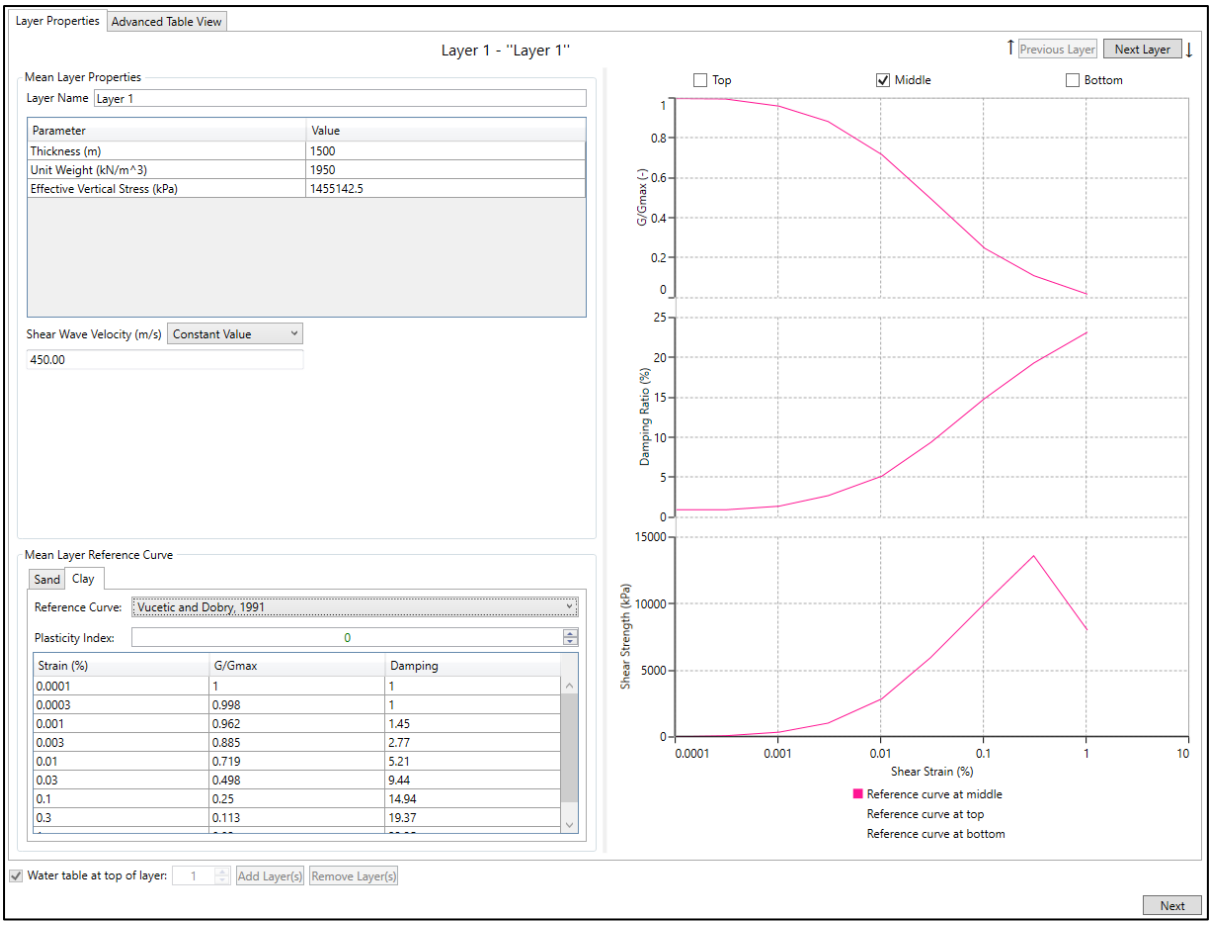

Figure-A II-4 Mean layer properties of the soil and the mean layer reference curve of the clay

For the bedrock layer known as the input record layer base, the semi Elastic Half-space behavior was considered, as shown in Figure-A II-5. The bedrock properties, including shear wave velocity and unit weight, were applied in this part.

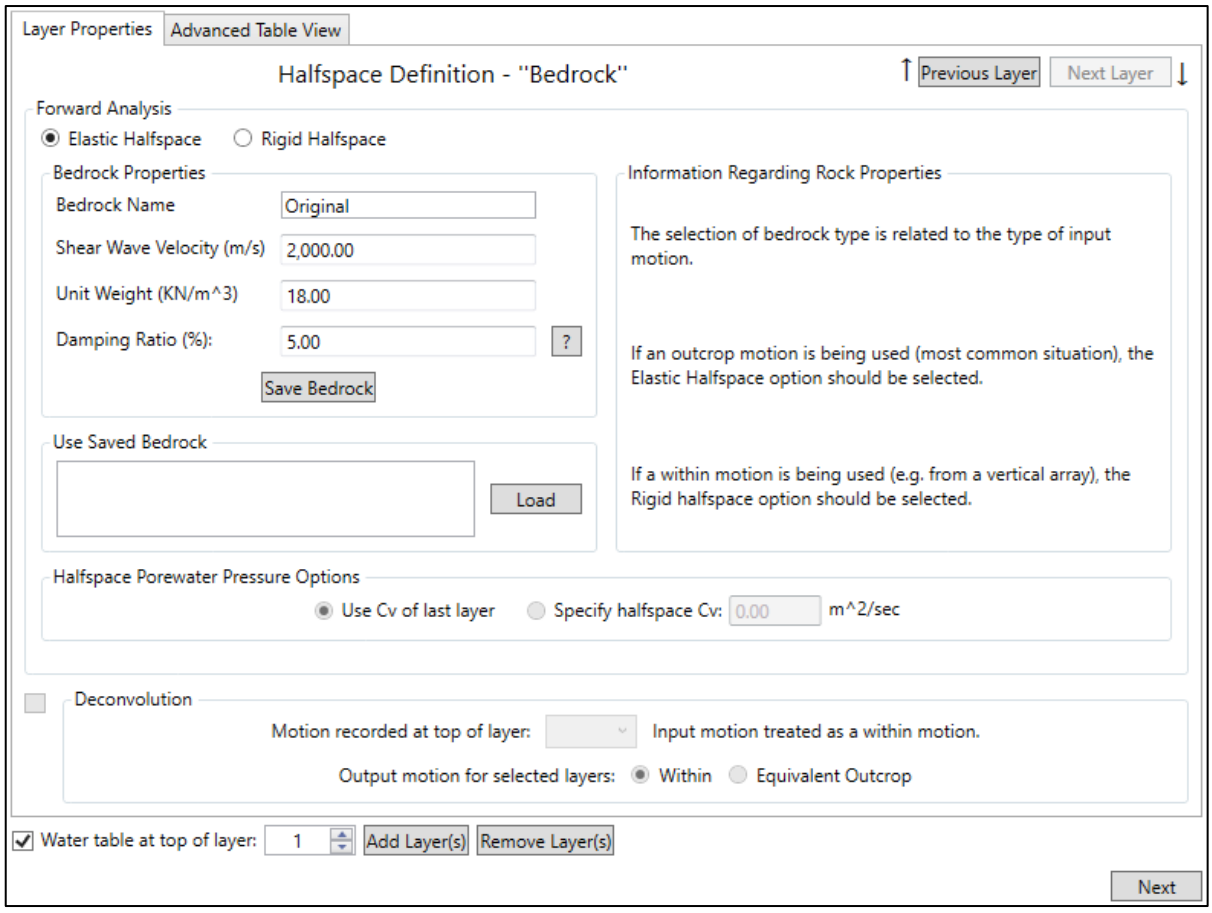

Figure-A II-5 Definition of the bedrock layer known as the original soil information

- **Generated Soil Profile Definition**

In the next step, according to the recommended references, a defined soil profile is generated, as can be seen in Figures-A II-6 and Figures-A II-7, respectively.

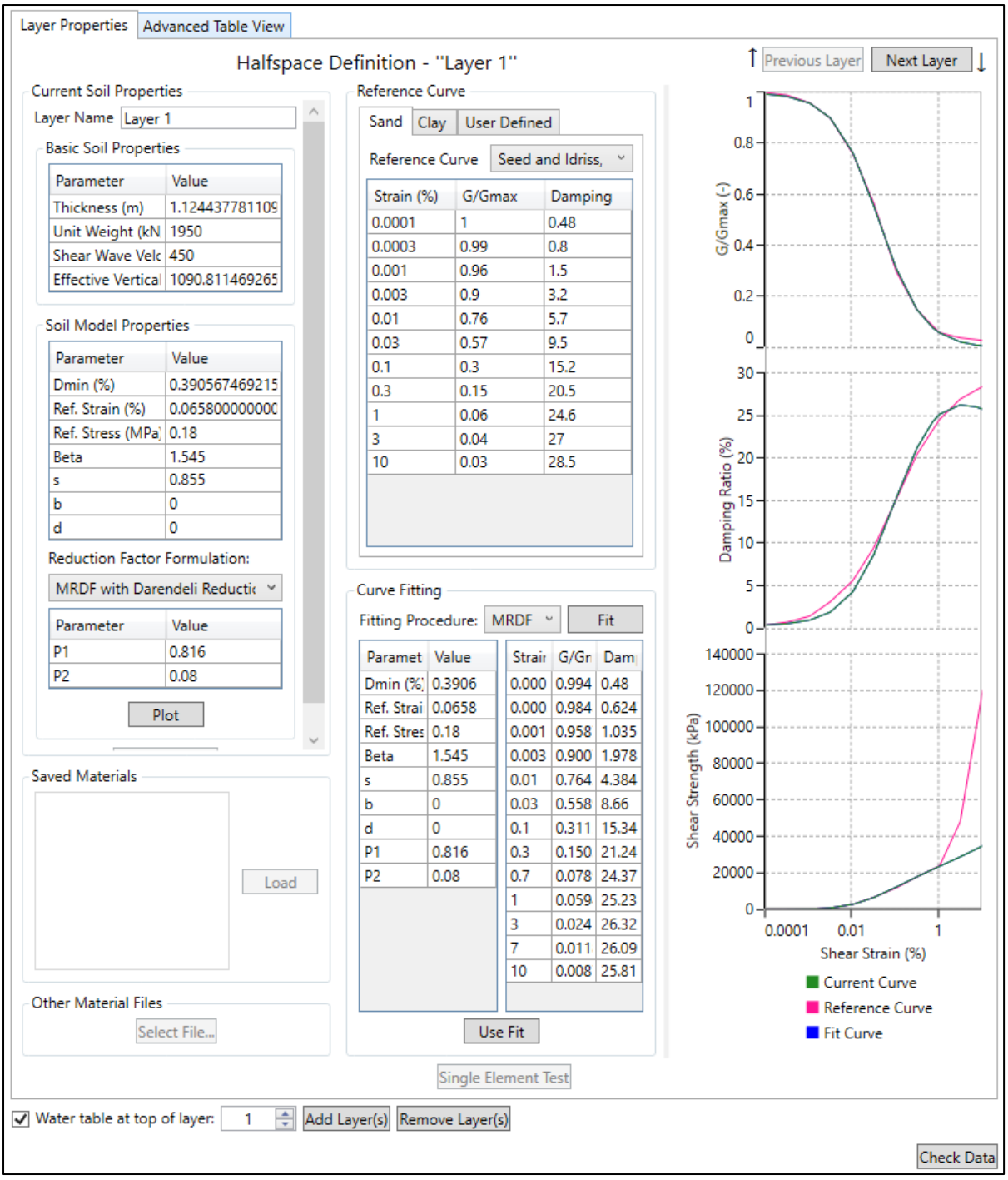

Figure-A II-6 Generated soil profile according to Seed and Idriss (1970) (mean) reference curve for the sand

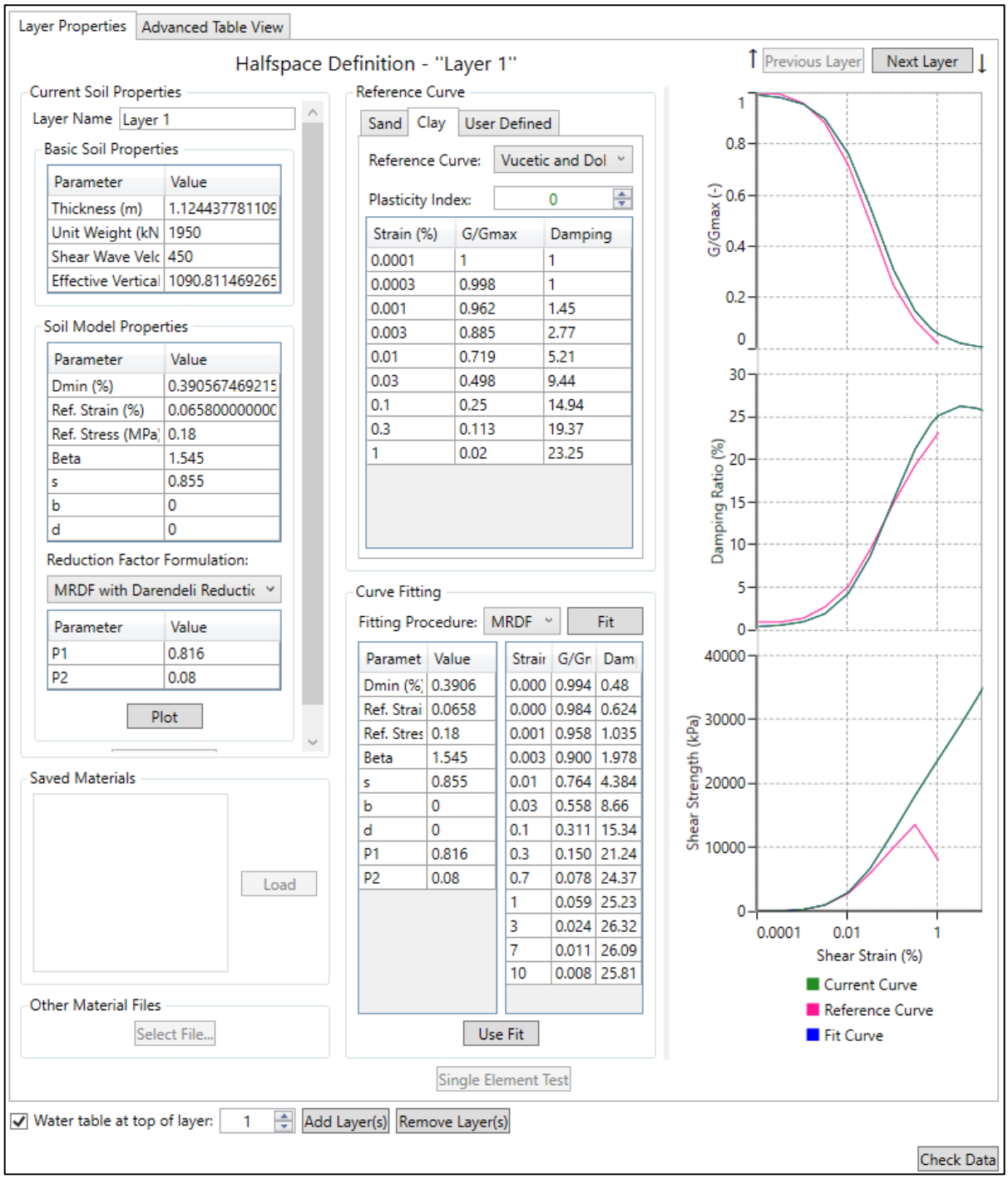

Figure-A II-7 Generated soil profile according to the proposed curve by Vucetic and Dobry (1991) for the clay

- **Selection of Input Motion**

In this step, the original acceleration time history record was entered. As shown in Figure-A II-8, the software automatically recognizes the type and format of the data and draws the initially recorded acceleration and time graph.

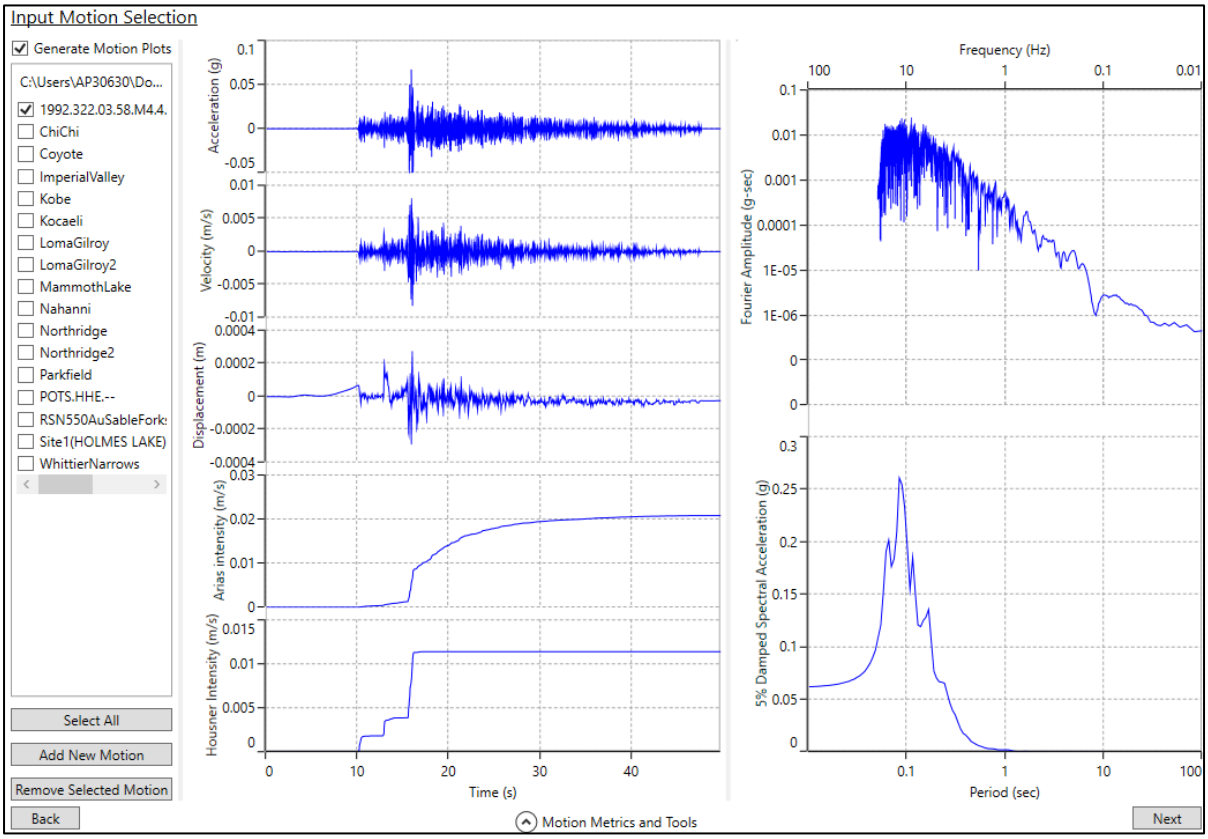

Figure-A II-8 Input time history acceleration recorded on the primary site

- **Output results**

Finally, the converted time history record for the target site class with the specific shear wave velocity was generated, and an example of the converted record was shown in Figure-A II-9. It is worth noting that results such as response spectra, stress-strain and other items related to the converted record can also be obtained in the output results.

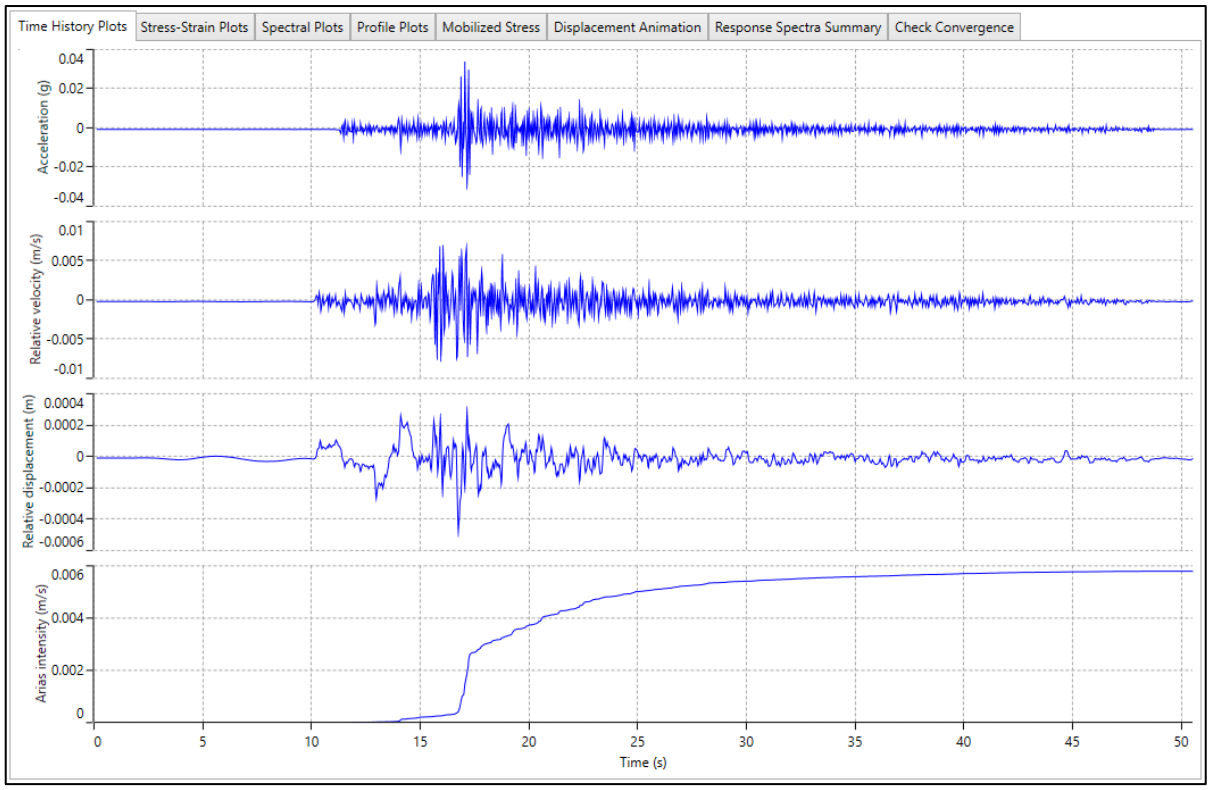

Figure-A II-9 Output time history acceleration converted for the target soil type

ANNEX III

GROUND MOTION PREDICTION EQUATIONS

- The proposed vertical-to-horizontal pseudo-spectral acceleration ratio in Ground Motion Prediction Equation (GMPE) by Bozorgnia and Campbell (2004) is given in the following equations. The proposed model of V/H spectra is a strong function of the natural period, distance from the epicentre and local site conditions and a weak function of earthquake magnitude and fault mechanism.

$$\ln V/H = \ln Y_V - \ln Y_H \quad \text{(A III-1)}$$

$$ln\,Y = c_1 + f_1(M_W) + c_4 ln\sqrt{f_2(M_W.\, r_{seis}.S)} + f_3(F) + f_4(S) + f_5(HW.F.M_W.r_{seis}) + \varepsilon \quad \text{(A III-2)}$$

- **Magnitude scaling factor:**

$$f_1(M_W) = c_2 M_W + c_3(8.5 - M_w)^2 \quad \text{(A III-3)}$$

- **Distance scaling factor:**

$$f_2(M_W, r_{seis}, S) = r_{seis}^2 + g(S)^2 (ex\,p[\,c_8 M_W + c_9(8.5 - M_w)^2])^2 \quad \text{(A III-4)}$$

- **Near-source effect of local site conditions:**

$$g(S) = c_5 + c_6(S_{VFS} + S_{SR}) + c_7 S_{FR} \quad \text{(A III-5)}$$

- **Effect of faulting mechanism:**

$$f_3(F) = c_{10} F_{RV} + c_{11} F_{TH} \quad \text{(A III-6)}$$

- **Far-source effect of local site conditions:**

$$f_4(S) = c_{12}S_{VFS} + c_{13}S_{SR} + c_{14}S_{FR} \quad \text{(A III-7)}$$

- **Effect of the hanging wall (HW):**

$$f_5(HW, F, M_W, r_{seis}) = HW f_3(F) f_{HW}(M_W) f_{HW}(r_{seis}) \quad \text{(A III-8)}$$

$$HW = \begin{cases} 0 & for\ r_{jb} \geq 5km\ or\ \delta > 70° \\ (S_{VFS} + S_{SR} + S_{FR})(5 - r_{jb})/5 & for\ r_{jb} < 5km\ and\ \delta \leq 70° \end{cases} \quad \text{(A III-9)}$$

$$f_{HW}(r_{seis}) = \begin{cases} c_{15}(r_{seis}/8) & for\ r_{seis} < 8km \\ c_{15} & for\ r_{seis} \geq 8km \end{cases} \quad \text{(A III-10)}$$

$$f_{HW}(M_W) = \begin{cases} 0 & for\ M_W < 5.5 \\ M_W - 5.5 & for\ 5.5 \leq M_W \leq 6.5 \\ 1.0 & for\ M_W > 6.5 \end{cases} \quad \text{(A III-11)}$$

- **Standard deviation:**

$$\sigma_{lnY} = \begin{cases} c_{16} - 0.07M_W & for\ M_W < 7.4 \\ c_{16} - 0.518 & for\ M_W \geq 7.4 \end{cases} \quad \text{(A III-12)}$$

$$\sigma_{lnY} = \begin{cases} c_{17} + 0.351 & for\ PGA \leq 0.07g \\ c_{17} - 0.132ln(PGA) & for\ 0.07g < PGA < 0.25g \\ c_{17} + 0.183 & for\ PGA \geq 0.25g \end{cases} \quad \text{(A III-13)}$$

Table-A III-1 Coefficients and statistical parameters from the regression analysis of the PGA and PSA Taken from Bozorgnia and Campbell (2004)

T_n (sec)	c_1	c_2	c_3	c_4	c_5	c_6	c_7	c_8	c_9	c_{10}	c_{11}	c_{12}	c_{13}	c_{14}	c_{15}	c_{16}	c_{17}	No.	r^2
Cor. PGA	-4																	443	0.949
0.05	-3																	435	0.940
0.075	-3.076	0.812	0.050	-1.252	0.121	-0.005	-0.051	0.648	0.040	0.243	0.333	-0.150	-0.196	-0.208	0.370	0.952	0.251	439	0.923
0.10	-2.661	0.812	0.060	-1.308	0.166	-0.009	-0.068	0.621	0.046	0.224	0.313	-0.146	-0.253	-0.258	0.370	0.958	0.257	439	0.901
0.15	-2.270	0.812	0.041	-1.324	0.212	-0.033	-0.081	0.613	0.031	0.318	0.344	-0.176	-0.267	-0.284	0.370	0.974	0.273	439	0.862
0.20	-2.771	0.812	0.030	-1.153	0.098	-0.014	-0.038	0.704	0.026	0.296	0.342	-0.148	-0.183	-0.359	0.370	0.981	0.280	439	0.844
0.30	-2.999	0.812	0.007	-1.080	0.059	-0.007	-0.022	0.752	0.007	0.359	0.385	-0.162	-0.157	-0.585	0.370	0.984	0.283	439	0.859
0.40	-3.511	0.812	-0.015	-0.964	0.024	-0.002	-0.005	0.842	-0.016	0.379	0.438	-0.078	-0.129	-0.557	0.370	0.987	0.286	439	0.871
0.50	-3.556	0.812	-0.035	-0.964	0.023	-0.020	-0.004	0.842	-0.036	0.406	0.479	-0.122	-0.130	-0.701	0.370	0.990	0.289	439	0.890
0.75	-3.709	0.812	-0.071	-0.964	0.021	-0.002	-0.002	0.842	-0.074	0.347	0.419	-0.108	-0.124	-0.796	0.331	1.021	0.320	438	0.917
1.0	-3.867	0.812	-0.101	-0.964	0.019	0	0	0.842	-0.105	0.329	0.338	-0.073	-0.072	-0.858	0.281	1.021	0.320	438	0.935
1.5	-4.093	0.812	-0.150	-0.964	0.019	0	0	0.842	-0.155	0.217	0.188	-0.079	-0.056	-0.954	0.210	1.021	0.320	428	0.960
2.0	-4.311	0.812	-0.180	-0.964	0.019	0	0	0.842	-0.187	0.060	0.064	-0.124	-0.116	-0.916	0.160	1.021	0.320	405	0.971
3.0	-4.817	0.812	-0.193	-0.964	0.019	0	0	0.842	-0.200	-0.079	0.021	-0.154	-0.117	-0.873	0.089	1.021	0.320	333	0.976
4.0	-5.211	0.812	-0.202	-0.964	0.019	0	0	0.842	-0.209	-0.061	0.057	-0.057	-0.261	-0.889	0.039	1.021	0.320	275	0.978
Vertical Component																			
Cor. PGA	-3.108	0.756	0	-1.287	0.142	0.046	-0.040	0.587	0	0.253	0.173	-0.135	-0.138	-0.256	0.630	0.975	0.274	439	0.958
0.05	-1.918	0.756	0	-1.517	0.309	0.069	-0.023	0.498	0	0.058	0.100	-0.195	-0.274	-0.219	0.630	1.031	0.330	434	0.934
0.075	-1.504	0.756	0	-1.551	0.343	0.083	0	0.487	0	0.135	0.182	-0.224	-0.303	-0.263	0.630	1.031	0.330	436	0.910
0.10	-1.672	0.756	0	-1.473	0.282	0.062	0.001	0.513	0	0.168	0.210	-0.198	-0.275	-0.252	0.630	1.031	0.330	436	0.900
0.15	-2.323	0.756	0	-1.280	0.171	0.045	0.008	0.591	0	0.223	0.238	-0.170	-0.175	-0.270	0.630	1.031	0.330	436	0.899
0.20	-2.998	0.756	0	-1.131	0.089	0.028	0.004	0.668	0	0.234	0.256	-0.098	-0.041	-0.311	0.571	1.031	0.330	436	0.915
0.30	-3.721	0.756	0.007	-1.028	0.050	0.010	0.004	0.736	0.007	0.249	0.328	-0.026	0.082	-0.265	0.488	1.031	0.330	436	0.941
0.40	-4.536	0.756	-0.015	-0.812	0.012	0	0	0.931	-0.018	0.299	0.317	-0.017	0.022	-0.257	0.428	1.031	0.330	436	0.949
0.50	-4.651	0.756	-0.035	-0.812	0.012	0	0	0.931	-0.043	0.243	0.354	-0.020	0.092	-0.293	0.383	1.031	0.330	436	0.957
0.75	-4.903	0.756	-0.071	-0.812	0.012	0	0	0.931	-0.087	0.295	0.418	0.078	0.091	-0.349	0.299	1.031	0.330	435	0.962
1.0	-4.950	0.756	-0.101	-0.812	0.012	0	0	0.931	-0.124	0.266	0.315	0.043	0.101	-0.481	0.240	1.031	0.330	435	0.967
1.5	-5.073	0.756	-0.150	-0.812	0.012	0	0	0.931	-0.184	0.171	0.211	-0.038	-0.018	-0.518	0.240	1.031	0.330	420	0.973
2.0	-5.292	0.756	-0.180	-0.812	0.012	0	0	0.931	-0.222	0.114	0.115	0.033	-0.022	-0.503	0.240	1.031	0.330	395	0.977
3.0	-5.748	0.756	-0.193	-0.812	0.012	0	0	0.931	-0.238	0.179	0.159	-0.010	-0.047	-0.539	0.240	1.031	0.330	321	0.978
4.0	-6.042	0.756	-0.202	-0.812	0.012	0	0	0.931	-0.248	0.237	0.134	-0.059	-0.267	-0.606	0.240	1.031	0.330	274	0.980

Table-A III-2 Guidance on evaluating local site conditions

Taken from Bozorgnia and Campbell (2004)

site classification	Site Parameter			Approximate $V_{S30}(m/s^2)$	Approximate site category	
	S_{VFS}	S_{SR}	S_{FR}		NEHRP	NBCC 2015
Firm Soil	0	0	0	298±92 (210-390)	D	D
Very firm soil	1	0	0	368±80 (290-490)	C & D	C & D
Soft rock	0	1	0	421±109 (310-530)	C & D	C & D
Firm rock	0	0	1	830±339 (490-1170)	B & C	B & C
Generic soil	0.25	0	0	≈310	D	D
Generic rock	0	0.5	0.5	≈620	C	C

Table-A III-3 Evaluation of faulting mechanism

Taken from Bozorgnia and Campbell (2004)

Faulting Category	Faulting Parameter	
	F_{RV}	F_{TH}
Strike-slip and normal	0	0
Reverse	1	0
Thrust	0	1
Reverse or thrust	0.5	0.5
Generic (unknown)	0.25	0.25

- The proposed vertical-to-horizontal pseudo-spectral acceleration ratio in Ground Motion Prediction Equation (GMPE) by Abrahamson and Gülerce (2011) is given in the following equation. The V/H ratio model depends on the magnitude, distance from the fault, faulting mechanism type, and site conditions and is applicable for earthquakes with a magnitude of 5.0 and above.

$$ln\left(V/H\right) = f_1\left(M.R_{rup}\right) + a_6F_{RV} + a_7F_{NM} + f_5\left(V_{S30}.P\hat{G}A_{1100}\right) \quad \text{(A III-14)}$$

- **Magnitude and distance dependence:**

$$f_1\left(M.R_{rup}\right) = \begin{cases} a_1 + a_4(M-c_1) + a_8(8.5-M)^2 + [a_2 + a_3(M-c_1)]\ln(R) & for\ M \le c_1 \\ a_1 + a_5(M-c_1) + a_8(8.5-M)^2 + [a_2 + a_3(M-c_1)]\ln(R) & for\ M > c_1 \end{cases} \quad \text{(A III-15)}$$

$$R = \sqrt{R_{rup}^2 + c_4^2} \quad \text{(A III-16)}$$

- **Site amplification dependence:**

$$f_5\left(P\hat{G}A_{1100}.V_{S30}^*\right) = a_{10}\,ln\left(\frac{V_{S30}^*}{V_{LIN}}\right) - \quad \text{(A III-17)}$$

$$\begin{cases} b\,ln\left[P\hat{G}A_{1100} + c\right] + b\,ln\left[P\hat{G}A_{1100} + c\left(\frac{V_{S30}^*}{V_{LIN}}\right)^n\right] & for\ V_{S30}^* < V_{LIN} \\ (b\cdot n)\,ln\left(\frac{V_{S30}^*}{V_{LIN}}\right) & for\ V_{S30}^* \ge V_{LIN} \end{cases}$$

$$V_{S30}^* = \begin{cases} V_{S30} & for\ V_{S30} < V_1 \\ V_1 & for\ V_{S30} \ge V_1 \end{cases} \quad \text{(A III-18)}$$

$$V_1 = \begin{cases} 1500 & for\ T \le 0.5\ sec \\ exp[8.0 - 0.795\,ln(T/0.21)] & for\ 0.5\ sec < T \le 1.0\ sec \\ exp[6.76 - 0.297\,ln(T)] & for\ 1.0\ sec < T < 2.0\ sec \\ 700 & for\ T \ge 2.0\ sec \\ 862 & for\ PGV \end{cases} \quad \text{(A III-19)}$$

- **Standard deviation:**

$$\sigma = \sqrt{\sigma_0^2 + \tau_0^2} \qquad \text{(A III-20)}$$

$$\sigma_0 = \begin{cases} S_1 & for\ M < 5 \\ S_1 + \left(\frac{S_2 - S_1}{2}\right)(M-5) & for\ 5 \le M \le 7 \\ S_2 & for\ M > 7 \end{cases}$$

$$\tau_0 = \begin{cases} S_3 & for\ M < 5 \\ S_3 + \left(\frac{S_4 - S_3}{2}\right)(M-5) & for\ 5 \le M \le 7 \\ S_4 & for\ M > 7 \end{cases}$$

Table-A III-4 Definition of the parameters
Taken from Abrahamson and Gülerce (2011)

Parameter	Definition
M	Earthquake moment magnitude
R_{rup}	Rupture distance (km)
R_{jb}	Joyner-Boore distance (km)
R_x	Horizontal distance (km) from the top edge of rupture and measured perpendicular to the fault strike
F_{RV}	Flag for reverse faulting earthquakes:1.0 for reverse or reverse/oblique earthquakes defined by rake angles between 30 and 150 degrees, 0 otherwise
F_{NM}	Flag for normal faulting earthquakes: 1.0 for normal earthquakes defined by rake angles between -60 and -120 degrees, 0 otherwise
V_{S30}	Shear-wave velocity over the top 30 m (m/s)
V_{LIN}	Period-dependent cutoff shear-wave velocity
V_1	Second period-dependent cutoff value
$P\hat{G}A_{1100}$	Median peak acceleration (g) for V_{S30}=1100 m/s

Table-A III-5 Constraints on the model parameters

Taken from Abrahamson and Gülerce (2011)

Parameter	Description	Estimation
V_{LIN}	Linear scaling for $V_{S30} > V_{LIN}$	Constrained by 1-D site simulation
a_1	Constant	Regression
a_2	Distance slope	Regression
a_3	Magnitude-dependent distance slope	PGA regression
a_4	Linear magnitude scaling, $M < c_1$	PGA regression
a_5	Linear magnitude scaling, $M \geq c_1$	Constrained to full saturation for PGA
a_8	Quadratic magnitude scaling	Regression
a_{10}	Linear site response scaling	Regression
b	Slope of non-linear soil response	Constrained by 1-D site simulation
c	Non-linear soil response term	Constrained by 1-D site simulation
c_1	Break in magnitude scaling	Constrained by hard-rock simulations and empirical data
c_4	Fictitious depth	PGA regression
n	Non-linear soil response term	Constrained by 1-D site simulation

Table-A III-6 Period-independent constants for the median V/H ratio

Taken from Abrahamson and Gülerce (2011)

c_1	c_4	a_3	a_4	a_5	n	c
6.75	10	0.0147	0.0334	-0.034	1.18	1.88

Table-A III-7 Coefficients for the median V/H ratios and standard deviations
Taken from Abrahamson and Gulerce (2011)

Period	V_{LIN}	b	a_1	a_2	a_6	a_7	a_8	a_{10}	s_1	s_2	s_3	s_4
PGA	865.1	-1.186	0.140	-0.160	-0.105	0.000	0.003	-1.230	0.422	0.333	0.213	0.161
0.010	865.1	-1.186	0.140	-0.160	-0.105	0.000	0.003	-1.230	0.450	0.330	0.230	0.150
0.020	865.1	-1.219	0.140	-0.160	-0.105	0.000	0.003	-1.268	0.450	0.330	0.230	0.150
0.029	898.6	-1.269	0.335	-0.185	-0.140	0.000	0.003	-1.366	0.450	0.330	0.230	0.150
0.040	994.5	-1.308	0.562	-0.238	-0.160	0.000	0.003	-1.457	0.450	0.341	0.230	0.150
0.050	1053.5	-1.346	0.720	-0.275	-0.136	0.000	-0.001	-1.533	0.450	0.351	0.230	0.150
0.075	1085.7	-1.471	0.552	-0.240	-0.019	0.000	-0.007	-1.706	0.450	0.370	0.230	0.150
0.10	1032.5	-1.624	0.214	-0.169	0.000	0.017	-0.010	-1.831	0.450	0.384	0.230	0.150
0.15	877.6	-1.931	-0.262	-0.069	0.000	0.040	-0.008	-2.114	0.450	0.403	0.230	0.150
0.20	748.2	-2.188	-0.600	0.002	0.000	0.057	-0.003	-2.362	0.450	0.416	0.230	0.150
0.26	639	-2.412	-0.769	0.023	0.000	0.072	0.001	-2.527	0.450	0.429	0.230	0.150
0.30	587.1	-2.518	-0.861	0.034	0.000	0.080	0.006	-2.598	0.450	0.436	0.230	0.150
0.40	503	-2.657	-1.045	0.057	0.000	0.097	0.015	-2.685	0.450	0.449	0.230	0.150
0.50	456.6	-2.669	-1.189	0.075	0.000	0.110	0.022	-2.657	0.450	0.460	0.230	0.150
0.75	410.5	-2.401	-1.250	0.090	0.000	0.133	0.022	-2.265	0.450	0.479	0.237	0.150
1.0	400	-1.955	-1.209	0.090	0.000	0.150	0.022	-1.685	0.450	0.492	0.266	0.150
1.5	400	-1.025	-1.152	0.090	0.029	0.150	0.022	-0.570	0.450	0.511	0.307	0.150
2.0	400	-0.299	-1.111	0.090	0.050	0.150	0.022	0.250	0.532	0.520	0.337	0.150
3.0	400	0.000	-1.054	0.090	0.079	0.150	0.022	0.460	0.648	0.520	0.378	0.213
4.0	400	0.000	-1.014	0.090	0.100	0.150	0.022	0.460	0.700	0.520	0.407	0.258
5.0	400	0.000	-1.000	0.090	0.100	0.150	0.022	0.460	0.700	0.520	0.430	0.292
7.5	400	0.000	-1.000	0.090	0.100	0.150	0.022	0.460	0.700	0.520	0.471	0.355
10.0	400	0.000	-1.000	0.090	0.100	0.150	0.022	0.460	0.700	0.520	0.500	0.400

ANNEX IV

DESIGN DETAILS OF STUDIED BUILDINGS

Table-A IV-1 Beam flexural design of the 3-storey building

Storey	Dim. (mm)	Bars loc.	A & D								B & C							
			1-2		2-1		2-3		3-2		1-2		2-1		2-3		3-2	
3rd	350 × 400	Top Bars	2	15M	2	15M	2	15M	2	15M	2	15M	2	15M	2	15M	2	15M
		Bottom Bars	3	20M	3	20M	3	15M	3	15M	3	20M	3	15M	3	15M	3	15M
2nd	350 × 400	Top Bars	4	20M	4	20M	3	20M	3	20M	3	25M	3	25M	3	25M	3	25M
		Bottom Bars	4	20M	4	20M	4	20M	4	20M	3	25M	3	25M	3	25M	3	25M
1st	350 × 400	Top Bars	3	25M	3	25M	3	25M	3	25M	4	25M	4	25M	3	25M	3	25M
		Bottom Bars	3	25M	3	25M	3	25M	3	25M	4	25M	3	25M	3	25M	3	25M

Table-A IV-2 Beam shear design of the 3-storey building

Storey	All Beams											
	Beam's end				Middle				Beam's end			
	Num.	Bar	s (mm)	L (mm)	Num.	Bar	s (mm)	L (mm)	Num.	Bar	s (mm)	L (mm)
1st - 3rd	1	10M	75	800	1	10M	200	5000	1	10M	75	800

Table-A IV-3 Main reinforcement design of the columns for the 3-storey building

Storey	Dim. (mm)	All Columns	
1st - 3rd	400 × 400	8	20M

Table-A IV-4 Shear design of the columns for the 3-storey building

Storey	Location	Stirrup Type	All Columns			
			Num.	Bar	s (mm)	L (mm)
1st - 3rd	top end	squared	1	10M	135	450
		lozenge	1	10M		
	middle	squared	1	10M	135	1700
		lozenge	1	10M		
	bot. end	squared	1	10M	135	450
		lozenge	1	10M		

Table-A IV-5 Beam flexural design of the 6-storey building

Storey	Dim. (mm)	Bars loc.	A & D								B & C							
			1-2		2-1		2-3		3-2		1-2		2-1		2-3		3-2	
6th	400 × 600	Top Bars	3	15M	3	15M	3	15M	3	15M	2	15M	2	15M	2	15M	2	15M
		Bottom Bars	4	15M	4	15M	4	15M	4	15M	3	20M	3	20M	3	20M	3	20M
5th	400 × 600	Top Bars	3	20M	3	20M	3	20M	3	20M	4	20M	4	20M	4	20M	4	20M
		Bottom Bars	4	20M	4	20M	4	20M	4	20M	4	20M	4	20M	4	20M	4	20M
4th	400 × 600	Top Bars	5	20M	5	20M	5	20M	5	20M	4	25M	3	25M	3	25M	3	25M
		Bottom Bars	4	25M	4	25M	4	25M	4	25M	4	25M	4	25M	4	25M	4	25M
3rd	400 × 600	Top Bars	5	25M	4	25M	4	25M	4	25M	5	25M	8	20M	5	25M	5	25M
		Bottom Bars	5	25M	5	25M	5	25M	5	25M	5	25M	5	25M	5	25M	5	25M
2nd	400 × 600	Top Bars	6	25M	5	25M	5	25M	5	25M	6	25M	6	25M	6	25M	6	25M
		Bottom Bars	6	25M	6	25M	6	25M	6	25M	6	25M	6	25M	6	25M	6	25M
1st	400 × 600	Top Bars	5	25M	5	25M	4	25M	4	25M	5	25M	5	25M	5	25M	5	25M
		Bottom Bars	5	25M	5	25M	5	25M	5	25M	5	25M	5	25M	5	25M	5	25M

Table-A IV-6 Beam shear design of the 6-storey building

Storey	All Beams											
	Beam's end				Middle				Beam's end			
	Num.	Bar	s (mm)	L (mm)	Num.	Bar	s (mm)	L (mm)	Num.	Bar	s (mm)	L (mm)
1st - 6th	1	10M	125	1200	1	10M	250	4000	1	10M	125	1200

Table-A IV-7 Main reinforcement design of the columns for the 6-storey building

Storey	Dim. (mm)	A1 – B1 – C1 - D1 - A4 – B4 – C4 - D4		A2 – B2 – C2 - D2 - A3 – B3 – C3 - D3	
6th	600 × 600	16	20M	16	20M
5th	600 × 600	16	20M	16	20M
4th	600 × 600	16	20M	16	25M
3rd	600 × 600	16	20M	16	25M
2nd	600 × 600	16	20M	16	25M
1st	600 × 600	16	20M	16	25M

Table-A IV-8 Shear design of the columns for the 6-storey building

Storey	Location	Stirrup Type	All Columns			
			Num.	Bar	s (mm)	L (mm)
1st - 6th	top end	squared	1	10M	100	600
		lozenge	1	10M		
	middle	squared	1	10M	100	1200
		lozenge	1	10M		

	bot. end	***squared***	1	10M	100	600
		lozenge	1	10M		

Table-A IV-9 Beam flexural design of the 9-storey building

Storey	***Dim. (mm)***	***Bars loc.***	***A & D***								***B & C***							
			1-2		**2-1**		**2-3**		**3-2**		**1-2**		**2-1**		**2-3**		**3-2**	
9th	500 × 650	***Top Bars***	3	20M	3	20M	3	20M	3	20M	4	20M	4	20M	4	20M	4	20M
		Bottom Bars	4	20M	4	20M	4	20M	4	20M	4	20M	4	20M	4	20M	4	20M
8th	500 × 650	***Top Bars***	3	20M	3	20M	3	20M	3	20M	4	20M	4	20M	4	20M	4	20M
		Bottom Bars	4	20M	4	20M	4	20M	4	20M	4	20M	4	20M	4	20M	4	20M
7th	500 × 650	***Top Bars***	5	20M	5	20M	5	20M	5	20M	4	20M	4	20M	4	20M	4	20M
		Bottom Bars	6	20M	6	20M	6	20M	6	20M	6	20M	6	20M	6	20M	6	20M
6th	500 × 650	***Top Bars***	5	25M	5	25M	5	25M	5	25M	5	20M	5	20M	5	20M	5	20M
		Bottom Bars	5	25M	5	25M	5	25M	5	25M	5	25M	5	25M	5	25M	5	25M
5th	500 × 650	***Top Bars***	6	25M	6	25M	6	25M	6	25M	5	25M	5	25M	5	25M	5	25M
		Bottom Bars	7	25M	7	25M	7	25M	7	25M	7	25M	7	25M	7	25M	7	25M
4th	500 × 650	***Top Bars***	6	30M	6	30M	6	30M	6	30M	5	30M	5	30M	5	30M	5	30M
		Bottom Bars	6	30M	6	30M	6	30M	6	30M	6	30M	6	30M	6	30M	6	30M
3rd	500 × 650	***Top Bars***	7	30M	7	30M	7	30M	7	30M	6	30M	6	30M	6	30M	6	30M
		Bottom Bars	7	30M	7	30M	7	30M	7	30M	7	30M	7	30M	7	30M	7	30M
2nd	500 × 650	***Top Bars***	7	30M	7	30M	7	30M	7	30M	7	30M	6	30M	6	30M	6	30M
		Bottom Bars	8	30M	8	30M	8	30M	8	30M	8	30M	8	30M	7	30M	7	30M
1st	500 × 650	***Top Bars***	6	30M	5	30M	5	30M	5	30M	6	25M	6	25M	6	25M	6	25M
		Bottom Bars	6	30M	6	30M	6	30M	6	30M	6	30M	6	30M	6	30M	6	30M

Table-A IV-10 Beam shear design of the 9-storey building

Storey	***All Frames***											
	Beam's end				***Middle***				***Beam's end***			
	Num.	***Bar***	***s (mm)***	***L (mm)***	***Num.***	***Bar***	***s (mm)***	***L (mm)***	***Num.***	***Bar***	***s (mm)***	***L (mm)***
4th - 9th	1	10M	145	1300	1	10M	300	3700	1	10M	145	1300
1st - 3rd	2	10M	145	1300	2	10M	350	3700	2	10M	145	1300

Table-A IV-11 Main reinforcement design of the columns for the 9-storey building

Storey	***Dim. (mm)***	**A1 – B1 – C1 - D1 - A4 – B4 – C4 - D4**		**A2 – B2 – C2 - D2 - A3 – B3 – C3 - D3**	
9th	700 × 700	20	20M	20	20M
8th	700 × 700	20	20M	20	20M
7th	700 × 700	20	20M	20	20M
6th	700 × 700	20	20M	20	20M
5th	700 × 700	20	20M	20	25M
4th	700 × 700	20	20M	20	25M
3rd	700 × 700	20	20M	20	25M

2nd	700 × 700	20	20M	20	25M
1st	700 × 700	20	20M	20	25M

Table-A IV-12 Shear design of the columns for the 9-storey building

Storey	*Location*	*Stirrup Type*	**All Columns**			
			Num.	*Bar*	*s (mm)*	*L (mm)*
1st - 9th	*top end*	*squared*	3	15M	150	700
		lozenge	0	15M		
	middle	*squared*	3	15M	150	950
		lozenge	0	15M		
	bot. end	*squared*	3	15M	150	700
		lozenge	0	15M		

Table-A IV-13 Beam flexural design of the 12-storey building

Storey	*Dim. (mm)*	*Bars loc.*	*A & D*								*B & C*							
			1-2		**2-1**		**2-3**		**3-2**		**1-2**		**2-1**		**2-3**		**3-2**	
12th	600 × 750	*Top Bars*	5	20M	5	20M	5	20M	5	20M	7	20M	7	20M	7	20M	7	20M
		Bottom Bars	5	20M	5	20M	5	20M	5	20M	5	20M	5	20M	5	20M	5	20M
11th	600 × 750	*Top Bars*	5	20M	5	20M	5	20M	5	20M	7	20M	7	20M	7	20M	7	20M
		Bottom Bars	5	20M	5	20M	5	20M	5	20M	5	20M	5	20M	5	20M	5	20M
10th	600 × 750	*Top Bars*	5	20M	5	20M	5	20M	5	20M	7	20M	7	20M	7	20M	7	20M
		Bottom Bars	6	20M	6	20M	6	20M	6	20M	5	20M	6	20M	6	20M	6	20M
9th	600 × 750	*Top Bars*	7	20M	6	20M	7	20M	7	20M	7	20M	7	20M	7	20M	7	20M
		Bottom Bars	5	25M	5	25M	5	25M	5	25M	5	25M	5	25M	5	25M	5	25M
8th	600 × 750	*Top Bars*	6	25M	6	25M	6	25M	6	25M	5	25M	4	25M	5	25M	5	25M
		Bottom Bars	7	25M	7	25M	7	25M	7	25M	6	25M	6	25M	7	25M	7	25M
7th	600 × 750	*Top Bars*	8	25M	7	25M	8	25M	8	25M	6	25M	6	25M	6	25M	6	25M
		Bottom Bars	8	25M	8	25M	8	25M	8	25M	8	25M	8	25M	8	25M	8	25M
6th	600 × 750	*Top Bars*	7	30M	6	30M	7	30M	7	30M	6	30M	5	30M	6	30M	6	30M
		Bottom Bars	7	30M	7	30M	7	30M	7	30M	7	30M	7	30M	7	30M	7	30M
5th	600 × 750	*Top Bars*	8	30M	8	30M	8	30M	8	30M	7	30M	7	30M	7	30M	7	30M
		Bottom Bars	8	30M	8	30M	8	30M	8	30M	8	30M	8	30M	8	30M	8	30M
4th	600 × 750	*Top Bars*	9	30M	9	30M	9	30M	9	30M	8	30M	8	30M	8	30M	8	30M
		Bottom Bars	10	30M	9	30M	9	30M	9	30M	9	30M	9	30M	9	30M	9	30M
3rd	600 × 750	*Top Bars*	10	30M	10	30M	10	30M	10	30M	9	30M	9	30M	9	30M	9	30M
		Bottom Bars	10	30M	10	30M	10	30M	10	30M	10	30M	10	30M	10	30M	10	30M
2nd	600 × 750	*Top Bars*	10	30M	10	30M	10	30M	10	30M	9	30M	9	30M	9	30M	9	30M
		Bottom Bars	11	30M	10	30M	10	30M	10	30M	10	30M	10	30M	10	30M	10	30M
1st	600 × 750	*Top Bars*	8	30M	7	30M	7	30M	7	30M	7	30M	6	30M	6	30M	6	30M
		Bottom Bars	8	30M	8	30M	8	30M	8	30M	8	30M	8	30M	8	30M	8	30M

Table-A IV-14 Beam shear design of the 12-storey building

Storey	*Frames A, B, C & D: Beam 1-2 & Beam 2-3*		
	Beam's end	*Middle*	*Beam's end*

	Num.	Bar	s (mm)	L (mm)	Num.	Bar	s (mm)	L (mm)	Num.	Bar	s (mm)	L (mm)
6^{th} - 12th	1	10M	150	1500	1	10M	300	3200	1	10M	150	1500
1^{st} - 5^{th}	2	10M	150	1500	2	10M	300	3200	2	10M	150	1500

Table-A IV-15 Main reinforcement design of the columns for the 12-storey building

Storey	Dim. (mm)	A1 – B1 – C1 - D1 - A4 – B4 – C4 - D4		A2 – B2 – C2 - D2 - A3 – B3 – C3 - D3	
12^{th}	800 × 800	24	20M	24	20M
11^{th}	800 × 800	24	20M	24	20M
10^{th}	800 × 800	24	20M	24	20M
9^{th}	800 × 800	24	20M	24	20M
8^{th}	800 × 800	24	20M	24	25M
7^{th}	800 × 800	24	20M	24	25M
6^{th}	800 × 800	24	20M	24	25M
5^{th}	800 × 800	24	20M	24	25M
4^{th}	800 × 800	24	20M	24	25M
3^{rd}	800 × 800	24	20M	24	25M
2^{nd}	800 × 800	24	20M	24	25M
1^{st}	800 × 800	24	20M	24	25M

Table-A IV-16 Shear design of the columns for the 12-storey building

Storey	Location	Stirrup Type	A1 – B1 – C1 - D1 - A4 – B4 – C4 - D4			
			Num.	Bar	s (mm)	L (mm)
1^{st} - 12^{th}	top end	squared	1	15M	125	800
		lozenge	1	15M		
	middle	squared	1	15M	125	650
		lozenge	1	15M		
	bot. end	squared	1	15M	125	800
		lozenge	1	15M		

Storey	Location	Stirrup Type	A2 – B2 – C2 - D2 - A3 – B3 – C3 - D3			
			Num.	Bar	s (mm)	L (mm)
5^{th} - 12^{th}	top end	squared	1	15M	125	800
		lozenge	1	15M		
	middle	squared	1	15M	125	650
		lozenge	1	15M		
	bot. end	squared	1	15M	125	800
		lozenge	1	15M		
1^{st} - 4^{th}	top end	squared	1	15M	100	800
		lozenge	1	15M		

	middle	***squared***	1	15M	125	650
		lozenge	1	15M		
	bot. end	***squared***	1	15M	100	800
		lozenge	1	15M		

ANNEX V

THE WORLDWIDE SELECTED STRONG GROUND MOTIONS USED IN THE SECOND AND THIRD PAPERS

Table-A V-1 Generic characteristics of the selected ground motions (PEER-NGA)

No.	Earthquake	Date	M_W	Mechanism	Station	R_{jb} (km)	R_{rup} (km)	V_{S30} (m/sec)	Site Class	Dir	PGA (g)	PGA_{ver} / PGA_{hor}
1	Friuli, Italy-01	1976/05/06	6.50	Reverse	Tolmezzo	14.97	15.82	505.23	C	H1	0.3571	0.8258
										H2	0.3151	
										V	0.2770	
2	Mammoth Lakes-01, USA	1980/05/25	6.06	Normal Oblique	Convict Creek	1.1	6.63	382.12	C	H1	0.4195	0.8981
										H2	0.4424	
										V	0.3869	
3	Mammoth Lakes-04, USA	1980/05/25	5.7	Strike-Slip	Convict Creek	1.37	5.32	382.12	C	H1	0.3715	0.7854
										H2	0.4845	
										V	0.3332	
4	Mammoth Lakes-06, USA	1980/05/27	5.94	Strike-Slip	Long Valley Dam (Upr L Abut)	9.65	16.03	537.16	C	H1	0.9453	0.5043
										H2	0.4137	
										V	0.3154	
5	Victoria, Mexico	1980/06/09	6.33	Strike-Slip	Cerro Prieto	13.8	14.37	471.53	C	H1	0.6454	0.4578
										H2	0.6325	
										V	0.2925	
6	Coalinga-05, USA	1983/07/22	5.77	Reverse	Oil City	1.99	8.46	398.49	C	H1	0.8412	0.8436
										H2	0.4222	
										V	0.5028	
					Transmitter Hill	3.7	9.51	477.25	C	H1	0.7798	0.4476
										H2	1.0219	
										V	0.3996	
7	Nahanni, Canada	1985/12/23	6.76	Reverse	Site 1	2.48	9.6	605.04	C	H1	1.1079	1.9776
										H2	1.2007	
										V	2.2808	

Continued Table-A V-1

No.	Earthquake	Date	M_W	Mechanism	Station	R_{jb} (km)	R_{rup} (km)	V_{S30} (m/sec)	Site Class	Dir	PGA (g)	PGA_{ver} / PGA_{hor}
8	N. Palm Springs, USA	1986/07/08	6.06	Reverse Oblique	Cabazon	6.84	7.92	376.91	C	H1	0.2213	1.6863
										H2	0.2041	
										V	0.3584	
					Morongo Valley Fire Station	3.62	12.03	396.41	C	H1	0.2225	1.5157
										H2	0.2172	
										V	0.3332	
					Whitewater Trout Farm	0	6.04	425.02	C	H1	0.4811	0.7469
										H2	0.6296	
										V	0.4111	
9	Baja California, USA	1987/02/07	5.5	Strike-Slip	Cerro Prieto	3.43	4.46	471.53	C	H1	1.2803	0.6282
										H2	0.9046	
										V	0.6760	
10	Whittier Narrows, USA	1987/10/01	5.99	Reverse Oblique	Garvey Res. - Control Bldg	0.36	14.5	468.18	C	H1	0.3741	0.8563
										H2	0.4762	
										V	0.3614	
					San Gabriel - E Grand Ave	0	15.2	401.37	C	H1	0.2623	1.0950
										H2	0.2125	
										V	0.2586	
11	Loma Prieta, USA	1989/10/18	6.93	Reverse Oblique	BRAN	3.85	10.72	476.54	C	H1	0.4564	1.0565
										H2	0.5023	
										V	0.5058	
					Corralitos	0.16	3.85	462.24	C	H1	0.6447	0.8205
										H2	0.4828	
										V	0.4578	
					LGPC	0	3.88	594.83	C	H1	0.5700	1.5229
										H2	0.6074	
										V	0.8960	
					UCSC Lick Observatory	12.04	18.41	713.59	C	H1	0.4601	0.8487
										H2	0.4168	
										V	0.3716	
					WAHO	11.03	17.47	388.33	C	H1	0.3732	0.5494
										H2	0.6540	
										V	0.2714	

Continued Table-A V-1

No.	Earthquake	Date	M_W	Mechanism	Station	R_{jb} (km)	R_{rup} (km)	V_{S30} (m/sec)	Site Class	Dir	PGA (g)	PGA_{ver} / PGA_{hor}
12	Manjil, Iran	1990/06/20	7.37	Strike-Slip	Abbar	12.55	12.55	723.95	C	H1	0.5146	1.0641
										H2	0.4969	
										V	0.5380	
13	Cape Mendocino, USA	1992/04/25	7.01	Reverse	Cape Mendocino	0	6.96	567.78	C	H1	1.49357	0.5931
										H2	1.03873	
										V	0.73876	
14	Northridge-01, USA	1994/01/17	6.69	Reverse	Beverly Hills - 12520 Mulhol	12.39	18.36	545.66	C	H1	0.6209	0.6165
										H2	0.4499	
										V	0.3258	
					LA - UCLA Grounds	13.8	22.49	398.42	C	H1	0.2779	0.7302
										H2	0.4738	
										V	0.2650	
					Simi Valley - Katherine Rd	0	13.42	557.42	C	H1	0.8043	0.6106
										H2	0.5354	
										V	0.4007	
15	Kobe, Japan	1995/01/16	6.9	Strike-Slip	Nishi-Akashi	7.08	7.08	609	C	H1	0.4832	0.8162
										H2	0.4643	
										V	0.3866	
16	Umbria Marche, Italy	1997/09/26	6	Normal	Nocera Umbra	8.29	8.92	428	C	H1	0.4723	0.8091
										H2	0.3831	
										V	0.3442	

Continued Table-A V-1

No.	Earthquake	Date	M_W	Mechanism	Station	R_{jb} (km)	R_{rup} (km)	V_{S30} (m/sec)	Site Class	Dir	PGA (g)	PGA_{ver} / PGA_{hor}
17	Chi-Chi, Taiwan	1999/09/20	7.62	Reverse Oblique	CHY028	3.12	3.12	542.61	C	H1	0.6364	0.4936
										H2	0.7604	
										V	0.3434	
					CHY080	0.11	2.69	496.21	C	H1	0.8092	0.8752
										H2	0.8601	
										V	0.7302	
					TCU071	0	5.8	624.85	C	H1	0.5286	0.7231
										H2	0.6513	
										V	0.4243	
					TCU072	0	7.08	468.14	C	H1	0.4771	0.6590
										H2	0.3799	
										V	0.2806	
					TCU074	0	13.46	549.43	C	H1	0.5964	0.5802
										H2	0.3797	
										V	0.2761	
					TCU079	0	10.97	363.99	C	H1	0.5922	0.7818
										H2	0.4244	
										V	0.3919	
					TCU084	0	11.48	665.2	C	H1	1.0089	0.4859
										H2	0.4311	
										V	0.3204	
					TCU129	1.83	1.83	511.18	C	H1	1.0049	0.4317
										H2	0.6240	
										V	0.3418	
18	Chi-Chi, Taiwan-02	1999/09/20	5.9	Reverse	TCU079	8.16	10.41	363.99	C	H1	0.4792	0.8346
										H2	0.2123	
										V	0.2662	
19	Chi-Chi, Taiwan-03	1999/09/20	6.2	Reverse	TCU076	13.04	14.66	614.98	C	H1	0.5216	0.8761
										H2	0.1611	
										V	0.2539	
20	Chi-Chi, Taiwan-06	1999/09/25	6.3	Reverse	TCU079	1.04	10.05	363.99	C	H1	0.7757	0.8259
										H2	0.6263	
										V	0.5757	

Continued Table-A V-1

No.	Earthquake	Date	M_W	Mechanism	Station	R_{jb} (km)	R_{rup} (km)	V_{S30} (m/sec)	Site Class	Dir	PGA (g)	PGA_{ver} / PGA_{hor}
21	Duzce, Turkey	1999/11/12	7.14	Strike-Slip	IRIGM 496	4.21	4.21	760	C	H1	0.7506	0.3776
										H2	1.0306	
										V	0.3321	
22	Tottori, Japan	2000/10/06	6.61	Strike-Slip	OKYH09	21.22	21.22	518.92	C	H1	0.1848	1.0967
										H2	0.2898	
										V	0.2538	
					SMNH01	5.83	5.86	446.34	C	H1	0.7330	0.9473
										H2	0.6170	
										V	0.6370	
					SMNH02	23.64	23.64	502.66	C	H1	0.5759	0.8685
										H2	0.3196	
										V	0.3726	
					TTR007	11.28	11.29	469.79	C	H1	0.7336	0.6267
										H2	0.5601	
										V	0.4017	
					TTR009	8.82	8.83	420.2	C	H1	0.6300	0.4690
										H2	0.6024	
										V	0.2889	
23	San Simeon, USA	2003/12/22	6.52	Reverse	Templeton - 1-storey Hospital	5.07	6.22	410.66	C	H1	0.4352	0.5743
										H2	0.4825	
										V	0.2632	
24	Bam, Iran	2003/12/26	6.6	Strike-Slip	Bam	0.05	1.7	487.4	C	H1	0.8077	1.3602
										H2	0.6290	
										V	0.9695	

Continued Table-A V-1

No.	Earthquake	Date	M_W	Mechanism	Station	R_{jb} (km)	R_{rup} (km)	V_{S30} (m/sec)	Site Class	Dir	PGA (g)	PGA_{ver} / PGA_{hor}
25	Parkfield, CA, USA	2004/09/28	6	Strike-Slip	PARKFIELD - JOAQUIN CANYON	3.83	4.57	378.99	C	H1	0.6200	0.5568
										H2	0.4924	
										V	0.3076	
					Parkfield - Cholame 3E	4.95	5.55	397.36	C	H1	0.5187	0.5078
										H2	0.7995	
										V	0.3270	
					Parkfield - Fault Zone 11	3.12	4	541.73	C	H1	0.5982	0.8739
										H2	1.1304	
										V	0.7186	
26	Niigata, Japan	2004/10/23	6.63	Reverse	NIG019	0.21	9.88	372.33	C	H1	1.3264	0.6442
										H2	1.1669	
										V	0.8015	
					NIG028	0.46	9.79	430.71	C	H1	0.5171	0.6645
										H2	0.8467	
										V	0.4397	
					NIGH01	0.49	9.46	480.4	C	H1	0.6698	0.5061
										H2	0.8370	
										V	0.3789	
					NIGH12	9.93	10.72	564.25	C	H1	0.3501	0.8489
										H2	0.4175	
										V	0.3245	
27	Chuetsu-Oki, Japan	2007/07/16	6.8	Reverse	Kashiwazaki City Takayanagicho	10.38	20.03	561.59	C	H1	0.3621	0.7902
										H2	0.7269	
										V	0.4054	
					Kashiwazaki Nishiyamacho Ikeura	0	12.63	655.45	C	H1	0.8948	0.6604
										H2	0.8519	
										V	0.5766	

Continued Table-A V-1

No.	Earthquake	Date	M_W	Mechanism	Station	R_{jb} (km)	R_{rup} (km)	V_{S30} (m/sec)	Site Class	Dir	PGAs (g)	PGA_{ver} / PGA_{hor}
28	Iwate, Japan	2008/06/13	6.9	Reverse	AKT023	11.68	16.96	555.96	C	H1	0.3658	0.6818
										H2	0.3678	
										V	0.2501	
					AKTH04	13.07	17.94	458.73	C	H1	2.4685	0.6073
										H2	1.3433	
										V	1.1058	
					IWTH24	3.1	5.18	486.41	C	H1	0.4381	0.7033
										H2	0.5186	
										V	0.3352	
					IWTH25	0	4.8	506.44	C	H1	1.4346	2.9877
										H2	1.1517	
										V	3.8405	
					IWTH26	5.97	6.02	371.06	C	H1	1.0692	0.9611
										H2	0.9049	
										V	0.9454	
					MYG005	10.71	13.47	361.24	C	H1	0.5355	1.3445
										H2	0.4456	
										V	0.6568	
					Kurihara City	12.83	12.85	512.26	C	H1	0.7027	0.5256
										H2	0.4220	
										V	0.2862	
29	L'Aquila, Italy	2009/04/06	6.3	Normal	L'Aquila - V. Aterno-Colle Grilli	0	6.81	685	C	H1	0.4816	0.5560
										H2	0.5170	
										V	0.2774	
30	Darfield, New Zealand	2010/09/03	7.00	Strike-Slip	Heathcote Valley Primary School	24.36	24.47	422	C	H1	0.5765	0.5014
										H2	0.6315	
										V	0.3025	
31	Christchurch, New Zealand	2011/02/21	6.2	Reverse Oblique	Heathcote Valley Primary School	0	3.36	422	C	H1	1.6469	1.4968
										H2	1.2894	
										V	2.1811	
					LPCC	2.52	6.12	649.67	C	H1	0.9097	0.5372
										H2	0.9539	
										V	0.5004	

ANNEX VI

THE SITE CLASSIFICATION FOR SEISMIC SITE RESPONSE

Table-A VI-1 Site classification for seismic site response specified in NBC (2015)

Taken from NBC (2015)

Site Class	Ground Profile Name	Average Properties in Top 30 m, as per Note A-4.1.8.4.(3) and Table 4.1.8.4.-A		
		Average Shear Wave Velocity, $\bar{V}_{s30}$, m/s	**Average Standard Penetration Resistance, $\bar{N}_{60}$**	**Soil Undrained Shear Strength, S_u**
A	Hard rock	$\bar{V}_{s30} > 1500$	n/a	n/a
B	Rock	$760 < \bar{V}_{s30} \leq 1500$	n/a	n/a
C	Very dense soil and soft rock	$360 < \bar{V}_{s30} < 760$	$\bar{N}_{60} > 50$	$S_u > 100$ kPa
D	Stiff soil	$180 < \bar{V}_{s30} < 360$	$15 \leq \bar{N}_{60} \leq 50$	50 kPa $< S_u \leq 100$ kPa
E	Soft Soil	$\bar{V}_{s30} < 180$	$\bar{N}_{60} < 15$	$S_u < 50$ kPa
		Any profile with more than 3.0m of soil with the following characteristics: • Plasticity index: PI > 20 • Moisture content: w ≥ 40%, and • Undrained shear strength: $S_u < 25$kPa		
F	Other soils	Site-specific evaluation required		

Table-A VI-2 Site classification provided in ASCE/SEI 7-16 (2017)

Taken from ASCE/SEI 7-16 (2017)

Site Class	Ground Type	$\bar{V}_s$	$\bar{N}$ or $\bar{N}_{ch}$	$\bar{S}_u$
A	Hard rock	> 5,000 ft/s	NA	NA
B	Rock	2,500 to 5,000 ft/s	NA	NA
C	Very dense soil and soft rock	1,200 to 2,500 ft/s	> 50 blows/ft	>2,000 lb/ft^2
D	Stiff soil	600 to 1,200 ft/s	15 to 50 blows/ft	1,000 to 2,000 lb/ft^2
E	Soft clay soil	< 600 ft/s	< 15 blows/ft	< 1,000 lb/ft^2
		Any profile with more than 10 ft of soil that has the following characteristics: - Plasticity index PI > 20, - Moisture content w ≥ 40%, - Undrained shear strength $\bar{s}_u$ < 500 lb /ft2		
F	Soil requiring site response analysis	Soils requiring site response analysis		

Table-A VI-3 Ground types classification provided in Eurocode 8-1 (2004)

Taken from Eurocode 8-1 (2004)

Ground type	**Description of stratigraphic profile**	**Parameters**		
		$v_{s,30}$ (m/s)	**N_{SPT} (blows/30cm)**	**c_u (kPa)**
A	Rock or other rock-like geological formation, including at most 5m of weaker material at the surface.	> 800	_	_
B	Deposits of very dense sand, gravel, or very stiff clay, at least several tens of meters in thickness, characterized by a gradual increase of mechanical properties with depth.	360 – 800	> 50	> 250
C	Deep deposits of dense or medium dense sand, gravel or stiff clay with a thickness from several tens to many hundreds of meters.	180 – 360	15 - 50	70 - 250
D	Deposits of loose-to-medium cohesionless soil (with or without some soft cohesive layers), or of predominantly soft-to-firm cohesive soil.	< 180	< 15	< 70
E	A soil profile consisting of a surface alluvium layer with v_s values of type C or D and thickness varying between about 5 m and 20 m, underlain by stiffer material with v_s > 800 m/s.			
S_1	Deposits consisting, or containing a layer at least 10 m thick, of soft clays/silts with a high plasticity index (PI > 40) and high-water content	< 100 (indicative)	–	10 - 20
S_2	Deposits of liquefiable soils, of sensitive clays, or any other soil profile not included in types A – E or S_1			

LIST OF BIBLIOGRAPHICAL REFERENCES

AC 156. (2010). Acceptance Criteria for Seismic Qualification by Shake-Table Testing of Nonstructural Components and Systems. *International Code Council, ICC Evaluation Service Inc.*

Acerra, C., Havenith, H.-B., & Zacharopoulos, S. (2004). Guidelines for the Implementation of the H/V Spectral Ratio Technique on Ambient Vibrations Measurements, Processing and Interpretation. *European Commission – Research General Directorate, Project No. EVG1-CT-2000-00026*(SESAME European research project WP12 – Deliverable D23.12).

Albarello, D., & Lunedei, E. (2013). Combining Horizontal Ambient Vibration Components for H/V Spectral Ratio Estimates. *Geophysical Journal International, 194*(2), 936-951.

Ambraseys, N. N., & Douglas, J. (2003). Effect of Vertical Ground Motions on Horizontal Response of Structures. *International Journal of Structural Stability and Dynamics, 3*(02), 227-265.

Ambraseys, N. N., & Douglas, J. (2003). Near-Field Horizontal and Vertical Earthquake Ground Motions. *Soil dynamics and earthquake engineering, 23*(1), 1-18.

Ambraseys, N. N., Douglas, J., Sarma, S. K., & Smit, P. M. (2005). Equations for the Estimation of Strong Ground Motions from Shallow Crustal Earthquakes Using Data from Europe and the Middle East: Horizontal Peak Ground Acceleration and Spectral Acceleration. *Bulletin of earthquake engineering, 3*(1), 1-53.

Anajafi, H., & Medina, R. A. (2018). Evaluation of ASCE 7 Equations for Designing Acceleration-Sensitive Nonstructural Components Using Data from Instrumented Buildings. *Earthquake Engineering & Structural Dynamics, 47*(4), 1075-1094.

ASCE/SEI 7-16. (2017). Minimum Design Loads and Associated Criteria for Buildings and Other Structures. In *ASCE Standard* (Vol. 7-16). Reston, Virginia, USA: American Society of Civil Engineers (ASCE) & Structural Engineering Institute (SEI).

ASCE/SEI 41-17. (2017). Seismic Evaluation and Retrofit of Existing Buildings. In (pp. 576). Reston, Virginia, USA: American Society of Civil Engineers (ASCE) & Structural Engineering Institute (SEI).

Asgarian, A. (2017). *New Methodology to Generate Floor Design Spectra (FDS) Directly from Uniform Hazard Spectra (UHS) for Seismic Assessment of Non-structural Components (NSCs) of Buildings.* (Doctor of Philosophy in Engineering), McGill University.

Assi, R., Dliga, M., & Yao, G. (2017). *Horizontal and Vertical Seismic Acceleration Demands in Multi-Storey Buildings.* Paper presented at the Structures Congress 2017, Denver, Colorado.

Assi, R., & McClure, G. (2015). Evolution of The NBCC Seismic Provisions For Operational and Functional Components in Buildings. *Canadian Journal of Civil Engineering, 42*(12), 993-999.

ATC. (2018). *Recommendations for Improved Seismic Design and Installation of Nonstructural Components*. (NIST grant-contract report; NIST grant contract report; 18-917-43). Applied Technology Council, Redwood City, CA: National Institute of Standards and Technology, U.S. Department of Commerce.

Atkinson, G. M. (2004). Empirical Attenuation of Ground-Motion Spectral Amplitudes in Southeastern Canada and the Northeastern United States. *Bulletin of the Seismological Society of America, 94*(3), 1079-1095.

Atkinson, G. M., & Boore, D. M. (2006). Earthquake Ground-Motion Prediction Equations for Eastern North America. *Bulletin of the Seismological Society of America, 96*(6), 2181-2205.

Baird, A., Tasligedik, A. S., Palermo, A., & Pampanin, S. (2014). Seismic Performance of Vertical Nonstructural Components in The 22 February 2011 Christchurch Earthquake. *Earthquake Spectra, 30*(1), 401-425. doi:10.1193/031013EQS067M

Baker, J. W. (2011). Conditional Mean Spectrum: Tool for Ground-Motion Selection. *Journal of Structural Engineering, 137*(3), 322-331.

Bartosh, I., & Bouaanani, N. (2014). Effect of Horizontal Component Definition on the Characterization of Vertical Ground Motions: Application to Eastern Canada. *Journal of Earthquake Engineering, 18*(6), 831-852.

Bas, S., Kalkan, I., & Lee, J.-H. (2016). *Structural Behavior of a High-Rise RC Structure under Vertical Earthquake Motion*. Paper presented at the 16th World Conference on Earthquake Engineering, Santiago, Chile.

Bent, A. L. (2009). A Moment Magnitude Catalog for the 150 Largest Eastern Canadian Earthquakes. *Geological Survey of Canada Open File, 6080*, 23.

Berto, L., Bovo, M., Rocca, I., Saetta, A., & Savoia, M. (2020). Seismic Safety of Valuable Non-Structural Elements in RC Buildings: Floor Response Spectrum Approaches. *Engineering Structures, 205*, 110081.

Boore, D. M., Watson-Lamprey, J., & Abrahamson, N. A. (2006). Orientation-Independent Measures of Ground Motion. *Bulletin of the Seismological Society of America, 96*(4A), 1502-1511.

Bozorgnia, Y., & Campbell, K. W. (2004). The Vertical-to-Horizontal Response Spectral Ratio and Tentative Procedures for Developing Simplified V/H and Vertical Design Spectra. *Journal of Earthquake Engineering, 8*(2), 175-207.

Bozorgnia, Y., & Campbell, K. W. (2016a). Ground Motion Model for the Vertical-to-Horizontal (V/H) Ratios of PGA, PGV, and Response Spectra. *Earthquake Spectra, 32*(2), 951-978.

Bozorgnia, Y., & Campbell, K. W. (2016b). Vertical Ground Motion Model for PGA, PGV, and Linear Response Spectra Using the NGA-West2 Database. *Earthquake Spectra, 32*(2), 979-1004.

Bozorgnia, Y., Campbell, K. W., & Niazi, M. (2000). Observed Spectral Characteristics of Vertical Ground Motion Recorded During Worldwide Earthquakes from 1957 to 1995. *Proceedings of the 12th World Conference on Earthquake Engineering, 2671*.

Bozorgnia, Y., Mahin, S. A., & Brady, A. G. (1998). Vertical Response of Twelve Structures Recorded During the Northridge Earthquake. *Earthquake Spectra, 14*(3), 411-432.

Bozorgnia, Y., Niazi, M., & Campbell, K. W. (1995). Characteristics of Free-Field Vertical Ground Motion During the Northridge Earthquake. *Earthquake Spectra, 11*(4), 515-515.

Bozorgnia, Y., Niazi, M., & Campbell, K. W. (1996). Relationship between Vertical and Horizontal Response Spectra for the Northridge Earthquake. *11th World Conference on Earthquake Engineering, 893*.

Breccolotti, M., & Materazzi, A. L. (2016). The Role of the Vertical Acceleration Component in the Seismic Response of Masonry Chimneys. *Materials and Structures, 49*(1-2), 29-44.

Broderick, B. M., Elnashai, A. S., Ambraseys, N. N., Barr, J. M., Goodfellow, R. G., & Higazy, E. M. (1994). The Northridge (California) Earthquake of 17 January 1994: Observations, Strong Motion and Correlative Response Analyses. In: London: Imperial College.

Campbell, K. W. (1997). Empirical Near-Source Attenuation Relationships for Horizontal and Vertical Components of Peak Ground Acceleration, Peak Ground Velocity, and Pseudo-Absolute Acceleration Response Spectra. *Seismological Research Letters, 68*(1), 154-179.

Campbell, K. W., & Bozorgnia, Y. (2003). Updated Near-Source ground-Motion (Attenuation) Relations for the Horizontal and Vertical Components of Peak Ground Acceleration and Acceleration Response Spectra. *Bulletin of the Seismological Society of America, 93*(1), 314-331.

Campbell, K. W., & Bozorgnia, Y. (2007). *Campbell-Bozorgnia NGA Ground Motion Relations for the Geometric Mean Horizontal Component of Peak and Spectral Ground Motion Parameters*. University of California, Berkeley, CA: Pacific Earthquake Engineering Research Center.

Campbell, K. W., & Bozorgnia, Y. (2009). *Background Information on the Proposed Procedure for Developing Vertical Design Response Spectrum*. Retrieved from PROPOSAL 3-3: ASCE 7-07 Chapter 23, Vertical Ground Motions for Seismic Design, 2nd Member Organization Ballot: https://cdn.ymaws.com/www.nibs.org/resource/resmgr/BSSC/ballotjuneaugp1_3-3.pdf

Chen, G., & Wu, J. (1999). Transfer-Function-Based Criteria for Decoupling of Secondary Systems. *Journal of engineering mechanics, 125*(3), 340-346.

Christopoulos, C. (1999). *A Study on the Characteristics of Vertical Accelerations and Their Effects on Civil Engineering Structures.* (Maîtrise ès sciences appliquées), École Polytechnique de Montréal.

Christopoulos, C., Léger, P., & Filiatrault, A. (2000). *Generation of Vertical Acceleration for Seismic Sliding Generation of Gravity Dams*. Paper presented at the 12th World Conference of Earthquake Engineering.

Collier, C. J., & Elnashai, A. S. (2001). A Procedure for Combining Vertical and Horizontal Seismic Action Effects. *Journal of Earthquake Engineering, 5*(04), 521-539.

CSA-A23.3. (2014). A23.3-14: Design of Concrete Structures (sixth edition). In. Mississauga, Ontario: Canadian Standards Association.

CSA-S832. (2014). S832-14: Seismic Risk Reduction of Operational and Functional Components (OFCs) of Buildings. In: Canadian Standard Association, CSA Group.

CSI, E. (2017). Structural and Earthquake Engineering Software (Version 17.01). USA, California: Computers and Structures Inc. (CSI).

Dana, M., Cussen, A., Chen, Y. N., Davis, C., Greer, M., Houston, J., Littler, P., & Roufegarinejad, A. (2014). *Effects of the Seismic Vertical Component on Structural Behavior - An Analytical Study of Current Code Practices and Potential Areas of Improvement.* Paper presented at the 10th U.S. National Conference on Earthquake Engineering: Frontiers of Earthquake Engineering, NCEE 2014, July 21, 2014 - July 25, 2014, Anchorage, AK, United States.

Dhari, R. (2019). Shear Wave Velocity Calculator. *Omni Calculator sp. z o.o., Reviewed by Steven Wooding.* Retrieved from https://www.omnicalculator.com/physics/shear-wave-velocity

Elgamal, A., & He, L. (2004). Vertical Earthquake Ground Motion Records: An Overview. *Journal of Earthquake Engineering, 8*(05), 663-697.

Elnashai, A. S., He, L., & Elgamal, A. (2004). *Spectra for Vertical Earthquake Ground Motion*. Paper presented at 13th World Conference on Earthquake Engineering,, Vancouver, BC, Canada.

Eurocode 8-1. (2004). Eurocode 8: Design of Structures for Earthquake Resistance-Part 1: General Rules, Seismic Actions and Rules for Buildings. *Brussels: European Committee for Standardization*.

FEMA E-74. (2012). Reducing the Risks of Nonstructural Earthquake Damage – A Practical Guide. In: FEMA Washington, DC.

FEMA P-1050-1. (2015). NEHRP Recommended Seismic Provisions for New Buildings and Other Structures (FEMA P-1050-1). In *FEMA P-1050-1*. Washington, DC: Federal Emergency Management Agency: BUILDING SEISMIC SAFETY COUNCIL, A council of the National Institute of Building Sciences.

Filiatrault, A., Perrone, D., Merino, R. J., & Calvi, G. M. (2021). Performance-Based Seismic Design of Nonstructural Building Elements. *Journal of Earthquake Engineering, 25*(2), 237-269.

Filiatrault, A., & Sullivan, T. (2014). Performance-Based Seismic Design of Nonstructural Building Components: The Next Frontier of Earthquake Engineering. *Earthquake Engineering and Engineering Vibration, 13*(1), 17-46.

Foo, S., & Lau, D. (2004). *Seismic Risk Reduction of Operational and Functional Components of Buildings: Research Perspective.* Paper presented at the 13th World Conference on Earthquake Engineering, Vancouver, B.C., Canada.

Freeman, S. A. (1998). *Design Criteria for Non-Structural Components Based on Tri-Services Manuals, ATC 29-1*.

Furukawa, S., Sato, E., Shi, Y., Becker, T., & Nakashima, M. (2013). Full-Scale Shaking Table Test of A Base-Isolated Medical Facility Subjected to Vertical Motions. *Earthquake Engineering & Structural Dynamics, 42*(13), 1931-1949.

Goltz, J. D. (1994). *The Northridge, California Earthquake of January 17, 1994: General Reconnaissance Report* (Technical Report NCEER-94-0005 ed.). State University of New York at Buffalo: National Centre for Earthquake Engineering Research.

Graizer, V. M. (2012). *Effect of Low-Pass filtering and Re-Sampling on Spectral and Peak Ground Acceleration in Strong-Motion Records*, Lisbon, Portugal.

Gülerce, Z., & Abrahamson, N. A. (2011). Site-Specific Design Spectra for Vertical Ground Motion. *Earthquake Spectra, 27*(4), 1023-1047.

Gupta, A. K. (1984). Seismic Response of Multiply Connected MDOF Primary and MDOF Secondary Systems. *Nuclear engineering and design, 81*(3), 385-394.

Guzman Pujols, J. C., & Ryan, K. L. (2018). Computational Simulation of Slab Vibration and Horizontal-Vertical Coupling in A Full-Scale Test Bed Subjected to 3D Shaking at E-Defense. *Earthquake Engineering & Structural Dynamics, 47*(2), 438-459.

Haghshenas, E., Bard, P. Y., Theodulidis, N., & Sesame, W. P. T. (2008). Empirical Evaluation of Microtremor H/V Spectral Ratios. *Bulletin of earthquake engineering, 6*(1), 75-108.

Hashash, Y. M. A., Musgrove, M. I., Harmon, J. A., Groholski, D., Phillips, C. A., & Park, D. (2019). DEEPSOIL V7.0.20, User Manual. Urbana, Illinois: Board of Trustees of University of Illinois at Urbana-Champaign.

Hilmy, S. I., & Masek, J. P. (1994). Failure Mechanisms of Parking Structures Damaged During the Northridge Earthquake, January 17, 1994. *Special Report, Dames & Moore Structural/Earthquake Engineering Group, June 1994*.

Huang, Y.-N., Yen, W.-Y., & Whittaker, A. S. (2016). Correlation of Horizontal and Vertical Components of Strong Ground Motion for Response-History Analysis of Safety-Related Nuclear Facilities. *Nuclear engineering and design, 310*, 273-279.

IRIS. (2018). *Incorporated Research Institutions for Seismology*. Retrieved from: http://ds.iris.edu/seismo-archives/

Jeong, S., Lee, K., & Jang, W. (2011). PRISM for Earthquake Engineering A Program for Seismic Response Analysis of SDOF System (Version Version 2.0.1): Version 2.0.1. Retrieved from http://sem.inha.ac.kr/prism/

Kalkan, E., & Gülkan, P. (2004). Empirical Attenuation Equations for Vertical Ground Motion in Turkey. *Earthquake Spectra, 20*(3), 853-882.

Kehoe, B., & Hachem, M. (2003). *Procedures for Estimating Floor Accelerations*. Paper published at the Wiss, Janney, Elstner Associates, Inc., Emeryville, California, USA.

Kim, S. J., & Elnashai, A. S. (2008). *Seismic Assessment of RC Structures Considering Vertical Ground Motion.* (Doctor of Philosophy in Civil Engineering), Mid-America Earthquake Center, Department of Civil and Environmental Engineering, University of Illinois at Urbana-Champaign, (MAE Center Report No. 08-03)

Kim, S. J., Holub, C. J., & Elnashai, A. S. (2011). Analytical Assessment of the Effect of Vertical Earthquake Motion on RC Bridge Piers. *Journal of Structural Engineering, 137*(2), 252-260.

Kinoshita, T., Nakamura, N., & Kashima, T. (2021). Characteristics of the First-Mode Vertical Vibration of Buildings Based on Earthquake Observation Records. *Japan Architectural Review, 4*(2), 290-301.

Kondner, R. L., & Zelasko, J. S. (1963). *A Hyperbolic Stress-Strain Formulation for Sands.* Paper presented at the Proceedings of the 2nd Pan American Conference on Soil Mechanics and Foundation Engineering, Sao Paulo, Brasil.

Kumar, A. (2014). *A Simplified Methodology for Seismic Design and Assessment of Nonstructural Elements.* (Master of Science), University of British Columbia, Vancouver.

Kumar, S. S., Krishna, A. M., & Dey, A. (2014). *Nonlinear Site-Specific Ground Response Analysis: Case Study of Amingaon, Guwahati.* Paper presented at the 15th Symposium on Earthquake Engineering, IIT Roorke.

Kupper, L. L. (1971). Probability, Statistics, and Decision for Civil Engineers. In: Taylor & Francis.

Lee, R., Bradley, B., & Franklin, M. (2013). *Characteristics of Vertical Ground Motions in the Canterbury Earthquakes*. Paper presented at the 2013 NZSEE Conference, Wellington.

Li, X., Dou, H., & Zhu, X. (2007). Engineering Characteristics of Near-Fault Vertical Ground Motions and Their Effect on The Seismic Response of Bridges. *Earthquake Engineering and Engineering Vibration, 6*(4), 345-350.

Look, B. G. (2007). *Handbook of Geotechnical Investigation and Design Tables*: Taylor & Francis Group/Balkema, London, UK.

Macias-Carrasco, M., Fereydouni, A., Goda, K., & Atkinson, G. (2010). Documentation for the 2009 Canadian Composite Seismicity Catalogue (CCSC09).

Magliulo, G., Ercolino, M., Petrone, C., Coppola, O., & Manfredi, G. (2014). The Emilia earthquake: seismic performance of precast reinforced concrete buildings. *Earthquake Spectra, 30*(2), 891-912.

Mase, L. Z. (2020). Seismic Hazard Vulnerability of Bengkulu City, Indonesia, Based on Deterministic Seismic Hazard Analysis. *Geotechnical and Geological Engineering, 38*(5), 5433-5455. doi:10.1007/s10706-020-01375-6

Mase, L. Z., Likitlersuang, S., & Tobita, T. (2018). Analysis of Seismic Ground Response Caused During Strong Earthquake in Northern Thailand. *Soil dynamics and earthquake engineering, 114*, 113-126. doi:https://doi.org/10.1016/j.soildyn.2018.07.006

Mase, L. Z., Likitlersuang, S., & Tobita, T. (2021). Ground Motion Parameters and Resonance Effect During Strong Earthquake in Northern Thailand. *Geotechnical and Geological Engineering, 39*(3), 2207-2219. doi:10.1007/s10706-020-01619-5

Mazloom, S., & Assi, R. (2022a). Estimate of V/H Spectral Acceleration Ratios for Firm Soil Sites in Eastern Canada. *Soil dynamics and earthquake engineering, 159*, 107350. doi:https://doi.org/10.1016/j.soildyn.2022.107350

Mazloom, S., & Assi, R. (2022b). Estimation of the Vertical Peak Floor Acceleration Demands in Linear Elastic RC Moment-Resisting Frame Buildings. *Journal of Earthquake Engineering*.

McGavin, G., & Patrucco, H. (1994). Survey of Non-Structural Damage to Healthcare Facilities in the January 17, 1994 Northridge Earthquake. *Report prepared for HMC Group, Ontario, Canada*.

McGuire, R. K. (1995). Probabilistic Seismic Hazard Analysis and Design Earthquakes: Closing the Loop. *Bulletin of the Seismological Society of America, 85*(5), 1275-1284.

McGuire, R. K., Silva, W. J., & Costantino, C. J. (2001). *Technical Basis for Revision of Regulatory Guidance on Design Ground Motions: Hazard-and Risk-Consistent Ground Motion Spectra Guidelines, NUREG/CR-6728*. Washington, DC 20555-0001: Division of Engineering Technology, U.S Nuclear Regulatory Commission, Office of Nuclear Regulatory Research.

Medina, R. A. (2013). *Seismic Design Horizontal Accelerations for Nonstructural Components*, Vienna Congress on Recent Advances in Earthquake Engineering and Structural Dynamics (VEESD). Vienna, Austria.

Ministère du Logement, & Ministère de l'Écologie. (2014). *DIMENSIONNEMENT PARASISMIQUE DES ÉLÉMENTS NON STRUCTURAUX DU CADRE BÂTI*.

Miranda, E., & Taghavi, S. (2003). *Estimation of Seismic Demands on Acceleration-Sensitive Nonstructural Components in Critical Facilities.* Paper presented at the Proceedings of the Seminar on Seismic Design, Performance, and Retrofit of Nonstructural Components in Critical Facilities, ATC, 29-2, Newport Beach, CA, 347−360.

Mitchell, D., Tinawi, R., & Law, T. (1989). The 1988 Saguenay Earthquake: A Site Visit Report. *Geological Survey of Canada, Open File 1999*, 92 pp.

Mohit, S. M. P., & Shimazu, T. (1987). The Behaviour of Beams in Reinforced Concrete Frames Under the Combined Action of Vertical and Horizontal Loadings. *Journal of Structural and Construction Engineering (Transactions of AIJ), 372*, 72-85.

Moschen, L. (2016). *Contributions to the Probabilistic Seismic Assessment of Acceleration Demands in Buildings.* (Ph.D. Thesis Ph.D. Thesis), University of Innsbruck, Innsbruck, Austria.

Moschen, L., Medina, R. A., & Adam, C. (2015). *Vertical Acceleration Demands on Nonstructural Components in Buildings*. Paper presented at the 5th International Conference on Computational Methods in Structural Dynamics and Earthquake Engineering (COMPDYN 2015) (pp. 25-27), Crete Island, Greece.

Moschen, L., Medina, R. A., & Adam, C. (2016). Vertical Acceleration Demands on Column Lines of Steel Moment-Resisting Frames. *Earthquake Engineering and Structural Dynamics, 45*(12), 2039-2060. doi:10.1002/eqe.2751

NBC. (2015a). National Building Code of Canada: Canadian Commission on Building Fire Codes. In *NBC 2015, Part 4 of Division B: Structural Design*: National Research Council of Canada, Canadian Commission on Buildings and Fire Codes.

NBC. (2015b). User's Guide-NBC 2015 Structural Commentaries. In: National Research Council of Canada, Canadian Commission on Buildings and Fire Codes.

Newmark, N. M., Blume, J. A., & Kapur, K. K. (1973). Seismic Design Spectra for Nuclear Power Plants. *American Society of Civil Engineers, Journal of the Power Division, 99*(PO2), 287-303.

Newmark, N. M., & Hall, W. J. (1982). *Earthquake Spectra and Design*. Berkeley, CA: Earthquake Engineering Research Institute.

NIST GCR 17-917-44 (ATC). (2017). *Seismic Analysis, Design, and Installation of Nonstructural Components and Systems – Background and Recommendations for Future Work* (17-917-44).

NRCAN. (2001). *Strong Motion Historical Events*. Retrieved from: ftp://ftp.seismo.nrcan.gc.ca

NRCAN. (2015). Determine 2015 National Building Code of Canada Seismic Hazard Values. Retrieved from https://www.earthquakescanada.nrcan.gc.ca/hazard-alea/interpolat/calc-en.php

Papadopoulou, O. (1989). *The Effect of Vertical Excitation on Reinforced Concrete Multi-Storey Structures.* (MSc. Dissertation), Imperial College of London, UK.

Papazoglou, A. J., & Elnashai, A. S. (1996). Analytical and Field Evidence of the Damaging Effect of Vertical Earthquake Ground Motion. *Earthquake Engineering and Structural Dynamics, 25*(10), 1109-1137.

PEER-NGA. (2018). PEER Ground Motion Database. from Pacific Earthquake Engineering Research Center https://ngawest2.berkeley.edu

Pekcan, G., Itani, A., & Staehlin, W. (2003). *Nonstructural System Response to Vertical Excitation and Implications for Seismic Design and Qualification*. Paper presented at the Proceedings of Seminar of Seismic Design, Performance, and Retrofit of Non-Structural Components in Critical Facilities, Applied Technology Council (ATC-29), Multidisciplinary Center for Earthquake Engineering Research.

Petrone, C., Magliulo, G., & Manfredi, G. (2016). Floor Response Spectra in RC Frame Structures Designed According to Eurocode 8. *Bulletin of earthquake engineering, 14*(3), 747-767.

Picozzi, M., Parolai, S., & Albarello, D. (2005). Statistical Analysis of Noise Horizontal-to-Vertical Spectral Ratios (HVSR). *Bulletin of the Seismological Society of America, 95*(5), 1779-1786.

Pileggi, D., Rossi, D., Lunedei, E., & Albarello, D. (2011). Seismic Characterization of Rigid Sites in the ITACA Database by Ambient Vibration Monitoring and Geological Surveys. *Bulletin of earthquake engineering, 9*(6), 1839-1854.

Reinhorn, A. M., Ryu, K. P., & Maddaloni, G. (2010). *Modeling and Seismic Evaluation of Nonstructural Components: Testing Frame for Experimental Evaluation of Suspended Ceiling Systems* (Technical Report MCEER-10-0004). Retrieved from Multidisciplinary Center for Earthquake Engineering Research, University of Buffalo, State University of New York.

Ryan, K. L., Soroushian, S., Maragakis, E., Sato, E., Sasaki, T., & Okazaki, T. (2016). Seismic Simulation of an Integrated Ceiling-Partition Wall-Piping System at E-Defense. I: Three-Dimensional Structural Response and Base Isolation. In *Journal of Structural Engineering* (Vol. 142, pp. 04015130 (04015115 pp.)). USA: ASCE - American Society of Civil Engineers.

SEAOC/OSHPD, S. D. M. (2019). Seismic Design Maps by Structural Engineers Association of California-SEAOC and California's Office of Statewide Health Planning and Development-OSHPD. Retrieved from https://seismicmaps.org/

Seed, H. B., & Idriss, I. M. (1970). *Soil Moduli and Damping Factors for Dynamic Response Analysis* (EERC 70-10). Retrieved from Earthquake Engineering Research Center, University of California, Berkeley, California.

SeismoSoft. (2018). Earthquake Software for Response Spectrum Matching (Version 2018): SeismoMatch, Earthquake Engineering Software Solutions. Retrieved from https://seismosoft.com/products/seismomatch/

Seismotoolbox. (2019). Engineering Seismology Toolbox. Available from Gail Atkinson, Karen Assatourians. Earthquake Data Auto-Processor (EDAP), Automatically Generated Interactive Ground Motion Maps For Southern Ontario https://www.seismotoolbox.ca/edap/index.php

Shirai, K., Ohmachi, T., & Arita, S. (2004). *Empirical Study on Relationship Between Horizontal and Vertical Ground Motions*. Paper presented at the 13th World Conference on Earthquake Engineering, Vancouver, BC, Canada.

Shome, N., & Cornell, C. A. (1999). Probabilistic Seismic Demand Analysis of Nonlinear Structures. Report no. RMS-35. *Research Management System (RMS) Program, Department of Civil Engineering, Stanford University, Stanford, CA*.

Shrestha, B. (2009). *Vertical Ground Motions and its Effect on Engineering Structures: A State-of-the-Art Review.* Paper presented at the International Seminar on Hazard Management for Sustainable Development, Kathmandu, Nepal.

Shteinberg, V. V., Graizer, V. M., & Ivanova, T. G. (1980). The May 17, 1976 Gazli Earthquake. *Izvestiya Academy of Sciences, USSR, Physics of the Solid Earth, 16*(3), 22-29.

Siddiqqi, J., & Atkinson, G. M. (2002). Ground-Motion Amplification at Rock Sites Across Canada as Determined from the Horizontal-to-Vertical Component Ratio. *Bulletin of the Seismological Society of America, 92*(2), 877-884.

Sonley, E., & Atkinson, G. M. (2005). Empirical Relationship Between Moment Magnitude and Nuttli Magnitude for Small-Magnitude Earthquakes in Southeastern Canada. *Seismological Research Letters, 76*(6), 752-755.

Stewart, J. P., Abrahamson, N. A., Atkinson, G. M., Baker, J. W., Boore, D. M., Bozorgnia, Y., Campbell, K. W., Comartin, C. D., Idriss, I. M., & Lew, M. (2011). Representation of Bidirectional Ground Motions for Design Spectra in Building Codes. *Earthquake Spectra, 27*(3), 927-937.

Taghavi, S., & Miranda, E. (2003). *Response Assessment of Nonstructural Building Elements*. Retrieved from Pacific Earthquake Engineering Research Center, University of California Berkeley, California, USA.

Taghavi, S., & Miranda, E. (2008). *Effect of Interaction Between Primary and Secondary Systems on Floor Response Spectra.* Paper presented at the 14th World Conference on Earthquake Engineering, Beijing, China.

Taghavi, S., & Miranda, E. (2012). *Probabilistic Study of Peak Floor Acceleration Demands in Nonlinear Structures.* Paper presented at the Proceedings of the 15th World Conference on Earthquake Engineering (15WCEE), Lisbon, Portugal.

Tso, W. K., Zhu, T. J., & Heidebrecht, A. C. (1992). Engineering Implication of Ground Motion A/V Ratio. *Soil dynamics and earthquake engineering, 11*(3), 133-144.

US NRC. (2014). Regulatory Guide 1.60: Design Response Spectra for Seismic Design of Nuclear Power Plants. *United States Nuclear Regulatory Commission*.

USGS. (2018). *United States Geological Survey, Search Earthquake Catalog*. Retrieved from: https://earthquake.usgs.gov/earthquakes/search/

VDC. (2018). Strong-Motion Virtual Data Center. from Center for Engineering Strong Motion Data (CESMD), The Consortium of Organizations for Strong-Motion Observation Systems (COSMOS) https://strongmotioncenter.org/vdc/scripts/default.plx

Vucetic, M. (1992). *Soil Properties and Seismic Response.* Paper presented at the Proceedings of the 10th World Conference on Earthquake Engineering, Madrid, Spain.

Vucetic, M., & Dobry, R. (1991). Effect of Soil Plasticity on Cyclic Response. *Journal of geotechnical engineering, 117*(1), 89-107.

Wang, M. (2008, 2008). *Seismic Risk Assessment of Operational and functional Components for New and Existing buildings.* Paper presented at the 14th World Conference on Earthquake Engineering, Beijing, China.

Wieser, J. D., Pekcan, G., Zaghi, A. E., Itani, A. M., & Maragakis, E. (2012). *Assessment of Floor Accelerations in Yielding Buildings.* Sponsored by the National Science Foundation, University of Nevada, Reno. (MCEER-12-0008)

Yamanouchi, T., & Hasegawa, H. (1996, 1996). *Seismic Performance of Model Structures Designed by Old and New Japanese Seismic Codes, Against the 1995 Kobe Earthquake Ground Motions*.